Characterization of Composite Dust generated during Milling of Uni-Directional and Random fiber composites

Anirudh Krishnan Iyer

A thesis
Submitted in partial fulfillment of the
Requirements for the degree of

Master of Science in Mechanical Engineering

University of Washington
2015

Committee:
Ramulu Mamidala
John. C. Kramlich
Jeffrey Lawrence Miller

Program Authorized to Offer Degree:
Mechanical Engineering

University of Washington

Abstract

Characterization of Composite Dust generated during Milling of Uni-Directional and Random fiber composites

Anirudh Krishnan Iyer

Chair of the Supervisory Committee:
Professor Ramulu Mamidala
Department of Mechanical Engineering

As every manufacturer of carbon-fiber composite structures knows, one of the most nettlesome aspects of the production process is that machining, drilling and sanding of carbon fiber composites produces fine dust. These composite materials typically consist of epoxy matrix material reinforced with carbon, graphite, glass, and/or para-aramid fibers. Matrix materials are usually epoxy, polyester, phenolic, fluorocarbon, polyether-sulfone, and silicon. The most commonly used are epoxies and polyesters, which are less expensive than epoxies. It can build up on and short out computers, control panels and servomotors. In the air, it can be inhaled and threaten human health. Further, the accumulation of any dust in a manufacturing facility can be problematic from the regulatory perspective. In fact, dust has been blamed for several explosions in manufacturing facilities, leading the U.S. Occupational Safety and Health Admin. (OSHA) and many local governments to more closely monitor and regulate dust accumulation in all manufacturing environments. An increase in human exposure to potentially toxic airborne fibers has accompanied the increased use of composite

materials. The dust emitted during the machining of composite materials is potentially damaging to the human lung. Several studies have attempted to characterize the damage to the lung caused by airborne particles from composites, while other studies have characterized the size and concentration of the dust emitted. Some studies have shown that the chip formation process affects the size distribution of the particles emitted during the machining of composites. Health hazard evaluation of composite matrix material is usually conducted by examining the individual materials that are in the resin system and using sound scientific judgment. The main objective of this research is to quantify the amount of dust generated during machining (predominantly milling) of composites and to calculate what percentage of this dust is harmful to the workers in such composite dust laden environments. This criteria is based on PM (Particulate matter) aerosol standards defined by OSHA in regard to safety and well-being. In addition this research will also highlight the effect of stacking sequence of laminates on the concentration of dust generated and the characterization of these particle sizes. This research also further aims to develop optimized cutting conditions that will help in reducing the amount of dust that would be generated by using an experimental study. During this study different tests were carried out to characterize the different effects that are observed during the machining of Uni-Directional and random fiber composites. The machining dust results showed a very good correlation between the different real time measuring instruments and validated the design of the iso-kinetic sampling tower. Mean aerodynamic diameters of particles found during the machining of Uni-Directional composites was 0.19 um and that of random fiber composites was found to be 0.28 um. Tests to find out the optimal cutting conditions for the lowest amount of dust generated was found to be that of using a low cutting speed, high feed and lower depth of cuts. These conditions however might not aid the best surface finish. Hence a compromise or a trade-off is required.

A. Acknowledgments

I cannot express enough thanks to my committee for their continued support and encouragement: Dr. Ramulu, my committee chair; Dr. John Kramlich and Dr. Jeffrey Miller. I offer my sincere appreciation for the learning opportunities provided by my committee. My completion of this thesis could not have been accomplished without the support of my lab-mates, Rishi Pahuja, Kapil Gangwar, Aditya Venkata, Eshetu Eneyew, Shanti Ravali and Neha Kulkarni. All of them have helped me in the course of this thesis, in whatever capacity they could. A very big part of this thesis is credited to my guide, Dr. M. Ramulu. I have never seen anybody work so hard and still find time to help you out. And oh yeah, did I mention the coffee he used to buy us free of cost? He is generally the first professor to check in in the department in the morning, and definitely the only one on campus on Saturdays. I always remember a thing he used to say "My life is all about Department and Apartment" meaning that work and home is his life. A hearty thanks to Jeffrey Miller, who taught me a lot about the instrumentation to be used in the thesis. His patience and knowledge really helped me grasp a lot of knowledge in a short period of time. Special thanks to Rishi Pahuja for his help on using the Scanning Electron Microscope. Thanks to my parents Mr. Kadayam Krishnan and Jayashree Krishnan. The amount of moral support you give me is immense. I would like to also thank my brother, Arvind Iyer for always supporting me. Last but not the least, I would like to thank Wanwisa Kisalang and the Mechanical Engineering Office staff for their prompt help, Eamon McQuaide the workshop in-charge for his help with tooling and materials and Bill Kuykendall for his help on small issues materials and more. Lastly, I would like to thank all the people whose names I may have missed, who have given me constructive criticism and good advice throughout the course of my study. A special thanks to the entire Mechanical Engineering Faculty for the knowledge they have endowed me with. This association is something I will cherish for life.

.

B. Dedication

I dedicate this work to my parents and my dear brother.

C. Table of contents

D. List of tables

E. List of figures

Figure Page

1 Chapter I: Introduction

Composites could be natural or synthetic. Wood is a good example of a natural composite, combination of cellulose fiber and lignin. The cellulose fiber provides strength and the lignin is the "glue" that bonds and stabilizes the fiber. Bamboo is a very efficient wood composite structure. The components are cellulose and lignin, as in all other wood, however bamboo is hollow. This results in a very light yet stiff structure. Composite fishing poles and golf club shafts copy this natural design. The ancient Egyptians manufactured composites! Adobe bricks are a good example. The combination of mud and straw forms a composite that is stronger than either the mud or the straw by itself. Composites are combinations of two materials in which one of the material is called the reinforcing phase, is in the form of fibers, sheets, or particles, and is embedded in the other material called the matrix phase. Typically, reinforcing materials are strong with low densities while the matrix is usually a ductile or tough material. If the composite is designed and fabricated correctly, it combines the strength of the reinforcement with the toughness of the matrix to achieve a combination of desirable properties not available in any single conventional material. The use of Carbon Fiber Reinforced Polymer (CFRP) composite has grown considerably over the recent years. Although their creation ascends to a half century ago, their use was initially limited to few niche aerospace and defense applications due to their high manufacturing costs. This can be attributed to their high production costs as well as to the fact that carbon fibers are a very expensive raw material. The development of new and innovative production technologies has reduced carbon fiber cost promoting their use across different industries. During the last decades CFRP have earned huge importance for applications in many industrial sectors such as automotive, sporting, wind energy, nuclear, construction, naval, biomedical and offshore oil and gas applications. A broad definition of composite is: *Two or more chemically distinct materials which when combined have improved properties over the individual materials*. While the advantages of composites over conventional materials are obvious, one must not overlook their limitations. There is an apparent lack in knowledge and experience that limits their fast incorporation into existing and new designs. The high

cost of materials and complexities in their manufacturing is perhaps the most serious problems that designers with composites have to deal with. Components fabricated from composite materials are endeavored to be made net shape. This is made possible because of the fact that many components are built layer by layer out of contoured two dimensional plies that closely captures the final shape of the product. Even though composite components are often made near-net shape, some machining is often unavoidable. In many cases excess material is added to compensate for material conformity to complex mold shapes and for locating and fixturing performs. Resin flashing may also result after molding and curing of fiber-resin performs. This excess material has to be removed by machining. Machining is also an indispensable process for shaping parts from stock composite materials and for finishing close-tolerance components. Some of the common machining processes used are edge trimming, turning, milling, drilling, and grinding. Despite the existing experience and knowledge in machining traditional material such as metals, it has been challenge to maintain consistent results in terms of machining quality for composite material [1].

The essence of the concept of composites is that the load is applied over a large surface area of the matrix. Matrix then transfers the load to the reinforcement, which being stiffer, increases the strength of the composite. It is important to note that there are many matrix materials and even more fiber types, which can be combined in countless ways to produce just the desired properties. In the United States, composites manufacturing is a 25 billion dollar a year industry. There are about 6000 composites related manufacturing plants and materials distributors across the U.S. The industry employs more than 235,000 people [2]. An additional 250,000 people are employed in businesses that support the composites industry, including materials suppliers, equipment vendors, and other support personnel. About 90% of all composites produced are comprised of glass fiber and either polyester or vinyl ester resin. Composites are broadly known as reinforced plastics.

2 Chapter II: Background and Literature Review

2.1 Composition of Composites

Composite materials are constructed from two materials; one material is called the reinforcement or discrete phase. The other is called a matrix or continuous phase. The fiber and the matrix have two different properties but when combined together they form a material with significantly different properties that are not found in either of the individual materials, such as high strength per weight ratio, high corrosion and thermal resistance and high stiffness, which are markedly superior to those of comparable metallic alloys. The duty of the matrix phase is to hold the reinforcement in order to form the desired shape; while the function of the reinforced is to carry the major external load thus improves the overall mechanical properties of the matrix. When the two phases are mixed properly, the new combined material present better strength than would each individual material [3]. The simplest explanation of a composite material is shown in figure below.

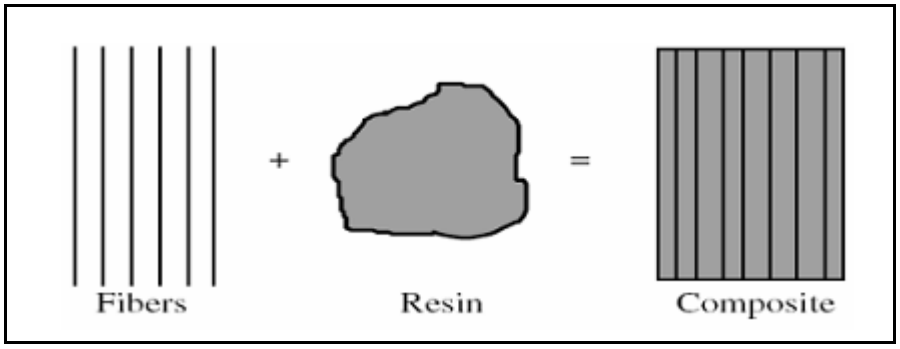

Figure 2-1: Formation of composite material using fibers and resins (Mazumdar.SK 2002)

2.2 Some Commonly Used Fibers and Matrix Materials

Table 2-1: Commonly used fibers and matrix materials

Material	Characteristics
Fibers	
Glass	High strength, low stiffness, high density; lowest cost; E (calcium aluminoborosilicate) and S (magnesia-aluminosilicate) types commonly used.
Graphite	Available as high-modulus or high-strength; low cost; less dense than glass.
Boron	High strength and stiffness; highest density; highest cost; has tungsten filament at its center.
Aramids (Kevlar)	Highest strength-to-weight ratio of all fibers; high cost.
Other fibers	Nylon, silicon carbide, silicon nitride, aluminum oxide, boron carbide, boron nitride, tantalum carbide, steel, tungsten, molybdenum.
Matrix materials	
Thermosets	Epoxy and polyester, with the former most commonly used; others are phenolics, fluorocarbons, polyethersulfone, silicon, and polyimides.
Thermoplastics	Polyetheretherketone; tougher than thermosets but lower resistance to temperature.
Metals	Aluminum, aluminum-lithium, magnesium, and titanium; fibers are graphite, aluminum oxide, silicon carbide, and boron.
Ceramics	Silicon carbide, silicon nitride, aluminum oxide, and mullite; fibers are various ceramics.

2.3 Types of Composites

2.3.1 Polymer Matrix Composites

Polymer matrix composites (PMC) (See Fig. 2-2) and fiber reinforced plastics (FRP) are referred to as Reinforced Plastics. Common fibers used are glass (GFRP), graphite (CFRP), boron, and aramids (Kevlar). These fibers have high specific strength (strength-to-weight ratio) and specific stiffness (stiffness-to-weight ratio).

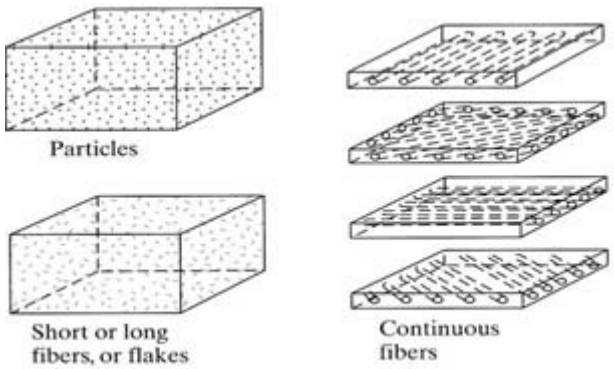

Figure 2-2: Polymer Matrix Composites[4]

2.3.2 *Fiber Reinforced Composites*

FRP (fiber reinforced polymer) is an acronym commonly used in the composite industry and it referees to plastic and polymer materials that are reinforced with structural fiber such as fiberglass, carbon fiber, or aramid fiber. FRP can also be used as a replacement for the term "composite". Most often, FRP products are constructed using thermoset resins such as polyester, vinyl ester or epoxy, but they can also use thermoplastic resins. The reinforcing fiber can not only be of various types (fiberglass, carbon fiber, or aramid) but the style of the fiber can very as well. The fiber can be discontinuous such as fiber that is found in chopped strand mat, or glass fiber used in gun roving (See Fig. 2-3). The fiber could be continuous direct-end roving, which is commonly used in filament winding and pultrusion. Other constructions of fiber include woven roving and stitched fabrics. Woven is similar to other textiles, and structural fibers are interwoven. With stitched fabrics, layers of fiber are stitched together [5].

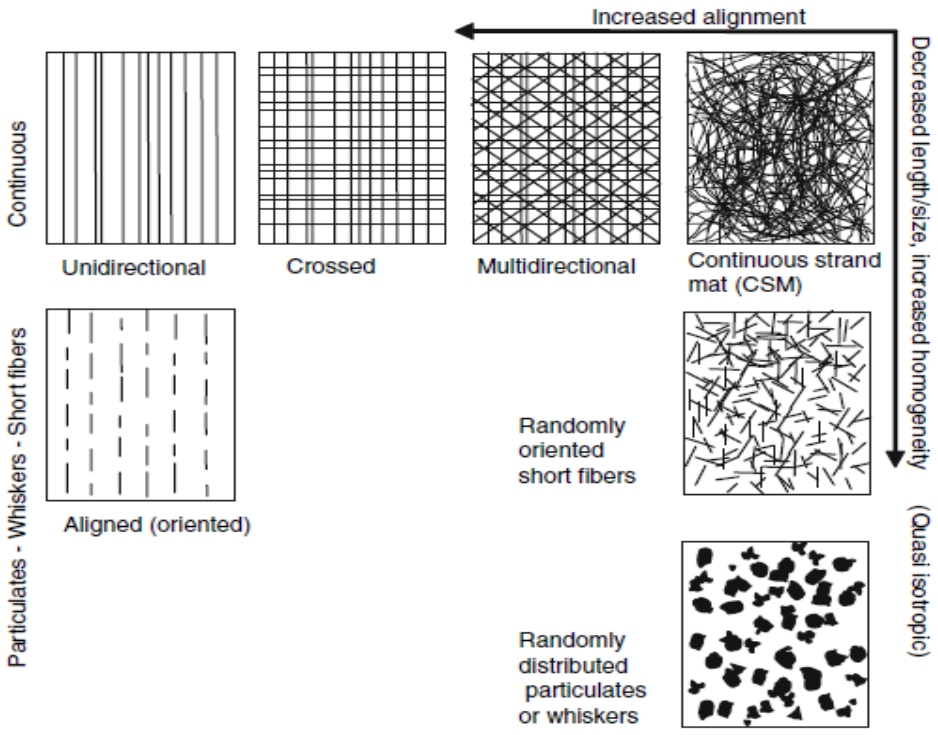

Figure 2-3: Different reinforcement arrangements in composites[5]

2.3.3 Metal Matrix Composites

The metal matrix composites offer higher modulus of elasticity, ductility, and resistance to elevated temperature than polymer matrix composites. But, they are heavier and more difficult to process. Details can be found in Table 2-2.

Table 2-2: Metal matrix composites

Fiber	Matrix	Applications
Graphite	Aluminum	Satellite, missile, and helicopter structures
	Magnesium	Space and satellite structures
	Lead	Storage-battery plates
	Copper	Electrical contacts and bearings
Boron	Aluminum	Compressor blades and structural supports
	Magnesium	Antenna structures
	Titanium	Jet-engine fan blades
Alumina	Aluminum	Superconductor restraints in fission power reactors
	Lead	Storage-battery plates
	Magnesium	Helicopter transmission structures
Silicon carbide	Aluminum, titanium	High-temperature structures
	Superalloy (cobalt-base)	High-temperature engine components
Molybdenum, tungsten	Superalloy	High-temperature engine components

2.3.4 Ceramic Matrix Composites

Ceramic matrix composites (CMC) are used in applications where resistance to high temperature and corrosive environment is desired. CMCs are strong and stiff but they lack toughness (ductility). Matrix materials are usually silicon carbide, silicon nitride and aluminum oxide, and Mullite (compound of aluminum, silicon and oxygen). They retain their strength up to 3000 ^{o}F. Fiber materials used commonly are carbon and aluminum oxide. Applications are in jet and automobile engines, deep-see mining, cutting tools, dies and pressure vessels.

2.4 Aerospace Applications of Composite Materials

Composites are versatile, used for both structural applications and components, in all aircraft and spacecraft, from hot air balloon gondolas and gliders, to passenger airliners, fighter planes and the Space Shuttle. Applications range from complete airplanes such as the Beech Starship, to wing assemblies, helicopter rotor blades, propellers, seats and instrument enclosures. These types have different mechanical properties and are used in different areas of aircraft construction in the Boeing 787 aircraft as shown in fig.2-4, 2-5.

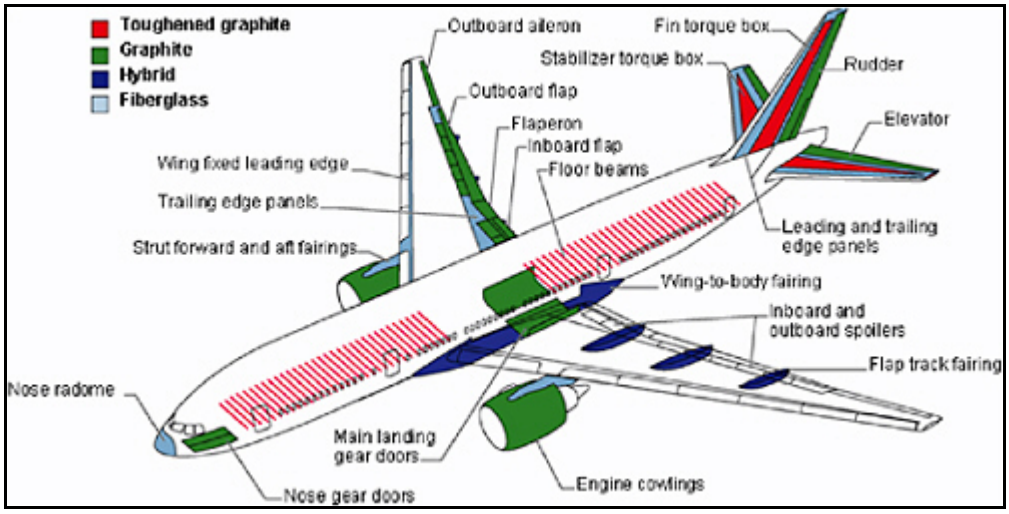

Figure 2-4: Use of composite materials pre 2001[6]

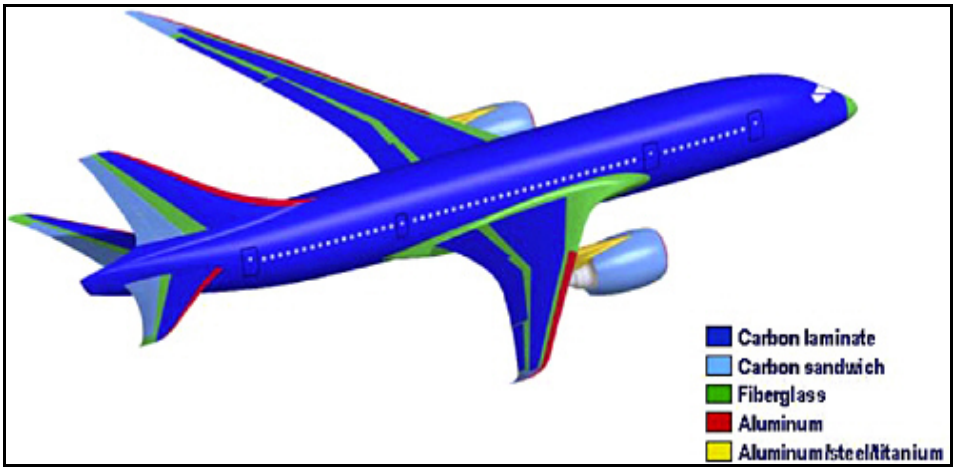

Figure 2-5: Use of Composites on Modern Aircrafts [6]

2.5 *Milling of Composites and Concerned Issues*

Machining of composites is widely performed in order to do the final processing of the near-net shape material in order to meet tolerance requirements in assembly. Drilling and milling are the most commonly used machining processes. In milling, material is removed from work-piece by rotating cutter head that may have more than one active cutting edge. The types milling operation that are most common in machining of FRPs are: peripheral milling or profiling and end milling. Fig. 2-6 (a) and Fig. 2-6 (b) illustrates these milling operations.

- **Peripheral milling** uses the cutting edges on the periphery of the tool. The machine surface is parallel to the axis of rotation of the cutter and the engagement into the work-piece is in radial direction of the cutter. Peripheral milling is appropriately called edge trimming because tool diameter is usually small and the axial engagement covers the entire thickness of the work piece.

- **End milling** is similar to peripheral milling, except that the axial engagement may be less than the thickness of the part and slot is obtained. The machine most commonly used is vertical milling machine but for side and face milling horizontal milling machine is used. Information about the tool used is listed near the figure below.

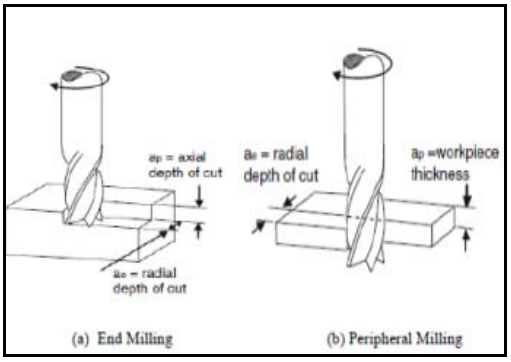

Tool : 12.7 mm (0.5") carbide end mill
Speed: 6000, 3000, 1000 Rpm
Feed: 635, 381, 127 mm/min
Depth of Cut (axial) : 6.35, 3.81, 2.54 mm
Depth of Cut (radial): 0.762 mm

Figure 2-6: (a) End Milling, (b) Peripheral Milling

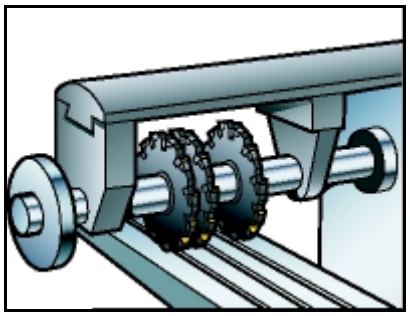

Figure 2-7: Side and face milling

- **Side and face milling cutters** can handle long, deep, open slot in more efficient manner, and provide the best stability and productivity for this type of milling. They can also be built into a "gang" to machine more than one surface in the same plane at the same time as shown in Fig. 2-7.

The milling machine provides the primary motion to the spindle (to which the cutter is held) and feed motions to the machine tables (to which the work-piece is held). The milling operation may be classified as conventional milling (or up cut milling) and climb milling (or down cut milling) operation depending on how the cutting edges approach the work-piece. The operations are depicted. *In up milling the direction of cutting speed of the edge in contact with work-piece is opposite to the direction of feed. In down milling, the direction of cutting speed is the same as that of the feed*. The resulting chip area in both the cases has a "comma" shape and length of the chip is described by a torchoid that results from the superposition of peripheral motion and feed motion. In up milling the cutting edge begins engaging the chips at the thin section of the comma shape. This results in low engagement forces and in lifting up of the work-piece. In down milling the cutting edge engages the chip at the thick section of the comma shape. The engagement forces are high and result in pushing the work piece against the work holding surface. Cutting forces in milling are also not continuous. In up milling, the forces gradually increase from zero at beginning of tool engagement to a maximum when the cutting edges about to leaves the work-piece.

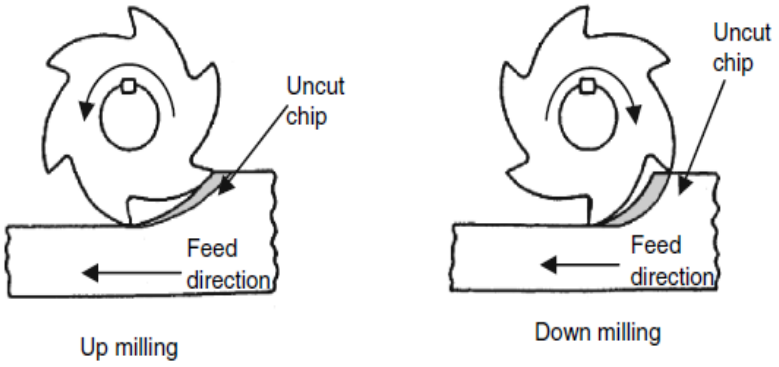

Figure 2-8: Up Milling (left), Down Milling (right) [7]

Milling is the one of the most frequently used material removal processes in manufacturing parts made of FRPs. However unlike the milling of metals which is characterized by high materials removal rates, milling of FRPs is conducted as much lower scale. The reason for this is that FRPs component are largely made near net shape and any subsequent milling is limited mainly to de-burring and trimming as well as to achieving the contour shape accuracy. In milling, as opposite to turning, the cutting tool is rotating and quite often more than one cutting edge is engaged in cutting at same time. This adds complexity to the milling processes in terms of fiber orientation, chip size and cutting forces that continuously vary with tool rotation. The machinability of FRPs in milling is mainly characterized by tool wear, surface roughness and delamination [5].

Composites are inhomogeneous materials consisting of two phases that are deliberately combined to form structures with desired properties. The two phases are the matrix phase and the reinforcement phase. Fiber-reinforced polymers consist of a combination of two separate phases within a single material microstructure, typically a fiber and matrix phase. The fibers in the microstructure typically carry the primary load and have a high strength and stiffness. The ductile matrix material provides several key functions including stabilizing the fibers in compression, distributing and transmitting loads between fibers, and providing off-axis properties. Common fiber-reinforcement materials include carbon, glass, aramid, and boron fibers. The matrix typically consists of a thermoset or thermoplastic such as epoxy, polycarbonate, or polyester. Fibers are typically produced by a pultrusion process, which results in the alignment of molecules in

the fiber longitudinal direction. The phases are macroscopically distinguishable with distinct boundaries between them known as interface. The role of the matrix phase is to hold the reinforcement phase, distribute the applied load and protect the composite from hostile environments such as heat, cold, moisture and corrosion. The reinforcement phase supplies strength to the composite, conducts or resists corrosion, resists or conducts electricity. The materials used for the matrix and reinforcement phase can be a metal, polymer or ceramic. Reinforcement materials in composite construction are used in the form of flakes, particles, sheets, whiskers and fibers. Composites are classified according to the type of matrix materials and the form of reinforcement material used. Since reinforcement improves the properties of the composite, selection of reinforcement material should be in such a way that they possess high strength and stiffness. Reinforcement materials retain their strength and stiffness in fibrous form than in any other form. Thus fibers are the most commonly used reinforcement materials in composite construction and hence called as fiber reinforced polymers (FRP). In general fiber reinforced composites are available in laminate form, which is obtained by stacking a number of thin layers of fibers and matrix and consolidating them into desired thickness. By controlling the stacking sequence and orientation of fiber in each layer a wide range of physical and mechanical properties can be obtained with the composite specific to the application purpose. This gives composites the edge over metals and alloys in industrial applications. The properties of fiber reinforced composites are highly dependent on the lay and the individual components of the composites that is the fiber-matrix interface. Fiber reinforced composites offer high strength-weight ratio, high modulus weight ratio, high fatigue strength-weight ratio, high fatigue damage tolerance, low coefficient of thermal expansion and high internal damping [5]. These properties make fiber reinforced composites emerge as the major structural material in the aerospace, vehicle and shipping industry where weight reductions as well as exceptional physical and mechanical properties are of major concern.

Machining of composites is very different from machining of metals and their Alloys. In composites, different material response depends on diverse properties of matrix and reinforcement. Responses can be different because the machining there is

alternatively hard and soft material (matrix and fiber). Hence the resultant mechanism of chip formation, cutting mechanism differs in composites from metals [8].

Conventional or Non-conventional techniques can be used for composite machining. Conventional techniques are milling drilling, boring, etc. Non-Conventional methods are Water jet machining, lasers etc. All methods have their own set of advantages and disadvantages Water jet has excellent contouring ability. It can also be used for bulk production. Lasers impart no cutting forces, hence there is no mechanical distortion. But the heat from lasers can cause thermal distortion [9].

Machining of polymers/Composites is employed when the quantity of items does not justify the cost for molds, or when a product needs accurate dimensional accuracy, better surface finish. As high performance polymers have been increasingly used for a large number of industrial applications, the machining quality was become predominate factor for the development of new processes and materials. Nevertheless the knowledge about the polymer under machining is very limited, as well as the definition of suitable models for predictions of cutting forces. In the scientific literature, machining of plastics is poorly treated. In the oldest references, an experimental approach is preferred, assuming the plastics behave as metals [10].

While FRP composite materials are generally fabricated net-shape, post-processing operations are often unavoidable. Net-shape composite manufacturing technologies generally have very loose tolerances and as such, post-curing machining operations are often required to improve dimensional accuracy [11, 12]. Due to the anisotropic and highly abrasive nature of typical fiber reinforcements, several machining complications arise which must be accounted for when designing the machining process for a FRP composite, as these have been observed to affect the fiber failure mechanisms occurring in the machining process. Due to the two-phase nature of most FRP composites, several new failure mechanisms and damage modes exist, which do not exist in the machining of homogenous metals. These include matrix cracking, transverse cracking, delamination, fiber pull-out, and fiber-matrix interfacial failure. A tool material with high stiffness and hardness and low coefficient of friction is often implemented to combat the rapid tool wear as high speed steel and cemented carbide have been observed to be unsuitable tool materials for the machining of FRPs [11].

2.6 Chip Formation, Delamination and Effect of Fiber Orientation on Chip Formation

Chip formation mechanism in orthogonal cutting of unidirectional carbon fiber reinforced polymer (CFRP) was studied first time by [13]. The purpose of the work was to investigate chip size and surface of machined work piece. Cutting experiments were conducted in both perpendicular and parallel to fibers direction. When cutting perpendiculars to fibers, downward pressure causes fiber fracture and cracks (0.3 mm into the composite) are produced below tool face. In machining parallel to fibers, tool applies pressure on composite to produce chip, start of next chip is indicated by crack appearing from tool tip. Crack depth in parallel cutting is small compared to the perpendicular cutting as shown in Figure 2-9.

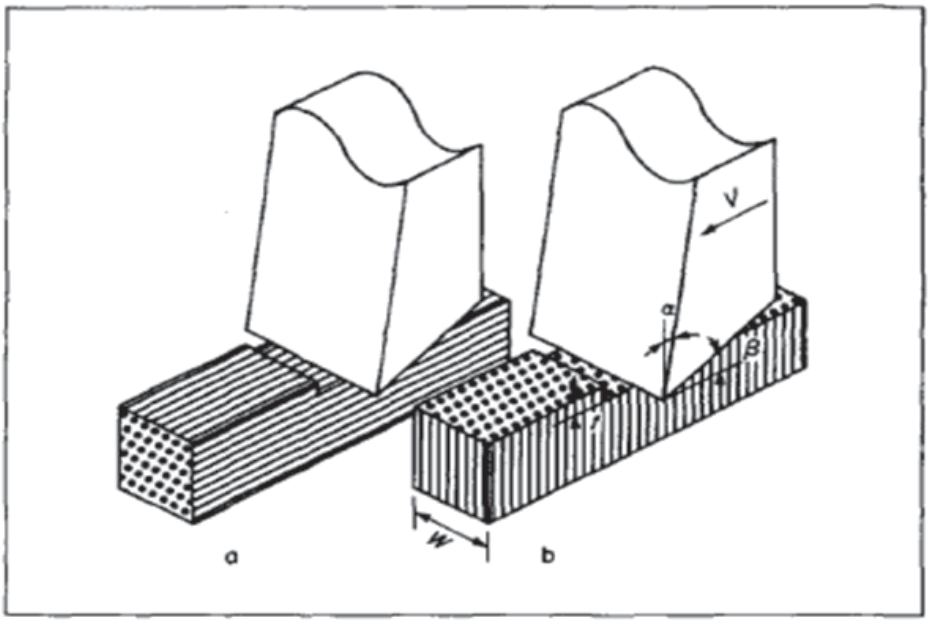

Figure 2-9: (a) Parallel Direction cut (b) Perpendicular direction cut [13]

Ramulu *et al* [14] carried out an experimental study of orthogonal cutting mechanism in edge trimming of unidirectional graphite/epoxy composite with polycrystalline diamond tools. They examined the effect of tool geometry and operating conditions from an analysis of chip formation, cutting force and machined surface

topography. Delamination is a mode of failure for composite materials. In laminated materials, repeated cyclic stresses, impact, and so on can cause layers to separate, forming a mica-like structure of separate layers, with significant loss of mechanical toughness. High transverse forces due to cutting action and low inter laminar strength of composite structures are main causes of delamination. In edge trimming of FRPs, axial force acting perpendicular to stacking plane causes interfacial separation. For up-milling cutting configuration, the axial force acts upward and material damages are observed more on the top ply. In down-milling the bottom ply does not have any support, therefore, damage is more due to downward push [15].

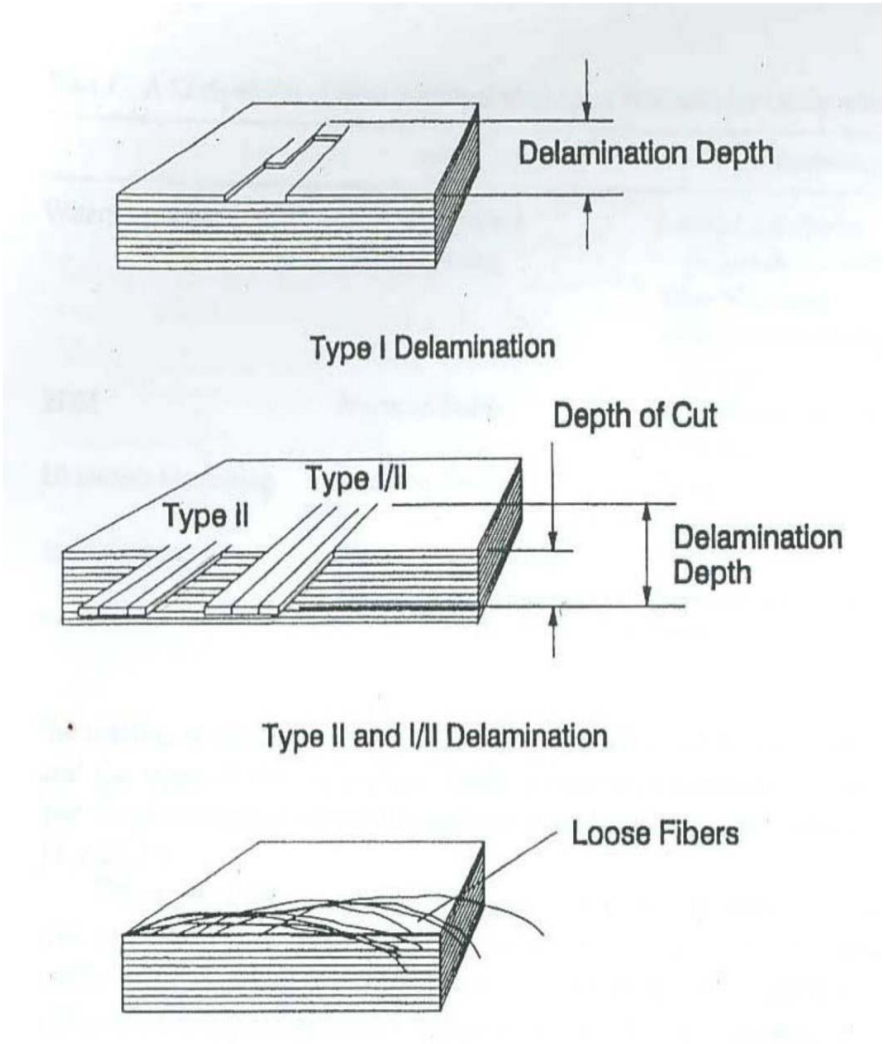

Figure 2-10: Delamination Types [15]

Table 2-3: Types of Delamination [15]

TYPE I DELAMINATION	Damage in the surface area where fibers have been broken and removed some distance inward from the machined edge
TYPE II DELAMINATION	Indicates fiber's upward protrusion from machined edge. These are fibers that bent ahead of the cutting edge and flexed back to their normal position after the cutting edge passed by.
TYPE III DELAMINATION	Describes partially attached fibers, Or cracks parallel to the machined surface. Both Type I/II and Type III delamination create a fuzzy appearance of the machined edge.

H.Y. Puw and H. Hocheng [16] Investigated the cutting of Uni-directional CFRP composites using a single square carbide insert. The experiments were conducted at cutting speeds ranging from 30 – 190 m/min, table feed speed of 50 to 150 mm/min and a constant depth of 1 mm. Based on the articles, the authors asserted that work piece fiber orientation has a significant effect on the formation of burrs and surface roughness. The cut was clean showing no fiber roots on the machined surface when the tool was fed along the fiber orientation (0 fiber orientation). Many uncut fibers were, unfavorably, observed when machining at 90° and 45 °fiber angle, as the cutting tool is liable to slip over the fibers during cutting.

A. I. Azmi [17] Conducted end milling experiments under different experimental parameters and their levels according to the Taguchi design of experimental method. They used 3 factors 3 levels for this optimization technique and had done nine experiments (L9). The process parameters varied had been name as feed rate, spindle speed and depth of cut. The responses were surface roughness, tool life and machining

forces. Taguchi analysis combined with statistical analysis of variance (ANOVA) was performed to quantify the effects of spindle speed, feed rate and depth of cut on those characteristics. Multiple regression analysis (MRA) was also employed to establish parametric relationship between the experimental parameters and the machinability outputs. The most influencing factor in the process was feed rate, then spindle speed is the second one and depth of cut has negligible effect on the process.

V. Schulze [18] examined the effect of cutting velocity and feed rate upon the machining force (F_w), delamination factor (F_d), surface roughness (R_a) and international dimensional precision (IT) using two types of GFRP composite materials, these are Viapal VUP 9731 and ATLAC 382-05. Analysis of variance is executed to evaluate the cutting characteristics of GFRP composite materials using a cemented carbide end mill. The results show that the end mill produces less damage on the Viapal VUP 9731 composite material than the ATLAC 382-05.

Davim [19] investigated the machinability in turning processes of glass fiber reinforced plastics (GFRPs) manufactured by hand lay-up. A statistical technique, using orthogonal arrays and analysis of variance (ANOVA), were employed to know the influence of cutting parameters on specific cutting pressure and surface roughness. The machining parameters considered were cutting velocity and feed rate. The chosen array was the L9 (2^4) with nine rows corresponding to the number of test with two columns with three levels. They developed the plan of tests to correlate the influence of the cutting velocity and the feed rate, with surface roughness and specific cutting pressure using two cutting tool materials (polycrystalline diamond tool and cemented carbide tool). They concluded that the polycrystalline diamond tool (PCD) presented smaller value of surface roughness and specific cutting pressure and the feed rate had the highest physical as well statistical influence on surface roughness and specific cutting pressure. A new machinability index had been proposed by them.

2.7 Fiber Orientation In Milling Uni-directional FRPS

The peculiar aspects of cutting with rotating tool such as in milling, drilling, and abrasive cutting, as opposed to linear orthogonal machining is that the fiber orientation angle, θ, is not constant, but varies continuously with cutting edge position around the cutter axis relative to the fiber direction. In milling the chip thickness also varies with cutting edge position. Fig. 2-10 (a, b) shows the scheme of up-milling and in Fig. 2-10 (c, d) shows the down milling operation, where ø is the engagement angle and Ψ is the laminate orientation angle. Consider for example Fig. 2-10(a) up milling of unidirectional laminate with fiber orientation Ψ< 90°. The cutting edge position is indicated by the engagement angle φ, measured from vertical line. At the current cutting edge position, the fiber is subjected to tensile and bending stresses. The fiber orientation angle, θ, is measured clockwise from cutting velocity vector [12]. Then for the case in

Fig. 2-10 a and for $\varphi \leq \Psi$ it can be shown that

$$\theta = \Psi - \varphi \text{ for } \varphi \leq \Psi. \quad (1)$$

As the tool engagement angle increases and become equal to laminate orientation, $\varphi = \Psi$, the fiber orientation angle become equal to zero. With further increase in the engagement angle so that $\Psi > \varphi$ as shown in Fig. 2-10 (b), the fibers will subject to compression and bending. The fiber orientation angle for this case is given by

$$\theta = \pi + \Psi - \varphi \text{ for } \varphi > \Psi \quad (1.1)$$

Similarly for down milling (Fig. 2-10 c, d) it can be shown that:

$$\theta = \pi + (\Phi - \Psi) \; \Phi \leq \Psi \quad (1.2)$$

$$\theta = \varphi - \Psi \; \varphi > \Psi \quad (1.3)$$

Because of this continuous evolution of fiber orientation angle and the associated chip formation modes, the characteristics of the instantaneous cutting forces (frequency and magnitude) will vary from one cutting edge position to another as shown in Fig. 2-10. The change in uncut chip thickness will also affect the magnitudes of the cutting forces.

The quality of the machined surface would depend on the fiber orientation at cutting edge entry for up milling and at cutting edges exits for down milling. Since φ=0 for both of these positions, the quality of the machined surface is function of angle Ψ for up milling and the angle (π-Ψ) for down milling [5].

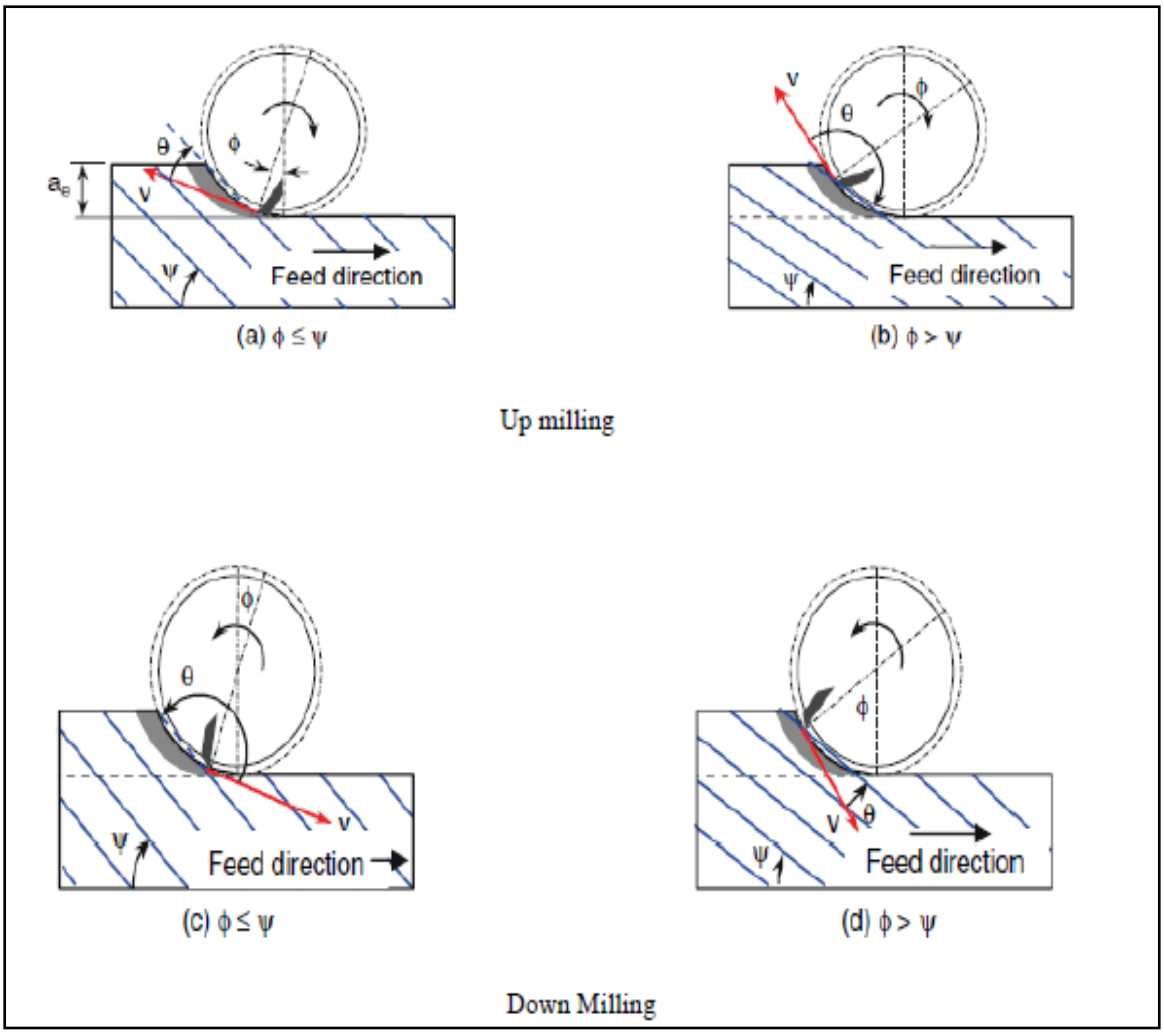

Ø – Engagement angle
Ψ – Laminate orientation
Θ – Relative angle between cutting edge and fiber Orientation

Figure 2-11: Fiber orientation convention in milling of unidirectional laminates: (a, b) up milling and (c, d) [5]

2.8 Tooling Materials for Composites

1. Carbon Steels

Carbon steels have been used since the 1880s for cutting tools. However carbon steels start to soften at a temperature of about 180oC. This limitation means that such tools are rarely used for metal cutting operations. Plain carbon steel tools, containing about 0.9% carbon and about 1% manganese, hardened to about 62 Rc, are widely used for woodworking and they can be used in a router to machine aluminum sheet up to about 3mm thick.

2. High Speed Steel (HSS)

HSS tools are so named because they were developed to cut at higher speeds. Developed around 1900 HSS are the most highly alloyed tool steels. The tungsten (T series) were developed first and typically contain 12 - 18% tungsten, plus about 4% chromium and 1 - 5% vanadium. Most grades contain about 0.5% molybdenum and most grades contain 4 - 12% cobalt. It was soon discovered that molybdenum (smaller proportions) could be substituted for most of the tungsten resulting in a more economical formulation which had better abrasion resistance than the T series and undergoes less distortion during heat treatment. Consequently about 95% of all HSS tools are made from M series grades. These contain 5 - 10% molybdenum, 1.5 - 10% tungsten, 1 - 4% vanadium, 4% Chromium and many grades contain 5 - 10% cobalt. HSS tools are tough and suitable for interrupted cutting and are used to manufacture tools of complex shape such as drills, reamers, taps, dies and gear cutters. Tools may also be coated to improve wear resistance. HSS accounts for the largest tonnage of tool materials currently used. Typical cutting speeds: 10 - 60 m/min.

3. Cast Cobalt Alloys

Introduced in early 1900s these alloys have compositions of about 40 - 55% cobalt, 30% chromium and 10 - 20% tungsten and are not heat treatable. Maximum hardness values of 55 - 64 Rc. They have good wear resistance but are not as tough as HSS but can be used at somewhat higher speeds than HSS. Now only in limited use.

4. Carbides

Also known as cemented carbides or sintered carbides were introduced in the 1930s and have high hardness over a wide range of temperatures, high thermal conductivity, high Young's modulus making them effective tool and die materials for a range of applications. The two groups used for machining are tungsten carbide and titanium carbide, both types may be coated or uncoated. Tungsten carbide particles (1 to 5 micro-m) are bonded together in a cobalt matrix using powder metallurgy. The powder is pressed and sintered to the required insert shape. Titanium and niobium carbides may also be included to impart special properties. A wide range of grades are available for different applications. Sintered carbide tips are the dominant type of material used in metal cutting. The proportion of cobalt (the usual matrix material) present has a significant effect on the properties of carbide tools. 3 - 6% matrix of cobalt gives greater hardness while 6 - 15% matrix of cobalt gives a greater toughness while decreasing the hardness, wear resistance and strength. Tungsten carbide tools are commonly used for machining steels, cast irons and abrasive non-ferrous materials. Titanium carbide has a higher wear resistance than tungsten but is not as tough. With a nickel-molybdenum alloy as the matrix, TiC is suitable for machining at higher speeds than those which can be used for tungsten carbide. Typical cutting speeds are: 30 - 150 m/min or 100 - 250 when coated.

5. Coatings

Coatings are frequently applied to carbide tool tips to improve tool life or to enable higher cutting speeds. Coated tips typically have lives 10 times greater than uncoated tips. Common coating materials include titanium nitride, titanium carbide and aluminum oxide, usually 2 - 15 micro-m thick. Often several different layers may be applied, one on top of another, depending upon the intended application of the tip. The techniques used for applying coatings include chemical vapor

deposition (CVD) plasma assisted CVD and physical vapor deposition (PVD). Diamond coatings are also in use and being further developed.

6. Cermet

Developed in the 1960s, these typically contain 70% aluminum oxide and 30% titanium carbide. Some formulation contain molybdenum carbide, niobium carbide and tantalum carbide. Their performance is between those of carbides and ceramics and coatings seem to offer few benefits. Typical cutting speeds: 150 - 350 m/min.

7. Ceramics

a. Alumina

Introduced in the early 1950s, two classes are used for cutting tools: fine grained high purity aluminum oxide (Al2O3) and silicon nitride (Si3N4) are pressed into insert tip shapes and sintered at high temperatures. Additions of titanium carbide and zirconium oxide (ZrO2) may be made to improve properties. But while ZrO2 improves the fracture toughness, it reduces the hardness and thermal conductivity. Silicon carbide (SiC) whiskers may be added to give better toughness and improved thermal shock resistance. The tips have high abrasion resistance and hot hardness and their superior chemical stability compared to HSS and carbides means they are less likely to adhere to the metals during cutting and consequently have a lower tendency to form a built up edge. Their main weakness is low toughness and negative rake angles are often used to avoid chipping due to their low tensile strengths. Stiff machine tools and work set ups should be used when machining with ceramic tips as otherwise vibration is likely to lead to premature failure of the tip. Typical cutting speeds: 150 - 650 m/min.

b. Silicon Nitride

In the 1970s a tool material based on silicon nitride was developed, these may also contain aluminum oxide, yttrium oxide and titanium carbide. SiN has an affinity for iron and is not suitable for machining steels. A specific type is 'Sialon', containing the elements: silicon, aluminum, oxygen and nitrogen. This has higher thermal shock resistance than silicon nitride and is recommended for machining cast irons and nickel based super alloys at intermediate cutting speeds.

c. Cubic Boron Nitride (cBN)

Introduced in the early 1960s, this is the second hardest material available after diamond. cBN tools may be used either in the form of small solid tips or as a 0.5 to 1 mm thick layer of polycrystalline boron nitride sintered onto a carbide substrate under pressure. In the latter case the carbide provides shock resistance and the cBN layer provides very high wear resistance and cutting edge strength. Cubic boron nitride is the standard choice for machining alloy and tool steels with a hardness of 50 Rc or higher. Typical cutting speeds: 30 - 310 m/min.

d. Diamond

The hardest known substance is diamond. Although single crystal diamond has been used as a tool, they are brittle and need to be mounted at the correct crystal orientation to obtain optimal tool life. Single crystal diamond tools have been mainly replaced by polycrystalline diamond (PCD). This consists of very small synthetic crystals fused by a high temperature high pressure process to a thickness of between 0.5 and 1mm and bonded to a carbide substrate. The result is similar to cBN tools. The random orientation of the diamond crystals prevents the propagation of cracks, improving toughness. Because of its reactivity, PCD is not suitable for machining plain carbon steels or nickel, titanium and cobalt based alloys. PCD is most suited to light uninterrupted finishing cuts at almost any speed and is mainly used for very high speed machining of aluminum - silicon alloys, composites and other non - metallic materials. Typical cutting speeds: 200 - 2000 m/min.

e. Other Materials

To improve the toughness of tools, developments are being carried out with whisker reinforcement, such as silicon nitride reinforced with silicon carbide whiskers.

2.9 End Mill Cutters

An end mill is a tool used on a milling machine, a machine found in a metal working shop that is used to remove material from a metal block to make it into a finished part. It is one of the tools used on the milling machine to make a particular type of cut. End mills come in single ended and double ended varieties. A single ended one has only one useful working end; the other end is just

a smooth shank for holding the tool in the tooling holder on the milling machine. A double ended one has two useful working ends. When one end becomes dull and no longer useful, it can be installed such that the opposite end can be used. These tools are made of carbide steels, with the cutting surfaces sometimes made entirely of carbides. Typical end mill cutters are shown in Fig. 2-12, its nomenclature in Fig. 2-13 and type of operations in Fig. 2-13. It is also common for end mills to be coated with a very thin layer of titanium nitrate. Titanium nitrate is a gold colored coating that prevents the metal chips being removed from the part from sticking to the tool, reducing its life and the quality of the cut. End mills come in a wide variety of shapes and sizes.

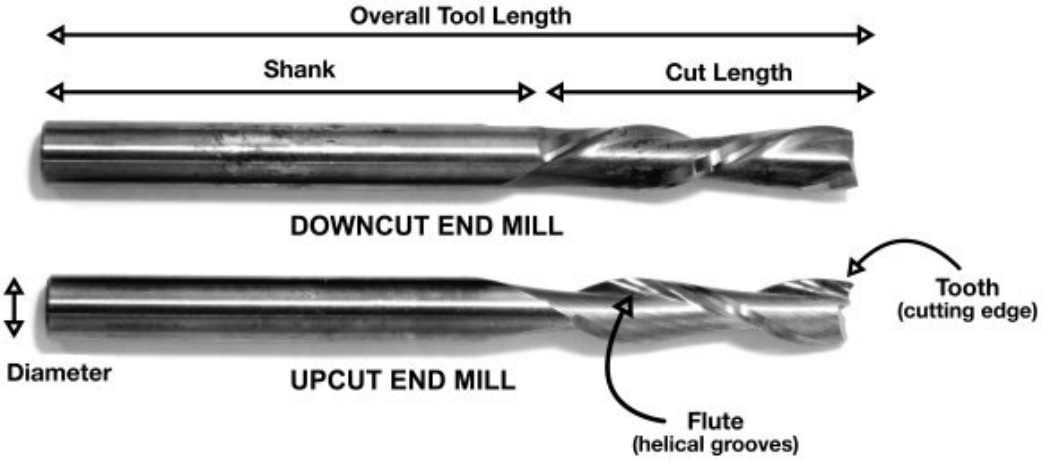

Figure 2-12: Standard End Mill [20]

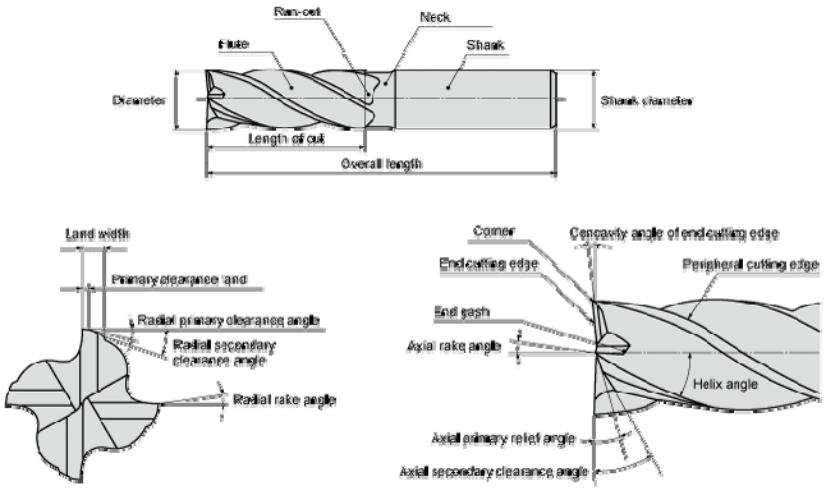

Figure 2-13: End Mill Nomenclature ASME[21]

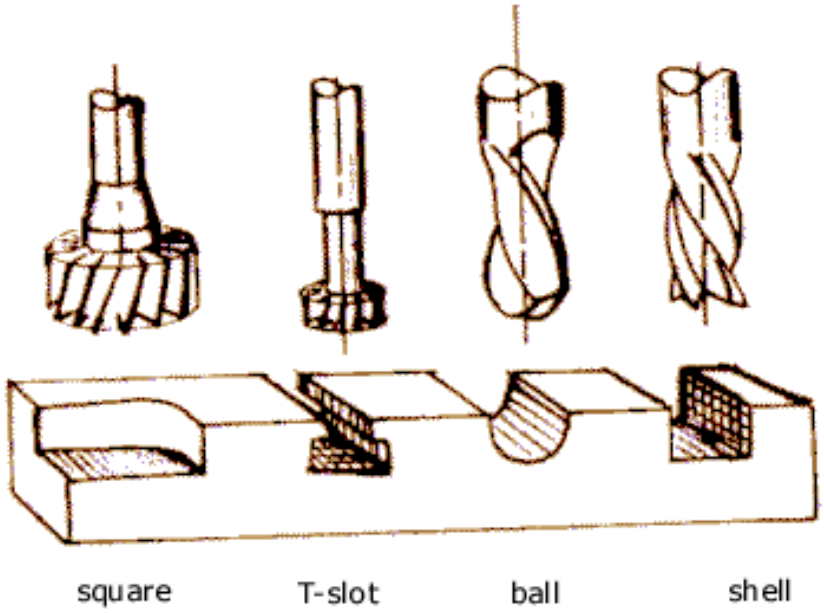

Figure 2-14: Types of End Mills [20]

2.10 Surface Roughness Measurement

In a machining process, a specific surface geometry is produced as a result of the prescribed machine tool kinematics. This surface geometry is called an ideal or theoretical surface geometry, which follows a repeated pattern. In real life, however the actual machined surface deviates from ideal surfaces because of the occurrence of tool wear, machine vibrations, material in-homogeneity, and other factor not related to machine tool kinematics. The actual machined surface may not have a regular geometry. This effect result is natural surface finish. Fig. 2-15 shows the different definitions used to describe machine surface geometric characteristics. The surface profile is typically described by its lay, waviness, and roughness. Lay is the macroscopic contour of the surface and described the direction of predominant surface pattern. The term lay is mostly used to describe flat surfaces and shape is used for contoured surfaces. Errors in lay and shape result from misalignment of machine component and from distortion resulting from clamping forces. Waviness is the repeated deviations from an ideal surface that are relatively of larger magnitude (>0.1mm). These deviations result from deflections in machine tool and cutting tool, form error in tool geometry and from machine vibrations. *Roughness is finely spaced irregularities or irregular deviations characterized by short wave length* as shown in figure

below. Roughness is affected by tool shape and feed (ideal surface finish) as well as by machining conditions (natural surface finish).[5]

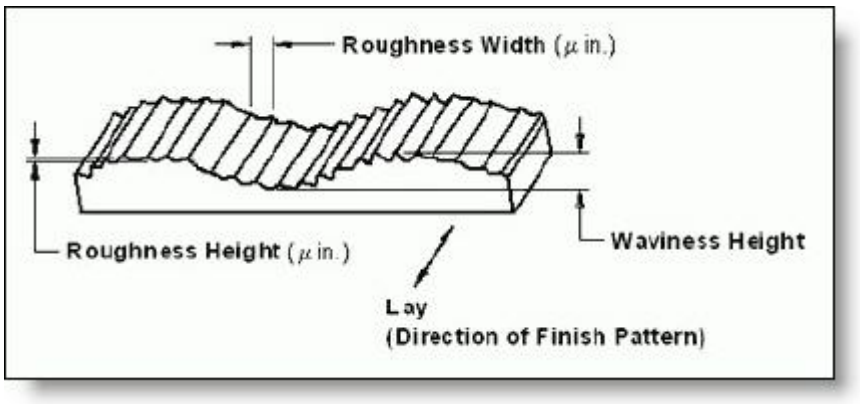

Figure 2-15: Schematic representation of a machined surface [22]

2.11 Aerosols

Aerosol is a dispersion of solid and liquid particles suspended in gas (air). "Aerosol" is defined as the dispersion of both particles and gas, but in common practice it is used to refer to the particles only. Primary aerosol are atmospheric particles that are emitted or injected directly into the atmosphere. Secondary aerosols are atmospheric particles that are created by in situ aggregation or nucleation from gas phase molecules (gas to particle conversion). Either type may be natural or anthropogenic or both. An aerosol can be defined as a system of solid or liquid particles suspended in air or other gaseous environment. Aerosols vary in size and composition, they can be naturally or manmade generated, and thus there are a wide range of them, from flame synthesized nanoparticles and nanomaterials (good aerosols), with fundamentally new properties and functions because of their small size (<100 nm) to airborne particulate matter resulted from the industrial production of nanomaterials, and viruses that have a negative effect in visibility and human health (bad aerosols). Aerosols can be naturally or manmade generated. The latter can also be produced inadvertently as a portion of combustion emissions, but they are also produced intentionally for commercial uses. Manufactured aerosols (nanoparticles and nanomaterials) are playing an increasing role in water, soil, and air treatments; efficient energy production and storage; and medicines.

2.11.1 Concepts Related To Aerosols

All properties of aerosols depend on particle size, thus it is the most important parameter to study the behavior of aerosols. Moreover the nature of laws governing the aerosol properties may change with particle size, so it is necessary to take a microscopic approach and characterize properties on an individual particles basis. Then averaged properties can be integrated over the size distribution. Nomenclature used in aerosols is shown in table 2-4.

Table 2-4: Aerosol Concepts

Concept	Definition	Units
Particle size, d	It is the diameter of a spherical particle, and is the major parameter to characterize the behavior of aerosols. All properties of aerosols depend on particle size, and many of the laws governing these properties change with particles size.	[μm], [nm]
Count average diameter, d (Mean diameter)	Is the sum of all the particles with a certain size d_i divided by the total number of particles. $d = \sum n_i d_i / \sum n_i = \sum n_i d_i / N$	[μm], [nm]
Diameter of average surface, d_s	$d_s = [\sum n_i d_i^2 / N]^{1/2}$	[μm], [nm]
Diameter of average volume, d_v	$d_v = [\sum n_i d_i^3 / N]^{1/3}$	[μm], [nm]

Number concentration, N	Total number of aerosol particles per unit volume of air.	[# particles / m^3 of air]
Surface area concentration, S	Total surface area of aerosol particles per unit volume of air.	[μm^2 of particles / m^3 of air]
Volume concentration, V	Total volume of aerosol particles per unit volume of air.	[μm^3 of particles / m^3 of air]
Mass concentration, M	Total mass of aerosol particles per unit volume of air.	[g of particles / m^3 of fluid]
Count Average, C	Total counts of aerosol particles per unit volume of air	[No of particles / m^3 of fluid]
Count Median Diameter	Defined as the particle size for which half the total number of particles are larger and half are smaller	[μm], [nm]
Mass Median Diameter	Defined as the diameter for which half the mass is contributed by particles larger than the MMD and half by particles smaller than the MMD. It is the diameter that divides the graphical representation of the distribution of mass into two segments of equal area. Important parameter to characterize aerosols.	[μm], [nm]
Mass Median Aerodynamic Diameter	Defined as the mass median of the distribution of mass with respect to aerodynamic diameter. Most important parameter to characterize aerosols.	[μm], [nm]
Count Median Aerodynamic Diameter	Defined as the count median of the distribution of count with respect to aerodynamic diameter	[μm], [nm]

Volume Equivalent Diameter	Defined as the diameter of a spherical particle of the same volume as the particle under consideration	[μm], [nm]
Mass Equivalent Diameter	Defined as the diameter of a non-porous sphere composed of a bulk particle material that has the same mass particle in question	[μm], [nm]
Projected Area Equivalent Diameter	Defined as diameter of a circle having the same area as that of a particle's sectional area projected on a plane.	[μm], [nm]

2.11.2 Size Ranges

Some of the characteristic size ranges of typical aerosols are shown in the figure 2-16.

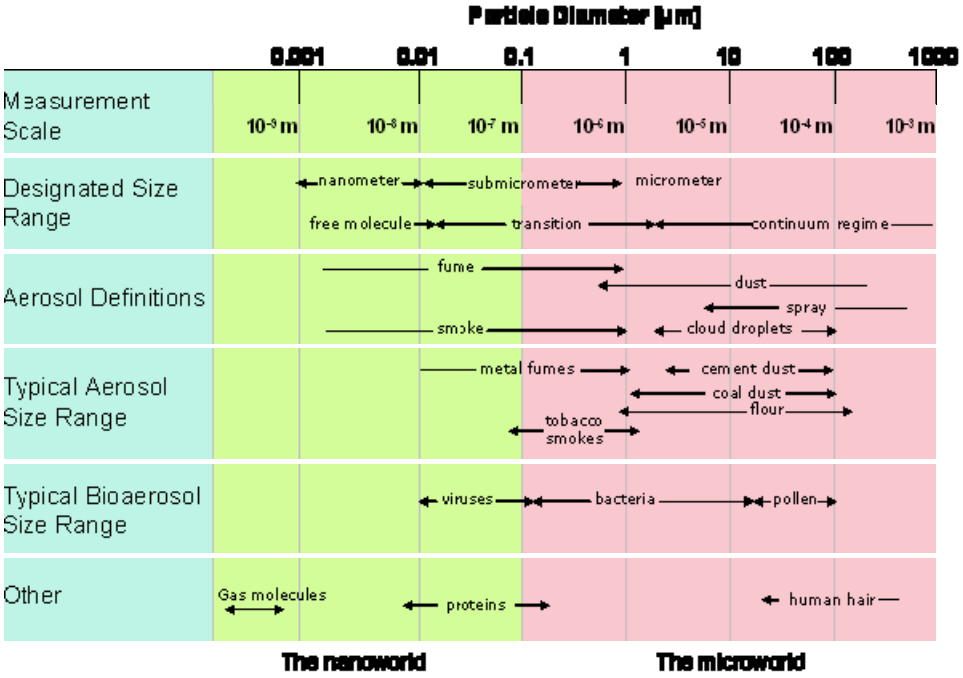

Figure 2-16: Different size ranges for aerosol particles [23]

2.11.3 Aerosol Physics

- **Reynolds Number**

Since an aerosol is a particle in air, it is important to understand how air moves before we can characterize the movement of an aerosol. In the fluid field, we call the calm flow the laminar flow, whereas the rapid one as turbulent flow. Now that the concept of these two types of flow is established, we then need to quantitatively define each flow regime. Reynolds number is one index we can use. The aerosols' Reynolds number (Re_p) is a dimensionless parameter to characterize fluid flow around an object. It is the ratio of inertial forces to viscous forces acting on the aerosol, as

$$\mathrm{Re}_p = \frac{(Inertial\ forces)}{(Viscous\ forces)} = \frac{\rho_g V d_p}{\eta} \tag{1.4}$$

Where ρ_g is gas density, V is gas velocity, d_p is aerosol diameter, and η is gas viscosity

When $Re_p > 1000$, the flow is turbulent. For laminar flow, $Re_p < 1$. If Re_p is between 1 and 1000, it's in the transition regime. It should be pointed out that the Reynolds number can be for a flow around a particle or through a pipe, and the criteria are different. For a flow in a pipe, the commonly accepted value of Reynolds number for turbulent flow is greater than 4000; for laminar flow, it is less than 2000.

- **Newton's Law**

When a ball is dropped, it falls due to the gravitational force. Meanwhile, the resistance of gas molecules (drag) tend to slow down the movement. To describe the drag force resulting from gas resistance, F_d, the following equation can be used: where C_D is the drag coefficient. This is the general form of Newton's resistance equation.

$$F_D = C_D \frac{\pi}{8} \rho_g d_p^2 V^2 \tag{1.5}$$

Where ρ_g is gas density, V is gas velocity, d_p is aerosol diameter

This Newton's resistance equation is valid in the turbulent flow regime (i.e. Rep > 1000), where inertial forces are much larger than viscous forces. The drag coefficient C_D has a nearly constant value of 0.44 [23].

- ***Stokes's Law***

When small particle size and low velocity are involved, the Reynolds number is small and the flow is laminar. Under this condition, inertial forces are negligible compared to viscous forces. Newton's Law is no longer valid and ***Stokes's Law*** shall be used, which has the following form:

$$F_D = 3\pi\eta V d_p \tag{1.7}$$

Where, V is gas velocity, d_p is aerosol diameter, and η is gas viscosity.

In order to determine the drag coefficient in the Stokes's regime, we can compare the above equation to the Newton's resistance equation:

$$F_D = C_D \frac{\pi}{8} \rho_g d_p^2 V^2 \tag{1.8}$$

$$C_D = \frac{24\eta}{\rho_g d_p V} = \frac{24}{\mathrm{Re}_p} \tag{1.9}$$

Then, we can get the drag coefficient in the laminar flow regime. It is inversely proportional to the drag coefficient Re_p as: There are several assumption associated with the Stokes's Law:

- The fluid is incompressible.
- There is no other particle nearby that would affect the flow pattern.
- The motion of the particle is constant.
- The particle is spherical and rigid.
- The air velocity right at the particle surface is zero

- ***Settling Velocity***

Once we can determine the force acting on an aerosol, we can then investigate how an aerosol moves. When a particle is released, it settles due to gravity, and the velocity increases. As the velocity increases, the drag also increases which counterbalances the gravitational force. Eventually, when these two forces are equal to each other, i.e. the net force is zero, there is no more acceleration and the velocity reaches a constant value. This is called ***terminal settling velocity***, i.e.

$$F_G\left(=mg=\frac{\rho_p \pi d_p^3 g}{6}\right)=F_D\left(=3\pi\eta V d_p\right)$$

(following Stokes's Law)

By solving the equation above, the terminal settling velocity can be obtained as:

$$V=V_{TS}=\frac{\rho_p d_p^2 g}{18\eta} \tag{1.10}$$

This equation is valid for $Re_p < 1.0$. For most aerosols we'll encounter, this is the case. If Re_p is rather large, Newton's resistance equation should be used for F_D in the equation above.

- ***Slip Correction Factor***

For very small particles (with a diameter less than 1 μm), scientists found that the settling velocity is faster than that predicted by the Stokes's law [23]. A critical assumption of Stokes's law is that the relative velocity of the gas right at the particle surface is 0. This is true when the medium is "continuous". As the particle gets smaller, the medium is no longer "continuous" to the particle and each molecule is no longer invisible to the particle. Gas molecules moving around the particle may miss the particle, which we call "slip". So, the velocity of the gas right at the surface is no longer 0 due to the missing collision. Since the collision is the source of drag. The particle's settling velocity becomes faster than previously theorized due to smaller-than-expected resistance. To quantify the 'slip' effect on the particles, first we need to define the mean free path of gas molecules. The definition of 'mean free path' of gas molecules is the average distance a gas molecule travels between collisions with other gas molecules. For air, the mean free path, λ, is 0.066 μm at room temperature. If a particle is much smaller than the mean free path, missed collisions are much more likely. Because the effect of 'slip', the drag force decreases and the settling velocity increases. Therefore, we have to modify our formula for them.

For the drag force,

$$F_D = \frac{3\pi\eta V d_p}{C_c}$$

For the settling velocity,

$$V_{TS} = \frac{\rho_p d_p^2 g C_c}{18\eta}$$

Where C_c is the Cunningham slip correction factor, and

$$C_c = 1 + \frac{\lambda}{d_p}\left[2.34 + 1.05\exp\left(-0.39\frac{d_p}{\lambda}\right)\right] \quad (1.11)$$

where λ is the mean free path of the gas and dp is diameter of the particle. For air, λ is 0.066 μm at standard temperature and pressure. The above equations are applicable to Rep < 1.0. The slip correction factor for a 1.0 μm particle at standard condition is 1.15, i.e., the settling velocity is 15% higher than without the slip.

- ***Relaxation Time***

Relaxation time characterizes the time required for a particle to adjust or "relax" its velocity to a new condition of forces. It's an indication of the particle's ability to quickly adjust to a new environment or condition. It depends on the mass and mechanical mobility of the particle, and is not affected by the external forces acting on the particle. The relaxation time, τ, can be obtained using the following equation:

$$\tau = mB = \rho_p \frac{\pi}{6} d_p^3 \left(\frac{C_c}{3\pi\eta d_p} \right) = \frac{\rho_p d_p^2 C_c}{18\eta}$$

Where m is the mass of the particle, and B is mobility coefficient.

Because relaxation time is proportional to the square of particle diameter, it increases rapidly with the increase of particle size. Usually, small particles "relax" to new environments (i.e. following the flow well) in a very short time, while larger particles are more "stubborn" and tend to stick to their original path. With the use of τ, we can easily calculate a particle's terminal settling velocity as:

$$V_{TS} = \tau g \qquad (1.12)$$

- ***Acceleration of a particle***

When the particle is released, there are two forces acting on it: the gravitational force pulling it down and the drag force to slow it. Therefore, the net force of these two results in the acceleration of the particle. According to the Newton's law,

$$F_G - F_D = mg - 3\pi\eta V(t)d_p = ma = m\frac{dV(t)}{dt}$$

If we multiple particle mobility (B) to each term of the above equation and knowing that the particle's relaxation time (τ) equals to mB, we can get:

$$\tau g - V(t) = \tau\frac{dV(t)}{dt}$$

Thus, knowing that τg equals to the settling velocity (VTS), the velocity of a particle at any time after it is released in still air in a gravitational field can be calculated by the following equation via integration of the above one:

$$V(t) = V_{TS}\left[1 - \exp\left(-\frac{t}{\tau}\right)\right] \qquad (1.13)$$

Where V (t) is the particle's velocity after it is released for a period of time, t. A particle will reach 63% of its terminal settling velocity after an elapsed time of τ, and reach 95% of the terminal settling velocity after 3τ [23].

2.11.4 Particulate Matter and Their Size Nomenclature:

Airborne particulate matter represents a complex mixture of organic and inorganic substances. Mass and composition in urban environments tend to be divided into two principal groups: coarse particles and fine particles. The barrier between these two fractions of particles usually lies between 1 µm and 2.5 µm. However, the limit between coarse and fine particles is sometimes fixed by convention at 2.5 µm in aerodynamic

diameter (PM2.5) for measurement purposes. The smaller particles contain the secondarily formed aerosols (gas-to-particle conversion), combustion particles and recondensed organic and metal vapours. The larger particles usually contain earth crust materials and fugitive dust from roads and industries. The fine fraction contains most of the acidity (hydrogen ion) and mutagenic activity of particulate matter, although in fog some coarse acid droplets are also present. Whereas most of the mass is usually in the fine mode (particles between 100 nm and 2.5 μm), the largest number of particles is found in the very small sizes, less than 100 nm [23]. As anticipated from the relationship of particle volume with mass, these so-called ultrafine particles often contribute only a few % to the mass, at the same time contributing to over 90% of the numbers.

Particulate air pollution is a mixture of solid, liquid or solid and liquid particles suspended in the air. These suspended particles vary in size, composition and origin. It is convenient to classify particles by their aerodynamic properties because: (a) these properties govern the transport and removal of particles from the air; (b) they also govern their deposition within the respiratory system and (c) they are associated with the chemical composition and sources of particles. These properties are conveniently summarized by the aerodynamic diameter , that is the size of a unit-density sphere with the same aerodynamic characteristics. Particles are sampled and described on the basis of their aerodynamic diameter, usually called simply the particle size. The aerodynamic properties of particles determine how they are transported in air and how they can be removed from it. These properties also govern how far they get into the air passages of the respiratory system. Additionally, they provide information on the chemical composition and the sources of particles. Particles have irregular shapes and their aerodynamic behaviour is expressed in terms of the diameter of an idealised sphere. The sampling and description of particles is based on this aerodynamic diameter, which is usually simply referred to as ‘particle size’. Particles having the same aerodynamic diameter may have different dimensions and shapes. Some airborne particles are over 10,000 times bigger than others in terms of aerodynamic diameter. Based on size, particulate matter is often divided into two main groups:

- The coarse fraction contains the larger particles with a size ranging from 2.5 to 10 μm (PM10 - PM2.5).
- The fine fraction contains the smaller ones with a size up to 2.5 μm (PM2.5). The particles in the fine fraction which are smaller than 0.1 μm are called ultrafine particles.

Most of the total mass of airborne particulate matter is usually made up of fine particles ranging from 0.1 to 2.5 μm. Ultrafine particles often contribute only a few percent to the total mass, though they are the most numerous, representing over 90% of the number of particles.

2.11.5 Effects of dust/ aerosols on human health

Carbon fiber is a material consisting of extremely thin fibers about 5-10 micron in diameter, which are composed of carbon atoms and are considered especially strong for their size. Several thousand carbon fibers are twisted together to form yarn, which can then be used in the raw form or woven into a fabric. When combined with a resin and wound or molded to form composite materials, a high strength to weight ratio is achieved. The principal health hazards of carbon fiber handling are due to mechanical irritation and abrasion similar to that of glass fibers. Carbon fibers are easily broken by stretching (by less than 2% elongation); the fibers can easily become a fine dust during cutting, machining or mechanical finishing and can then be released into the surrounding atmosphere. These micro fibers if uncontrolled have a potential to stick into human skin or the mucous membranes causing irritation. Most fibers have a coating (called a 'sizing' which is often an epoxy or other resin) that can also cause chemical irritation. Many of the solvents used in advanced composite processes are volatile, flammable and irritating to skin and eyes. Health effects typical of these chemicals include irritation of the eyes and upper respiratory tract, dizziness, drowsiness, nausea, and vomiting. Visual disturbances may also occur. Repeated or prolonged skin contact with these liquids may cause dermatitis.

2.11.6 *Human Respiratory System*

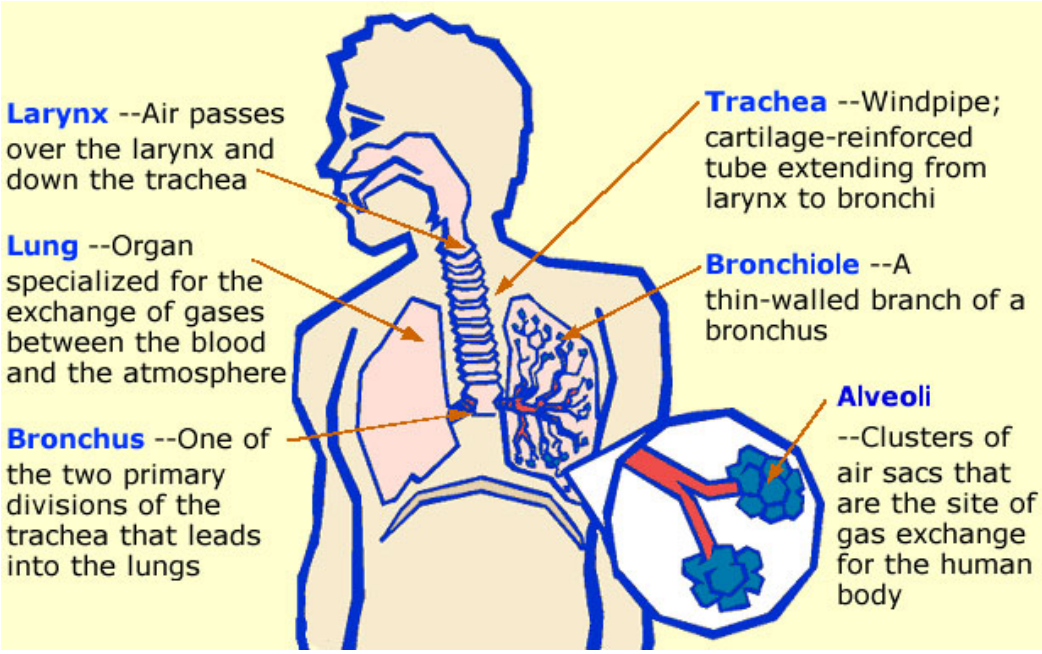

Figure 2-17: Human Respiratory System [2]

Figure 2-17 shows the human respiratory system. Breathing starts at the nose and mouth. The air is inhaled air in the nose or mouth, and it travels down the back of the throat and into the windpipe, or trachea. The trachea then divides into air passages called bronchial tubes. For the lungs to perform their best, these airways need to be open during inhalation and exhalation and free from inflammation or swelling and excess or abnormal amounts of mucus. As the bronchial tubes pass through the lungs, they divide into smaller air passages called bronchioles. The bronchioles end in tiny balloon-like air sacs called alveoli. The body has over 300 million alveoli. The alveoli are surrounded by a mesh of tiny blood vessels called capillaries. Here, oxygen from the inhaled air passes through the alveoli walls and into the blood. After absorbing oxygen, the blood leaves the lungs and is carried to the heart. The heart then pumps it through the body to provide oxygen to the cells of the tissues and organs. As the cells use the oxygen, carbon dioxide is produced and absorbed into the blood. The blood then carries the carbon dioxide back to the lungs, where it is removed from the body when one exhales. The average person who is moderately active during the daytime breathes about 20,000 liters (more than 5,000

gallons) of air every 24 hours. Inevitably, this air (which would weigh more than 20 kilograms [44 pounds]) contains potentially harmful particles and gases. Particles, such as dust and soot, mold, fungi, bacteria, and viruses deposit on airway and alveolar surfaces. Fortunately, the respiratory system has defense mechanisms to clean and protect itself. Only extremely small particles, less than 3 to 5 microns (0.000118 to 0.000196 inches) in diameter, penetrate to the deep lung. One of the respiratory system's defense mechanisms involves tiny, muscular, hair-like projections (cilia) on the cells that line the airways (Refer fig. 2-18). The airways are covered by a liquid layer of mucus that is propelled by the cilia. These tiny muscles beat more than 1,000 times a minute, moving the mucus that lines the trachea upwards about 0.5 to 1 centimeter per minute (0.197 to 0.4 inch per minute). Particles and pathogens that are trapped on this mucus layer are coughed out or moved to the mouth and swallowed. Because of the requirements of gas exchange, alveoli are not protected by mucus and cilia—mucus is too thick and would slow movement of oxygen and carbon dioxide. Instead, the body has another defense system. Mobile cells on the alveolar surface called phagocytes seek out deposited particles, bind to them, ingest them, kill any that are living, and digest them. The phagocytes in alveoli of the lungs are called alveolar macrophages. When the lungs are exposed to serious threats, additional white blood cells in the circulation, especially neutrophils, can be recruited to help ingest and kill pathogens (foreign particles). For example, when the person inhales a great deal of dust or is fighting a respiratory infection, more macrophages are produced and neutrophils are recruited. Cleaning areas and rate of cleaning are sown in the Table 2-5.

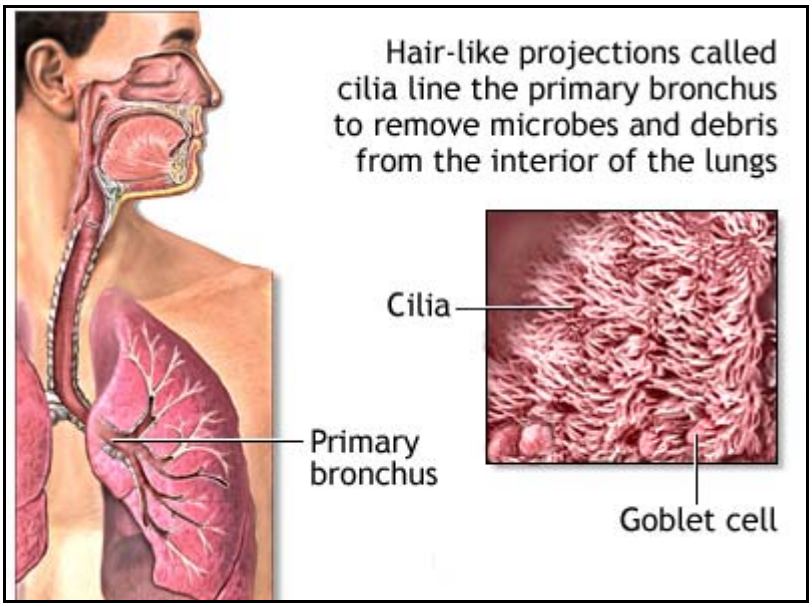

Figure 2-18: Cleaning in lungs [24]

Table 2-5: Cleaning areas and rate of cleaning

Clearance Mechanism	***Site Cleaned***	***Rate of Cleaning***
Cough	Trachea, bronchus	Instantaneous
Ciliary	Large Bronchi bronchiole tree Bronchiole airways	0.5 hr. 3 hrs. 6 hrs.
macrophages	Alveoli (air sacs)	24 hrs.
lymphatics	Lung tissue	Months, years

2.11.7 Review of Machining Dust

Source point capture of dust by vacuum systems integrated with sanding equipment has long been used by the composites industry to minimize dust accumulation in the air and the facility. In the past few years, however, particularly in the aerospace industry, many composites manufacturers have decided to segregate dust management in a separate structure. The result is large dust-mitigation chambers within a facility. Usually, these are big enough to accommodate the plant's largest composite structure. Sometimes called a room within a room, a chamber usually features directed airflow systems that remove dust as it's created and pass it through self-cleaning filters, which then accrete the dust into bins that can be cleaned out daily. Ventilation concerns for composites include safe working environment for their workers, contamination-free process areas, elimination of cross-contamination from one product to another and reduction in energy consumption. In 2007, a law was passed that forced OSHA to emphasize the risk of explosive and composite dust, and this is driving some awareness. Fire marshals are also starting to pay attention more to dust than they have in the past, some more than others. It depends on the authority of jurisdiction. Customer needs, driven by regulatory requirements, employee safety concerns, a general need for cleanliness and, sometimes, requirements from customers promote the need for dust-generating activities be separated from other manufacturing activities.

Response personnel are exposed to hazards posed by the fibrous particulates following a crash and the subsequent fire from spilled fuel. In recent years, a number of incidents have been reported on the irritant and toxic effects of fibrous matter and aerosols on personnel responding to the crash site. Firefighters and emergency crews involved in post-crash cleanup and restoration operations have expressed concerns about long-term effects from exposure to carbon fibers released from burning composites and in the special needs for extinguishing and handling the incinerated fiber composites. Incident reports vary concerning the nature and severity of short- and long-term adverse effects on the responding crews. Rescue and recovery personnel have suffered varying degrees of adverse health effects, ranging from eye and skin irritation to severe

respiratory problems. In certain instances, response teams equipped with enhanced protective clothing reportedly suffered from penetration by strands of needle-sharp carbon fibers [25].

The inhalation hazard from fibers poses the greatest potential for adverse health effects on humans and depends on the total dosage and the physical dimensions of the fibers. Smaller particles are deposited in the lower regions of the lungs and chronic toxicity is associated with this type of exposure. For purposes of hazard assessment, fibers are defined as high aspect ratio particles having a length-to-diameter ratio (L/D) greater than three [26]. The criterion L/D >3 has been established as an essential condition for chronic toxicity in studies of natural and manmade mineral fibers.

The volume of fibers deposited in the pulmonary region depends on the fiber density, size, and shape. Fibers entering the respiratory tract are restricted to those with dimensions capable of penetrating the tracheobronchial path after traversing through the nose and the upper respiratory tract. The ease of respiration of a fiber is characterized in terms of the aerodynamic diameter Da, which refers to the diameter of an equivalent spherical particle having the same terminal velocity as the fiber. Fibers with Da <10 μm are most likely to penetrate into the gas exchange region of the pulmonary system. Fibers with diameters smaller than 3 μm and lengths < 80 μm fall in the respirable range and can penetrate deep into the lungs [27].

In reviewing the toxicology research on carbon fibers, Thomson concluded that animal studies data indicate that there are no long-term health risks associated with exposure to PAN-based carbon fibers under occupational conditions. The health effects are limited to temporary irritations of the skin and upper respiratory tract since exposure is limited to relatively large-diameter fibers (6-8 μm) [28].

Kwan characterized the physical size and aerodynamic properties of particulates generated during laser machining of composites. The particle size analysis did not reveal generation of any fiber-like particles with L/D>3. The respirable fraction consisted of spherical particles with D_a <2 pm. Chemical analysis of the sampled particulate matter

revealed the presence of adsorbed volatile organic compounds with aromatic structure. Most of these chemicals were poly-nuclear aromatic hydrocarbons (PAH). The NIOSH database of toxic chemical substances describes the toxicological effects of these PAH species to range from sensory irritation to carcinogenicity [29].

Table 2.1. Conventional machining operations.

Sample Number	Matrix Material	Operation
R1	Fiberite 934 epoxy	Drilling 2000 RPM
R2	Hexel F263 epoxy	Drilling 2000 RPM
R3	Hexel F263 epoxy	Milling 2000 RPM
R4	Hexel F263 epoxy	Milling 4000 RPM
R5	Dow 332 epoxy	Grinding 4000 RPM

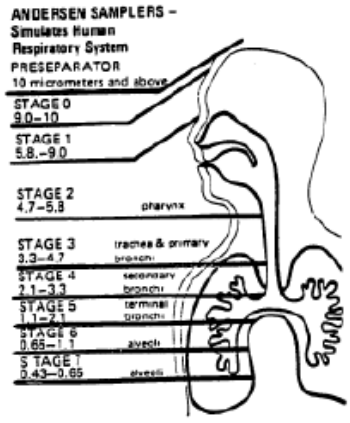

Figure 2-19: Penetration in the respiratory system[29]

A study was conducted by Ramulu and Kramlich that was focused on environmental effects of carbon fiber composites. Fiber orientation seems to play an important role in the dust size characterization. Size distribution depends on different machining parameters, materials and tools. Hence it is possible to develop optimal cutting conditions that would help reduce the machining dust [30].

Haddad studied the effect of machining parameters on dust generation and particle counts. They used a GRIMM 1.209 dust monitor which measures the percentages of dust sizes from .25 μm to above 30 μm to estimate average particle size. The material was T700/M21 with a fiber volume of 59%. Spindle speed was varied between 18570 and 74270 rpm with linear feed rate between 125 to 500 mm/min. Depth of cut was 2 mm and

cutting direction was down milling. Highest particles were between 0.25 to I micro meter. Chip size measurements showed that 87% – 95% of the inhaled dust could reach the pulmonary alveoli. They found an increase in the number of particles with increasing cutting speed. The feed-rate appeared to have less of an effect at a constant cutting speed on the number of particles generated [31], [32].

Jeffrey Miller [33] carried out a variety of tests on machining of composite materials and their different particulate sizes of the machined dust. He performed a variety of tests using Uni-directional and multi-directional laminates. He observed that the aerodynamic diameter of particles obtained by machining the Uni-directional composites was about 0.15 μm. He also questioned the credibility in the measurement of the percentage of particles that are alveolic by Haddad [32] and stated a possible misjudgment of the definition and measurement of alveolic fractions by the author.

3 Chapter III: Methodology

3.1 Materials Used and Tests Performed

The materials used in this tests include Aerospace grade composite materials. Uni-Directional CFRP composites and Random fiber HexMC® composites were used to perform the tests. These composites were in the form of rectangular plates that were ten cut into smaller pieces in order to perform the tests. Table 3-1 shows the materials used while Figure 3-1 shows the specimens cut in order to perform the tests.

Table 3-1: Materials used

#	TEST	Mfg.	Length (in)	Width (in)	Thick (in)	Type	# Plies	Layup
1	Uni Directional CFRP Edge trim	Toray	48	48	0.25	Uni	67	[100%/0%/0%], $[0]_{67}$
2	Semi-Circular Slot Test	Toray	48	48	0.75	Uni	100	[100%/0%/0%], $[0]_{100}$
3	Octagon Slot Test	Toray	48	48	0.25	Uni	67	[100%/0%/0%], $[0]_{67}$
4	HexMC® Edge Trimming	Hexcel	35	35	0.5	Random		Random

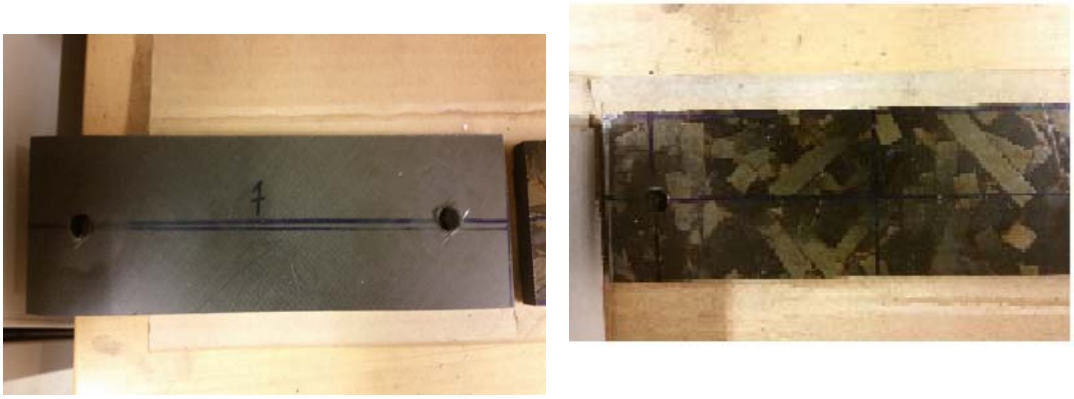

Figure 3-1: Uni directional (UDC) (left) and HexMC (right) Composites

3.2 Experimental Setup

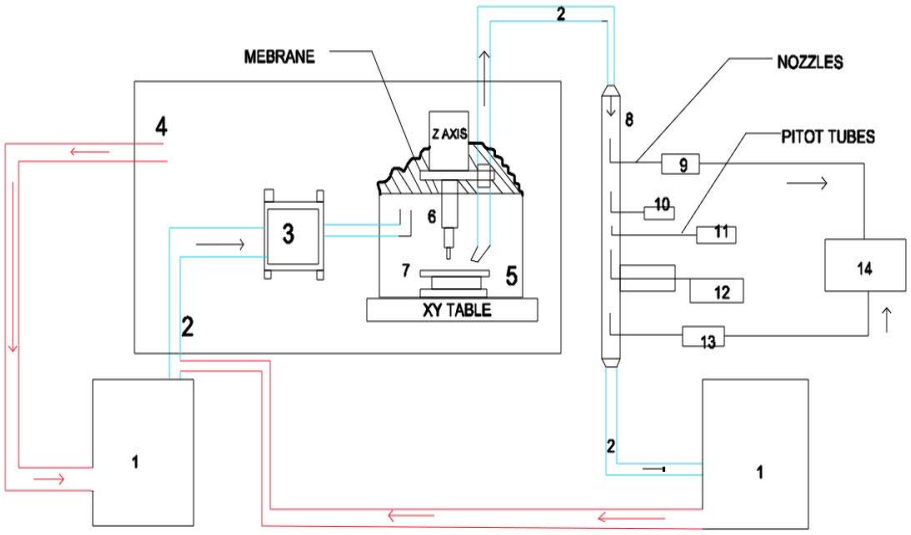

Figure 3-2 (a): Experimental Setup

Table 3-1 (a): List of associated instrumentation corresponding to the experimental setup

Number	Description
1	Shopvacs (2 vacuums , one 6HP other 6.5 HP)
2	Conductive Hose (Polyurethane hoses of 20mm diameter)
3	HEPA Filter (SBM BioMax -Model H10A3X1, 203.2 mm x 203.2 mm x 149.2 mm deep (8 in. x 8 in. x 5.875 in.)
4	Haas TM 1P CNC Mill - 7.5-hp vector drive spindle that spins to 6,000 rpm
5	Plexiglas working chamber- 689 mm x 419 mm x 343 mm (27.125 in. x 16.5 in. x 13.5 in.) , machine travel - 236 mm (9.3 inch) in X, 145 mm (5.7 inch) in Y by approximately 102 mm (4 inch) in Z motion directions
6	Machine Spindle
7	Base fixture and machining fixture - 0.375mm (3/8”), Grade 5 Bolts used
8	Iso- Kinetic sampling Tower
9	114.3 mm (4.5 inch) OD, 3.17 mm (.125 inch) wall thickness pipe made of Aluminum 6061, duct velocity passing through the tube is about 7.9 m/sec, 0.15 inches of water column.
10	Casella Micro-dust Pro
11, 12	Tsi© P-TRAK , Pitot's, Nozzles
12	Grimm Aerosol Spectrometer 1.109
13	Sioutas Cascade Impactor
14	Vacuum pump

Figure 3-2(a) and Table 3-1(a) represents the schematic diagram of the experimental setup and the associated instrumentation developed by Jeffrey Miller [33]. It was modified to be used as a part of this research. Each component of the setup will be explained as per the numbering on the diagram and Table 3-1(a).

1. Craftsman Shop Vacuum (Figure 3-3): Two shopvacs were used as a part of the setup. The one on the left is a 6HP vacuum, basically used to suck in air from the ambient atmosphere and feed it back into the system via a filter. The one on the right is a 6.5HP, primarily used to suck the dust created from machining.

Figure 3-3: Shop Vac

2. Conductive Hose (Figure 3-4): The conductive hose is an essential part of the setup because of the fact that the conductivity is what prevents the dust particles from sticking to the walls of the tube and thereby ensures accurate readings. Polyurethane hoses of 20mm diameter were used throughout the setup.

Figure 3-4: Conductive hose

3. HEPA Filter (Figure 3-5): Filters are a key component of cleanrooms, so it's no surprise they come in a variety of designs. Manufacturers provides HEPA units for isolation rooms, surgery suites, pharmaceutical compounding, and biotech and medical-device applications. For example, electrically enhanced filtration (EEF) units charge particles and bacteria with an ion flux inside an ionizing field where the bacteria are killed upon entry into the grid. The remaining particles are efficiently filtered, according to the company — down to 1% of the penetration of conventional filters with the same pressure drop and flow rate. In this experiment the main aim of this filter is to make sure that the air that enters the concerned system is as pure as it can get to avoid contamination of the measured dust. The HEPA filter used is a SBM BioMax Model H10A3X1, 203.2 mm x 203.2 mm x 149.2 mm deep (8 in. x 8 in. x 5.875 in.)

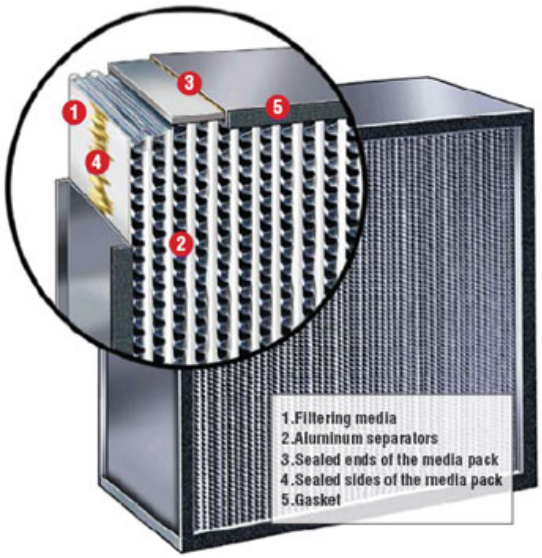

Figure 3-5: HEPA Filter

4. Haas TM 1P CNC Mill (Figure 3-6): It has a reliable 7.5-hp vector drive spindle that spins to 6,000 rpm and uses standard 40-taper tools. Rapids and cutting feed rates are 400 ipm. The machine's 762 x 305 x 406 mm travels provide plenty of room for work holding and larger parts, and a 10-pocket tool changer is standard. The TM-1P operates on either single- or three-phase power, and a one-piece cast-iron base/column damps vibration and provides rigidity – ensuring a high level of precision and repeatability as shown in Table 3-2.

Detail	Data	Units
Maximum speed	6000	rpm
Maximum torque	44.74	Nm
Spindle power	5.6	kW
Maximum thrust force (Z)	8900	N

Maximum feed rate	10.16	m/min
Accuracy	.01	mm

Table 3-2: Specifications of Haas TM 1P

Figure 3-6: Haas TM 1P Mill

5. Plexiglas working chamber (Figure 3-7): This is the enclosure designed for keeping the dust uncontaminated. The box dimensions stretch from about 689 mm x 419 mm x 343 mm (27.125 in. x 16.5 in. x 13.5 in.).The box is supported by an aluminum frame that helps the side panels of the box bolted on. The box allows a machine travel of 236 mm (9.3 inch) in X, 145 mm (5.7 inch) in Y by approximately 102 mm (4 inch) in Z motion directions. Care must be taken so that the tool travel in either directions does not exceed the boundaries of the box. The box has a removable trap door that is held together by four wing-nuts. The door hands easy access for changing the test piece, changing the tool. The membrane above the box remains inflated during the tests thereby providing a visual balance between the inlet air and outgoing dust.

Figure 3-7: Plexiglas Chamber

6. Machine Spindle (Figure 3-8): Acts as the tool holder for the milling cutter.

Figure 3-8: Milling Spindle

7. Base fixture and machining fixture (Figure 3-9): The Plexiglas chamber is held on using a nut on to the base plate as seen in the figure. On top of the base plate is a

multi-holed plate that contains many holes 0.375mm (3/8”) equivalent tapped through holes. Above the holed plate lies the aluminum raise block that helps to raise the height of the work piece in order to avoid interference between the top of the chamber and bottom of the Z axis spindle holder. The actual work piece is then fixtured onto this block using two 0.375mm (3/8”) grade 5 bolts.

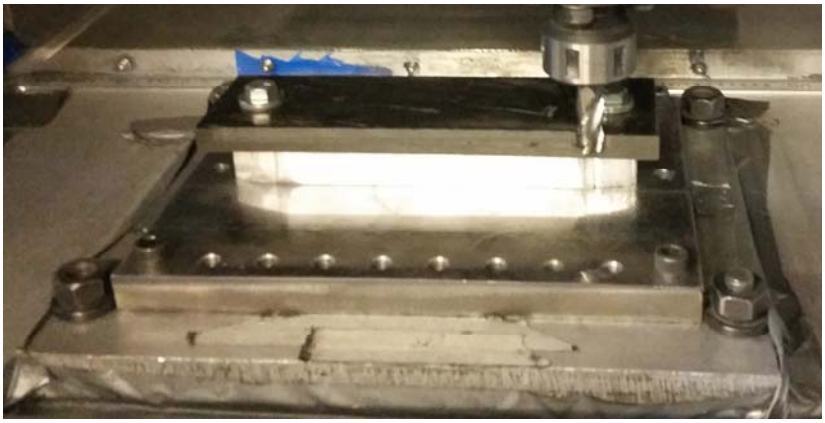

Figure 3-9: Base and Machining fixtures

8. Iso- Kinetic sampling Tower (Figure 3-12): Isokinetic sampling collects particles in a moving stream which moves at the same velocity in the sampling nozzle as elsewhere in the stream. This can increase the accuracy and reliability of results. It is used for activities like monitoring pollution in factory stacks, taking general air samples in an area of interest, and checking equipment for dust and other concerns. The term “isokinetic” comes from root words meaning “same” and “velocity.” In an isokinetic sampling procedure, the testing nozzle is set up to allow the sample stream to enter without changing speed. This reduces the risk of concentrating larger or smaller particles. If the stream moves too slowly into the collector, it increases the number of large particles. Too fast, and large particles are lost (Refer Fig. 3-10). In either case, the sample collected wouldn’t be an accurate reflection of what is in the overall stream.

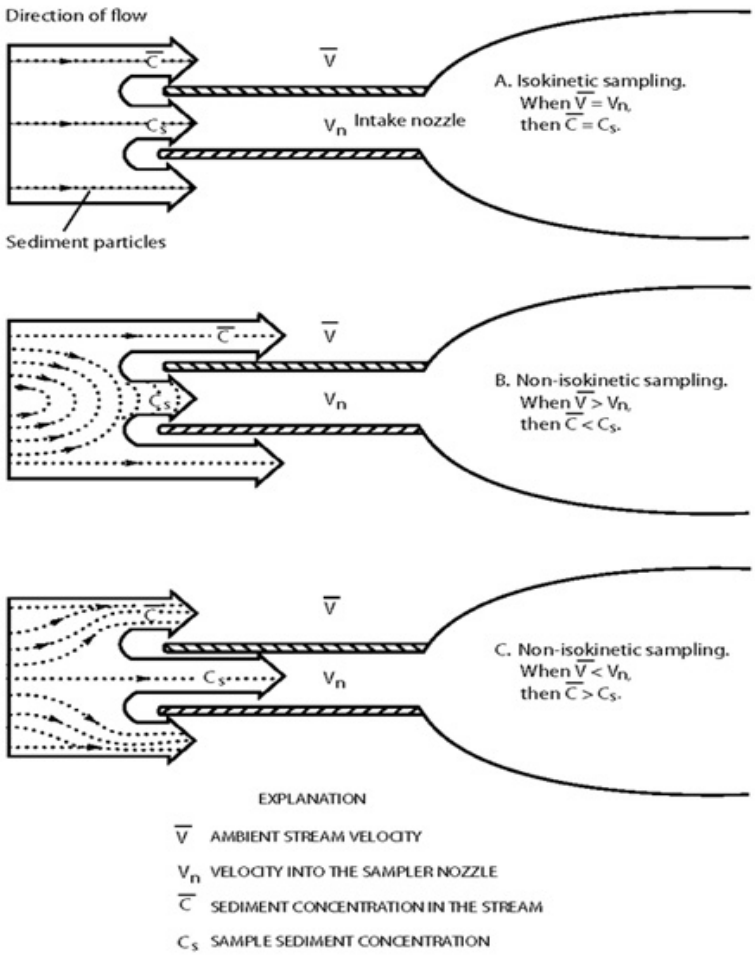

Figure 3-10: Iso Kinetics [34]

The iso- kinetic sampling tower built for the purpose of the tests performed in this series of experiments consists of a 114.3 mm (4.5 inch) OD, 3.17 mm (.125 inch) wall thickness pipe made of Aluminum 6061 (Refer Fig. 3-11(c)). The tube has cap fittings at the top and bottom in order to connect the flexible hoses that help capture the dust. Holes are drilled into the tube in order to insert the pitot tubes (Refer Fig. 3-11(b)) for measuring the pressure and nozzles for instruments that are sampling dust. The duct velocity passing through the tube is about 7.9 m/sec based on the flow through the Shopvacs in the arrangement. This was further confirmed by using the pressure feedback from magnahelics pressure gauge (Refer Fig. 3-11(a)) that takes feedback from the pipe and

reports it on the pressure gauge. The registered reading through the system was 0.15 inches of water column.

(a)

(b)

(c)

Figure 3-11: (a) Magnahelics gauge (b) Pitot tubes (c) Isokinetic tower

Design of the nozzle arrangements were perfected using a model and then testing the layout with the corresponding tests to make sure that there is no boundary layer effect. While designing the entire setup, it was made sure that there is ample space to meet the requirements of setting up multiple instruments that would be needed in order to run these tests. Hence a part of the CNC machine frame was used to make racks where the instruments could be mounted and used safely without interference. This can be seen in Fig. 3-12 (a)

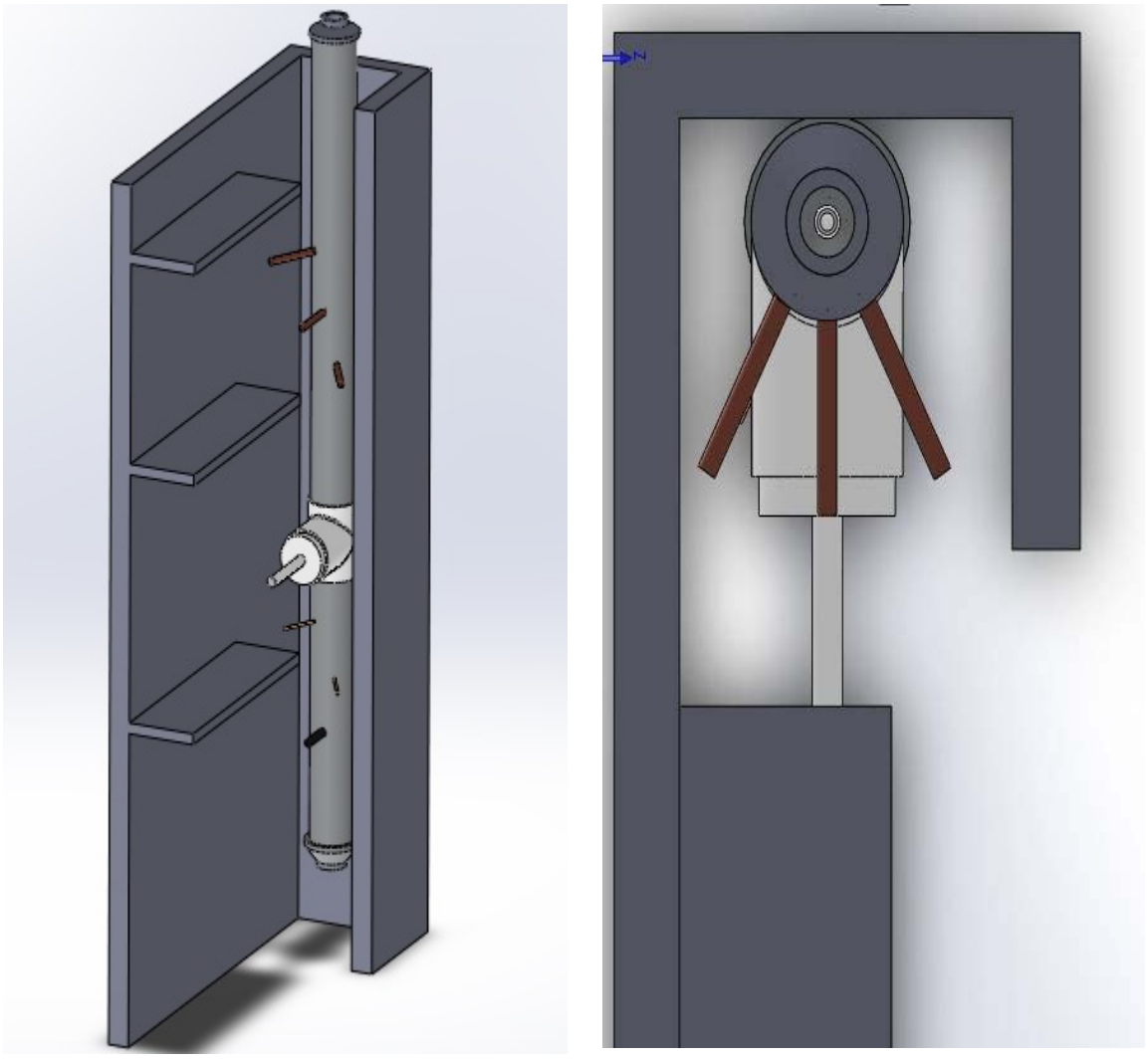

(a) (b)

Figure 3-12: (a) Isokinetic Tower Nozzle arrangements (b) Angular arrangements of Nozzles to prevent boundary layer effect

The arrangement of the different nozzles are angular in order to avoid the effect of boundary layer inertia. This can be seen from the Figure 3-12 (a). In the Figure 3-13 we can see the stream diverges as soon as it touches over the first Pitot tube in the Figure. If the second Pitot tube is very close to the first one, there is not enough time for the particles to get back into the required flow path in order to efficiently enter the second

tube. This affects the readings of the instruments. The same applies to nozzles as well. Hence this elaborate arrangement of placing the nozzles in angular direction across the tube helps to maintain a steady flow to all the nozzles and pitot tubes in the setup.

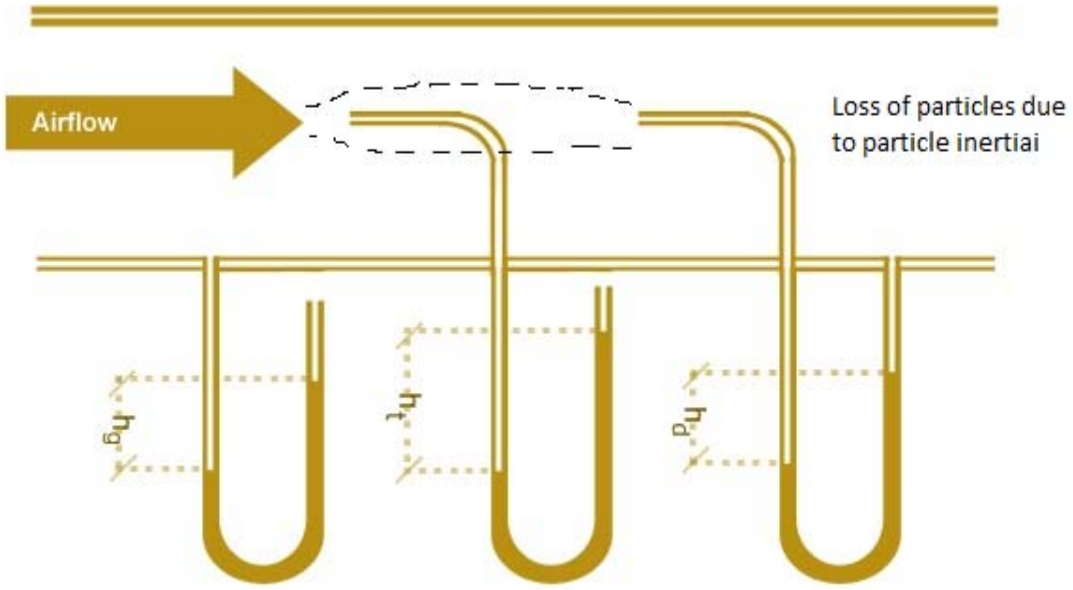

Figure 3-13: Inertia effect in Nozzles and Pitot Tubes [35]

9. Casella Micro-dust Pro

The CEL-712 Micro dust Pro shown in Fig. 3-14 is a rugged, hand-held, data logging instrument for the real time detection of airborne dusts, fumes and aerosols. It has a large color display and a graphical facility, allowing the user to instantly view the dust level and trends. It is ideal for walk-through surveys of ambient and indoor workplace environments. A quick, easy to use instrument, giving the user additional qualitative data which cannot be gained by gravimetric air sampling methods alone. This extremely versatile instrument can also be used with a range of accessories for static and size selective sampling applications. It has an extensive range of concentration measurement from 0.001mg/m3 to 250g/m3.It also comes with its own custom software package that

helps us analyze the results from the instrument. It also can use polyurethane foam (PUF) filters or a cyclone for size segregation.

Figure 3-14: Casella Micro-dust Pro

10. Tsi© P-TRAK: The TSI's P-TRAK® Ultrafine Particle Counter (UPC) 8525 shown in Fig. 3-15 is an ideal instrument measuring workplace ultrafine particulate levels. This portable instrument detects and counts ultrafine particles (smaller than 1 micrometer) that often accompany or signal the presence of a pollutant that is the root cause of complaints. Ultrafine particles are defined as having a diameter less than 0.1 μm (or 100 nm). Engineered nanoparticles (nanomaterials) are a subset of ultrafine particles with dimensions from 1 to 100 nm. Nanomaterials are produced and used for industrial and high-tech applications, while ultrafine particles are the byproducts of combustion and other chemical reactions. Measures particle counts from zero to 5 x 10^5 counts/cm^3. Particle size ranges from 0.02 to 1 micrometer. Sample flow rate is 100 cm^3/min.

Figure 3-15: Tsi© P-TRAK

11. Pitot Tubes and Nozzles: Pitot Tubes shown in Fig. 3-16 (a) were used for measuring pressure across the duct while nozzles shown in Fig. 3-16 (b) helped to serve as the inlet for the dust measurement inputs. Choices for nozzle diameter are listed in the subsequent sections.

(a) (b)

Figure 3-16: (a) Pitot tube (b) Nozzles

12. Grimm Aerosol Spectrometer 1.109: Grimm is a leading engineering technology provider undertaking research and design and production of different aerosol spectrometers for research as well as indoor and outdoor air quality monitoring.

This powerful instrument shown in Fig. 3-17 gives us the ability to continuously measure in real time particles in 31 different size channels and present the data as Particle Size Concentration, Particule Mass Distribution, and Outdoor PM/Monitor. Measures particles sizes from 0.25 to 32 μm in 31 size channels. In general are all data stored on the integrated 80 Kb memory, but with the use of the removable data logger card it is possible to store data up to 6 MB in the unit at all times. Data can be exported to Microsoft Excel. Even the instrument performance as well as (optional) sensor data are stored on the same card. These results can be called off simply by attachment of any PC and the use of the GRIMM Software As mentioned in the specification only with one GRIMM instrument it is possible to obtain many different results. As an example below are the data obtained as a single particle counter. The GRIMM Software shows the count and size distribution in ambient atmosphere. It is also possible to show the mass distribution in many different size channels mass as well. As a typical application the unit is used at a work place study with the EN 481 it is possible to use the same instrument. Three important fractions as mass by volume over time are shown. Even the atmospheric aerosol values used in the environmental data base such as PM10 and PM2.5 and even PM1 can be shown. Three PM fractions as mass by volume over time can be plotted as well. Because the concentrations of the particulate sample were way higher than what the machine could take, a diluter had to be used. A Topas DIL 550 diluter with a 10:1 dilution ratio was used with the GRIMM. In order to get the final concentration or counts, the data had to be multiplied by a factor of 10.

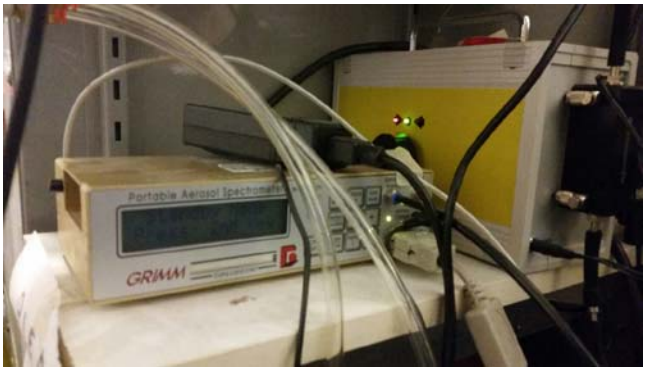

Figure 3-17: Grimm Spectrometer 1.109 and Topas Diluter.

13. Sioutas Cascade Impactor: The Sioutas Cascade Impactor shown in Fig. 3-18 separates and collects airborne particles in five size ranges: > 2.5 µm, 1.0 to 2.5 µm, 0.50 to 1.0 µm, 0.25 to 0.50 µm, and < 0.25 µm. It has a series of filters in the sizes aforementioned. When used with PTFE (Teflon) collection filters, the Sioutas Impactor is highly efficient at collecting particles without the use of impaction grease or substrate coatings and at retaining unstable compounds for size-fractionated chemical analysis. The Sioutas Impactor is simply clipped to a worker's collar or lapel for personal sampling or attached at a sampling site for area sampling. In our experiment it was clipped onto a nearby table.

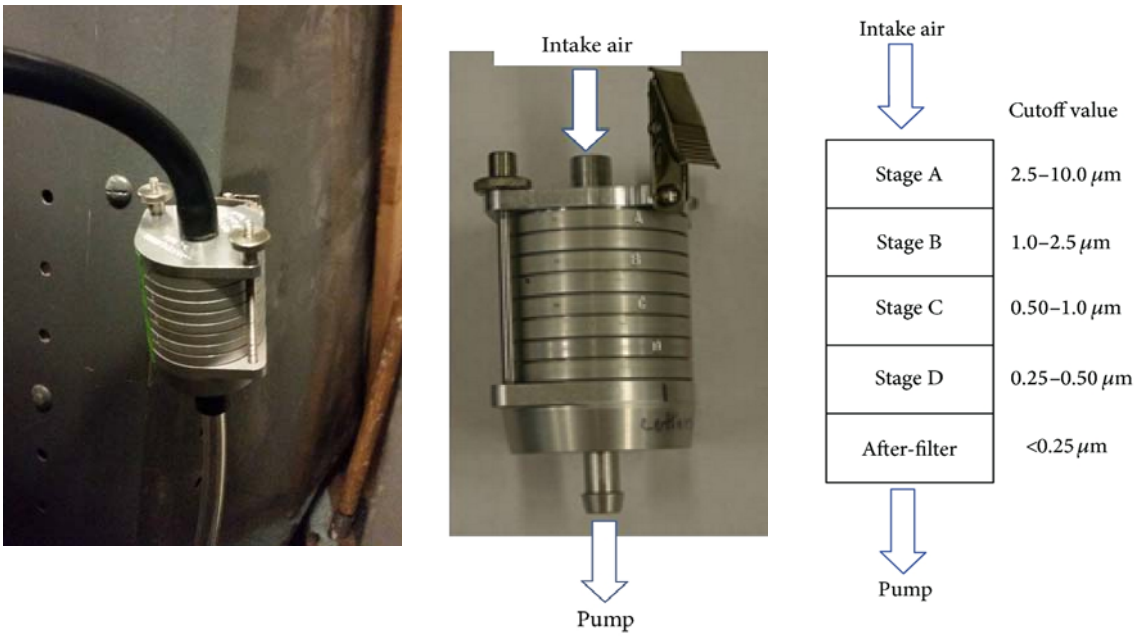

Figure 3-18: Cascade Impactor

14. Vacuum pump: The Grimm aerosol spectrometer and the P-Trak have their own pumps. While the Casella and impactor need an external pump. Hence an external vacuum pump was used for the Casella and the impactor. A manifold setup of valves was used to route and control the flow. Fig. 3-19 shows the vacuum pump and manifold setup.

Figure 3-19: Vacuum pump and Manifold

3.3 Selection of Nozzles Diameter for Different Instruments

In this experiment, there are multiple instruments. Hence it becomes extremely important to designate the required flow rate through each instrument. This can be done by choosing the correct nozzle diameters in the isokinetic tower. As mentioned earlier, the final duct velocity through the tube was 7.9 m/sec corresponding to a pressure of 0.15 in of water column.

Per Dwyer, the equation for calculating air velocity,

$V = 1096.2 \times (\Delta P/D)^{1/2}$

Where ΔP is the differential pressure in inches of water column, D is air density in lbs. /cubic feet.

At 70 F and 29.9" barometric pressure, the density of air, ΔP, is 1.201 kg/m3 (0.075 lb. /ft3).

Using Q = VA, where Q is he flow rate.
Here area, A= $\pi d^2/4$, solving for diameter, d, provides the nozzle diameter.

Based on the requirements of the different instruments and the setup variables including the vacuum setup pressures and velocities, the following diameter nozzles (Table 3-3) were used for the corresponding instruments. All nozzles were built using 306 Stainless Steel. A 15° knife edge design was used for the nozzle tip.

Table 3-3: Nozzle Design Parameters and Sizes

	KNOWN PARAMETERS		DESIGNED PARAMETERS	
Device	Flow (lpm)	Velocity (m/s)	Nozzle dia (mm)	Nozzle dia(in)
GRIMM	1.2	7.9	1.8	0.071
Casella	3.5	7.9	3.075	0.121
PTRAK	0.7	7.9	1.375	0.054
Sioutas Impactor	10	7.9	5.195	0.205

3.4 Tool Used

In all the experiments performed with the setup, only one type of tool was used. The tool geometry used was a 4 flute, 0.5" (12.7 mm) diameter carbide end mill cutter with a 30° helix angle shown in Fig. 3-20. A total of 6 tools were used in this investigation.

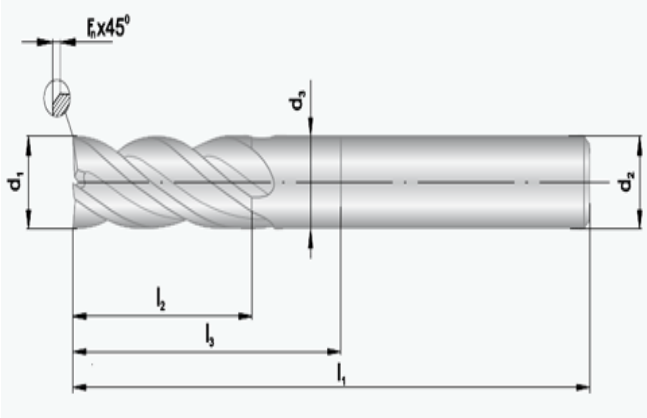

- Geometry - 4-flute helix
- Helix angle - λ - ~30°
- Chamfer of edge - Fn x45°-0.13”
- Flute diameter – 0.48”
- Shank diameter – 0.5”
- Depth Of Cut - l2 – 2.2”
- Overall Length - l1 – 4”
- Material - Micro grain solid carbide
- Coating - None
- Origin – Niagara Cutters

Figure 3-20: Flat nose end mill [20]

3.5 Design of Experiments Matrix for Edge Trimming of Unidirectional Composites

Machining of composites is a complex process and the determination depends on the material machined and the tool geometry and material used in addition to process conditions. In order to evaluate the effect of process variables on dust emissions it is necessary to conduct statistical analysis to draw meaningful conclusions. The statistical design test matrix is designed using Stat-Ease Design of Experiments. The factors considered were spindle speed, feed rate and cutting distance and the response were particle counts and particle concentration. Since particle counts play a very important role in determining aerodynamic diameter, the counts response was used for analysis. Mass concentration was also used in this analysis. The statistical design selected for this study is Response surface design since it is the design used for factors subjected to three levels. In our study for Uni Directional composites, we had three spindle speeds, three feed rates and three axial depth of cuts. The spindle speeds are 1000, 3000 and 6000 rpm. The feed rates are 635, 381, 127 mm/min and the axial depth of cut are 2.54, 3.81 and 6.35 mm. Following sections discuss in detail the statistical results. Based on the Factorial design we selected the Stat-Ease software will generate an experimental matrix where we have

to enter the experimental data for analysis. Table 3-4 shows the statistical design matrix for edge trimming of Uni Directional Composites. Statistical analysis helps in removing experimental errors obtained from the data, provide validity to the experimental results and attach a level of confidence to the results. This gives the experimenter the confidence that the experimental methods, results and conclusions are sound and valid.

Table 3-4: Statistical Design Matrix for UDC Composites

RUN NO	FACTOR 1 A:SPEED (RPM)	FACTOR 2 B:FEED(MM/MIN)	FACTOR 3 C:DOC (MM)
1	6000	635	3.81
2	3000	635	3.81
3	6000	635	2.54
4	6000	635	6.35
5	3000	635	2.54
6	1000	635	2.54
7	1000	635	6.35
8	1000	635	3.81
9	6000	381	6.35
10	6000	381	3.81
11	6000	381	2.54
12	3000	381	6.35
13	3000	381	3.81
14	3000	381	2.54
15	1000	381	2.54
16	1000	381	6.35
17	6000	127	3.81
18	3000	127	3.81
19	1000	127	3.81
20	1000	127	2.54

21	3000	127	2.54
22	6000	127	6.35
23	3000	127	6.35
24	1000	127	6.35

3.6 Design of Experiments for Edge Trimming Of HexMC® Composites

In these series of experiments the factors considered were spindle speed, feed rate and cutting distance and the response were particle counts and particle concentration. Since particle counts play a very important role in determining aerodynamic diameter, the counts response was used for analysis. Mass concentration was also used in this analysis. The statistical design selected for this study is Response surface design since it is the design used for factors subjected to 2 levels. The test matrix is shown in the Table 3-5. In our study for Uni Directional composites (UDC), we had two spindle speeds, two feed rates and two axial depth of cuts (DOC). The spindle speeds are 1000 and 6000 rpm. The feed rates are 635 and 127 mm/min and the axial depth of cut are 2.54 and 6.35 mm.

Table 3-5: Statistical Design Matrix for HexMC® Composites

RUN NO	FACTOR 1 A:SPEED (RPM)	FACTOR 2 B:FEED(MM/MIN)	FACTOR 3 C:DOC (MM)
1	6000	635	6.35
2	6000	635	2.54
3	6000	127	6.35
4	6000	127	2.54
5	1000	635	6.35
6	1000	635	2.54
7	1000	127	6.35
8	1000	127	2.54

4 Chapter IV: Results

4.1 Uni- Directional CFRP Linear Edge Trimming Results

During the process of edge trimming of Uni-directional composites the results observed are summarized below. During all the tests, the radial depth of cut was kept constant with a value of 0.076 mm (0.03”). Like mentioned previously, the tool used was a 4 flute, 12.7mm (0.5”) diameter flat nose carbide end mill. During this test, the data was recorded by the Grimm, Casella and PTRAK instruments.

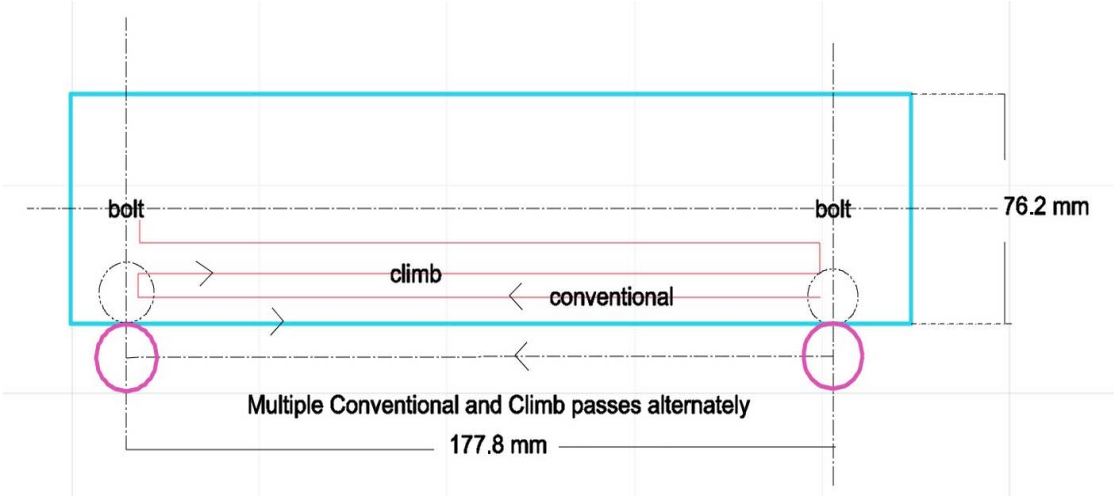

Figure 4-1: Edge Trim test

In this test, a one direction pass of about 177.78 mm (7 inches) was used because the distance between the 2 blots were close to 200 mm and we had restrictions on tool travel in the X direction due to the Plexiglas chamber. Hence multiple passes both conventional and climb were used as shown in the figure 4-1. In order to achieve the dust sampling time of close to 3 minutes, multiple passes were used. Since we were dealing with 3 different feed rates, the number of passes varied, as shown in Table 4.1.Fig 4-2 shows a composite piece after edge trim

#	FEED RATE (mm/min)	NO OF PASSES
1	635	10
2	381	6
3	127	3

Table 4-1: No of Passes in Edge Trim

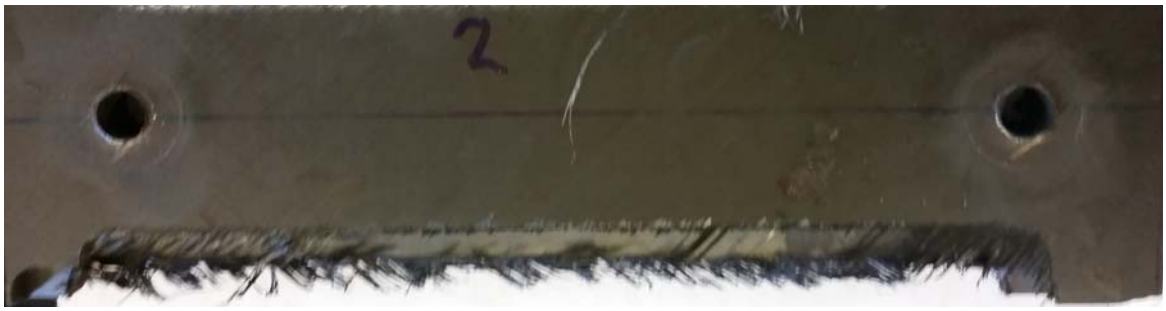

Figure 4-2: Uni Directional composite sample after edge trim (Plan View)

4.1.1 Grimm Aerosol Spectrometer Measurements

The Grimm aerosol spectrometer records both the particle mass concentration and the particle counts. It measures the particle counts in counts/liter and the concentration in $\mu g/m^{3.}$ Table 4-2 summarizes the results from Grimm instrument. The maximum counts observed during this experiment was observed at 33 million counts/liter in Run #22 and the minimum being around 11 million counts/liter in Run #6. As far as the mass concentration is concerned, the maximum was observed at around 67000 $\mu g/m^3$ and the minimum was around 20000 $\mu g/m^{3.}$Typical Grimm's data for particle concentration and particle counts are shown in Fig. 4-3. All the remaining plots can be found in Appendix A as a combined plot.

Table 4-2: Grimm spectrometer results

#	SPEED (RPM)	FEED (mm/min)	AXIAL DEPTH OF CUT (mm)	AVG PARTICLE COUNTS (COUNTS/LITER)	AVG PARTICLE CONCENTRATION (µg/m3)
1	6000	635	3.81	23487560	29289
2	3000	635	3.81	19825690	27245
3	6000	635	2.54	18627540	34270
4	6000	635	6.35	26752190	38230
5	3000	635	2.54	17659070	32560
6	1000	635	2.54	11453280	20230
7	1000	635	6.35	16347590	30130
8	1000	635	3.81	13258970	25130
9	6000	381	6.35	26629430	53230
10	6000	381	3.81	23145680	42234
11	6000	381	2.54	19674540	43950
12	3000	381	6.35	26897450	34230
13	3000	381	3.81	24379570	38230
14	3000	381	2.54	17682140	40160
15	1000	381	2.54	19545340	29950
16	1000	381	6.35	25408680	47066.4
17	6000	127	3.81	31248970	53236
18	3000	127	3.81	25432730	51271
19	1000	127	3.81	23457860	48230
20	1000	127	2.54	18675420	37210
21	3000	127	2.54	24112960	48220
22	6000	127	6.35	33531500	67097
23	3000	127	6.35	29112960	51220
24	1000	127	6.35	27786290	60722

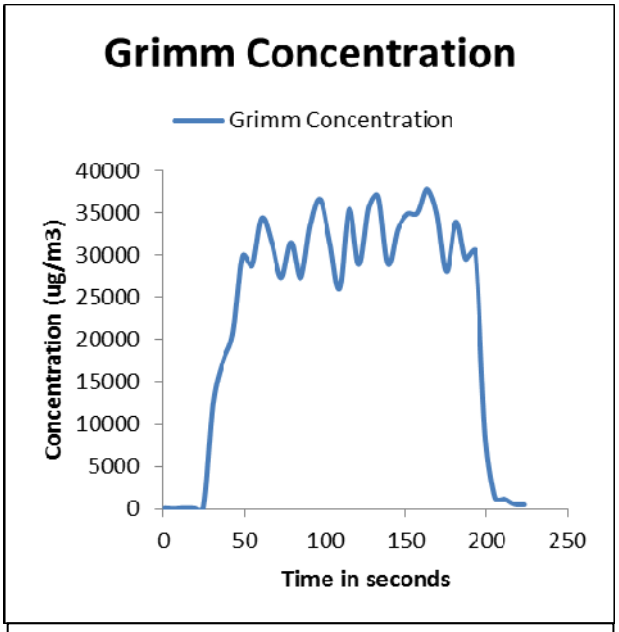

Speed: 6000 RPM

Feed: 635 mm/min

DOC: 2.54 mm

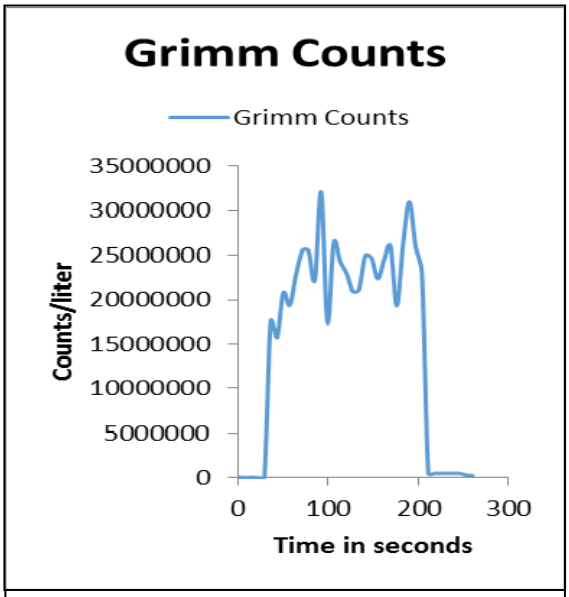

Speed: 6000 RPM

Feed: 635 mm/min

DOC: 2.54 mm

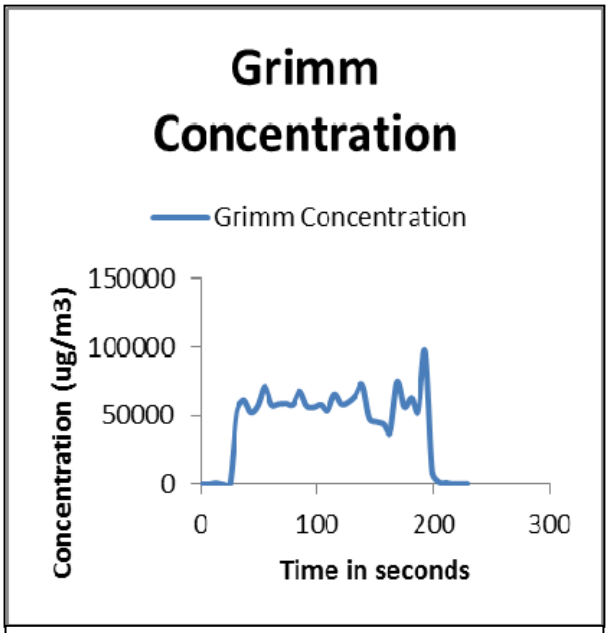

Speed: 1000 RPM

Feed: 635 mm/min

DOC: 2.54 mm

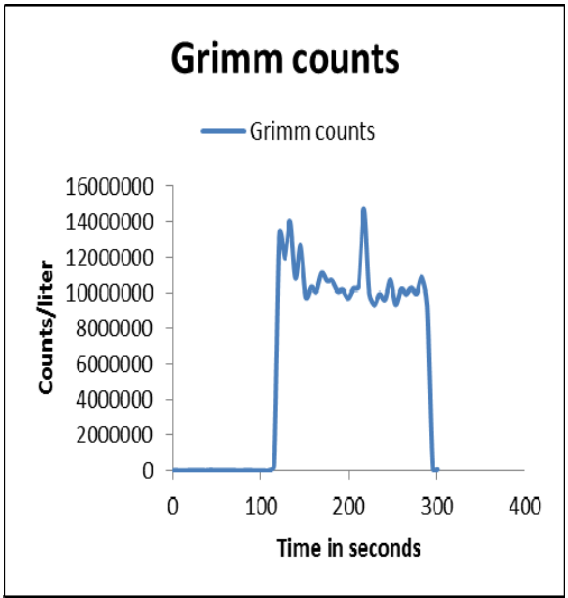

Speed: 1000 RPM

Feed: 635 mm/min

DOC: 2.54 mm

Figure 4-3: Sample Grimm Data for Uni-Directional CFRP Composites

4.1.2 Casella Micro-Dust Pro Measurements

The Casella Micro dust Pro records only particle mass concentration. It measures the concentration in mg/m^3 as shown in Table 4-3.

Table 4-3: Casella edge trim results

#	SPEED (RPM)	FEED (mm/min)	AXIAL DEPTH OF CUT (mm)	AVG PARTICLE CONCENTRATION (mg/m3)
1	6000	635	3.81	28.89
2	3000	635	3.81	28.45
3	6000	635	2.54	36.27
4	6000	635	6.35	39.29
5	3000	635	2.54	34.76
6	1000	635	2.54	20.57
7	1000	635	6.35	33.78
8	1000	635	3.81	25.63
9	6000	381	6.35	51.23
10	6000	381	3.81	44.24
11	6000	381	2.54	41.65
12	3000	381	6.35	31.13
13	3000	381	3.81	39.15
14	3000	381	2.54	42.46
15	1000	381	2.54	27.36
16	1000	381	6.35	45.13
17	6000	127	3.81	54.36
18	3000	127	3.81	49.221
19	1000	127	3.81	50.13
20	1000	127	2.54	39.41
21	3000	127	2.54	49.45

22	6000	127	6.35	67.397
23	3000	127	6.35	49.45
24	1000	127	6.35	61.7342

The maximum concentration observed during this experiment was observed at 68 mg/m^3 and the minimum being around 20 mg/m^3.It's interesting to see that Run #6 and Run #22 gave minimum and maximum concentration values respectively. Typical sample plots from the Casella instrument are shown in Fig. 4-4. All the remaining plots can be found in the appendix A as a combination plot.

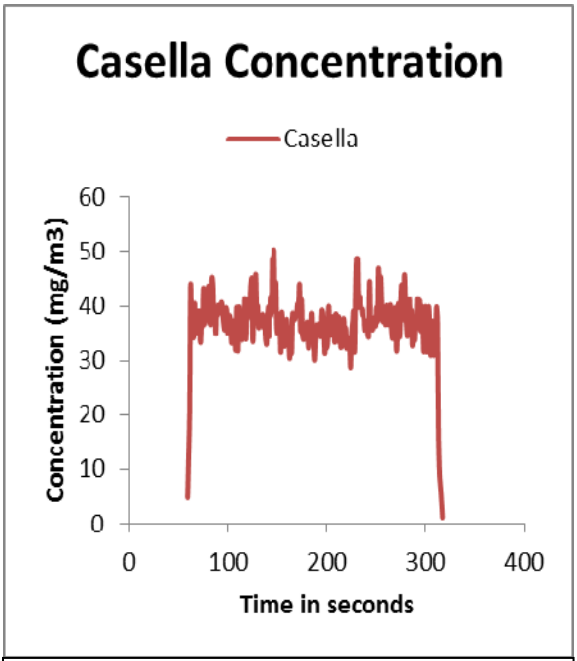

Speed: 1000 RPM

Feed: 127 mm/min

DOC: 2.54 mm

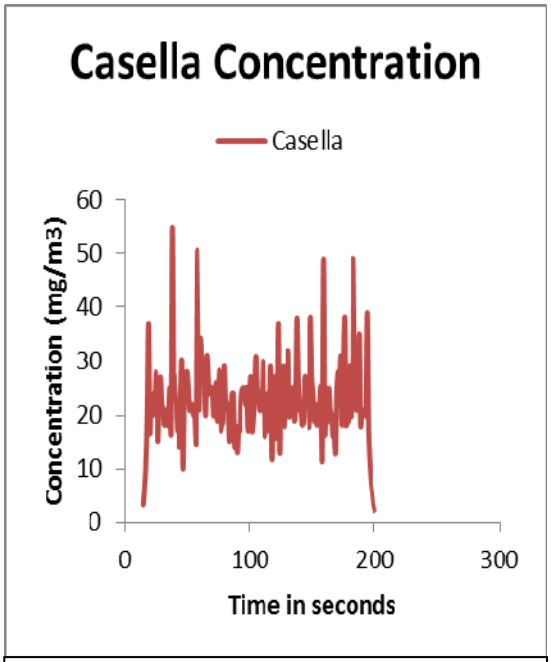

Speed: 1000 RPM

Feed: 635 mm/min

DOC: 3.81 mm

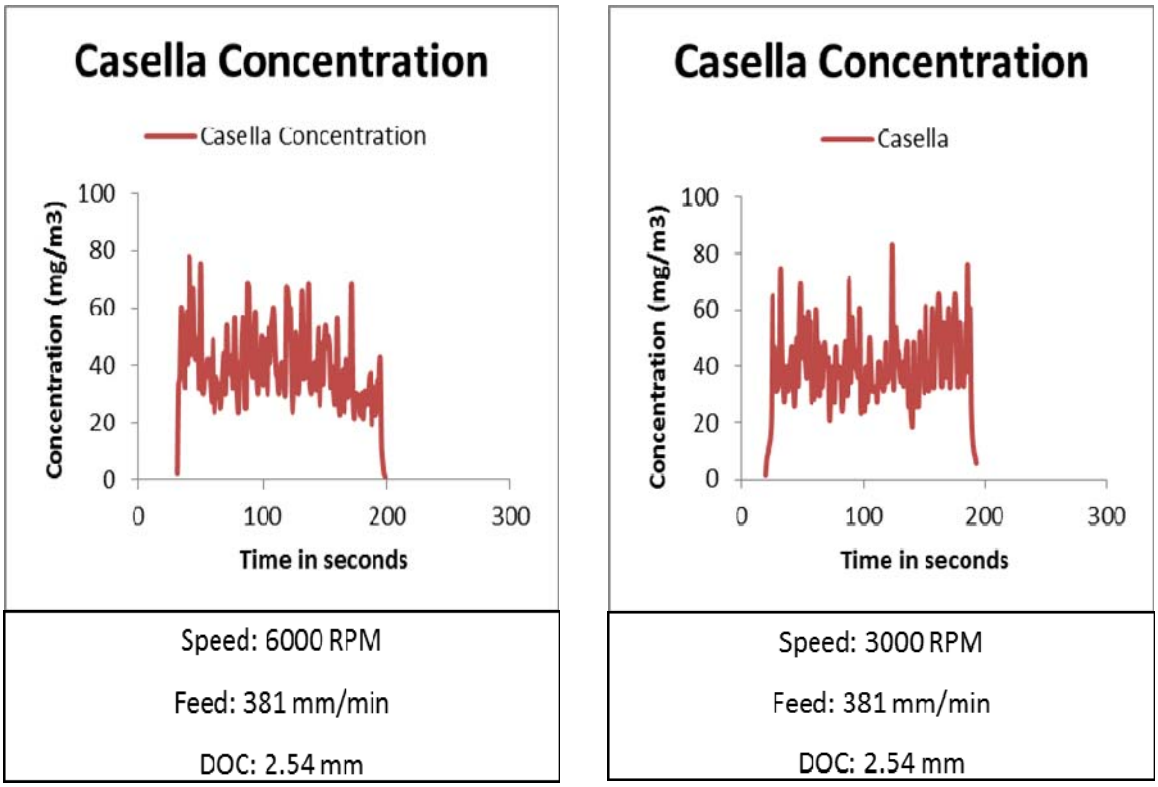

Figure 4-4: Sample Casella Data for Uni-Directional CFRP Composites

4.1.3 PTRAK Particle Counter Measurements

The P-TRAK particle counter records only particle mass concentration. It measures the counts in counts/cm^3 as seen in Table 4-4.

Table 4-4: PTRAK Edge trim results

#	SPEED (RPM)	FEED (mm/min)	AXIAL DEPTH OF CUT (mm)	AVG PARTICLE COUNTS (COUNTS/CC)
1	6000	635	3.81	27011
2	3000	635	3.81	22800
3	6000	635	2.54	21422
4	6000	635	6.35	30765
5	3000	635	2.54	20308

6	1000	635	2.54	13171
7	1000	635	6.35	18800
8	1000	635	3.81	14585
9	6000	381	6.35	29292
10	6000	381	3.81	25460
11	6000	381	2.54	21642
12	3000	381	6.35	29587
13	3000	381	3.81	26818
14	3000	381	2.54	19450
15	1000	381	2.54	21500
16	1000	381	6.35	27950
17	6000	127	3.81	34374
18	3000	127	3.81	27976
19	1000	127	3.81	25804
20	1000	127	2.54	20543
21	3000	127	2.54	26524
22	6000	127	6.35	36885
23	3000	127	6.35	32024
24	1000	127	6.35	30565

The maximum average counts observed during this experiment was observed at 37000 counts/cc (Run #22) and the minimum being around 14000 counts/cc (Run #6). A few sample plots from the instrument are shown below. All the remaining plots can be found in the appendix A as a combination plot.

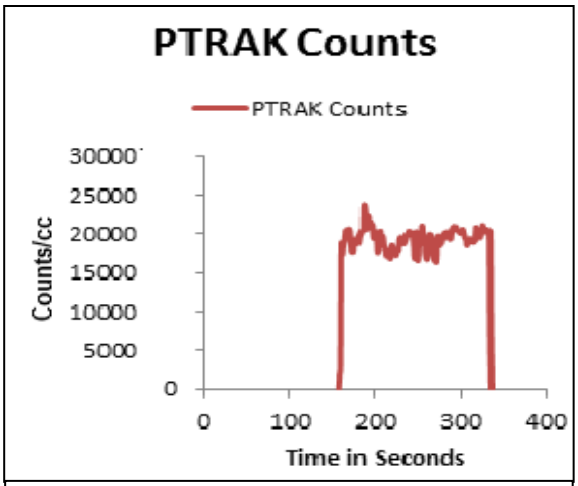

Speed: 3000 RPM

Feed: 635 mm/min

DOC: 2.54 mm

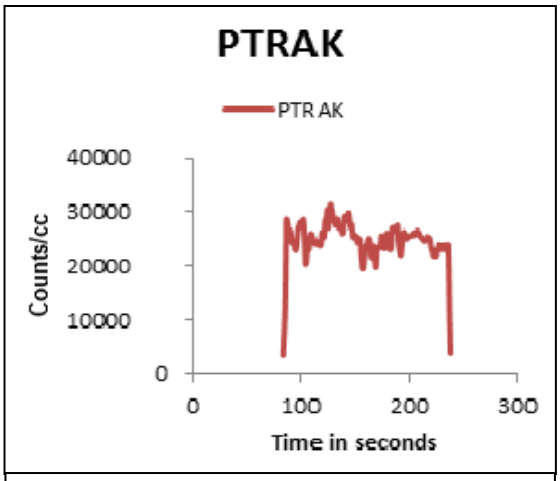

Speed: 1000 RPM

Feed: 635 mm/min

DOC: 2.54 mm

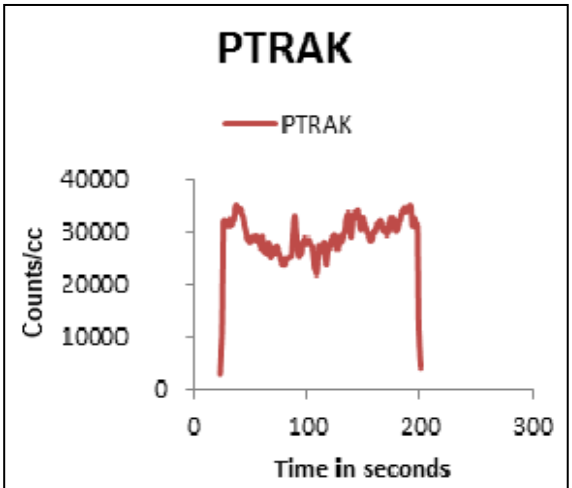

Speed: 6000 RPM

Feed: 381 mm/min

DOC: 6.35 mm

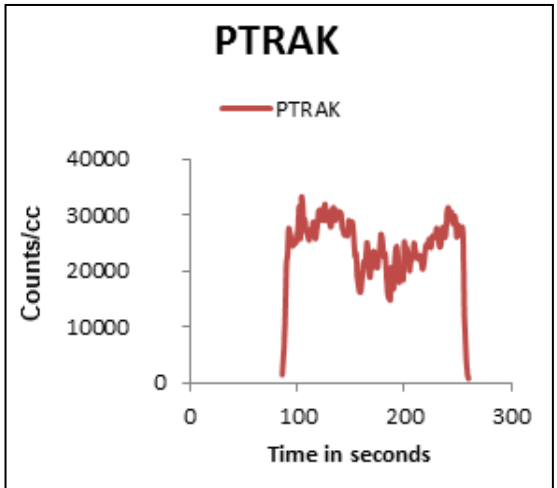

Speed: 3000 RPM

Feed: 381 mm/min

DOC: 6.35 mm

Figure 4-5: **Sample PTRAK Data for Uni-Directional CFRP Composites**

4.2 Uni-Directional CFRP Circular Slot Test

A machining test for semicircular slots were performed on a 25.4 mm (1 inch) thick Uni directional composite piece. The reason for performing this test was to see the change in the influence of direction of cutting with the fiber orientation on the generated dust. The dimensions of the piece were approximately 215 mm x 115 mm. The tool used was a 12.7 mm (1 inch) flat nose carbide end mill with 4 flutes, similar to the one used in the previously conducted investigations. Data was recorded for the Casella and PTRAK instruments. A schematic representation of the test is shown in Fig. 4-6.

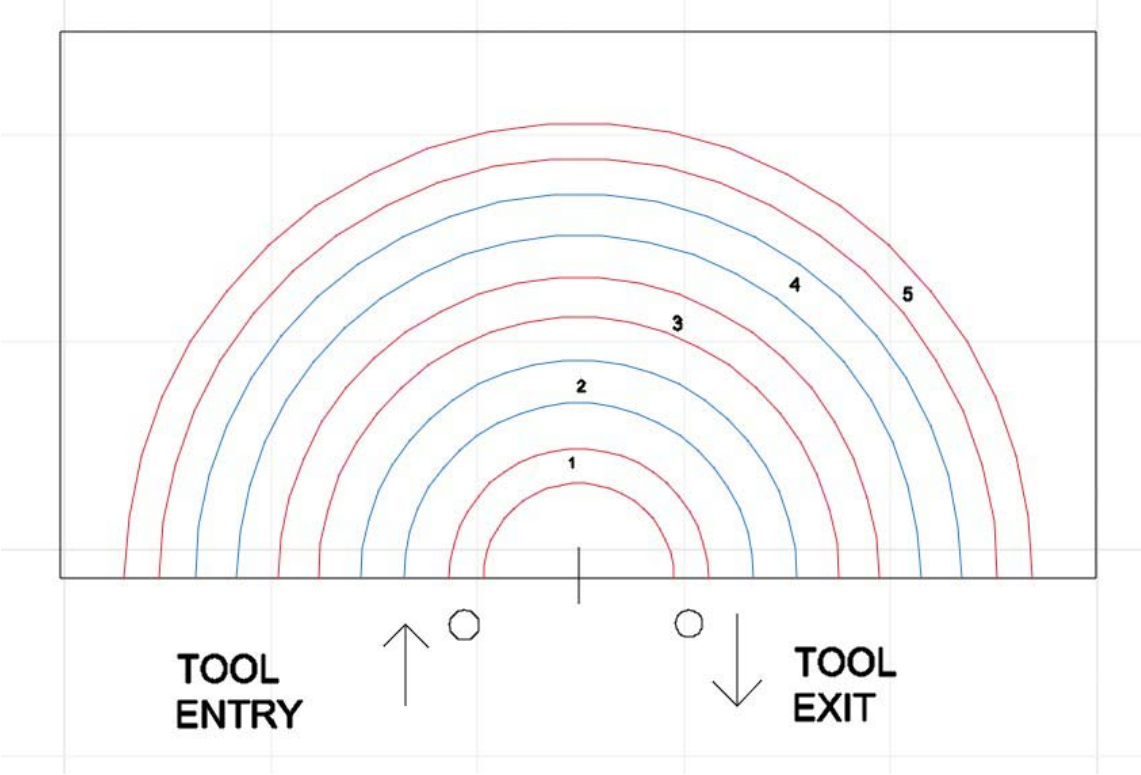

Figure 4-6: Circular slot test

In order to perform this test, a CNC program was written. This program starts the operation at the center of the work piece (marked by a line in the diagram) and then moves left equal to the amount of the corresponding slot radius. It then finishes the slot cut and returns back to the center of the work piece. It then repeats the same routine till all the slots are done. At the end it once again returns back to the center. After each slot

when the tool reaches the center, the program was paused in order to set-up the dust measuring instruments (Casella and PTRAK) for the next slot. It was made sure that there is no dust build up in the chamber or the tube by ensuring that we pause the process for a sufficient time so that the vacuum can suck out the residual dust. Parameters for the slot test are represented in the following table. Table 4-5 shows the parameters for the machined slots, while Fig. 4-7 shows the picture macrographs of the machined slots immediately after machining (left) and after cleaning (right).

Table 4-5: SLOT TEST PARAMETERS

SLOT No.	SLOT DIAMETER (mm)	SPEED (RPM)	FEED (mm/min)	DEPTH OF CUT (mm)
1	50.8	1000	127	5.08
2	82.55	6000	254	5.08
3	114.3	6000	381	5.08
4	146.05	3000	508	5.08
5	177.8	3000	635	5.08

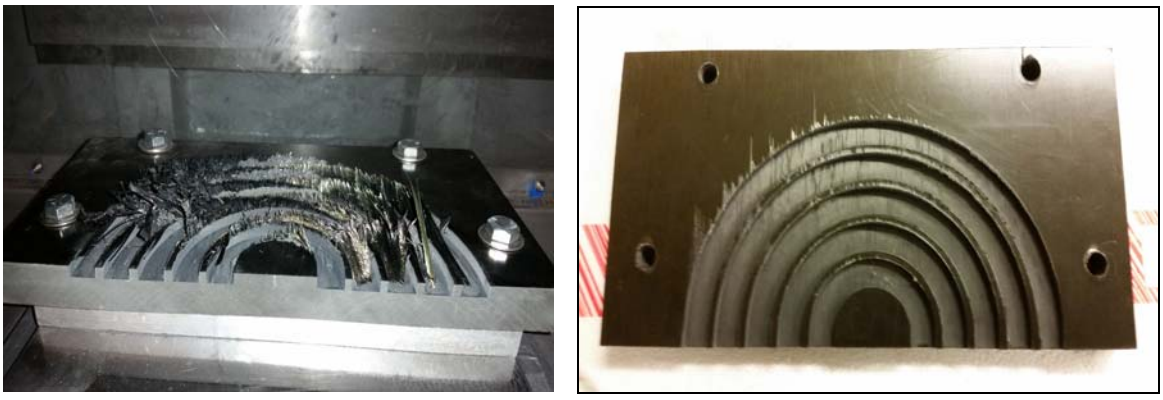

Figure 4-7: Semi Circular Slot Cut

Figure 4-8 shows the Casella recorded particle concentration for slots individually (a-e) and Fig 4-8 (f) shows all the five slots together. We can clearly see in the Fig. 4-8 (f) that concentrations for the slot #1 is lowest while that for the slot#5 is highest. A similar trend can be seen in the concentration recording of all the slots.

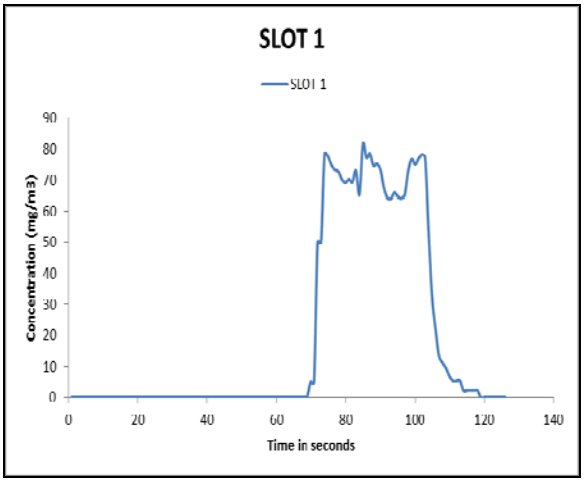

(a)

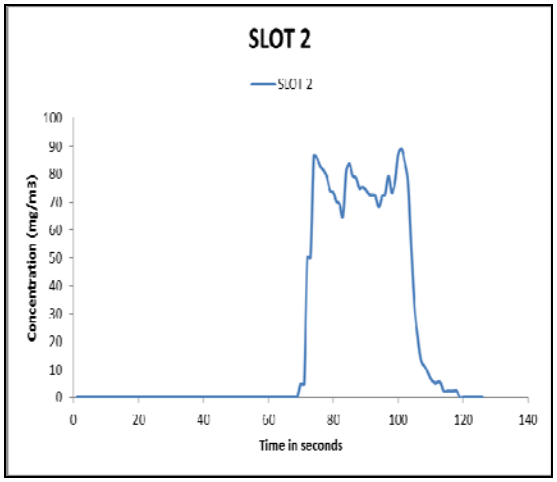

(b)

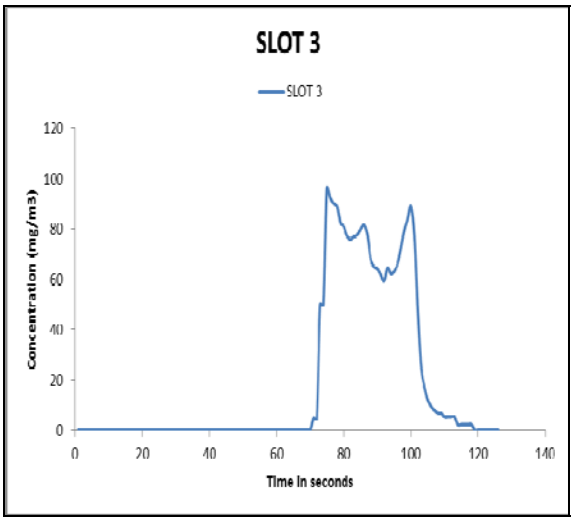

(c)

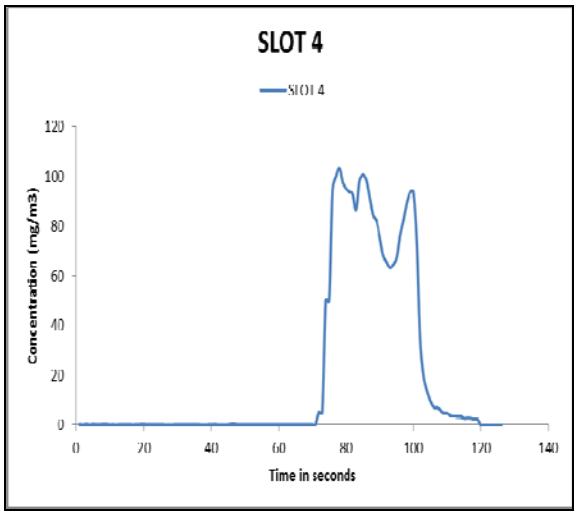

(d)

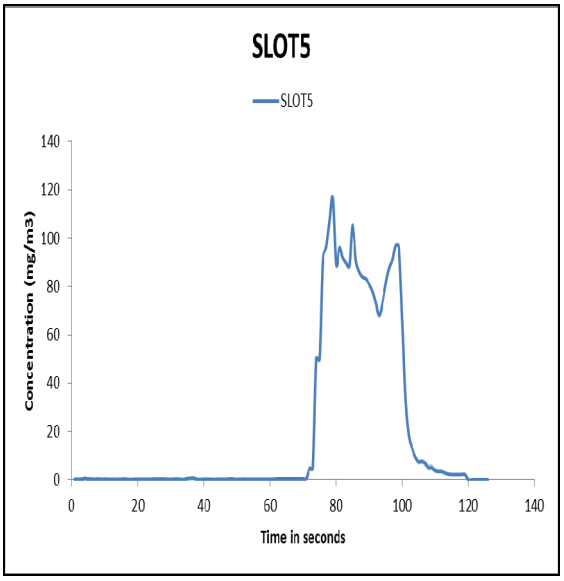

(e)

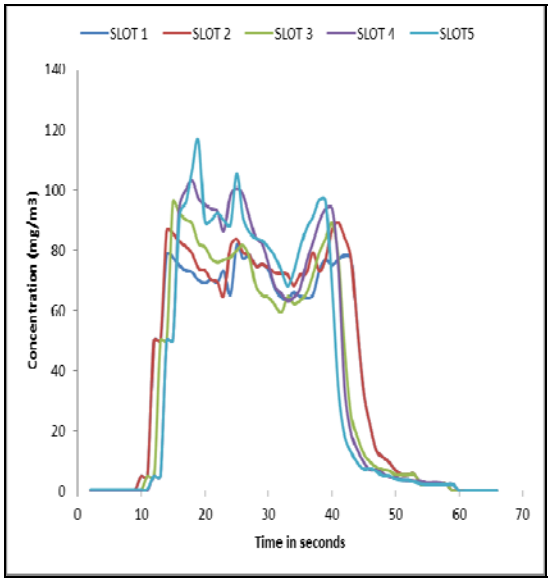

(f)

Figure 4-8: (a), (b), (c), (d), (e) - Casella data for the individual slots (1-5), (f) Combined Casella data for all slots together

Figure 4-9 shows the PTRAK recorded particle counts for slots individually (a-e) and Fig 4-9 (f) shows all the five slots together. We can clearly see in the Fig. 4-9 (f) that counts for the slot #1 is lowest while that for the slot#5 is highest. A similar trend can be seen in the counts recording of all the slots.

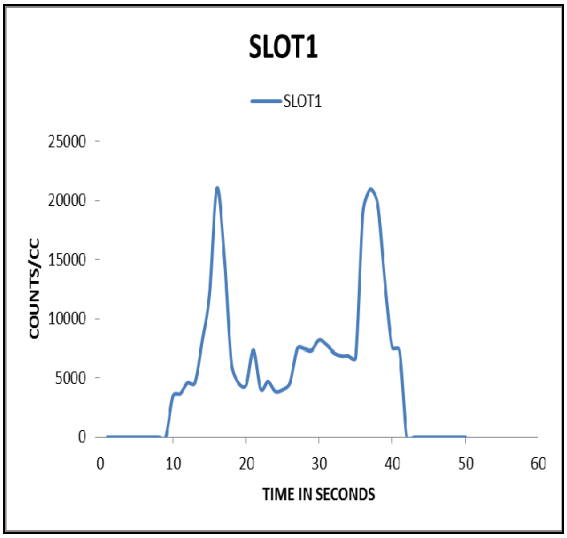

(a)

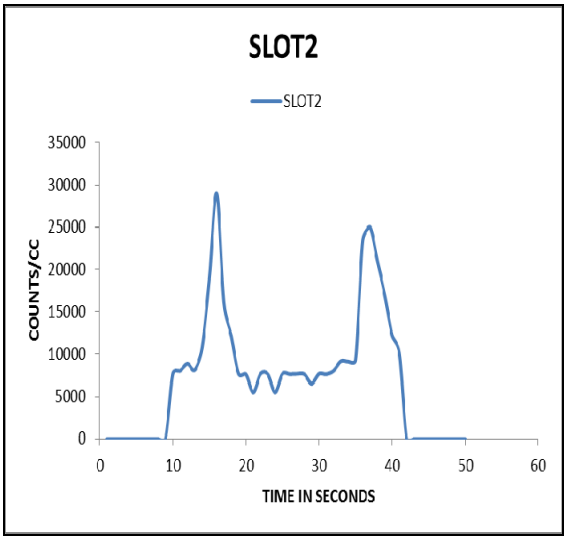

(b)

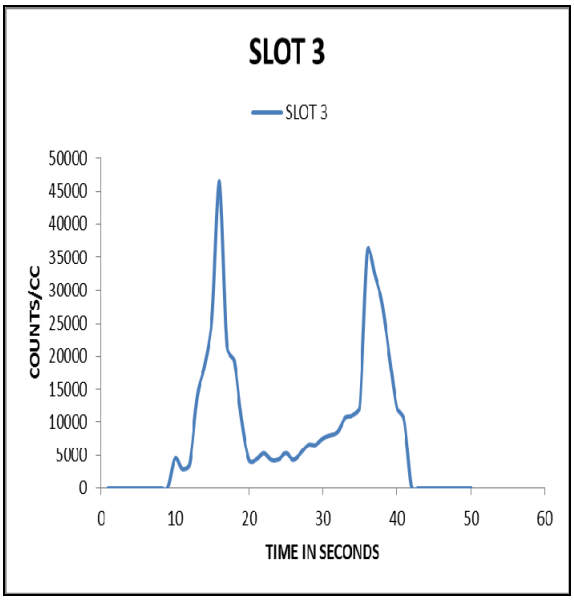

(c)

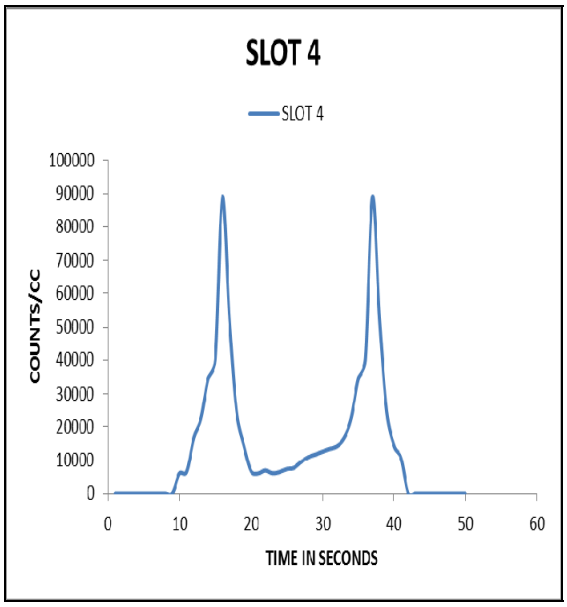

(d)

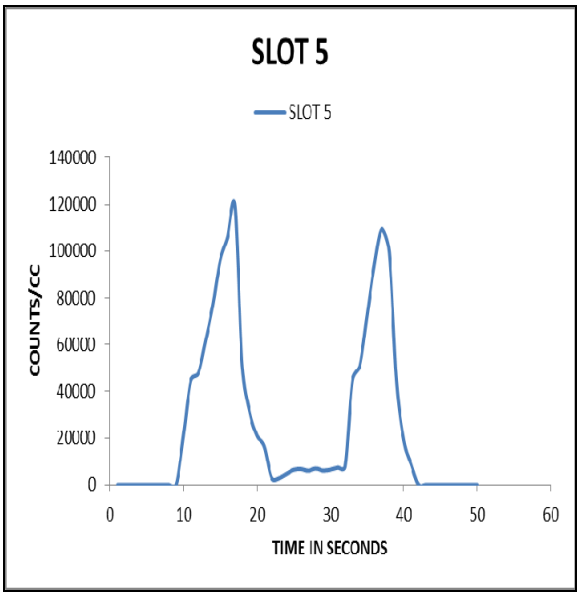

(e)

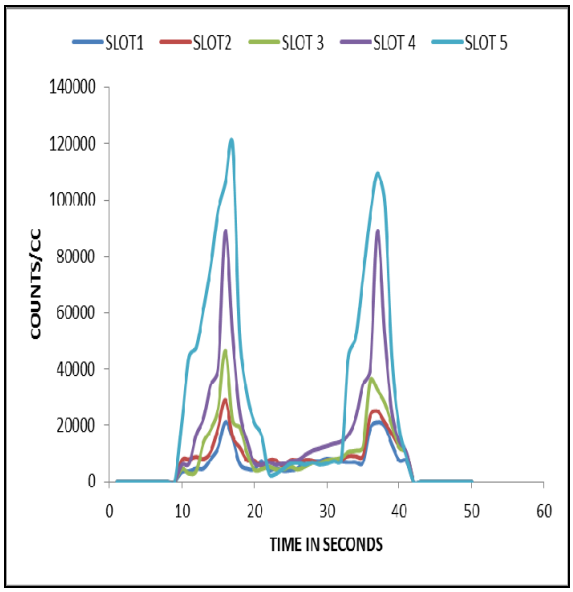

(f)

Figure 4-9: (a), (b), (c), (d), (e) - PTRAK data for the individual slots, (f) Combined PTRAK data for all slots together

4.3 Uni Directional CFRP Octagon Slot Test

A machining test for octagonal slot cutting pattern were performed on a 25.4 mm (1 inch) thick Uni directional composite piece. The reason for performing this test was to see the change in the influence of direction of cutting with the fiber orientation on the generated dust especially at ± 45° where maximum delamination are generally observed. The dimensions of the piece were approximately 175 mm x 115 mm. The tool used was a 12.7 mm (1 inch) flat nose carbide end mill with 4 flutes, similar to the one used in the previous investigations. Data was recorded for the Casella and PTRAK instruments. A schematic representation of the test is provided below.

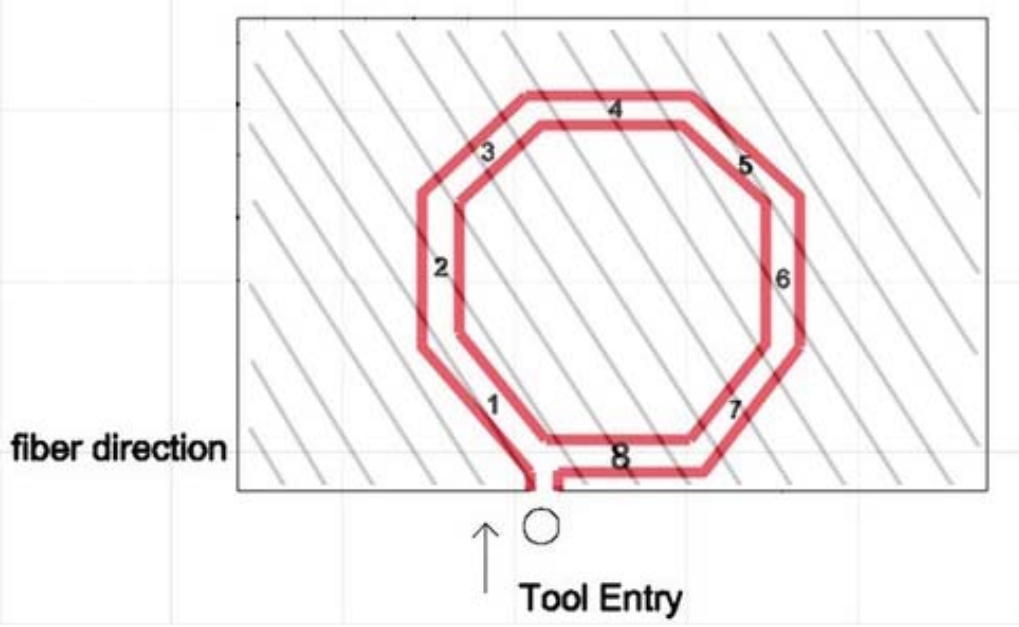

Figure 4-10: Octagon slot test

In order to perform this test, a CNC program was written. This program starts the operation at the point of entry shown in the Figure 4-10. It then moves on in the order of the numbers shown in the figure. It then finishes the cut at the last point and then stops. The program was paused in order to set-up the dust measuring instruments for each of the slots. It was made sure that there is no dust build up in the chamber or the tube by ensuring that we pause the process for a sufficient time so that the vacuum can suck out

the residual dust. Cutting parameters for the Octagonal slot test are represented in the following Table 4-6, while Fig. 4-11 shows the picture macrographs of the machined slots immediately after machining (left) and after cleaning (right).

Table 4-6: Data for Octagon Slots

SLOT No.	SLOT LENGTH (mm)	SPEED (RPM)	FEED (mm/min)	DEPTH OF CUT (mm)	RELATIVE ANGLE WRT FIBER DIRECTION (degrees)
1	35.96	1000	25.4	5.08	0
2	38.1	1000	25.4	5.08	45
3	35.96	1000	25.4	5.08	90
4	50.8	1000	25.4	5.08	135
5	35.96	1000	25.4	5.08	180
6	38.1	1000	25.4	5.08	225
7	35.96	1000	25.4	5.08	270
8	50.8	1000	25.4	5.08	315

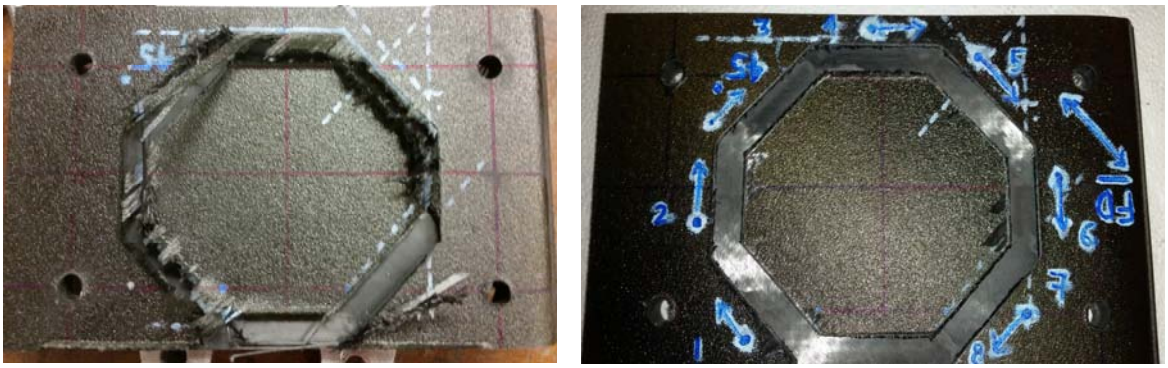

Figure 4-11: Octagonal Slot Cut

Figure 4-12 and Figure 4-13 show the mass concentration data from the Casella and particle counts from PTRAK respectively. Note that the data for time at 20, 45, 66 and 90 are significant.

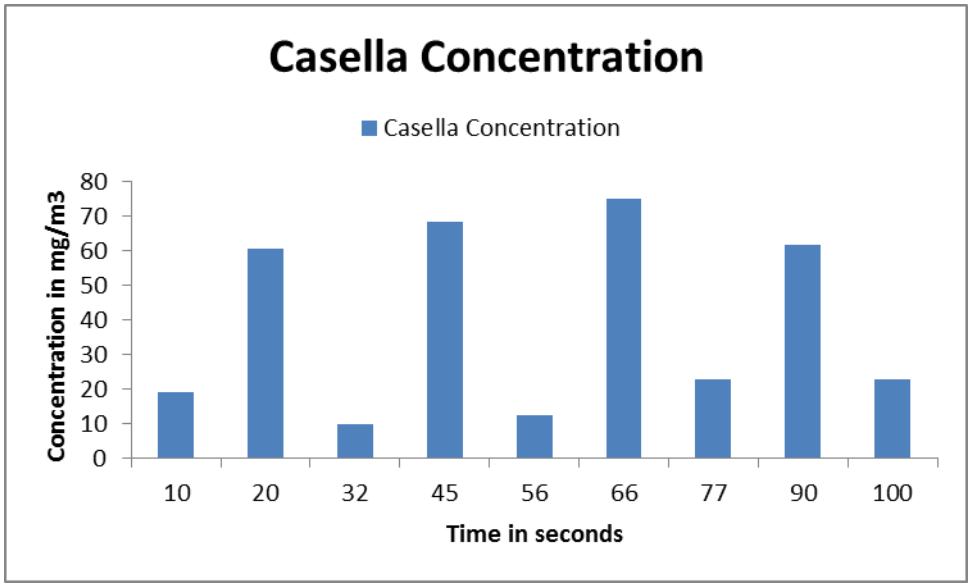

Figure 4-12: Casella Data for Octagon Slot

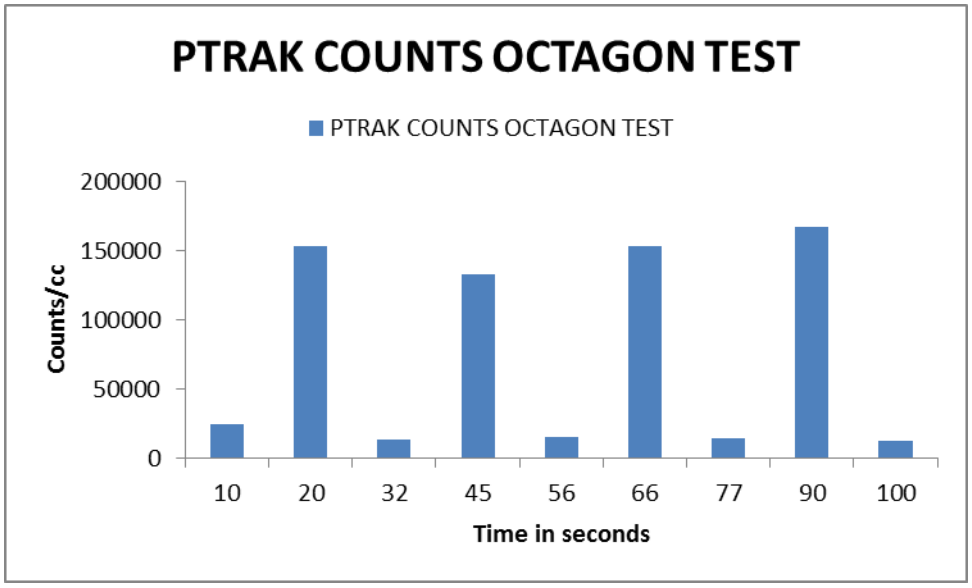

Figure 4-13: PTRAK Data for Octagon Slot

4.4 HexMC® PRELIMNARY EDGE TRIMMING RESULTS

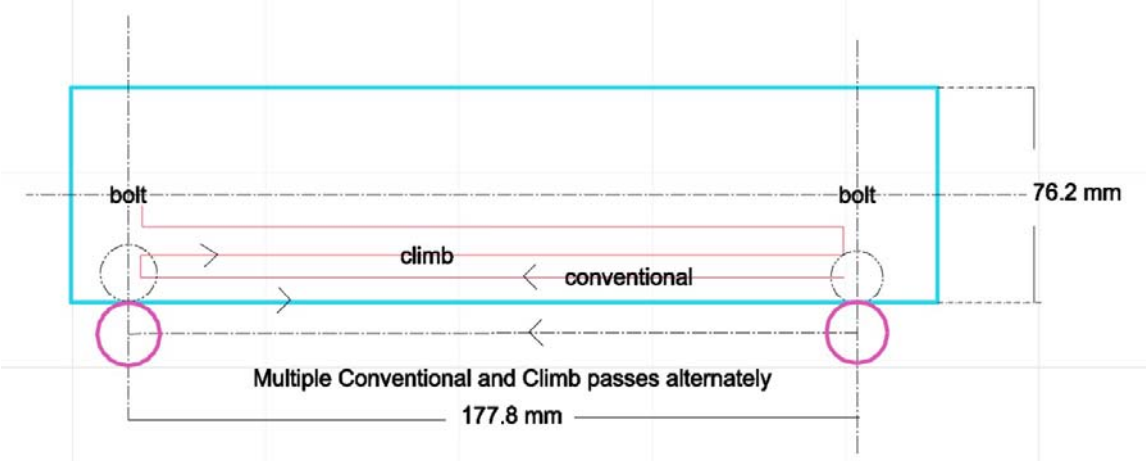

In edge trimming of HexMC® the experimental method of performing the edge trim is same as that of Uni-Directional CFRP Composites. Designed experiments and responses are given in Table 4-7 for Grimm instrument while the cutting distances and passes are shown in Table 4-8. Machined edge is shown in photo macrograph in Fig 4-14.

Table 4-7: Grimm data for HexMC

#	SPEED (RPM)	FEED (mm/min)	AXIAL DEPTH OF CUT (mm)	AVG PARTICLE COUNTS (COUNTS/LITER)	AVG PARTICLE CONCENTRATION (µg/m3)
1	6000	635	6.35	31531914	41594.24
2	6000	635	2.54	27684009	37285.76
3	6000	127	6.35	39522462	73001.54
4	6000	127	2.54	33599836	49874.56
5	1000	635	6.35	19268363	32781.44
6	1000	635	2.54	13499598	22010.24
7	1000	127	6.35	32750774	66065.54
8	1000	127	2.54	22012100	40484.48

From Table 4-7 the maximum average counts observed during this experiment was observed at 39 million counts/liter and the minimum being around 13 million counts/liter. As far as the mass concentration is concerned, the maximum average was observed at around 73000 $\mu g/m^3$ and the minimum was around 22000 $\mu g/m^3$. These values are associated with Run #3 and Run #6 respectively. A few sample plots from the instrument are shown fig. 4-15. All the remaining plots can be found in the appendix B as a combined plot.

Table 4-8: No of passes for HexMC Composites

#	FEED RATE (mm/min)	NO OF PASSES
1	635	10
2	381	6
3	127	3

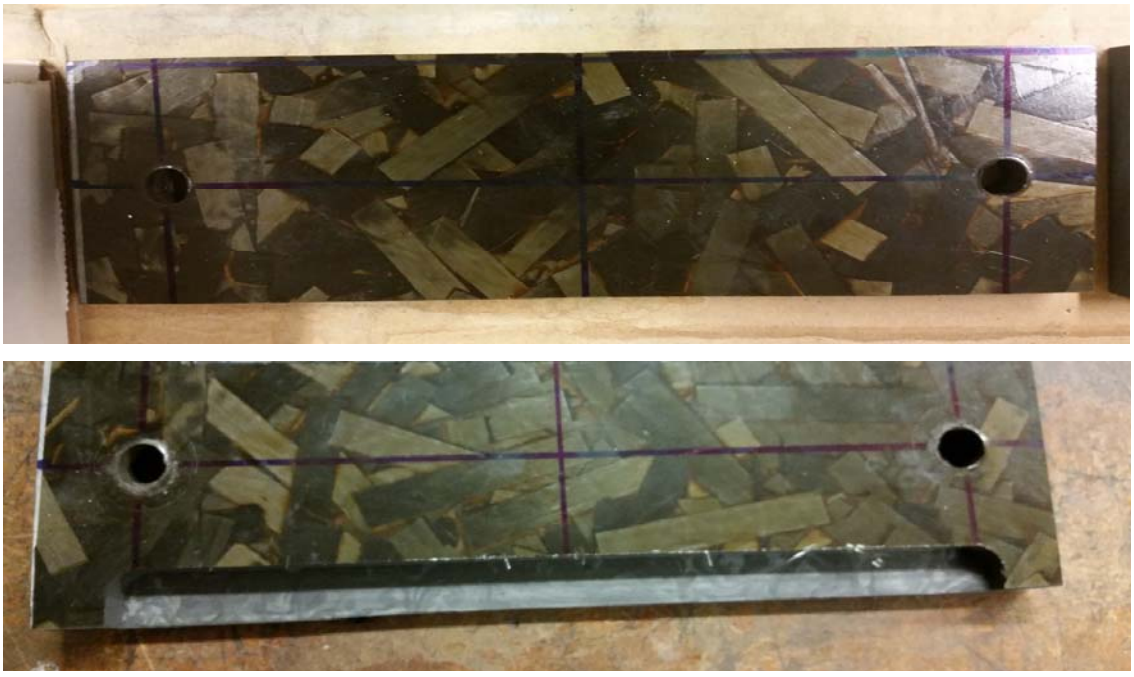

Figure 4-14: HexMC Before and after edge trimming

Mass concentrations recorded with the Casella and particle counts recorded with the PTRAK for the 8 runs are shown in Table 4-9 and Table 4-10 respectively.

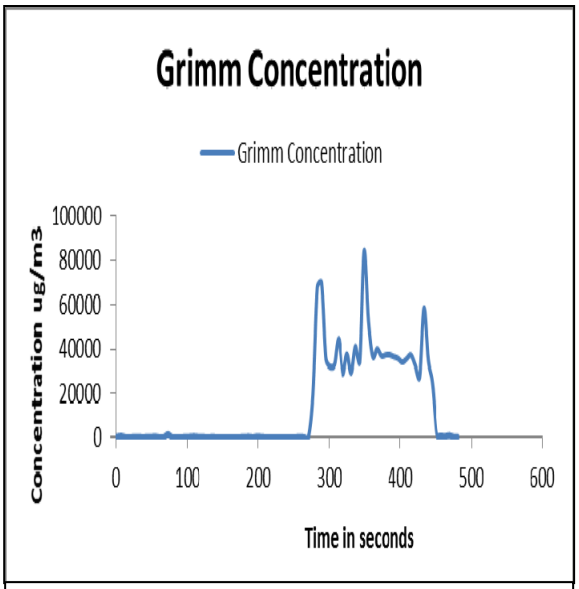

Speed: 6000 RPM

Feed: 635 mm/min

DOC: 6.35 mm

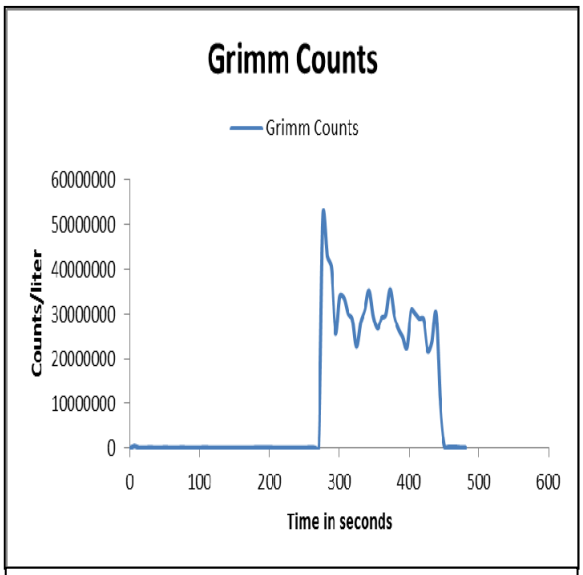

Speed: 6000 RPM

Feed: 635 mm/min

DOC: 6.35 mm

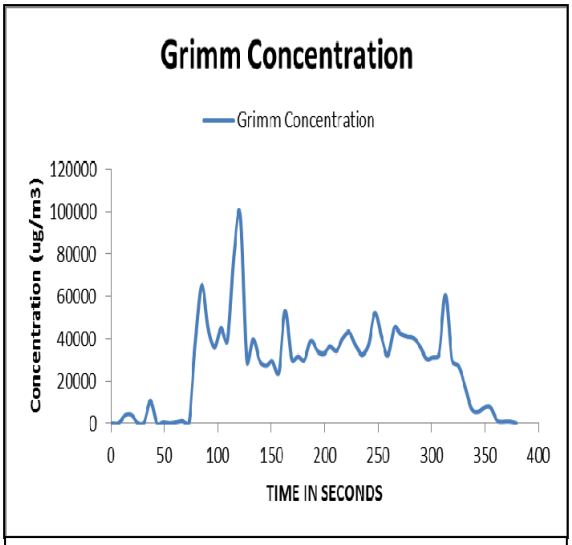

Speed: 6000 RPM

Feed: 635 mm/min

DOC: 2.54 mm

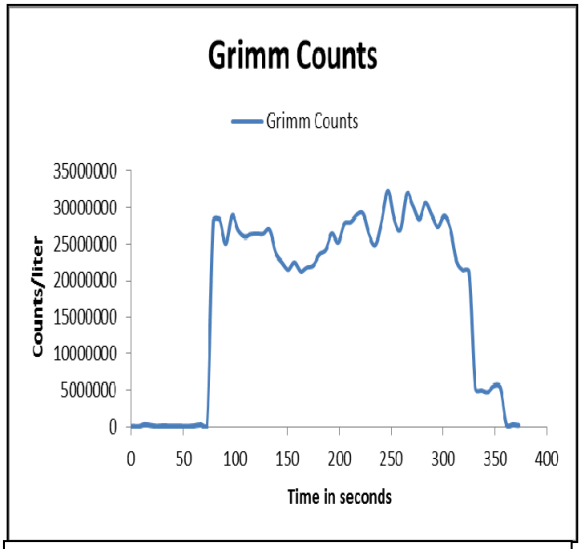

Speed: 6000 RPM

Feed: 635 mm/min

DOC: 2.54 mm

Figure 4-15: Grimm data for HexMC® Edge Trim

Table 4-9: Casella concentration measurements

#	SPEED (RPM)	FEED (mm/min)	AXIAL DEPTH OF CUT (mm)	AVG PARTICLE CONCENTRATION (mg/m3)
1	6000	635	6.35	42.74752
2	6000	635	2.54	39.46176
3	6000	127	6.35	73.32794
4	6000	127	2.54	53.13696
5	1000	635	6.35	36.75264
6	1000	635	2.54	22.38016
7	1000	127	6.35	67.16681
8	1000	127	2.54	42.87808

The maximum average counts observed during this experiment was observed at 74 mg/m^3 and the minimum being around 22 mg/m^3. A sample plots from the instrument is shown below. All the remaining plots can be found in the appendix B as a combined plot. Figure 4-16 shows the typical Casella concentration and Figure 4-17 shows typical PTRAK counts. Remaining plots can be found in appendix B as a combined plot.

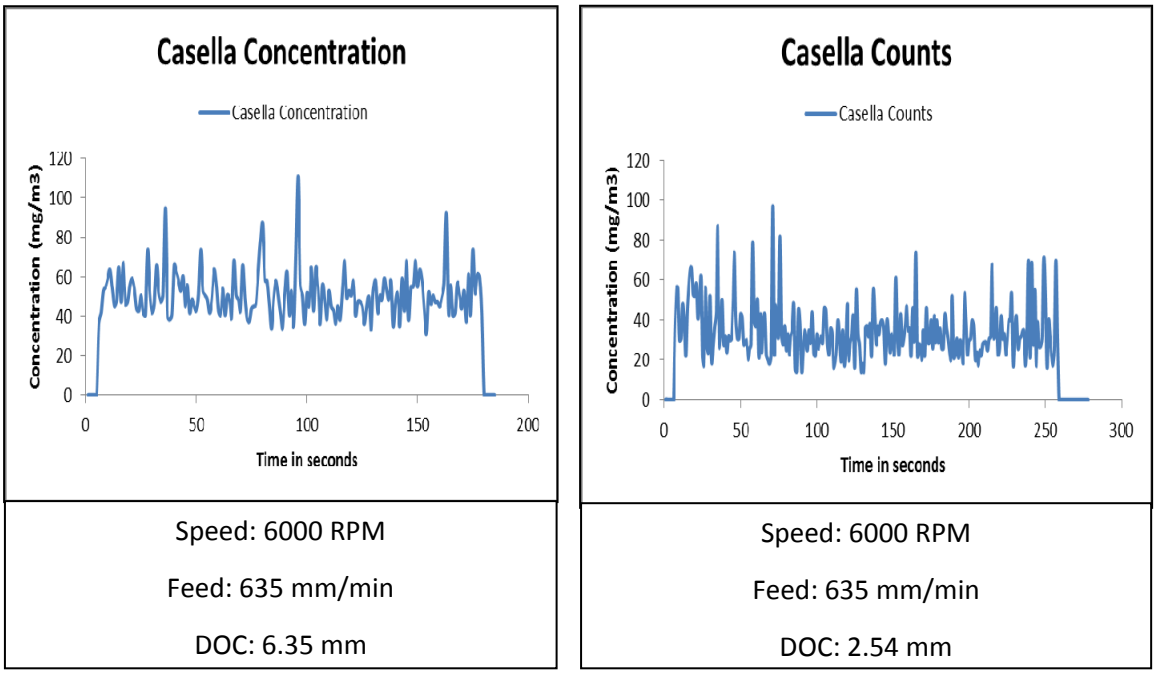

Speed: 6000 RPM Feed: 635 mm/min DOC: 6.35 mm	Speed: 6000 RPM Feed: 635 mm/min DOC: 2.54 mm

Figure 4-16: Casella results for HexMC Edge Trim

Table 4-10: PTRAK Counts Measurements

#	SPEED (RPM)	FEED (mm/min)	AXIAL DEPTH OF CUT (mm)	AVG PARTICLE COUNTS (COUNTS/CC)
1	6000	635	6.35	32236
2	6000	635	2.54	26504
3	6000	127	6.35	40272
4	6000	127	2.54	30922
5	1000	635	6.35	18091
6	1000	635	2.54	12197
7	1000	127	6.35	32560
8	1000	127	2.54	24137

The maximum counts observed during this experiment was observed at 40000 counts/cc and the minimum being around 12000 counts/cc. Remaining plots can be found in appendix B as a combined plot.

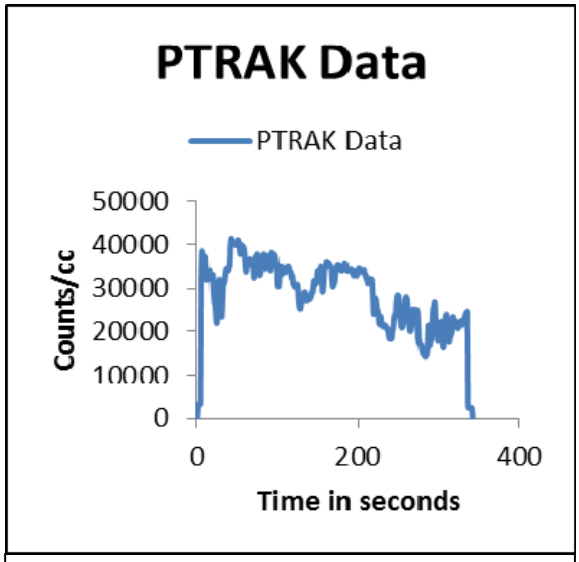

Speed: 6000 RPM

Feed: 635 mm/min

DOC: 6.35 mm

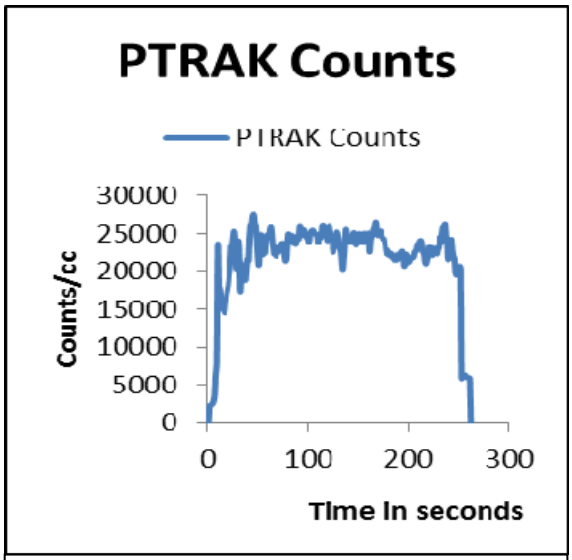

Speed: 6000 RPM

Feed: 635 mm/min

DOC: 2.54 mm

Figure 4-17: PTRAK EDGE TRIM HexMC

5 Chapter V: Analysis and Discussions

5.1 Multi - Instrument Isokinetic Correlation in CFRP Composites

During the course of the tests that have been conducted on the CFRP Composites, it was previously explained that the 3 instruments were used simultaneously to measure the data. If the isokinetic theory of optimization is valid, then the measurement made by the instruments must be similar in trend. In order to check this, it's necessary to convert the system of units to a common one so that they can be compared. The Grimm measures concentration in $\mu g/m^3$ while the Casella measures concentration in mg/m^3. When it comes to counts, the Grimm measures the counts in Counts/liter while the PTRAK measures the counts in Counts/cc. Hence in order to check the instruments measuring data compared to each other, the counts of the PTRAK were converted from counts/cc to counts per liter by multiplying by a factor of 1000. Also to compare the concentrations, it was preferred to convert the Grimm data from $\mu g/m^3$ to mg/m^3 by dividing the Grimm data with a factor of 1000. After making these changes to the data and then plotting the Grimm mass concentration data with the Casella Concentration data and plotting the Grimm counts data with the PTRAK data, results were found to be very similar. The correlation between the data measured by the instruments were extremely good, indicating that the isokinetic sampling technique is very close to being optimum. Some of the plots for UDC composites are shown in the figure 5-1. Since they were plotted for each and every test, it becomes pointless to plot all of them in the main thesis. Hence the rest of them are added in the appendix A.

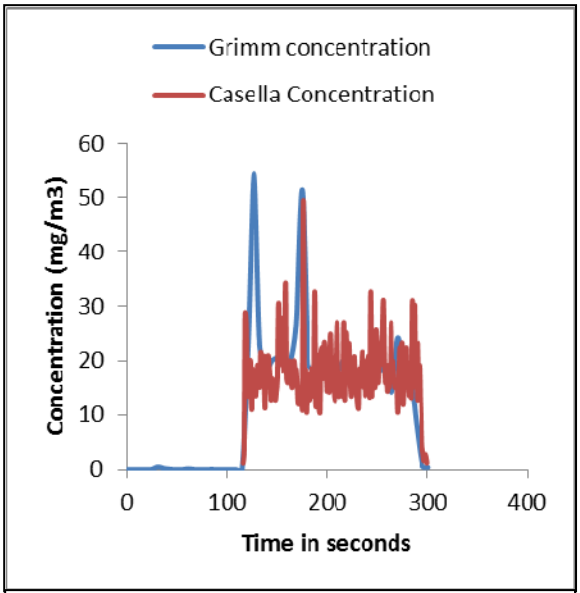

Speed: 1000 RPM

Feed: 635 mm/min

DOC: 2.54 mm

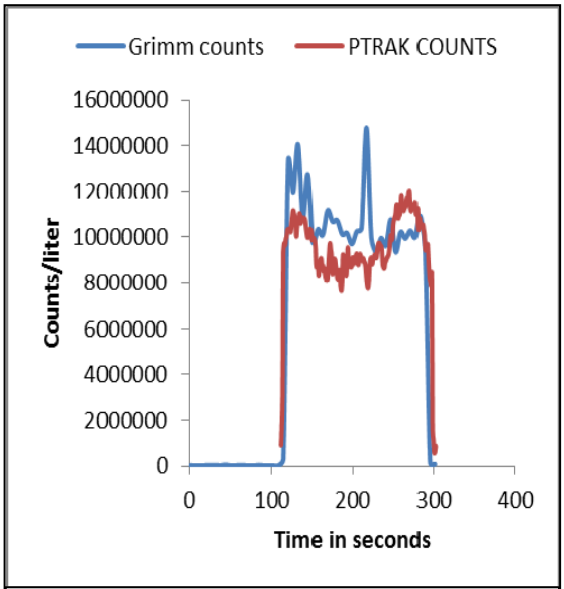

Speed: 1000 RPM

Feed: 635 mm/min

DOC: 2.54 mm

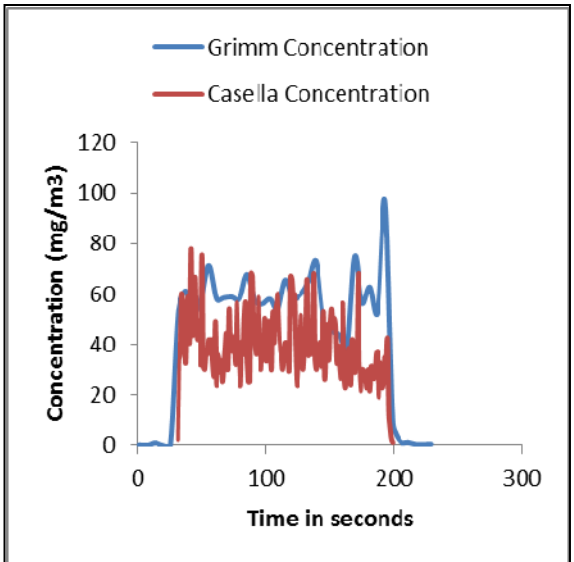

Speed: 6000 RPM

Feed: 381 mm/min

DOC: 2.54 mm

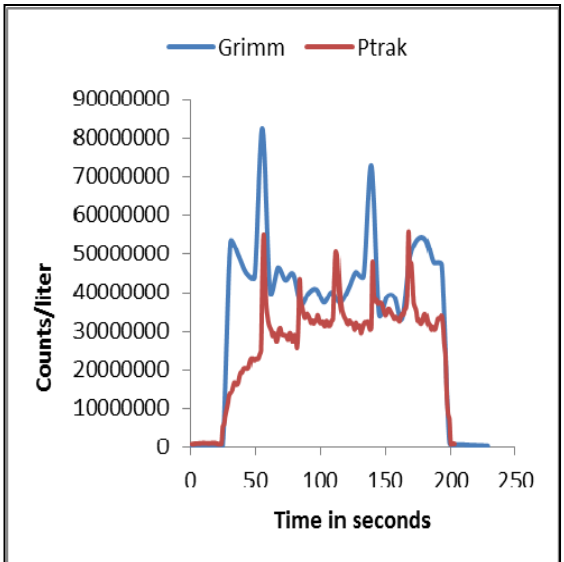

Speed: 6000 RPM

Feed: 381 mm/min

DOC: 2.54 mm

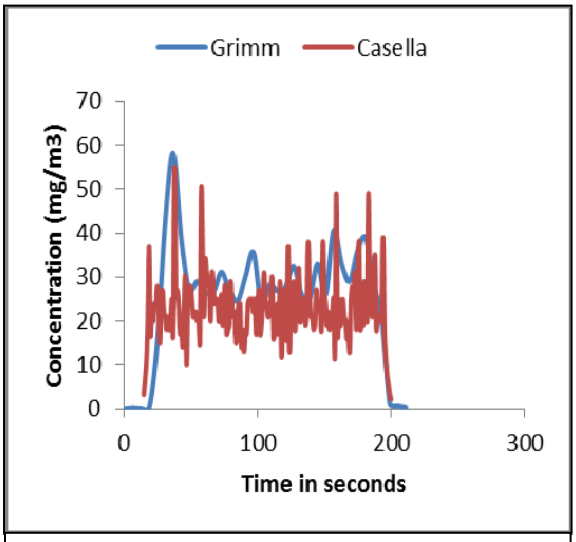

Speed: 1000 RPM

Feed: 635 mm/min

DOC: 3.81 mm

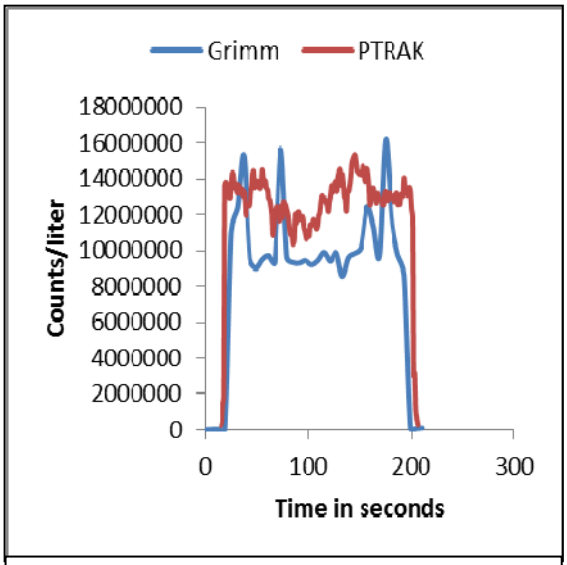

Speed: 1000 RPM

Feed: 635 mm/min

DOC: 3.81 mm

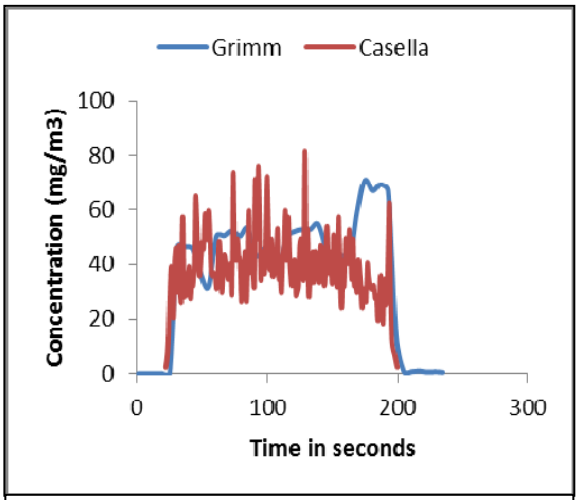

Speed: 6000 RPM

Feed: 381 mm/min

DOC: 3.81 mm

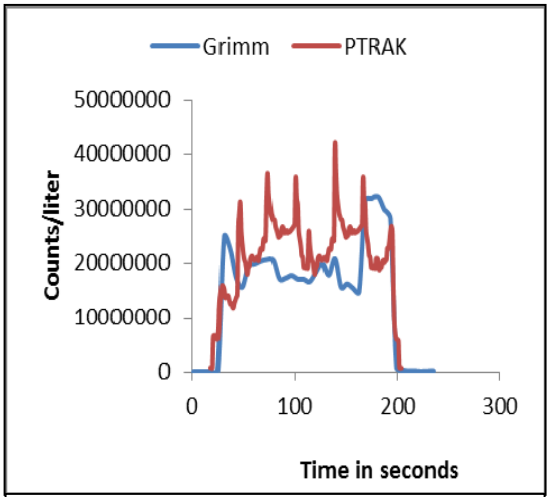

Speed: 6000 RPM

Feed: 381 mm/min

DOC: 3.81 mm

Figure 5-1: Multi-Instrument Kinetic Plots for UDC Composites

5.2 *Effect of Cutting Instantaneous Cutting Angle With Respect To Fiber Direction on the Machining Dust*

As mentioned in the previous sections, Semicircular slot tests were performed on the Uni Directional Composites. In order to find the effect of instantaneous cutting angles with respect to the fiber direction the total dust concentration and the counts were plotted against the angles of a semicircle from 0 to 180° in order to evaluate fiber direction effect.

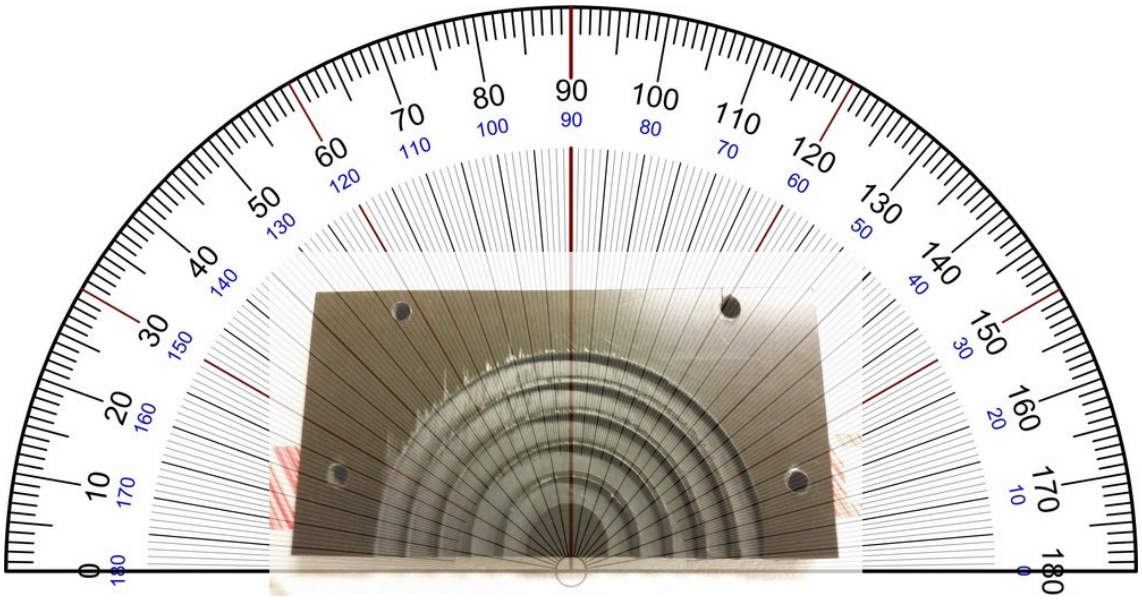

Figure 5-2: Circular slot

Fig. 5-2 shows a schematic of the angular variation of the machined slot and the angles associated with the data points being plotted. Using the total time of the test, it was simple enough to find the start and the end time of the experimental test because at the start the dust concentration is almost close to zero. Also similarly at the end of the test, the dust concentration goes almost close to zero as well. This gives us the time of the test that in turn helps us to associate the angles with the corresponding time data. The results are plotted mass concentration given by Casella and the particle counts given by PTRAK in Fig 5-3.

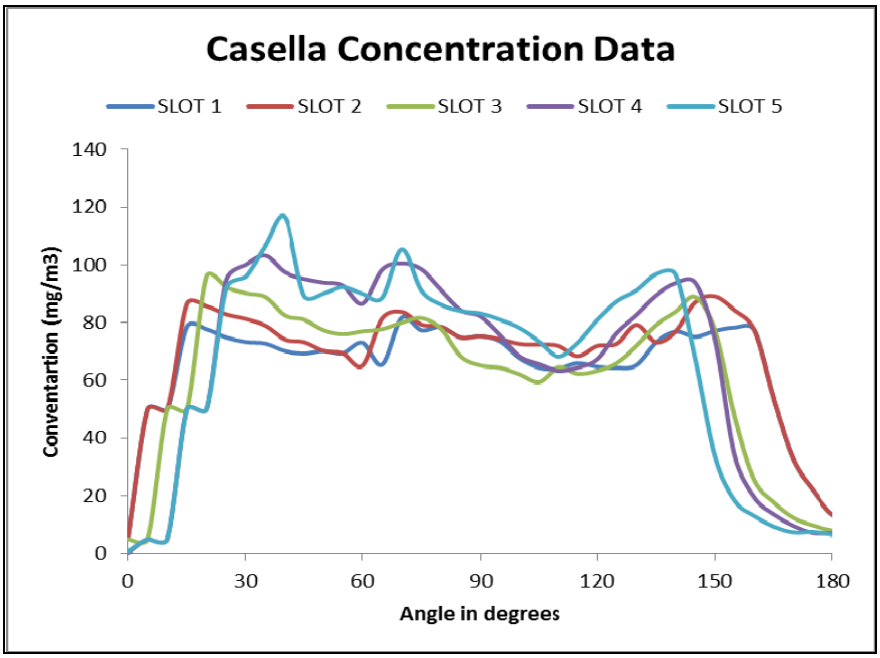

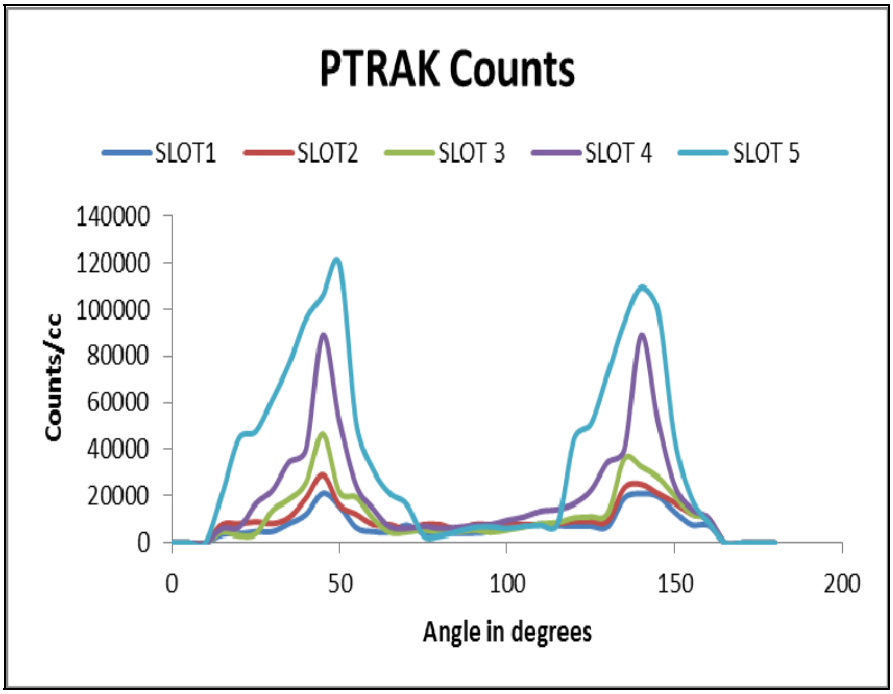

Figure 5-3: Casella and Grimm counts vs relative angle between the tool and fibers

As mentioned in the literature, the maximum damage is observed around the ± 45° relative angles [32] between the fiber direction and the instantaneous tool travel direction. In the above plots it's clear that the maximum counts and the maximum mass concentration are observed around the same mark of 45° and 135° relative angles. As the damages in machining is high, it's expected that the dust would higher because of the relatively high forces involved.

5.3 Effect of Cutting Instantaneous Cutting Angle With Respect Fiber Direction on The Machining Dust In Octagon Test

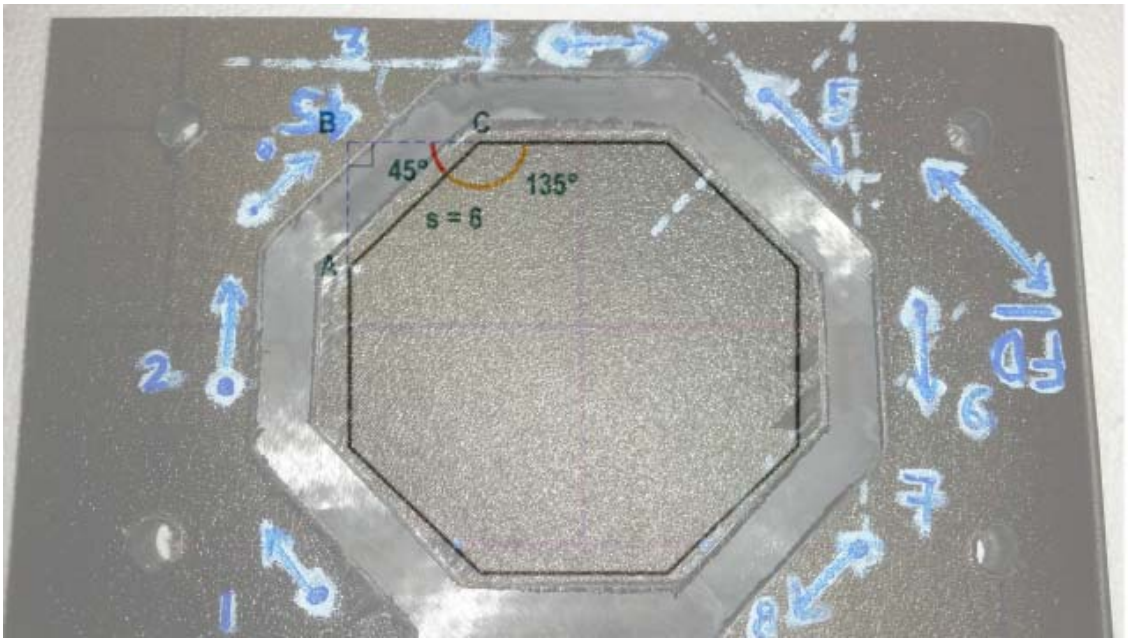

Figure 5-4: Octagon Test

In the case of this octagon in Fig. 5-4, the effect of instantaneous cutting angle with respect to fiber direction was achieved by taking average counts/ concentration in each of the slots and then plotting them versus the angle that the particular slot makes with the fiber direction and relative tool angle. The same is repeated for all the eight slots and the

data is represented as a histogram plot separately for the Casella and the PTRAK in Fig. 5-5.

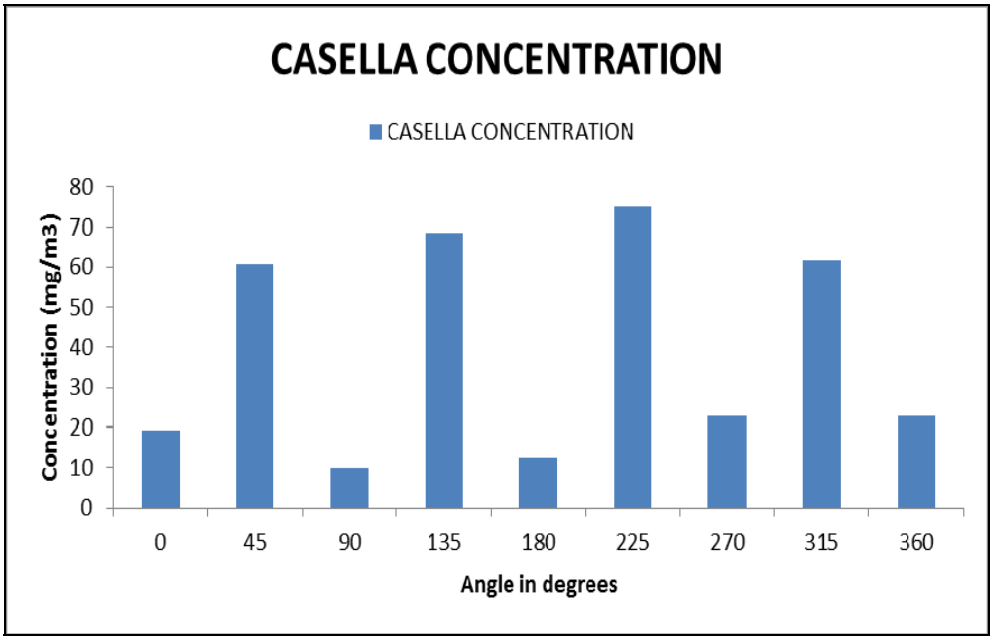

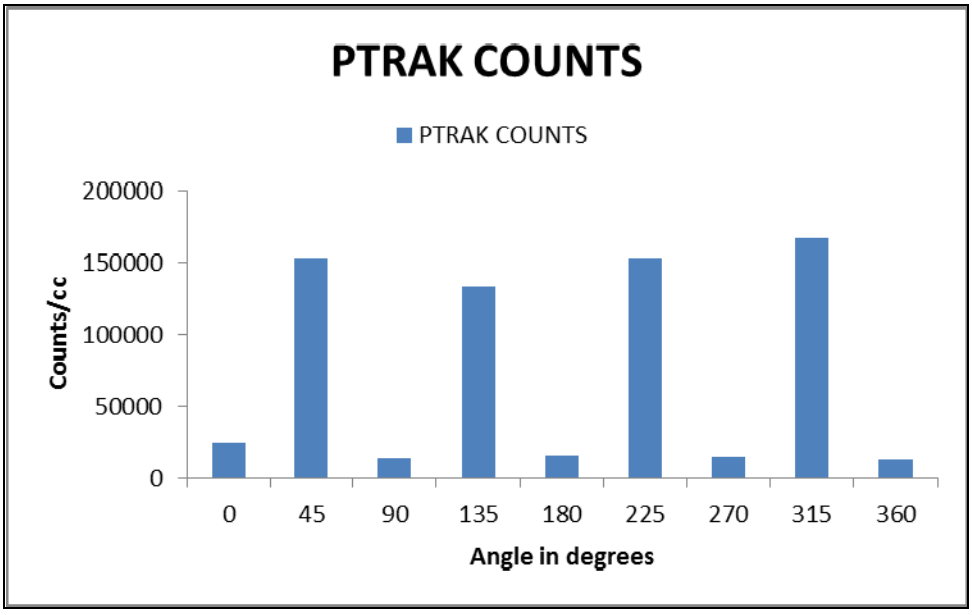

Figure 5-5: Casella and PTRAK data vs relative angle

In the above plots it's clear that the maximum counts and the maximum mass concentration are observed around the same mark of 45°, 135°, 225°, and 315° relative angles. As the damages in machining is high, it's expected that the dust would higher because of the relatively high forces involved.

5.4 Effects Of Linear Vs Contour Cutting

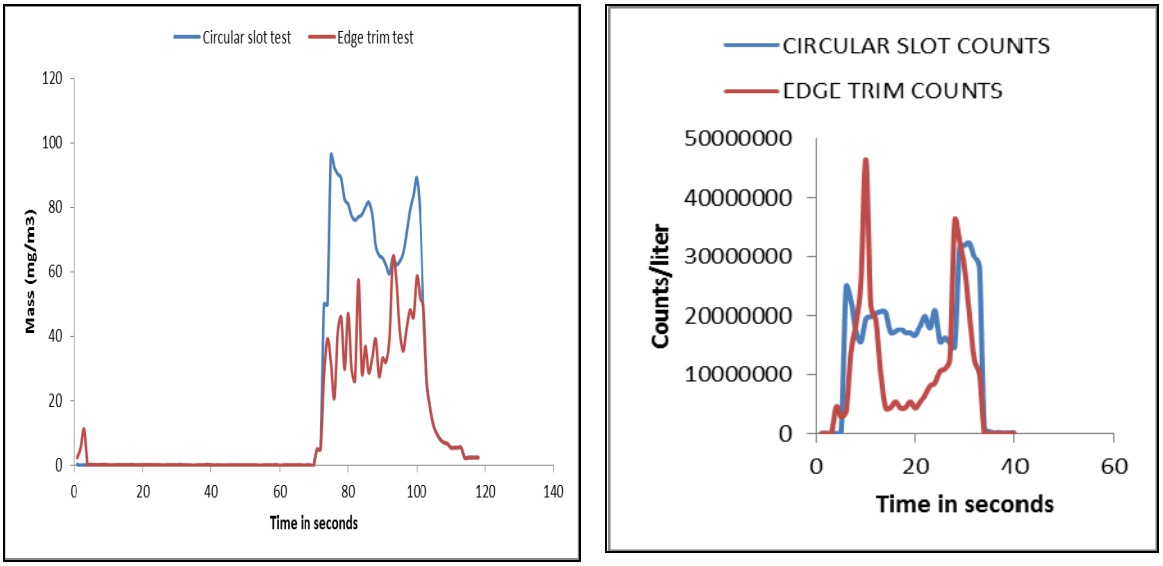

Figure 5-6: Linear vs Contour cutting

Fig. 5-6 shows the comparison of linear cut to contour cut in terms of dust emissions. Plots showing a circular slot test and edge trim was plotted for both counts and concentration from Grimm instrument in order to observe the behavior. The slot test was performed at speed of 6000 rpm, feed of 381 mm/min and depth of cut of 5.08 mm. The edge trim is performed 6000 rpm, feed of 381 mm/min and depth of cut of 3.81 mm. As the depths are different, direct comparison may not be valid. But conclusions can be drawn from the graph above. In both the graphs, we can clearly see that the disparity between the maximum and minimum counts or concentration is higher in circular slot cutting rather than in edge trimming. As explained in section 5.2, at relative tool to fiber angles between 45° and 315° the counts and concentrations are lower. In edge trim, there is no such zone where the counts and concentrations are lower. This advantage of cutting at an angle to the fibers can be utilized for low dust emission machining.

In an experiment was conducted by Jeffrey Miller [33], he performed edge trimming in a variety of conditions. He used multidirectional laminate composite and used different feeds, speeds and depth of cut to see the variation in dust using a similar setup of the instrument P-TRAK and Grimm to the one used in this thesis. A small comparison has been made between his data and the data collected in this thesis, in order to know the magnitude of measurements made and relative trend. In either case the speed was 6000 rpm, feed of 635 mm/min and depth of cut of 6.35 mm/min. Fig 5-7 represents the data from P-TRAK collected by Jeffrey Miller [33] for multi-directional laminate, while Figure 5-8 represents the P-TRAK data collected during edge trimming of UDC Composites used in the tests performed over the course of this thesis. The lowering of counts after each peak in Fig 5-7 is because of the overshoot of the milling cutter from the work-piece after each pass. In Fig 5-8 there is no drop in counts as there is no overshoot of the milling cutter. But a close look at the magnitudes suggest that the maximum number of counts recorded in both cases are very close to 27000 counts/cc which gives a good benchmark for data consistency. A similar trend is observed for Grimm counts and mass concentration as well as seen in Fig. 5-10.

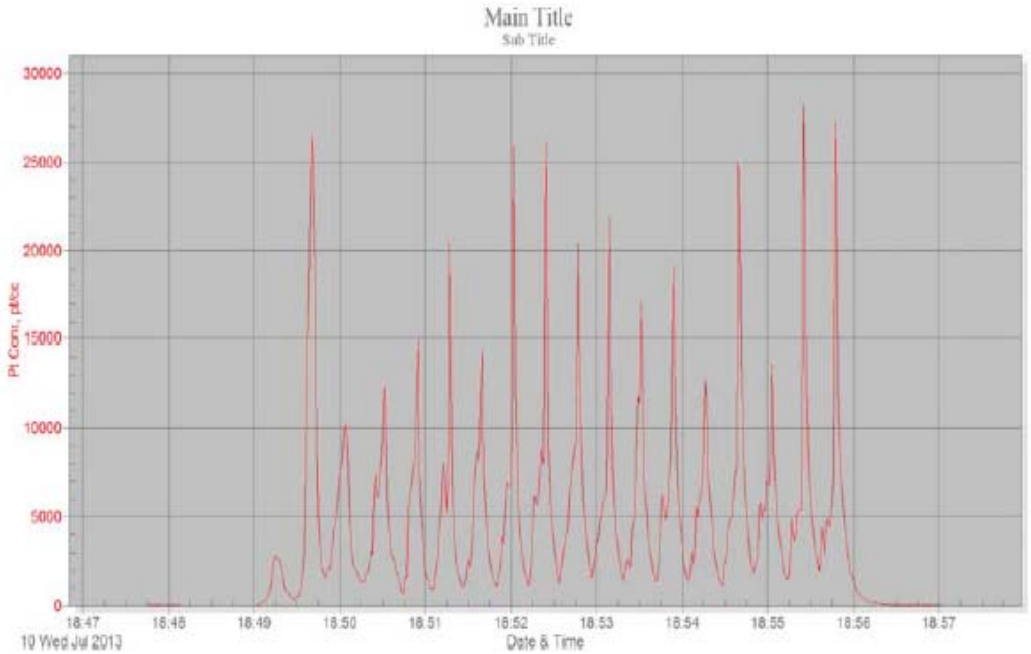

Figure 5-7: P-TRAK Data (Multidirectional)

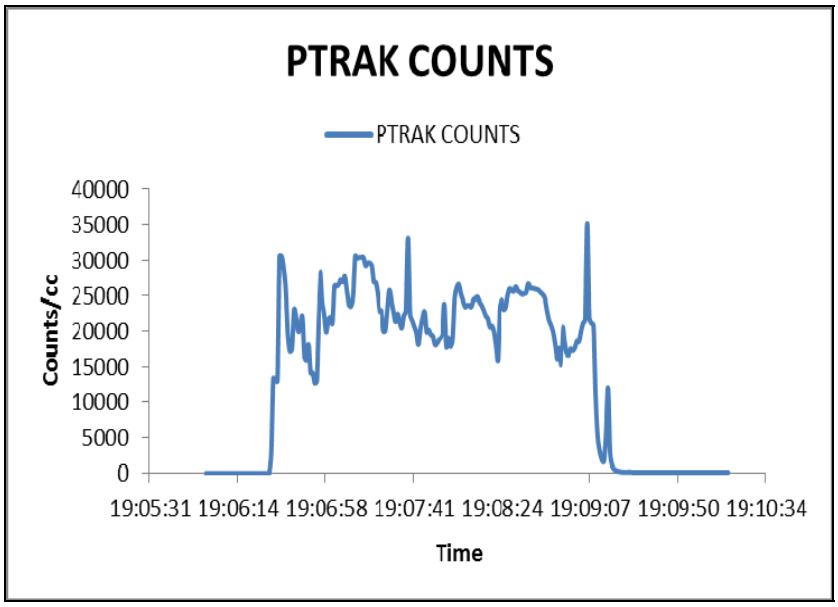

Figure 5-8: P-TRAK Data (Uni-Directional)

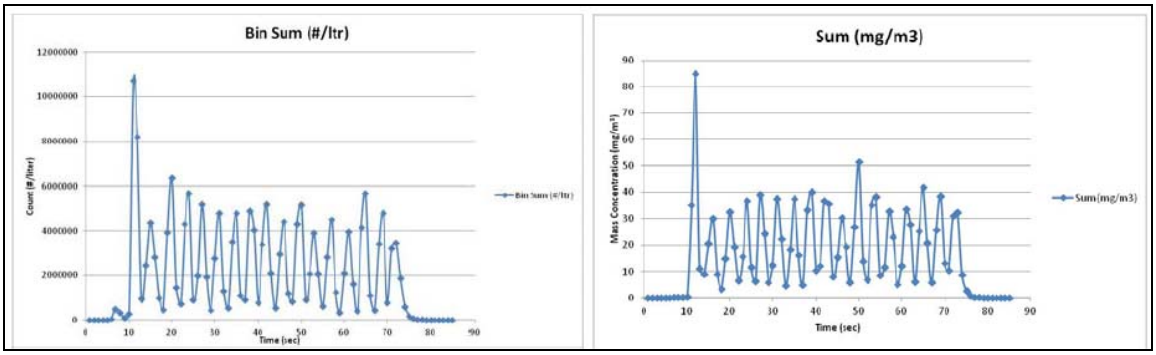

Figure 5-9: Grimm Data (Multidirectional)

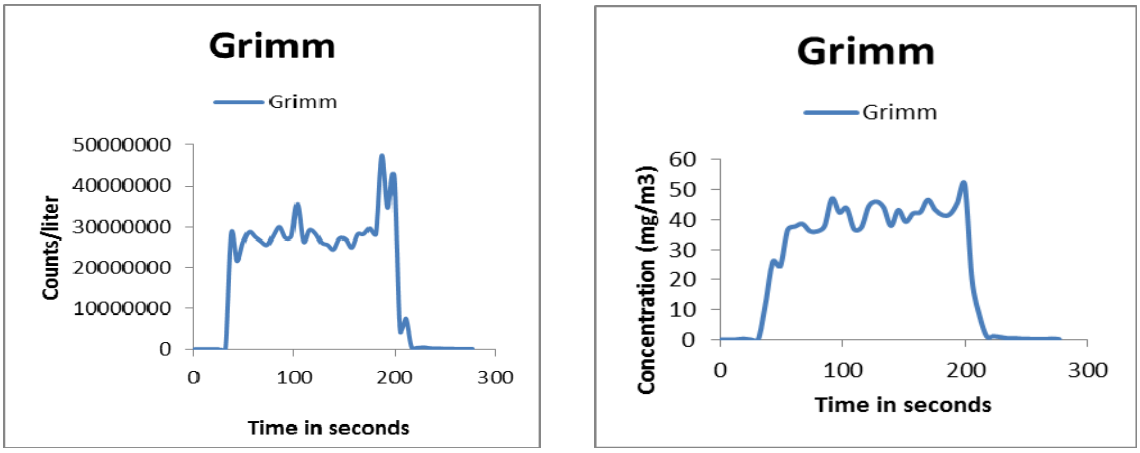

Figure 5-10: Grimm Data (Uni-Directional)

5.5 *Multi - Instrument Isokinetic Correlation in HexMC® Composites*

After unit conversions as described in section 5.1 and plotting the Grimm mass concentration data with the Casella Concentration data and the Grimm counts data with the PTRAK data, results were found to be very similar. The correlation between the data measured by the instruments were extremely good, indicating that the isokinetic sampling technique is very close to being optimum. Some of the plots are shown in the fig 5-11. Since they were plotted for each and every test, it becomes pointless to plot all of them in the main thesis. Hence the rest of them are added in the appendix B.

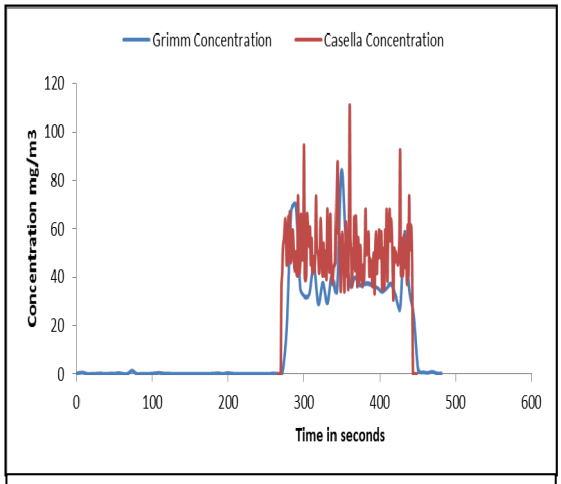

Speed: 6000 RPM

Feed: 635 mm/min

DOC: 6.35 mm

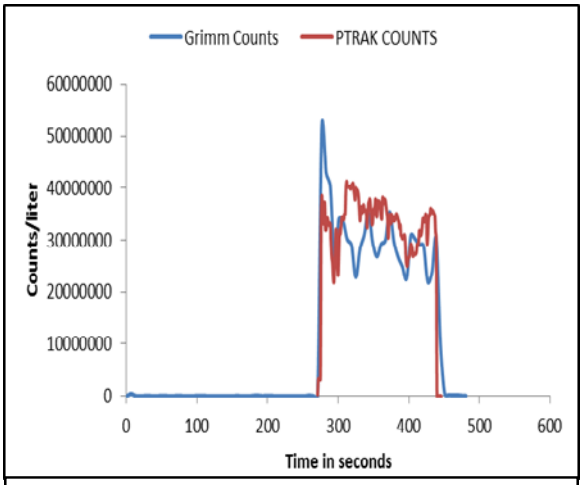

Speed: 1000 RPM

Feed: 635 mm/min

DOC: 6.35 mm

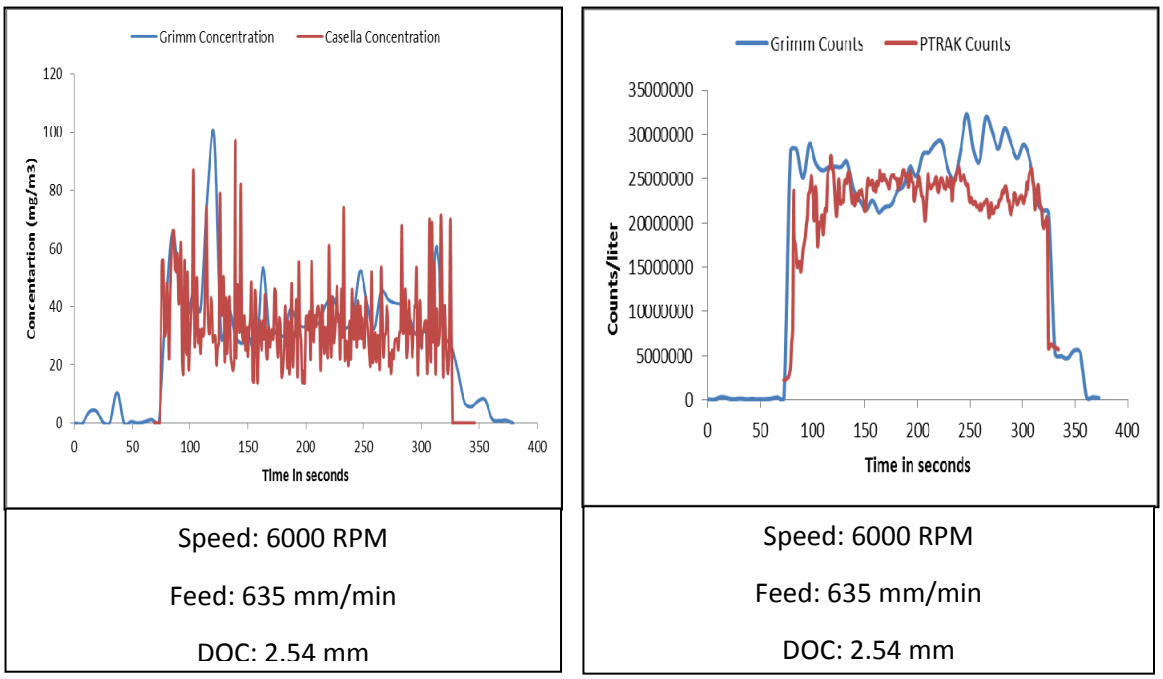

Speed: 6000 RPM Feed: 635 mm/min DOC: 2.54 mm	Speed: 6000 RPM Feed: 635 mm/min DOC: 2.54 mm

Figure 5-11: Multi-Instrument Kinetic Plots for HexMC

5.6 Sioutas Impactor Stages SEM Samples

The patented Sioutas Cascade Impactor separates and collects ultrafine, fine, and > 2.5-micron airborne particles (five size ranges including > 2.5 (Stage A), 1.0 to 2.5 (Stage B), 0.50 to 1.0 (Stage C), 0.25 to 0.50 (Stage D), and < 0.25 micron (Not used). Particles above each cut-point are collected on a 25-mm PTFE filter in each appropriate stage when the Sioutas Impactor is used with a 9 L/min sample pump. Particles less than the 0.25-micron cut-point of the last stage are collected on a 37-mm PTFE after-filter. This filter was not available, and hence not used in the test. Scanning electron images were taken for each filter stage for the unidirectional composites. For each stage, the images were taken at 6 to 7 different magnifications namely 50x, 500x, 1000x, 2000x, 5000x and a few at 10000x and 25000x. The ones detailed below are in the ones taken at 50x, 500x, 1000x and 2000x in the stated order for each stage. Fig 5-12 shows the photo micrographs taken for edge trimmed UD CFRP (a) and HexMC (b) for four filter stages A-D, while Fig 5-13 shows the smallest particle size in UDC and HexMC respectively. All additional SEM images can be found in Appendix F.

UDC Edge trim SEM Images

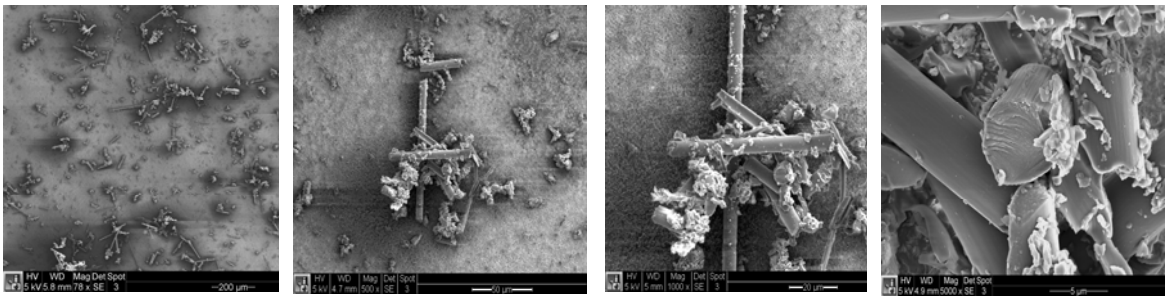

STAGE A

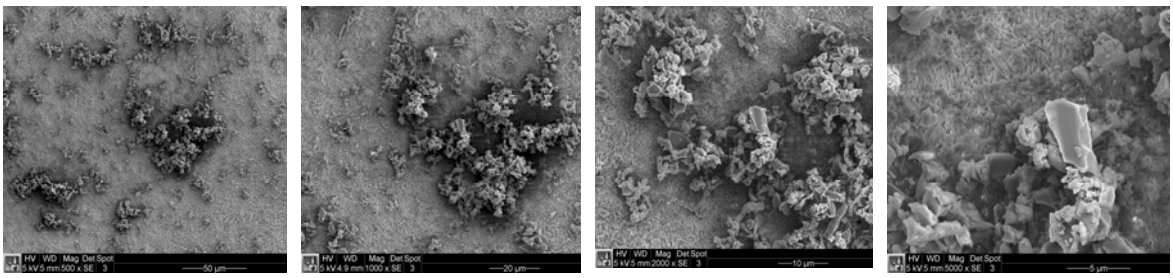

STAGE B

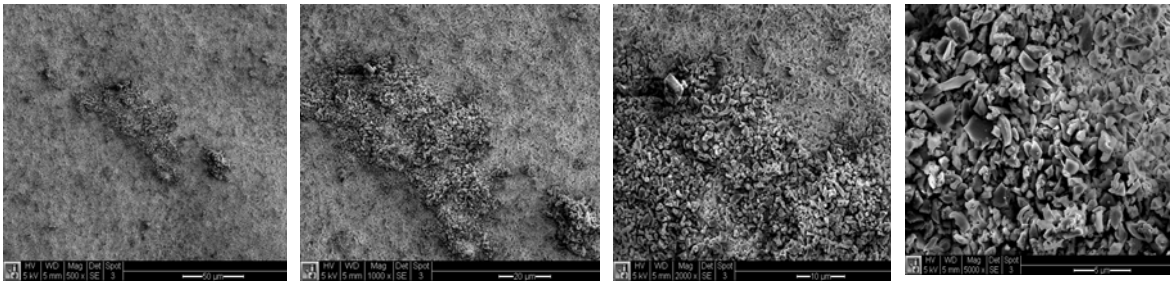

STAGE C

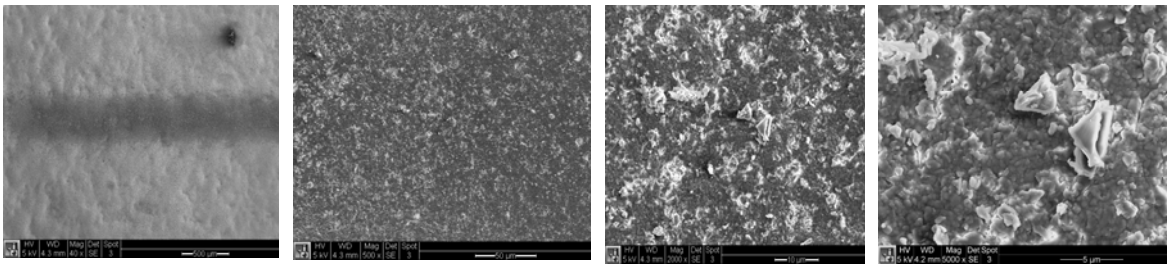

STAGE D

Figure 5-12 (a): Impactor micrographs UDC

HexMC® Edge trim SEM Images

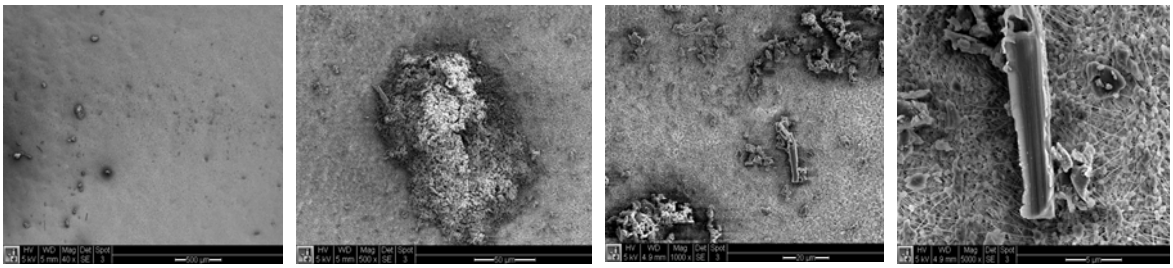

STAGE A

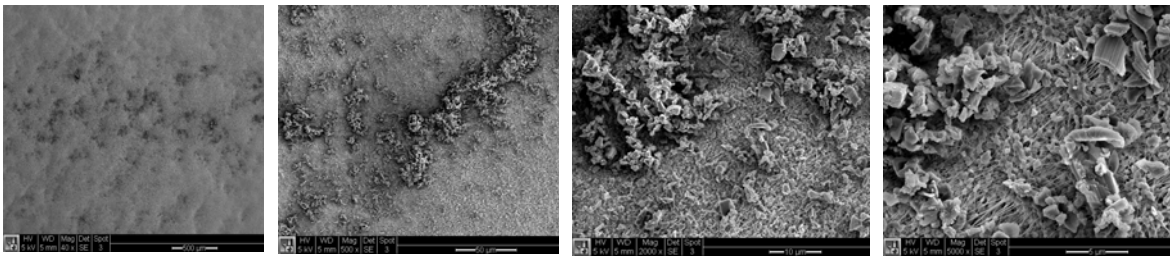

STAGE B

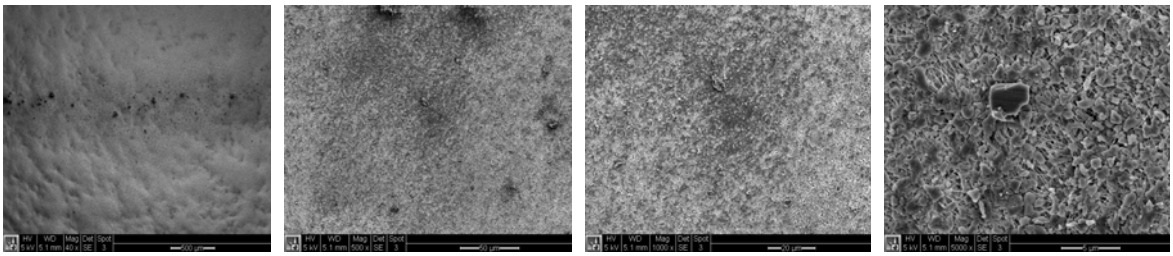

STAGE C

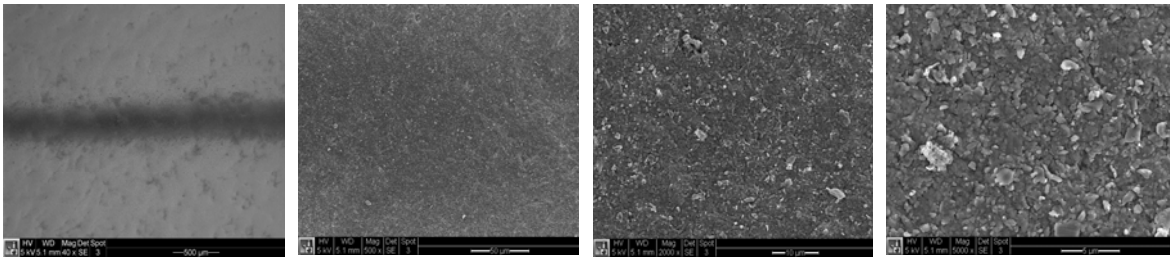

STAGE D

Figure 5-13 (b): Impactor micrographs HexMC®

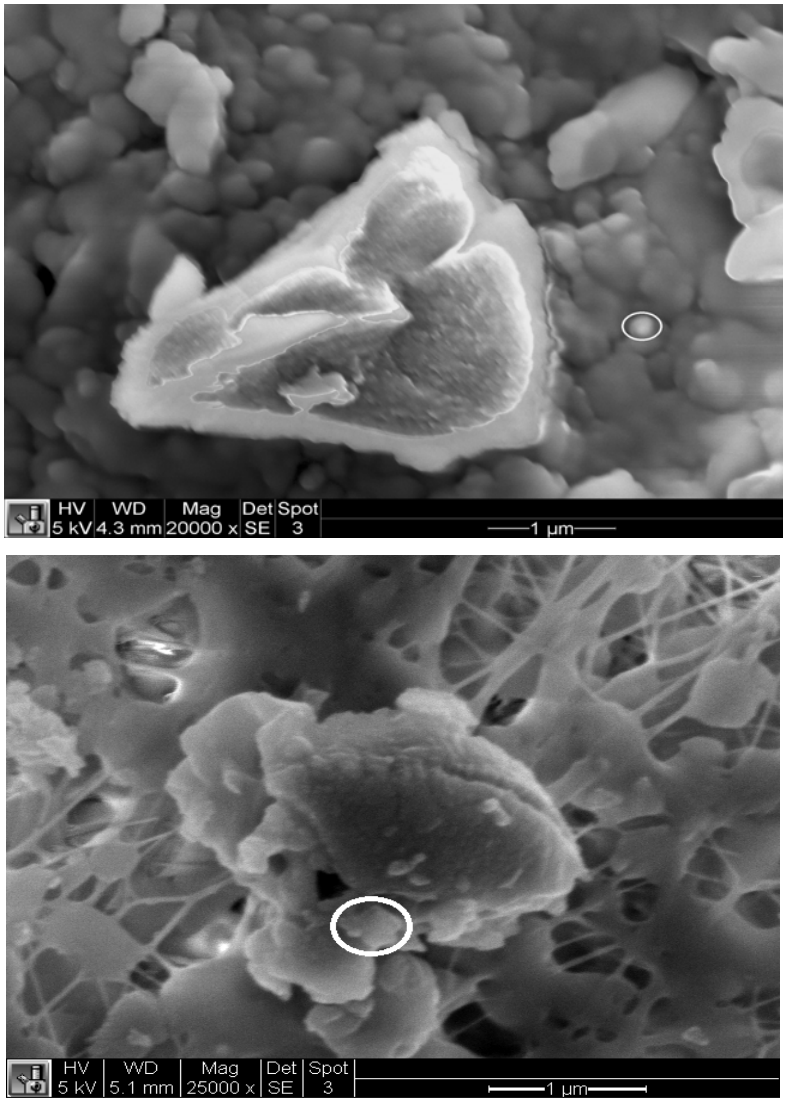

Figure 5-14: Magnified images of Stage D filter of UDC (Top) and HexMC® (Bottom)

From the image for UDC at the top, it can clearly be seen that the there are multiple particles smaller than about 0.2 µm. The one circled in the image at the top has a diameter of about 0.2 µm. In HexMC® composites the particle sizes are clearly larger. In the second figure, we can see that the smallest particle that can be seen in the image (circled) has a diameter of about 0.35 µm.

5.7 SEM Images Of Machining Dust On Carbon Tape

In this setup, a small piece of carbon tape was placed below the edge that was being trimmed. The vacuum was switched off and different feeds were varied. The test used constant speed of 6000 rpm and constant axial depth of cut of 6.35 mm. The feed used were 635 mm/min, 381 mm/min, and 127 mm/min. This was performed for both materials UDC and HexMC® Composites. Dust collected on tapes were also examined with SEM at 50x, 500x, 1000x and 2000x for each tape and corresponding material. Fig 5-15 represents the SEM images for varying federate for UDC (a) and HexMC (b) at different magnifications. Fig. 5-16 represents the SEM images taken at high magnification for UDC and HexMC at high feed rate for comparison. All remaining SEM images can be found in Appendix E.

UDC Edge trim on Carbon tape SEM Images

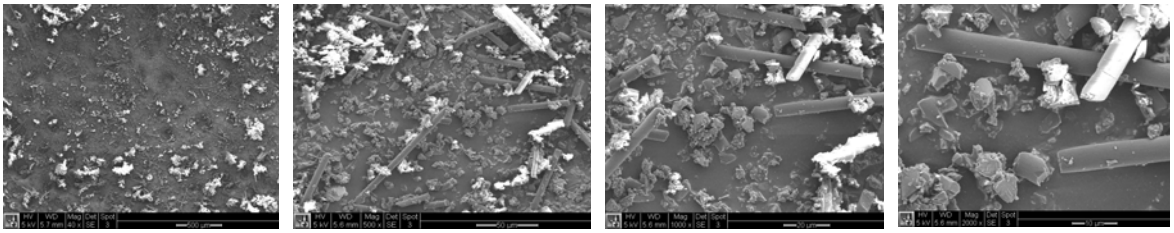

Feed : 127 mm/min

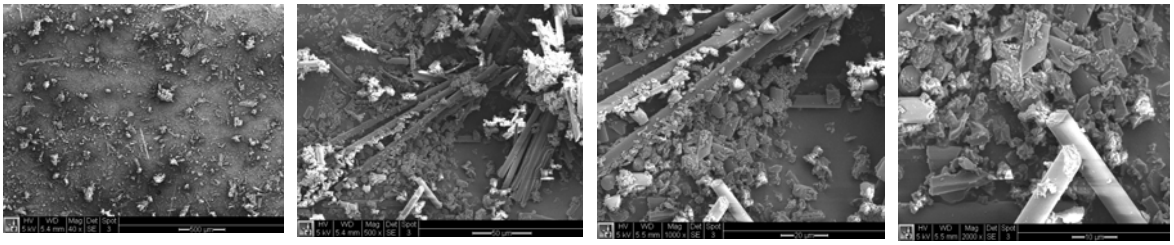

Feed : 381 mm/min

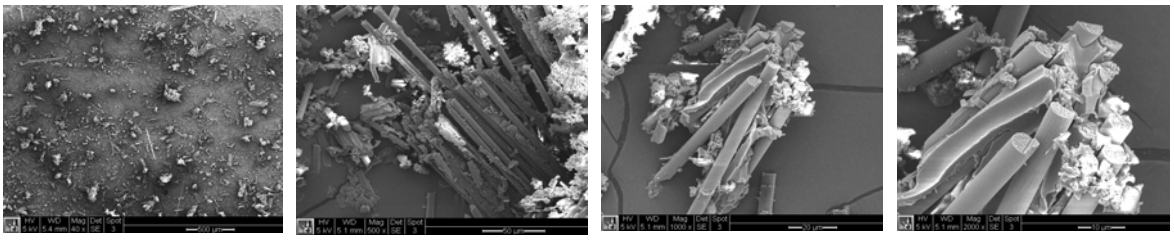

Feed : 635 mm/min

Figure 5-15 (a): Tape SEM UDC

HexMC® Edge trim on Carbon tape SEM Images

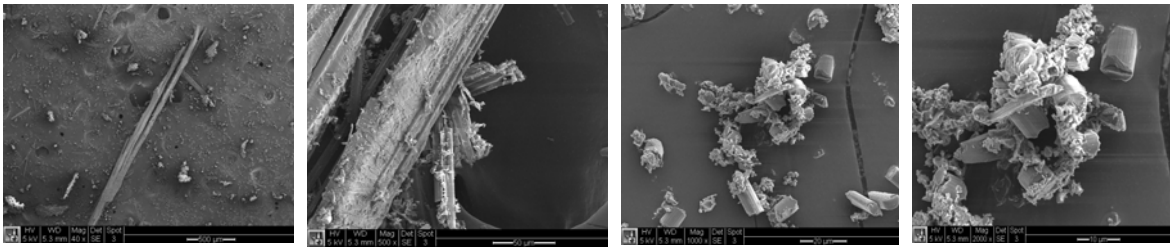

Feed : 127 mm/min

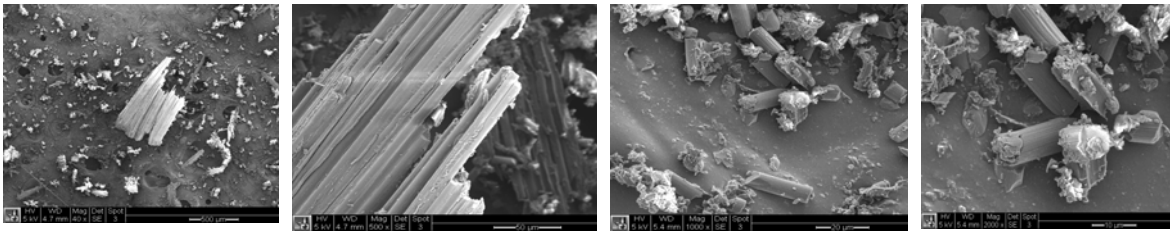

Feed : 381 mm/min

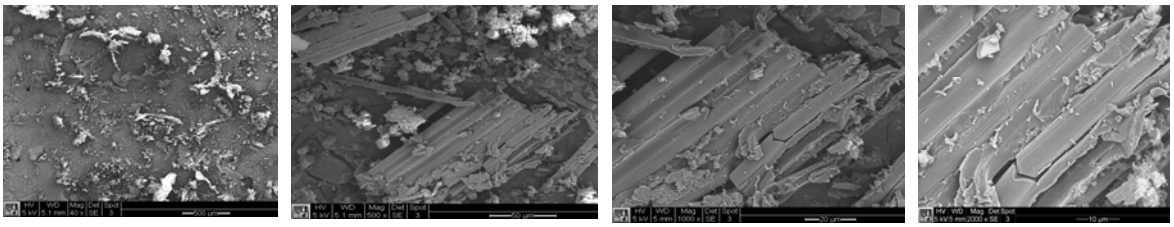

Feed : 635 mm/min

Figure 5-16 (b): Tape SEM HexMC®

As seen from the images from the tapes, we can clearly see that the particles sizes increases as the feed increases in both the materials. This explains the lower counts recorded by the instruments as the particle sizes are higher.

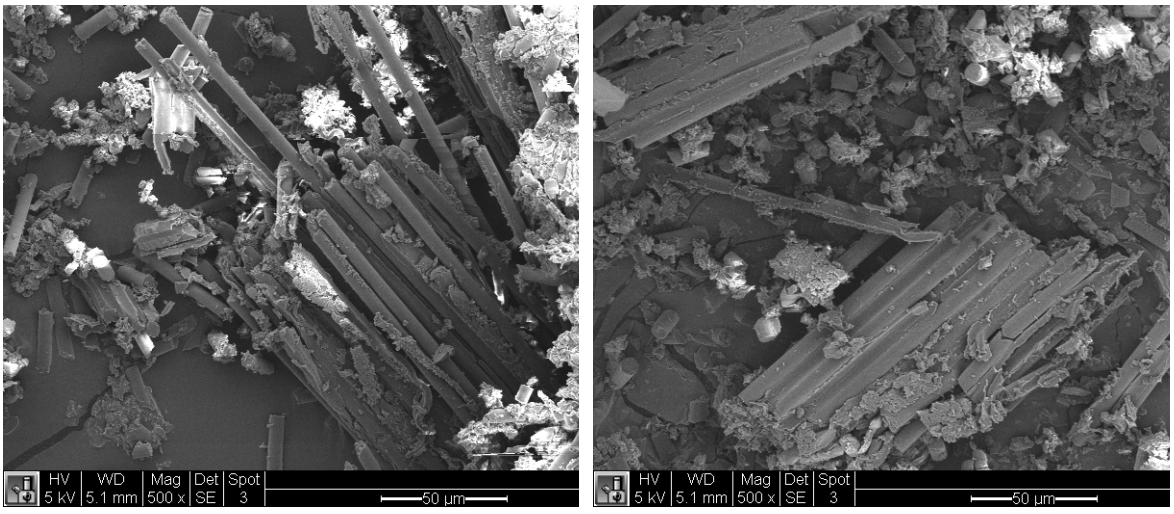

Figure 5-17: SEM Image (500x) at 635 mm/min feed for UDC (left) and HexMC® (Right)

From the image above, it can be clearly seen that in the UDC Composite, the fibers are pulled out of the matrix or fractured lengthwise or transverse. We can clearly see that the fibers are separated from each other and hence counts are recorded separately. This explains the higher counts. On the other hand, in the HexMC® composite the fibers are stuck together (this is because the fibers are in the form of a tape) and hence the particle sizes are much higher in HexMC®, leading to lower counts being registered.

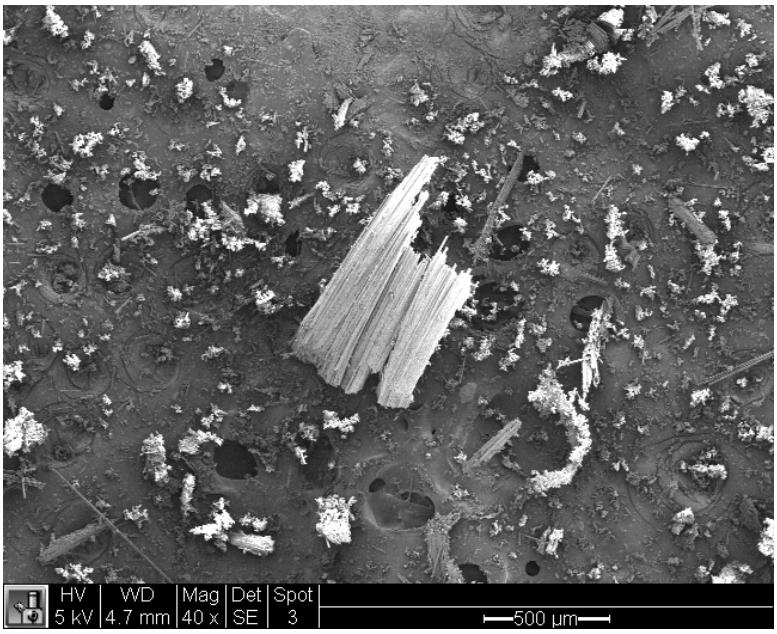

Figure 5-18: Large tape like fused particles in HexMC® Composite

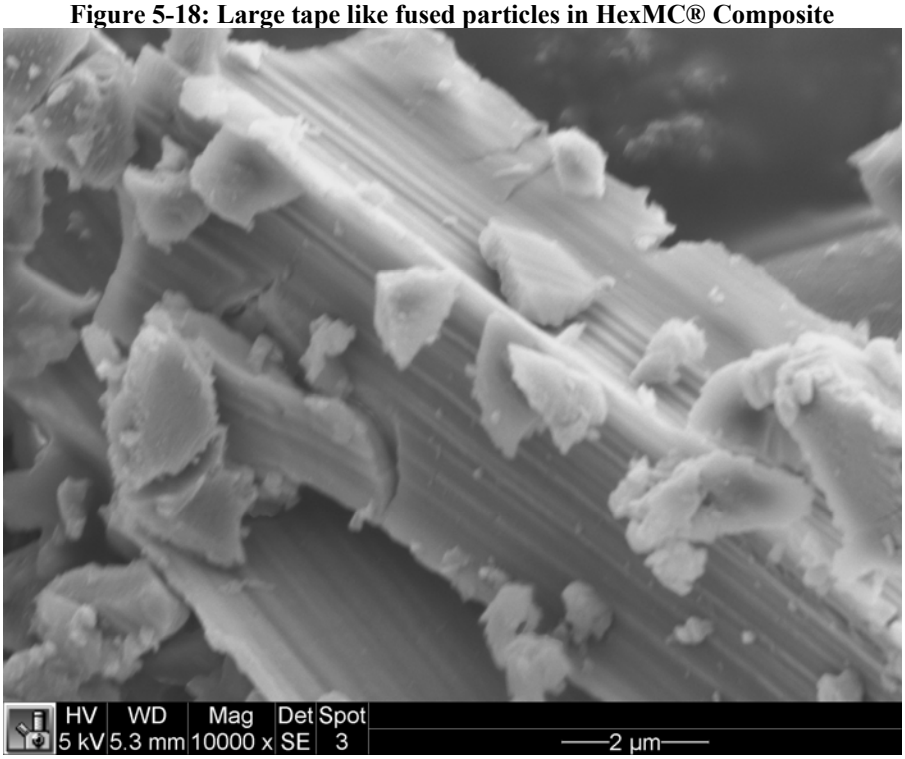

Figure 5-19: Fine particles in UDC Composites

Many particles comfortably smaller than 2 µm can be seen in fig. 5-11 to 5-18 suggesting that these smaller particles drive down the mean aerodynamic diameter to less than 0.3

μm. This can be verified using a calculation procedure for aerodynamic diameter shows as a flow chart in Fig. 5-19. Detailed steps are explained with pertinent equations.

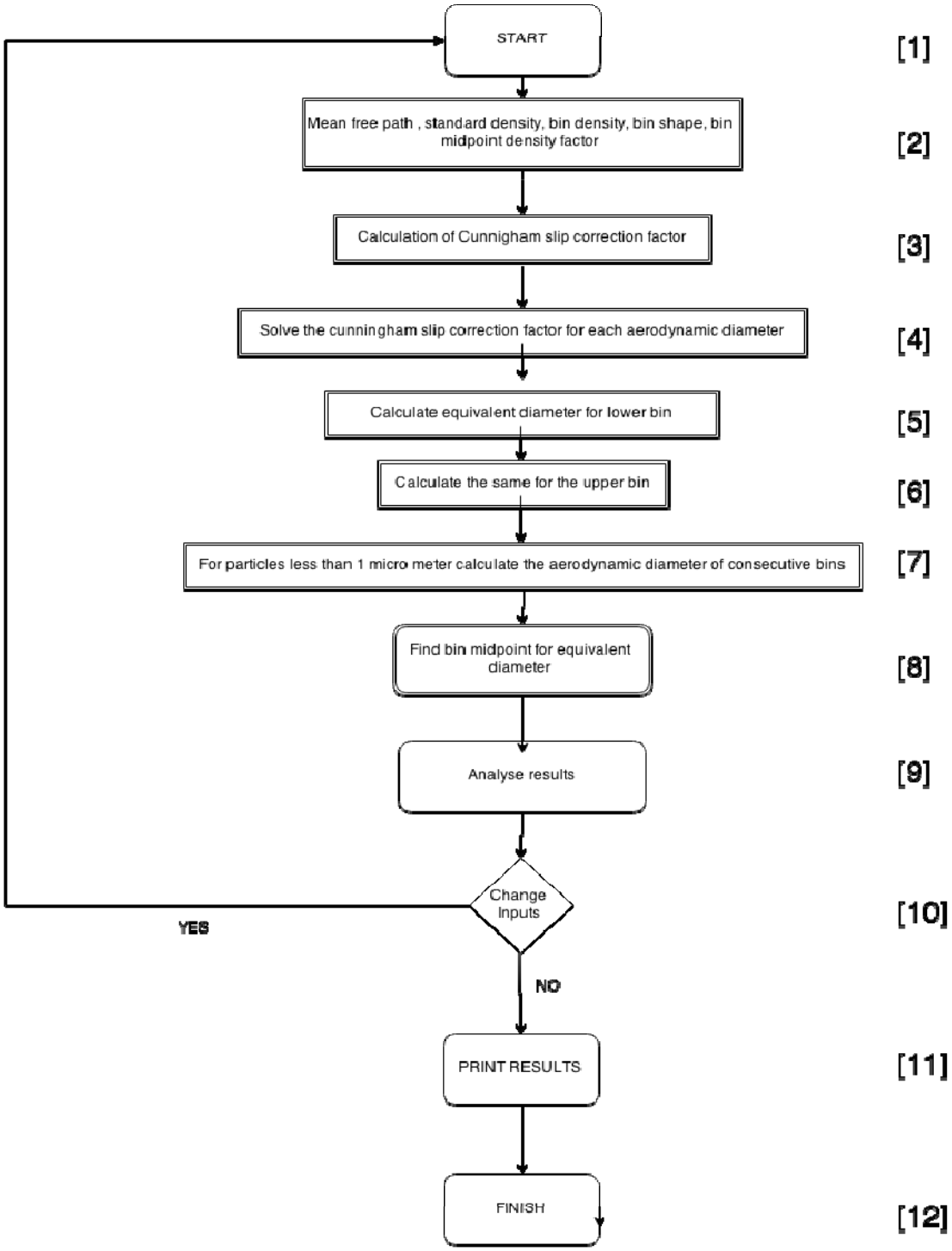

Figure 5-20: Aerodynamic diameter Model

SECTIONS AND THEIR PURPOSE

2	For this block, the mean free path, λ, standard density, ρ_a, estimated particle density, ρ_e, shape factor, χ, and midpoint factor are entered. Also d_e is the lower bin diameter. Pe is taken as 1.67 g/cc while χ is commonly taken at 1.5.
3	The Cunningham Slip Correction Factor, C_e, for direct particle measurement is calculated using equation with, d_e, being the low bin range diameter for a directly measured particle. The equation $C_e = 1 + \frac{2.52\lambda}{d_e}$ is used for particles between 0.1 µm and 1 µm While the equation $C_c = 1 + \frac{\lambda}{d}\left[2.34 + 1.05exp\left(-0.39\frac{d}{\lambda}\right)\right]$ is used for particles less than 0.1 µm
4	The equations $d_a = d_e\sqrt{\frac{C_e\rho_e}{C_a\rho_a\chi}}$ and $d_a = \frac{2.52\lambda}{C_a - 1}$ are combined in order to achieve the equation $\frac{2.52\lambda}{C_a-1} = d_e\sqrt{\frac{C_e\rho_e}{C_a\rho_a\chi}}$, which on simplification yields the equation $\frac{d_e\sqrt{\frac{C_e\rho_e}{C_a\rho_a\chi}}(C_a-1)}{2.52\lambda} = 1$
5	Here the lower aerodynamic bin diameter is calculated using $d_a = \frac{2.52\lambda}{C_a-1}$
6	The upper bin aerodynamic diameter, calculated in this section is simply an alternating substitution of the lower bin aerodynamic diameter as the upper bin diameter of a preceding bin is the same as the lower bin diameter of the

	following bin. Half of the Grimm bin sizes are less than 2.5 µm The equation used is $d_a = d_e\sqrt{\frac{\rho_e}{\rho_a \chi}}$.
7	The midpoints for all bin sizes are calculated in Section 6 and are nothing but the average of the upper and lower bin ranges
8	Results can be tabulated if desired in section 7.
9,10	Results of the findings are analyzed and decisions are taken to play around with different values of shape factors to get the correct aerodynamic variables nailed on.

Grimm aerodynamic bin diameter based model is used for analysis. An excel spreadsheet for aerodynamic diameter coupled with a Matlab solver for the slip correction factors was developed. Details of this spreadsheet can be found in the Appendix C.

5.8 Comparison of Aerodynamic Diameters

Aerodynamic diameters were calculated using the above model for both the materials i.e. unidirectional composites and HexMC ® composites. Plots for the counts were used as the input for the above model and the results of aerodynamic diameter vs particle counts for UDC and HexMC composites are shown in fig. 5-20

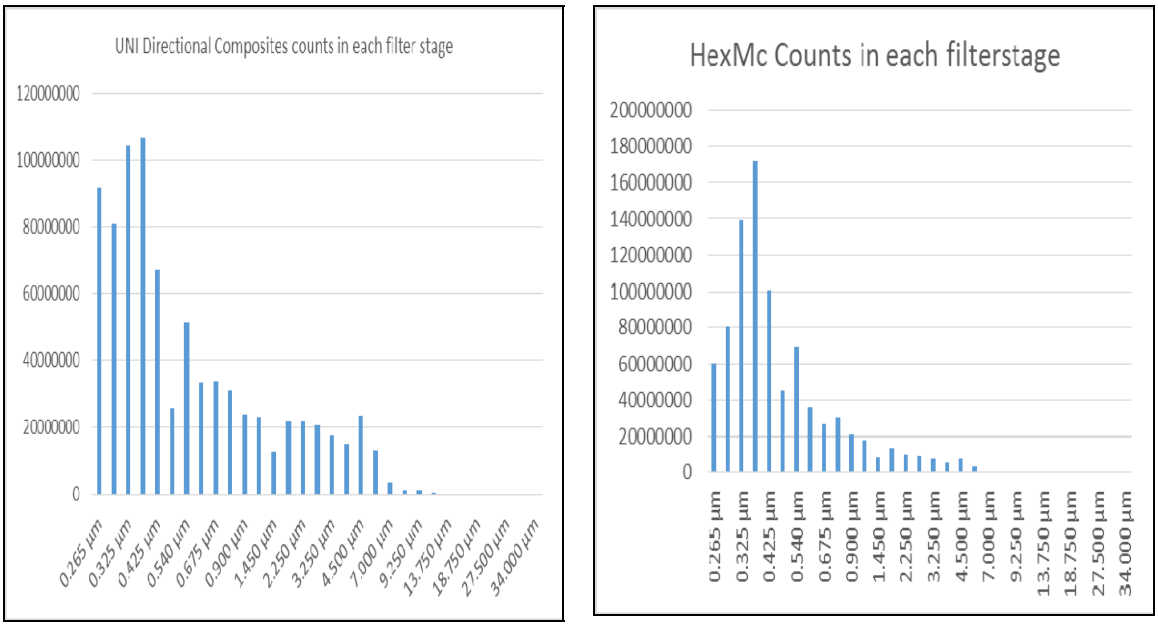

Figure 5-21: Counts in each filter stage for each material

From the spread sheet after inputting all the value into the bin diameters, data was calculated that the aerodynamic diameters for the material are tabulated below.

Material	Aerodynamic Diameter
Uni Directional Composites	0.17 µm
HexMC®	0.28 µm

The above can be explained by the fact that Unidirectional composites use carbon fiber cloth as the base material (carbon fibers in the cloth are separated and aligned and finer) while the HexMC® uses chopped carbon fiber tape (tape is 3mm wide).

5.9 Comparison of the Generated Dust on Human Health

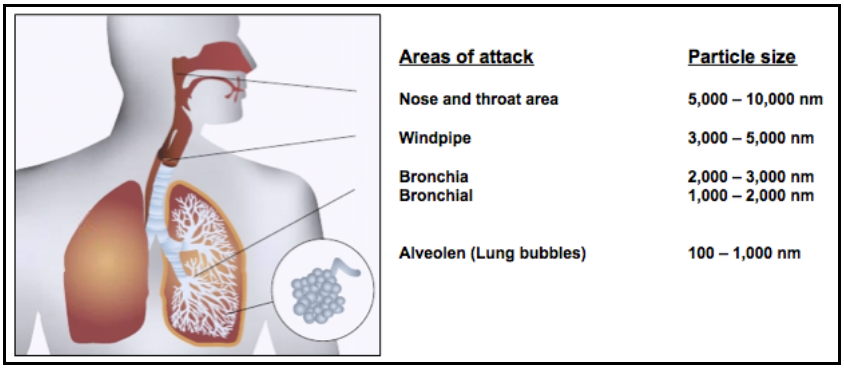

Figure 5-22: Areas of attack on human lungs[24]

Fig. 5-19 highlights the area of attack in human lungs [24]. The particles in between 5 to 10 µm cause irritation in the nose and throat, while those in between 3 to 5 µm enter the windpipe. The particle sizes in between 1 to 2 µm enter the arteries and veins in the lungs. Particle sizes less than 1µm enter the alveolen and can enter the blood stream via the ciliary interchange. A comparison of the different concerned particle sizes for Uni Directional and HexMC® composites are shown in the following pie-charts shown in fig. 5-23.

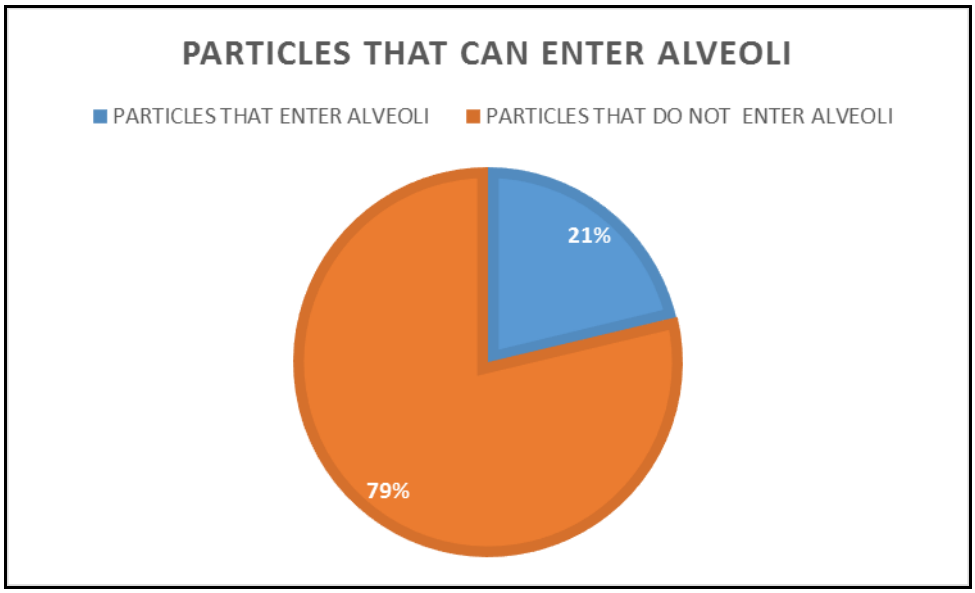

Figure 5-23: Particles entering alveoli UD-CFRP

Similar comparison was done for the HexMC® material.The results from that test are shown in fig 5-24.

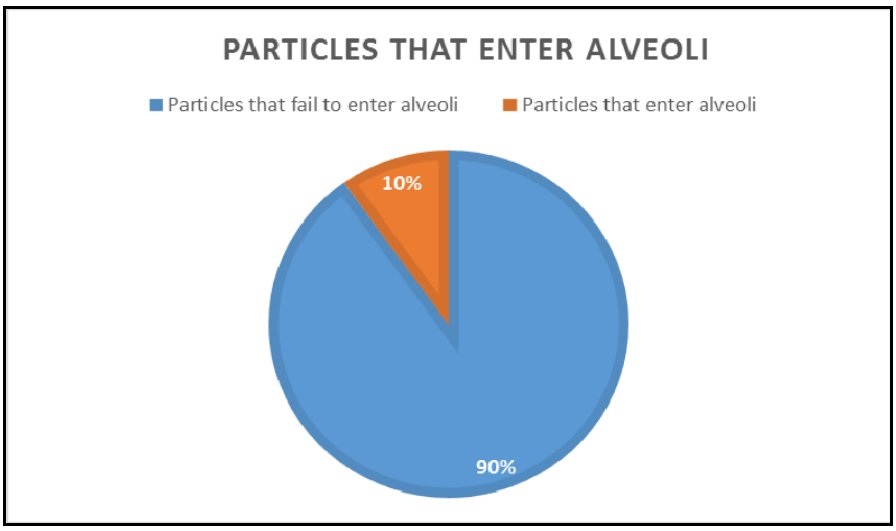

Figure 5-24: Particles entering alveoli HexMC

As it can be seen from the above figures that because the particle sizes (mean aerodynamic diameter) are larger in HexMC® the percentage of dangerous particles (particles that can enter alveoli) are smaller in HexMC® than in Uni-directional composites. Hence we can conclude that HEXMC® particles have less of a chance to enter the alveoli than Uni-Directional Composites. Even though in a comparison one appears safer than the other, the mean aerodynamic diameter ranges in between 0.19 to 0.28 µm these materials are not safe to machine out in the open. Heavy style gloves should always be worn when handling materials to protect against penetration of these fibers as well as contact with resins Protection of eyes and throat from carbon fiber dust is paramount. Users must wear full goggles and a dust mask to prevent dust inhalation. Dust particulate masks must be fit tested to the individual. Protective clothing should be worn whenever dust is created (such as while machining). The use of elastic cuffs on the protective clothing will keep dust from getting inside protective suits. Carbon fibers are electrically conductive and dust or waste can cause short-circuits within electrical equipment. Specific vacuum cleaners (designed specifically for extraction of conductive substances) should be used in conjunction with a suitable HEPA filter.

6 Chapter VI: Statistical Analysis of Experimental Data

6.1 Design of Experiments for Edge Trimming of Unidirectional Composites

To validate the experimental results it is necessary to conduct statistical analysis to draw meaningful conclusions. Statistical analysis helps in removing experimental errors obtained from the data, provide validity to the experimental results and attach a level of confidence to the results. This gives the experimenter the confidence that the experimental methods, results and conclusions are sound and valid. The statistical analysis is conducted using Stat-Ease Design of Experiments. The factors considered were spindle speed, feed rate and cutting distance and the response were particle counts and particle concentration. Since particle counts play a very important role in determining aerodynamic diameter, the counts response was used for analysis. The statistical design selected for this study is Response surface design since it is the design used for factors subjected to three levels. In our study for Uni Directional composites, we had three spindle speeds, three feed rates and three axial depth of cuts. The spindle speeds are 1000, 3000 and 6000 rpm. The feed rates are 635, 381, 127 mm/min and the axial depth of cut are 2.54, 3.81 and 6.35 mm. Following sections discuss in detail the statistical results.

6.1.1 Statistical Design Matrix for Average Counts

Based on the Factorial design we selected the Stat-Ease software will generate an experimental matrix where we have to enter the experimental data for analysis. Table 6-1 shows the statistical design matrix for edge trimming of Uni Directional Composites.

Table 6-1: DOE COUNTS TABLE FOR UNI-DIRECTIONAL EDGE TRIM

RUN NO	FACTOR 1 A:SPEED (RPM)	FACTOR 2 B:FEED(MM/MIN)	FACTOR 3 C:DOC (MM)	RESPONSE R1: GRIMM COUNTS(AVG) : Million Counts/liter
1	6000	635	3.81	23.48756
2	3000	635	3.81	19.82569
3	6000	635	2.54	18.62754
4	6000	635	6.35	26.75219
5	3000	635	2.54	17.65907
6	1000	635	2.54	11.45328
7	1000	635	6.35	16.34759
8	1000	635	3.81	13.25897
9	6000	381	6.35	26.62943
10	6000	381	3.81	23.14568
11	6000	381	2.54	19.67454
12	3000	381	6.35	26.89745
13	3000	381	3.81	24.37957
14	3000	381	2.54	17.68214
15	1000	381	2.54	19.54534
16	1000	381	6.35	25.40868
17	6000	127	3.81	31.24897
18	3000	127	3.81	25.43273
19	1000	127	3.81	23.45786
20	1000	127	2.54	18.67542
21	3000	127	2.54	24.11296
22	6000	127	6.35	33.5315

23	3000	127	6.35	29.11296
24	1000	127	6.35	27.78629

6.1.2 ***Statistical Output Analysis***

Once the data has been entered to the statistical design matrix, significance of the factors on the responses is analyzed using ANOVA, which is the statistical output. To identify the effect of factors on the response ANOVA analysis is conducted at a specific significance level or confidence interval known as α. Here Hierarchical Regression with Alpha to Enter = 0.050 has been used. Main things we have to note in this output are the ANOVA table, diagnostic plots, response surface and contour plot. Here we have Grimm average counts (Million counts/liter) as the Response data.

6.1.3 ***Anova Output for Average Counts***

Table 6-2: ANOVA OUTPUT FOR COUNTS

Analysis of Variance table (partial sum of squares)						
Source	SS	DF	MS	F-value	Prob>F	
Model	665.13	7	95.0178593	51.59161	<0.0001	*Significant*
A-Speed	0.33	1	0.33155069	0.180021	0.677005	*Not Significant*
B-Feed	238.11	1	238.1124714	129.2873	<0.0001	*Significant*
C-DOC	166.32	1	166.3189668	90.30579	<0.0001	*Significant*
Speed*Feed	1.67	1	1.667860668	0.905594	0.355442	*Not Significant*
Feed^2	0.04	1	0.035111586	0.019064	0.891905	*Not Significant*
DOC^2	9.81	1	9.813467195	5.328394	0.034673	*Not Significant*
Speed *Feed^2	50.27	1	50.26570995	27.29265	<0.0001	*Significant*
Residual	29.47	16	1.84173089			
Cor Total	694.59					
Std. Dev.	1.36		R-Squared	0.957576		
Mean	22.67		Adj R-Squared	0.939015		
C.V. %	5.99		Pred R-Squared	0.917577		
PRESS	57.25		Adeq Precision	28.95225		

From the ANOVA table 6-2 for average Counts we see that the model we have selected is significant since the prob>F value .00001 is less than the significance start level value 0.05, which indicates the model terms are significant. Here the model terms refer to A, B,

C that is spindle speed, feed rate and depth of cut. The ANOVA table shows that the response average counts mainly depends on individual effect of the factors and not on some interaction effect of the factors. ANOVA also gives an empirical relation between the responses and factors in the form of an equation from the experimental data. The equation is,

Average Counts =

+2.64063

+3.31588E-003 * Speed

+0.044620 * Feed

+5.61581 * Depth of Cut

-1.74913E-005 * Speed * Feed

-8.19340E-005 * Feed^2

-0.43793 * Depth of Cut^2

+2.37753E-008 * Speed * Feed^2

This relation will be very useful in process optimization so that the researcher can select the parameters depending on the counts set by the researcher. Another useful information we can get from the ANOVA output is the variability in the data which is given by R-squared and adjusted R-squared values. R-squared values should be between 0 and 1. Difference between R-squared and adjusted R-squared values should be below 0.2 which indicates that variability in data is minimum. Here counts R-squared is 0.9576 and adjusted R-squared is 0.9390. This indicates that there is a high level of fit.

6.1.4 Residual Analysis for Average Counts

In order to check the validity of the Anova model, examination of residuals plots is conducted. To see that our model assumptions are not violated we need to see that the

residuals for the normal probability plot are distributed along a straight line. For outlier plots we need to see that there is no unusual response in the experiment conducted, if our model is good all the residuals lie within the ± 3.5 limit. For residuals vs factor plots we need to see that the residuals are of constant variance. For residuals vs predicted we need to see that residuals do not follow any trend. Residual plots for average counts are shown in the figure 6-1.

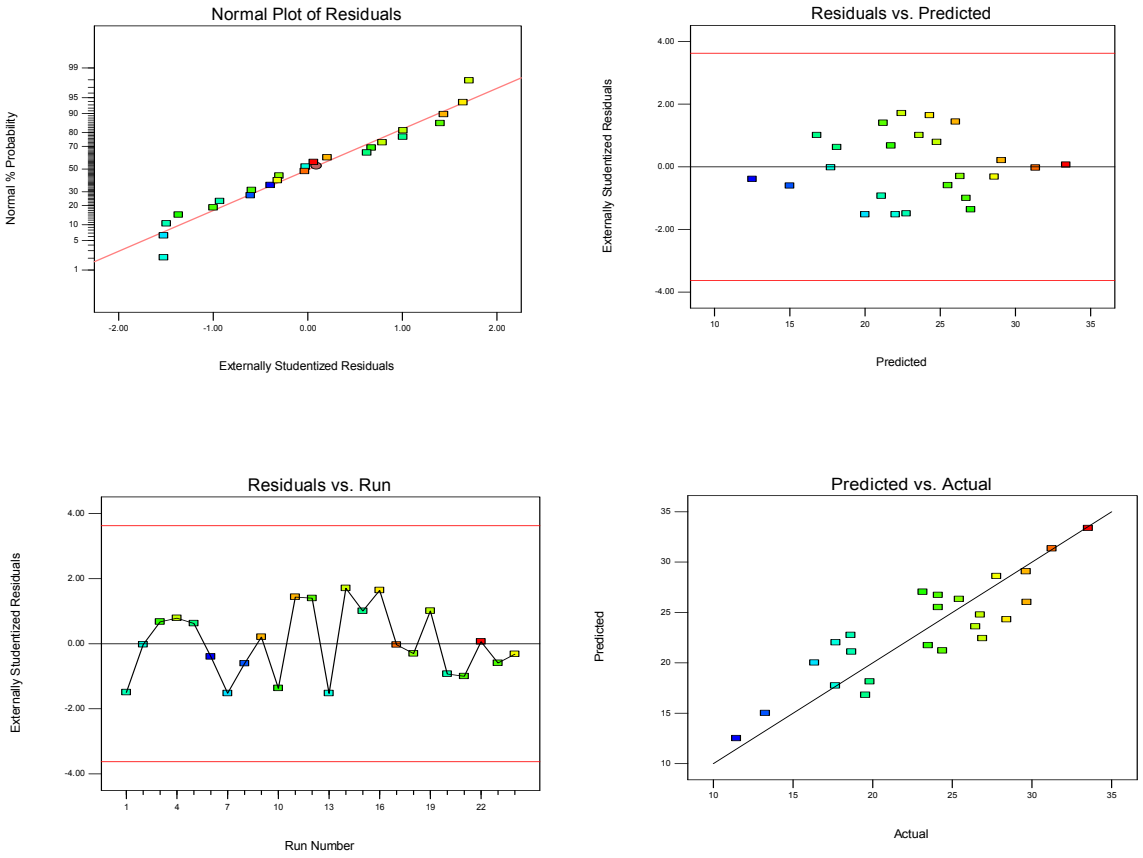

Figure 6-1: Residual Plots

All the plots in fig 6-1 do not show any violation of model assumption and we can conclude that our model is good for prediction.

6.1.5 Contribution of the Different Factors on Counts

Table 6-3: Contribution of different factors on response

Model Parameters		% Contribution
A-Speed	0.33	*negligible*
B-Feed	238.11	*48*
C-Depth of Cut	166.32	*34*
Speed*Feed	1.67	
Feed^2	0.04	*negligible*
DOC ^ 2	9.81	*2*
Speed *Feed^2	50.27	*10*
Residual	29.47	6
Correlated Total	694.59	100

The percentage contribution of the main factors is found by dividing the sum of squares of the individual factors by the correlated total is and shown in Table 6-3. The above table clearly shows that among the individual factors, feed is the most important factor, followed by depth of cut and then by the speed. It is important to note that the interaction factors also play an important role.

6.1.6 Effect of the Important Model Terms on Counts

As seen from the table 6-3, we can clearly say that feed, speed and interaction between the square of speed and feed play an important role in the responses.

6.1.7 ***Effect of Feed Rate***

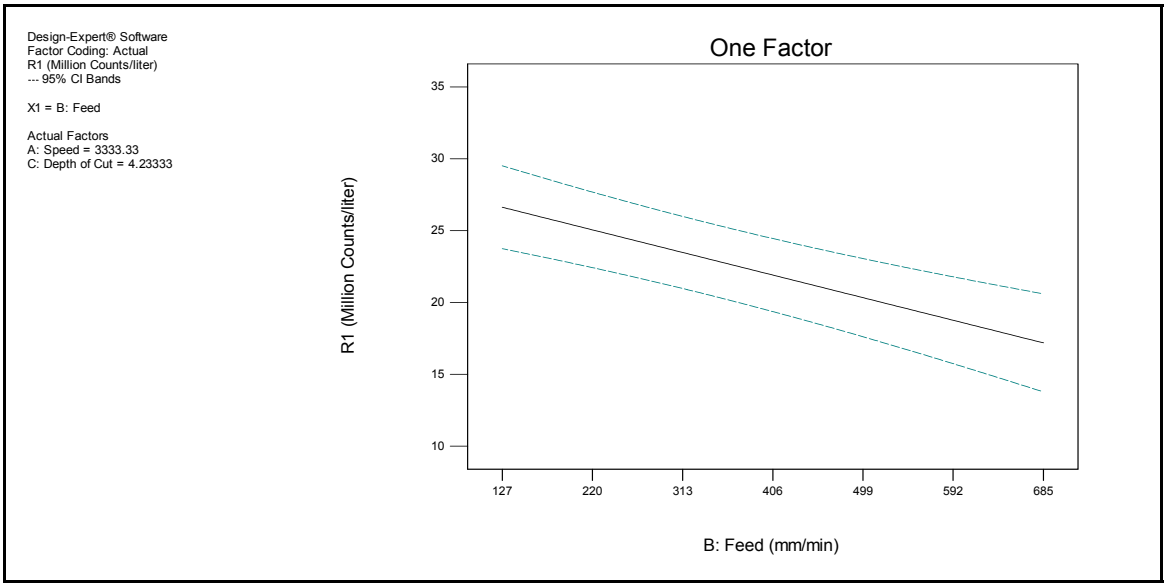

Figure 6-2: Effect of Feed Rate

From Fig. 6-2 it can be clearly seen that the counts of particles decreases with an increase in feed rate. This can be explained from the fact that at a higher feed rate, the exposure time per area of the work piece is lower than in a low feed. Also when machining at a high feed rate, the cut is very coarse, meaning the particle sizes would be higher than in a slow feed. But for the same volume of material machined, the number of particles generated for a coarse cut would be leaser because of their larger sizes and overall equivalent higher cumulative mass. In case for a low feed, the particles will be much finer, leading to higher counts.

6.1.8 *Effect of Spindle Speed*

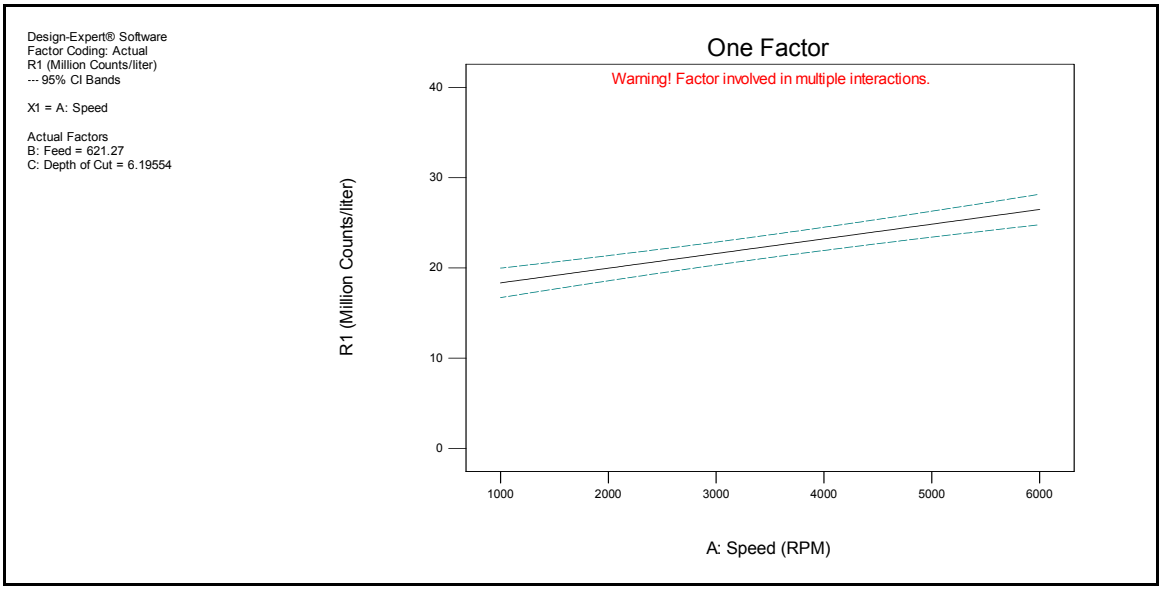

Figure 6-3: Effect of Spindle Speed

From Fig. 6-3 we can clearly see that the particle counts are higher at higher spindle speed and lower at lower spindle speed even though the contribution to the model is negligible This can be explained by the definition of spindle speed. Spindle speed is defined as the number of revolutions that the cutter makes per minute. Since the tool used was a four flute cutter, the number of times the teeth of the end mill would contact the work piece would depend upon the spindle speed. At 1000 rpm the no of contacts of the cutting edges with the cutting material will be 6 times less than that of a 6000 rpm spindle at the same feed and depth and equivalent cutting time. Since the contact made in a given period time is more in 6000 rpm spindle speed than in 1000 rpm spindle speed, the counts are higher at higher rpm.

6.1.9 *Effect of Depth of Cut*

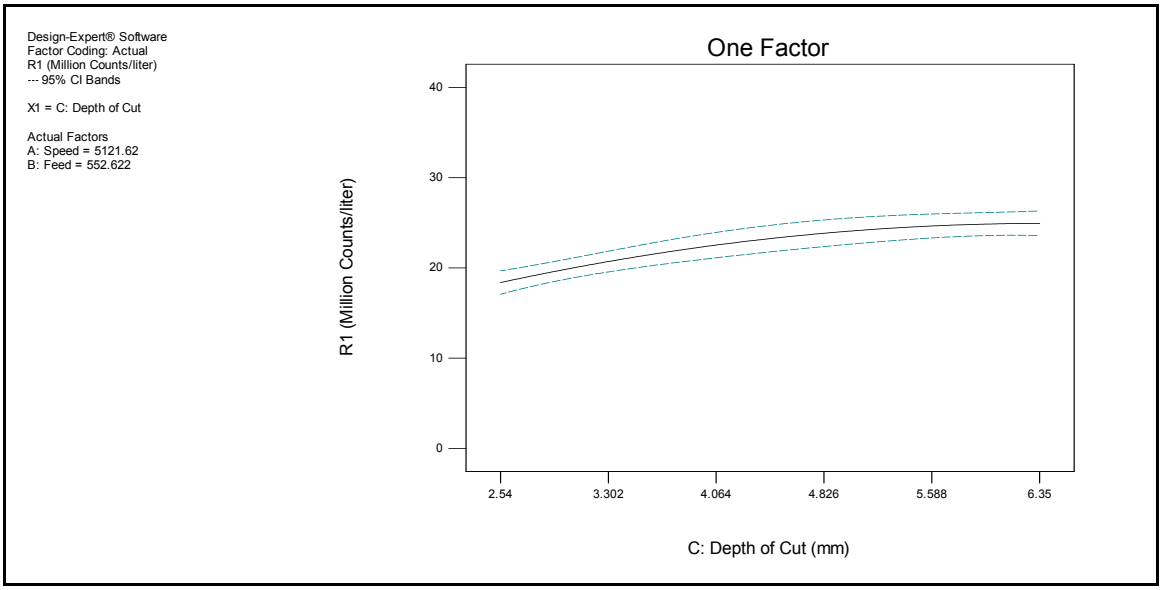

Figure 6-4: Effect of Depth of Cut

The depth of cut is a significant factor that affects the counts. As we can clearly see from the fig. 6-4, the counts increase with the increase of the depth. This can be explained by the fact that the higher depth causes higher contact with the work piece causing higher volume of material removal.

6.1.10 ***Interaction Effects of Feed and Speed***

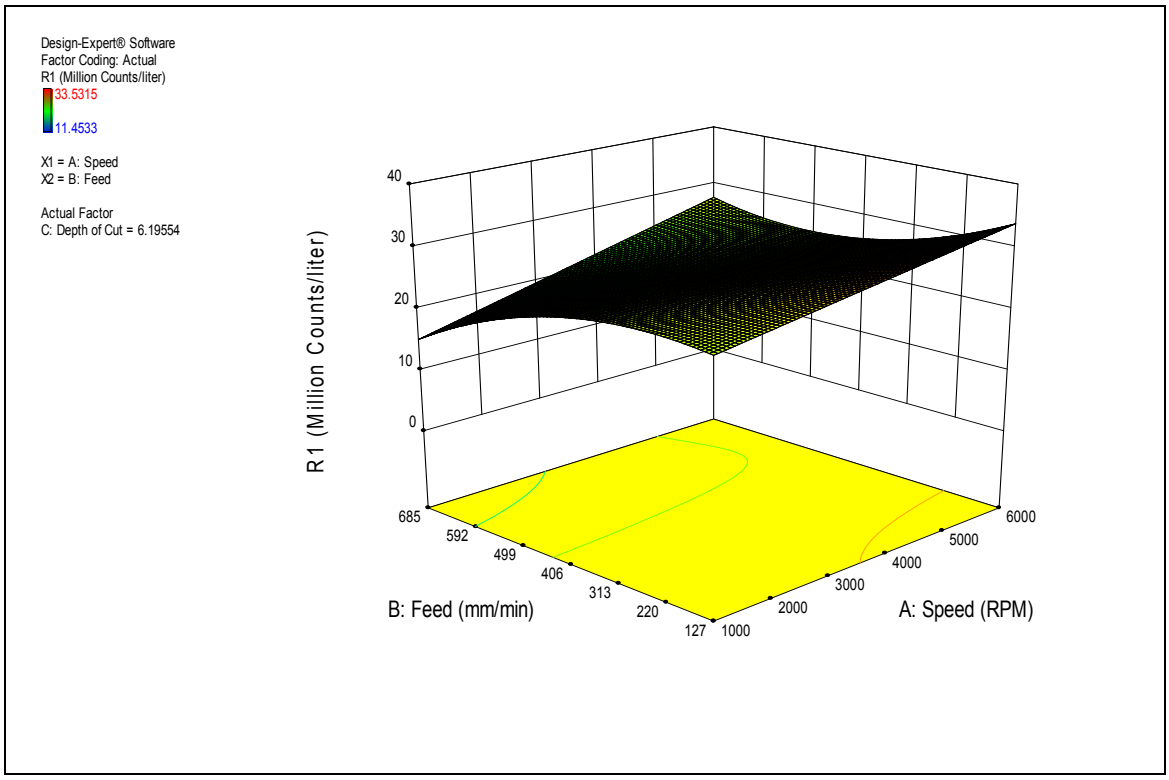

Figure 6-5: Effect of feed and speed

From the Fig 6-5, it can be clearly seen that interaction effect plays a significant role in the response. It can be seen that almost at all the areas of the plot except at higher speed, the dust counts seems to reduce with an increase in feed.

.

6.2 Statistical Design Matrix for Average Concentration

Table 6-4: DOE MASS TABLE FOR UNI-DIRECTIONAL EDGE TRIM

RUN NO	FACTOR 1 A:SPEED (RPM)	FACTOR 2 B:FEED(MM/MIN)	FACTOR 3 C:DOC (MM)	RESPONSE R1: GRIMM CONCENTRATION (AVG) : mg/m^3
1	6000	635	3.81	28.89
2	3000	635	3.81	34.76
3	6000	635	2.54	36.27
4	6000	635	6.35	39.29
5	3000	635	2.54	28.45
6	1000	635	2.54	20.57
7	1000	635	6.35	33.78
8	1000	635	3.81	25.63
9	6000	381	6.35	51.23
10	6000	381	3.81	44.24
11	6000	381	2.54	41.65
12	3000	381	6.35	31.13
13	3000	381	3.81	39.15
14	3000	381	2.54	42.46
15	1000	381	2.54	27.36
16	1000	381	6.35	45.13
17	6000	127	3.81	54.36
18	3000	127	3.81	49.221
19	1000	127	3.81	50.13
20	1000	127	2.54	39.41
21	3000	127	2.54	49.45
22	6000	127	6.35	67.397
23	3000	127	6.35	49.45
24	1000	127	6.35	61.7342

6.2.1 Anova Output for Average Concentration

Once the data has been entered to the statistical design matrix seen in Table 6-4, significance of the factors on the responses is analyzed using ANOVA, which is the statistical output. To identify the effect of factors on the response ANOVA analysis is conducted at a specific significance level or confidence interval known as α. Here Hierarchical Regression with Alpha to Enter = 0.010 has been used. Main things we have to note in this output are the ANOVA table, diagnostic plots, response surface and contour plot. Here we have Grimm average concentration in mg/m^3 as the Response data.

Analysis of variance table [Partial sum of squares]						
Source	SS	DF	MS	F-Value	Prob > F	
Model	2942.78	8.00	367.85	36.21	<0.0001	*significant*
A-Speed	2.36	1.00	2.36	0.23	0.636951	*Not significant*
B-Feed	1901.32	1.00	1901.32	187.19	<0.0001	*significant*
C-DOC	68.13	1.00	68.13	6.71	<0.0001	*significant*
Speed*DOC	65.11	1.00	65.11	6.41	0.023014	*Not significant*
Speed^2	53.17	1.00	53.17	5.23	0.037073	*Not significant*
DOC^2	0.72	1.00	0.72	0.07	0.793709	*Not significant*
Speed^2*DOC	347.49	1.00	347.49	34.21	<0.0001	*significant*
Speed*DOC^2	53.08	1.00	53.08	5.23	0.037225	*Not significant*
Residual	152.36	15.00	10.16			
Lack of Fit	152.36	14.00	10.88			
Pure Error	0.00	1.00	0.00			
Cor Total	3095.14	23.00				
Std. Dev.	3.19		R-Squared	0.95		
Mean	41.30		Adj R-Squared	0.92		
C.V. %	7.72		Pre R-Squared	0.87		
PRESS	390.72		Adeq Precision	24.23		

ANOVA also gives an empirical relation between the responses and factors in the form of an equation from the experimental data. The equation is,

Dust Concentration =

-16.90053

+0.036442 * Speed

-1.17947 * Feed
+640.24317 * Depth of Cut
-0.28502 * Speed * Depth of Cut
-3.40147E-006 * Speed^2
-1064.45439 * Depth of Cut^2
+2.25101E-005 * Speed^2 * Depth of Cut
+0.32629 * Speed * Depth of Cut^2

This empirical relation will be very useful in process optimization so that the researcher can select the parameters depending on the counts set by the researcher. Another useful information we can get from the ANOVA output is the variability in the data which is given by R-squared and adjusted R-squared values. R-squared values should be between 0 and 1. Difference between R-squared and adjusted R-squared values should be below 0.2 which indicates that variability in data is minimum. Here counts R-squared is 0.95 and adjusted R-squared is 0.92. This indicates that there is a high level of fit.

6.2.2 Residual Analysis for Average Concentration

In order to check the validity of the Anova model, examination of residuals plots is conducted. To see that our model assumptions are not violated we need to see that the residuals for the normal probability plot are distributed along a straight line. For outlier plots we need to see that there is no unusual response in the experiment conducted, if our model is good all the residuals lie within the ± 3.5 limit. For residuals vs factor plots we need to see that the residuals are of constant variance. For residuals vs predicted we need to see that residuals do not follow any trend. Residual plots for average counts are shown in the fig 6-6. All the plots below do not show any violation of model assumption and we can conclude that our model is good for prediction.

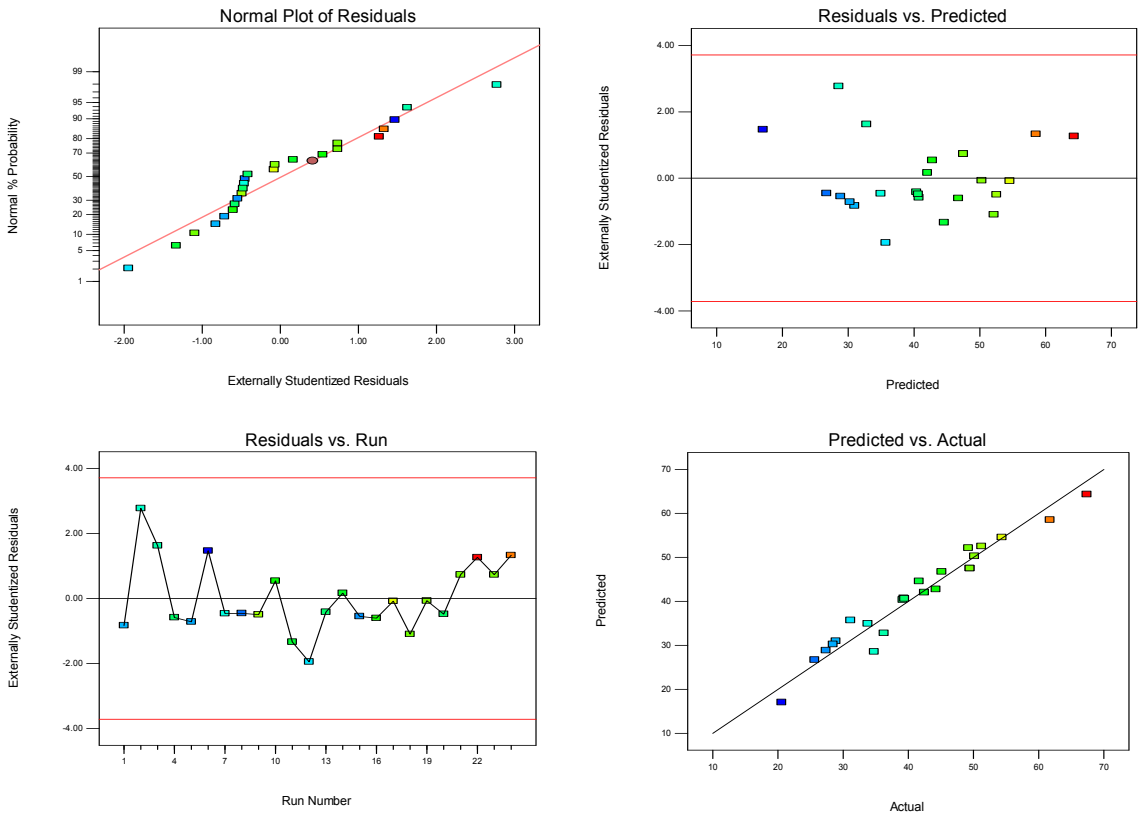

Figure 6-6: Residual Plots

6.2.3 ***Contribution of the Different Factors on Concentration***

Table 6-5: Contribution of different factors on response

Model Parameters		% Contribution
A-Speed	2.36	*negligible*
B-Feed	1901.32	*61*
C-DOC	68.13	*3*
Speed*DOC	65.11	*2*
Speed^2	53.17	*2*
DOC^2	0.72	*2*
Speed^2*DOC	347.49	*15*
Speed*DOC^2	53.08	6
Residual	152.36	9
Cor Total	3095.14	100

The percentage contribution of the main factors is found by dividing the sum of squares of the individual factors by the correlated total as seen in table 6-5. The above table clearly shows that among the individual factors, feed is the most important factor, followed by depth of cut and then by the speed. It is important to note that the interaction factors also play an important role.

6.2.4 *Effect of the Important Model Terms on Concentration*

As seen from the Table 6-5, we can clearly say that feed, speed and interaction between the square of speed and depth of cut play an important role in the responses.

6.2.5 *Effect Of Feed Rate*

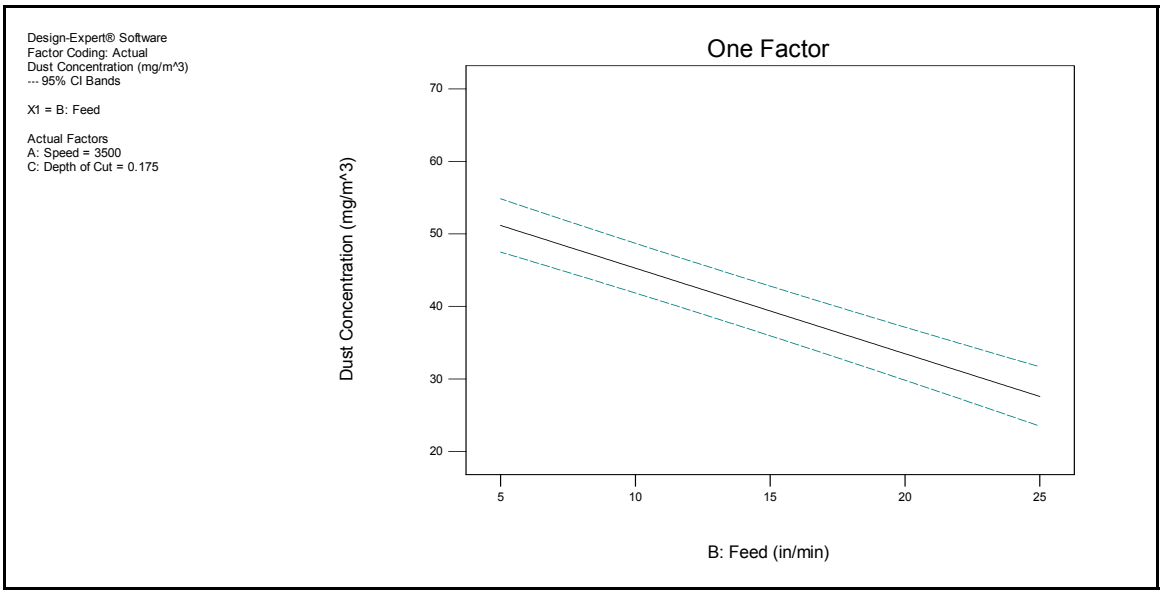

Figure 6-7: Effect of Feed rate on concentration

From fig 6-7 it can be clearly seen that the concentration of particles decreases with an increase in feed rate. This can be explained from the fact that at a higher feed rate, the exposure time per area of the work piece is lower than in a low feed. Also when machining at a high feed rate, the cut is very coarse, meaning the particle sizes would be

higher than in a slow feed. Cumulatively, the variation in the mass is very subtle as compared to the variation in counts. This means that at high feed even though the counts were lower by quite a few million particles, the excessive mass of the larger particles makes the difference in mass concentration seem subtle.

6.2.6 ***Effect of Spindle Speed***

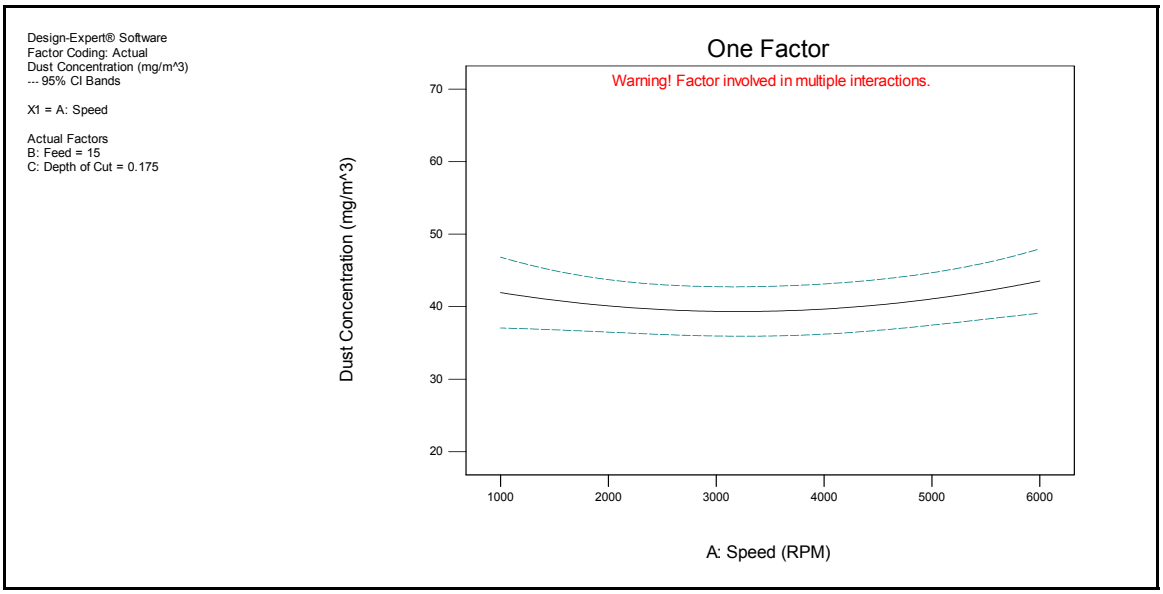

Figure 6-8: Effect of Spindle Speed

As seen from the figure 6-8, even though spindle speed has a negligible effect on the concentration, we can see that at mid-range speed we see lowest mass concentration.

6.2.7 ***Effect of Depth of Cut***

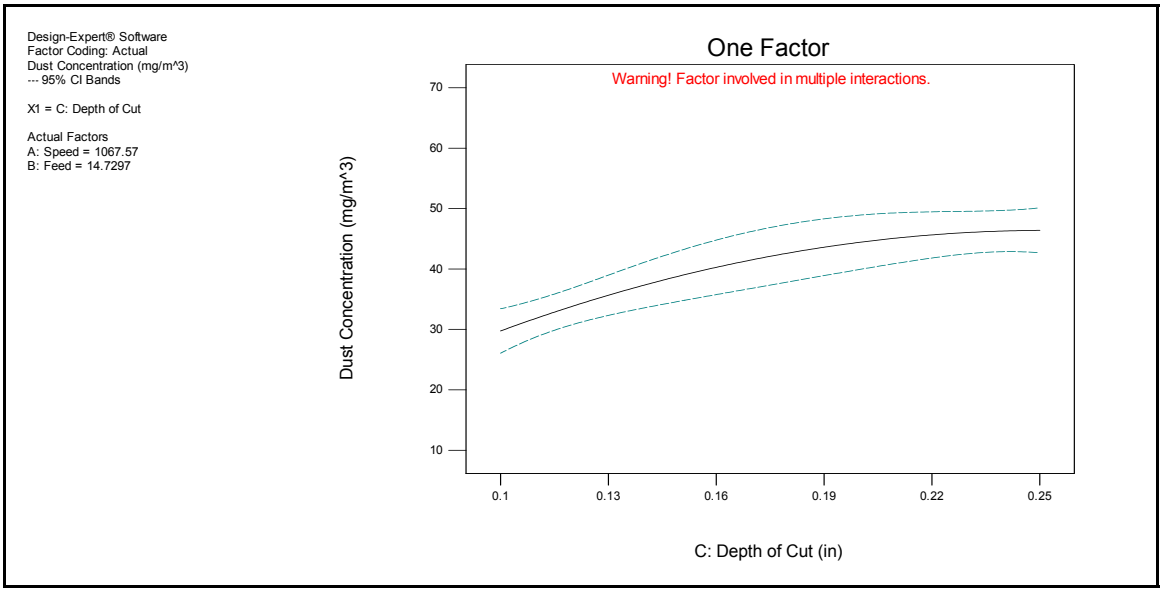

Figure 6-9: Effect of Depth of Cut

We can clearly see in Fig 6-9 that as the depth increases the concentration increases. This can be explained by the fact that higher volume of dust is cut per pass than at a lower depth of cut. So we should see a higher concentration at a higher depth of cut, which is what we observe.

6.2.8 Interaction Effects of Speed and Depth of Cut

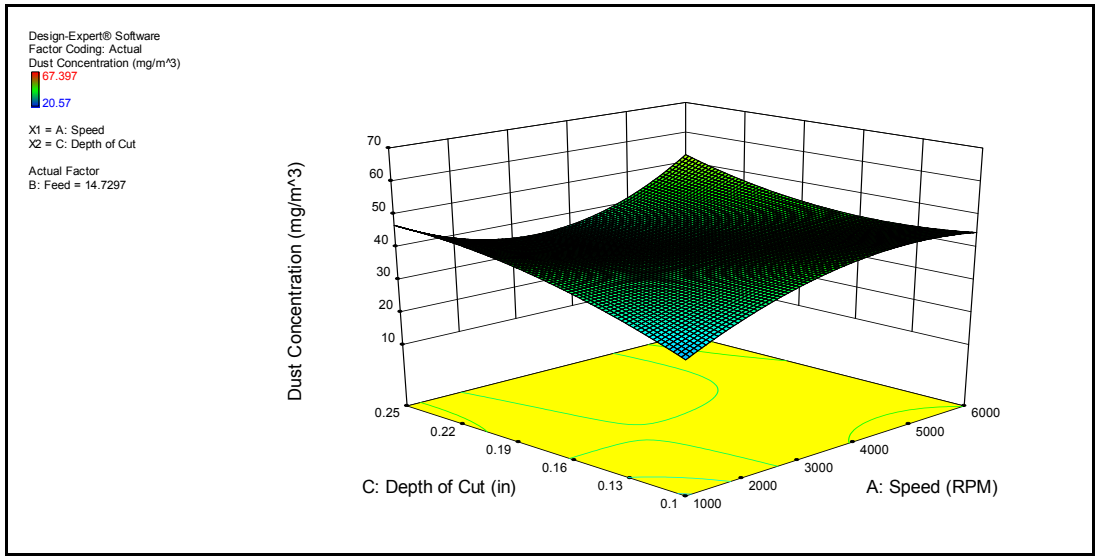

Figure 6-10: Interaction effect of speed and depth of cut

From fig. 6-10, it can be clearly seen that interaction effect plays a significant role in the response. It can be seen that at lower depth of cut, dust concentration increases with increase in speed. While at higher depth of cut, there seems to be a mid-range speed that gives the lower concentration.

6.3 Conclusion

From the above design of experiments for both counts and concentration, it's clear that feed and depth of cut are the most important factors that affect the particle counts. The best cutting conditions for the least particle counts is low speed, high feed and low depth of cut. Cutting speed effects are negligible. It's a commonly researched fact that has been accepted which says that slow feed and high spindle speed are best cutting parameters for best surface finish and least delamination. But this needs to be taken care of during machining composites, in order to generate least amount of dust, higher feeds and lower spindle speeds help. Hence in order to ensure a good finish and lower dust generation, a compromise is required.

6.4 Design of Experiments for Edge Trimming of HexMC® Composites

The statistical analysis is conducted using Stat-Ease Design of Experiments. The factors considered were spindle speed, feed rate and cutting distance and the response were particle counts and particle concentration. Since particle counts play a very important role in determining aerodynamic diameter, the counts response was used for analysis. The statistical design selected for this study is Response surface design since it is the design used for factors subjected to 2 levels. In our study for Uni Directional composites, we had two spindle speeds, two feed rates and two axial depth of cuts. The spindle speeds are 1000 and 6000 rpm. The feed rates are 635 and 127 mm/min and the axial depth of cut are 2.54 and 6.35 mm. Following sections discuss in detail the statistical results. The design matrix is shown in Table 6-6.

6.4.1 Statistical Design Matrix for Counts

Table 6-6: Design matrix for HexMC

RUN NO	FACTOR 1 A:SPEED (RPM)	FACTOR 2 B:FEED(MM/MIN)	FACTOR 3 C:DOC (MM)	RESPONSE R1: GRIMM COUNTS(AVG) : Million Counts/liter
1	6000	635	6.35	31.53191
2	6000	635	2.54	25.68401
3	6000	127	6.35	39.52246
4	6000	127	2.54	34.59984
5	1000	635	6.35	29.26836
6	1000	635	2.54	22.4996
7	1000	127	6.35	34.75077
8	1000	127	2.54	30.0121

6.4.2 *Anova Output for Average Counts*

Table 6-7: ANOVA OUTPUT

Analysis of variance table [Partial sum of squares]						
Source	SS	DF	MS	F-Value	Prob> F	
Model	204.21	5.00	40.84	370.53	<0.05	*significant*
A-Speed	27.41	1.00	27.41	248.64	<0.05	*significant*
B-Feed	111.76	1.00	111.76	1013.91	<0.05	*significant*
C-DOC	62.04	1.00	62.04	562.82	<0.05	*significant*
Speed*Feed	1.91	1.00	1.91	17.35	<0.05	*significant*
Feed*DOC	1.09	1.00	1.09	9.90	0.09	*Not significant*
Residual	0.22	2.00	0.11			
Cor Total	204.43	7.00				
Std. Dev.	0.332006		R-Squared	0.998922		
Mean	30.98363		Adj R-Squared	0.996226		
C.V. %	1.071552		Pre R-Squared	0.982746		
PRESS	3.527287		Adeq Precision	58.24414		

From the ANOVA table (Table 6-7) for average Counts we see that the model we have selected is significant since the prob>F value .05 is less than the significance start level value 0.1, which indicates the model terms are significant. Here the model terms refer to A, B, C that is spindle speed, feed rate and depth of cut. The ANOVA table shows that the response average counts mainly depends on individual effect of the factors and not on some interaction effect of the factors. ANOVA also gives an empirical relation between the responses and factors in the form of an equation from the experimental data. The equation is,

Average Counts =

+27.76730

+1.03373E-003 * Speed

-0.39151 * Feed

+29.74153 * Depth Of Cut

-1.95573E-005 * Speed * Feed

+0.49256 * Feed * Depth Of Cut

This relation will be very useful in process optimization so that the researcher can select the parameters depending on the counts set by the researcher. Another useful information we can get from the ANOVA output is the variability in the data which is given by R-squared and adjusted R-squared values. R-squared values should be between 0 and 1. Difference between R-squared and adjusted R-squared values should be below 0.2 which indicates that variability in data is minimum. Here counts R-squared is 0.998 and adjusted R-squared is 0.9962. This indicates that there is a high level of fit.

6.4.3 ***Residual Analysis for Average Counts***

In order to check the validity of the Anova model, examination of residuals plots is conducted. To see that our model assumptions are not violated we need to see that the residuals for the normal probability plot are distributed along a straight line. For outlier plots we need to see that there is no unusual response in the experiment conducted, if our model is good all the residuals lie within the ± 3.5 limit. For residuals vs factor plots we need to see that the residuals are of constant variance. For residuals vs predicted we need to see that residuals do not follow any trend. Residual plots for average counts are shown in the figure 6-11.

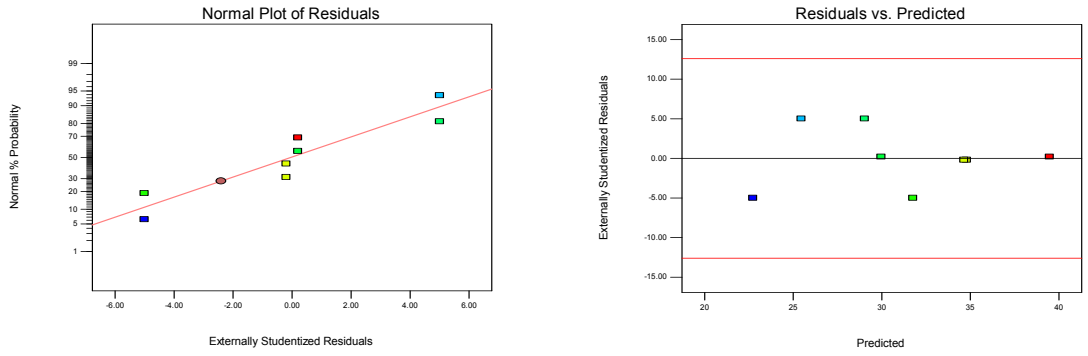

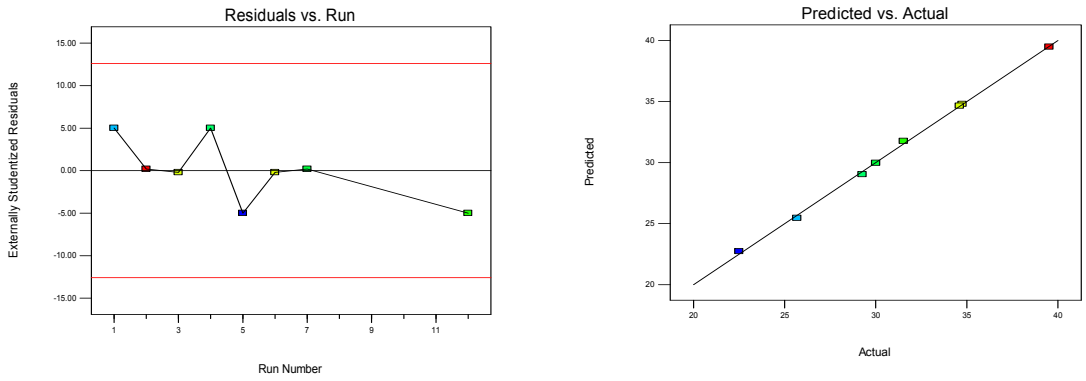

Figure 6-11: Plots for residuals

All the plots do not show any violation of model assumption and we can conclude that our model is good for prediction.

6.4.4 Contribution of the Different Factors on Counts

Table 6-8: Contribution of factors

Source	Squares	% Contribution
A-Speed	*27.41*	*13*
B-Feed	*111.76*	*54*
C-Depth Of Cut	*62.04*	*30*
AB	*1.91*	*2*
BC	*1.09*	*1*
Residual	0.22	negligible
Correlated Total	204.43	100

The percentage contribution of the main factors is found by dividing the sum of squares of the individual factors by the correlated total as seen in Table 6-8. The above table

clearly shows that among the individual factors, feed is the most important factor, followed by depth of cut and then by the speed. It is important to note that the interaction factors also play an important role.

6.4.5 *Effect of Feed Rate*

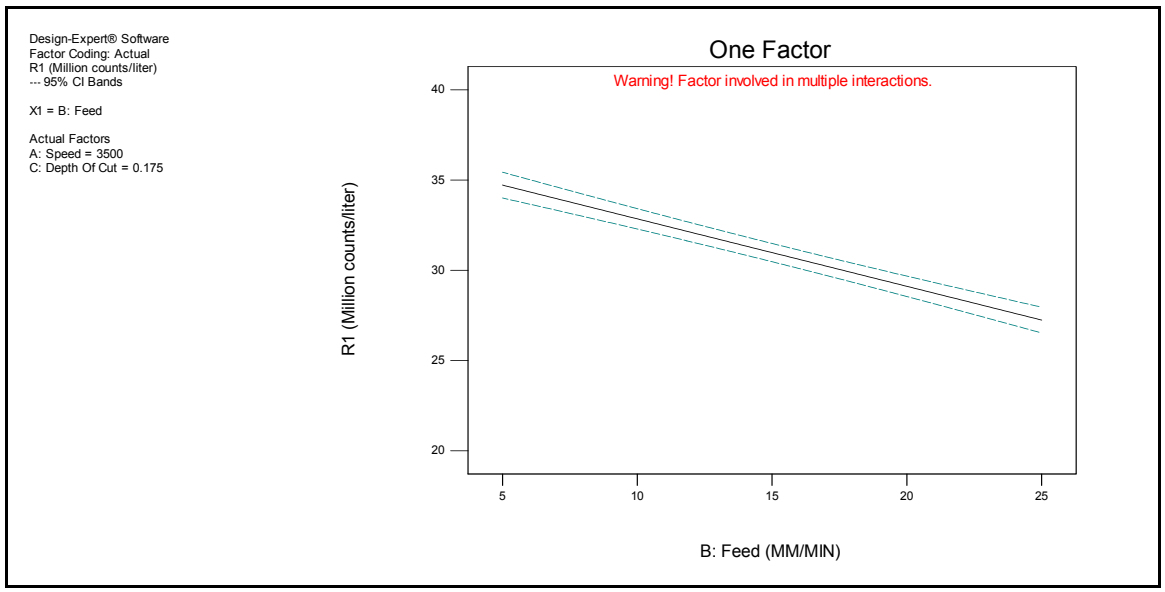

Figure 6-12: Effect of feed rate

From Fig. 6-12 it can be clearly seen that the counts of particles decreases with an increase in feed rate. This can be explained from the fact that at a higher feed rate, the exposure time per area of the work piece is lower than in a low feed. Also when machining at a high feed rate, the cut is very coarse, meaning the particle sizes would be higher than in a slow feed. But for the same volume of material machined, the number of particles generated for a coarse cut would be leaser because of their larger sizes and overall equivalent higher cumulative mass. In case for a low feed, the particles will be much finer, leading to higher counts

6.4.6 ***Effect of Spindle Speed***

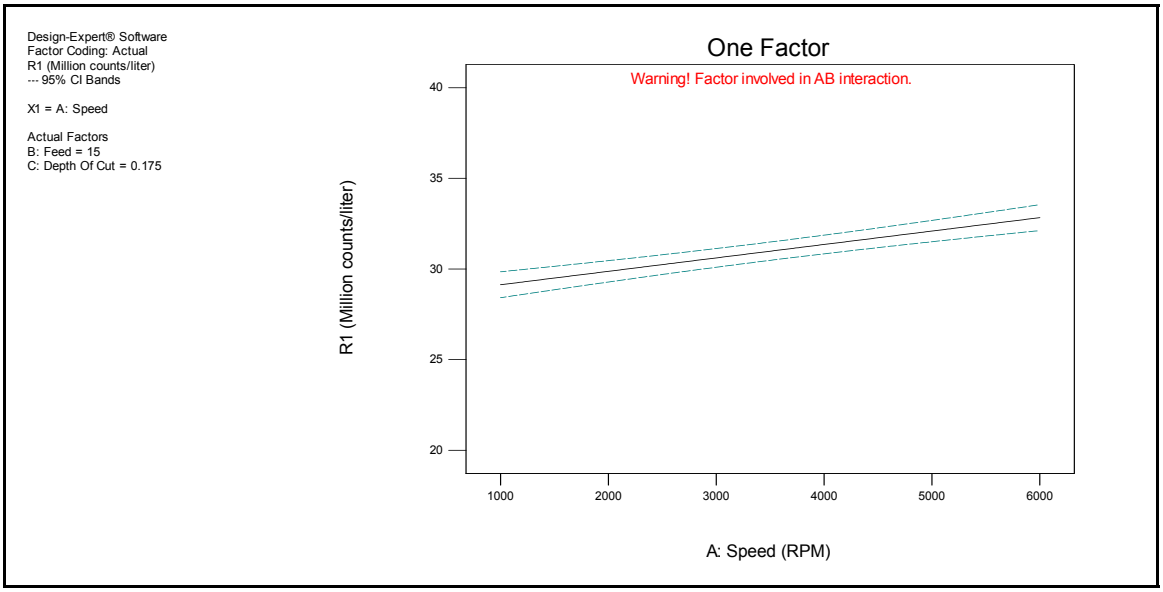

Figure 6-13: Effect of Spindle speed

From Fig 6-13 we can clearly see that the particle counts are higher at higher spindle speed and lower at lower spindle speed. This can be explained by the definition of spindle speed. Spindle speed is defined as the number of revolutions that the cutter makes per minute. Since the tool used was a four flute cutter, the number of times the teeth of the end mill would contact the work piece would depend upon the spindle speed. At 1000 rpm the no of contacts of the cutting edges with the cutting material will be 6 times less than that of a 6000 rpm spindle at the same feed and depth and equivalent cutting time. Since the contact made in a given period time is more in 6000 rpm spindle speed than in 1000 rpm spindle speed, the counts are higher at higher rpm.

6.4.7 *Effect of Depth of Cut*

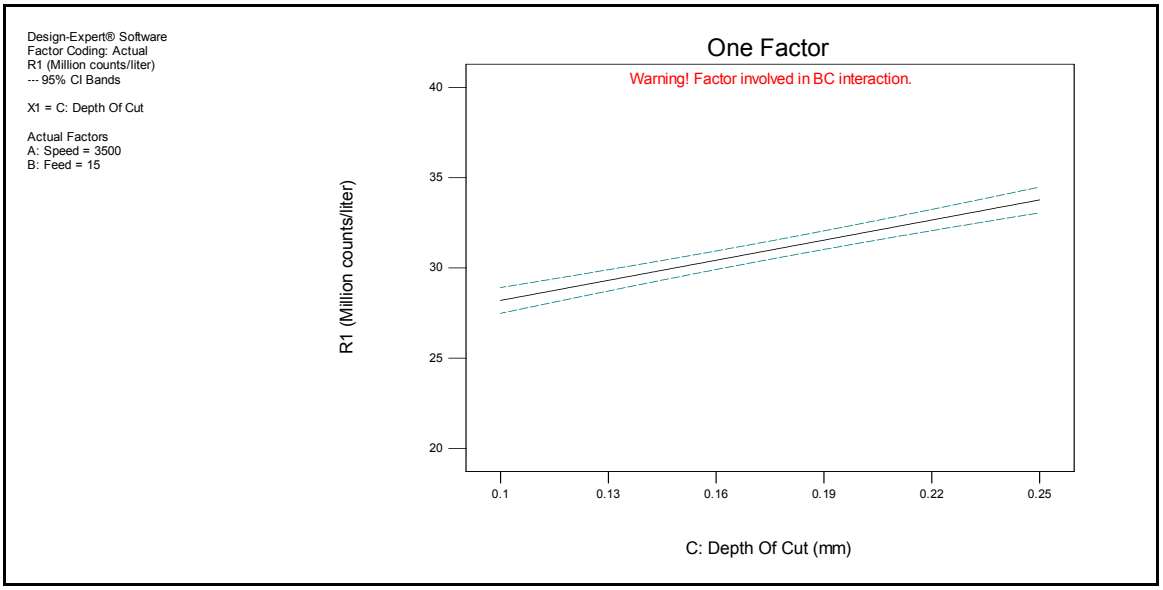

Figure 6-14: Effect of depth of cut

The depth of cut is a significant factor that affects the counts. As we can clearly see from the Fig 6-14, the counts increase with the increase of the depth. This can be explained by the fact that the higher depth causes higher contact with the work piece causing higher volume of material removal

6.4.8 *Interaction Effects of Feed and Speed*

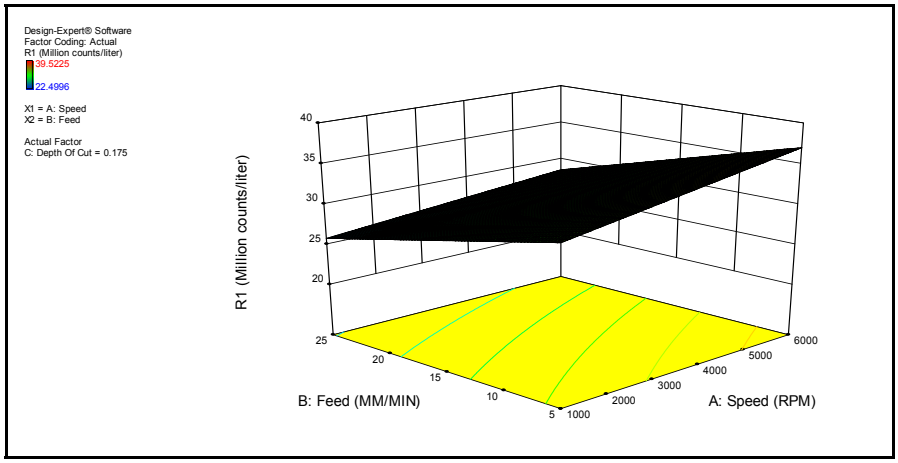

Figure 6-15: Effect of feed and speed

From the above Contour plot, it can be clearly seen that interaction effect plays a significant role in the response. It can be seen that almost at all the areas of the plot except at higher speed, the dust counts seems to reduce with an increase in feed

6.4.9 Interaction Effects of Feed and Depth of Cut

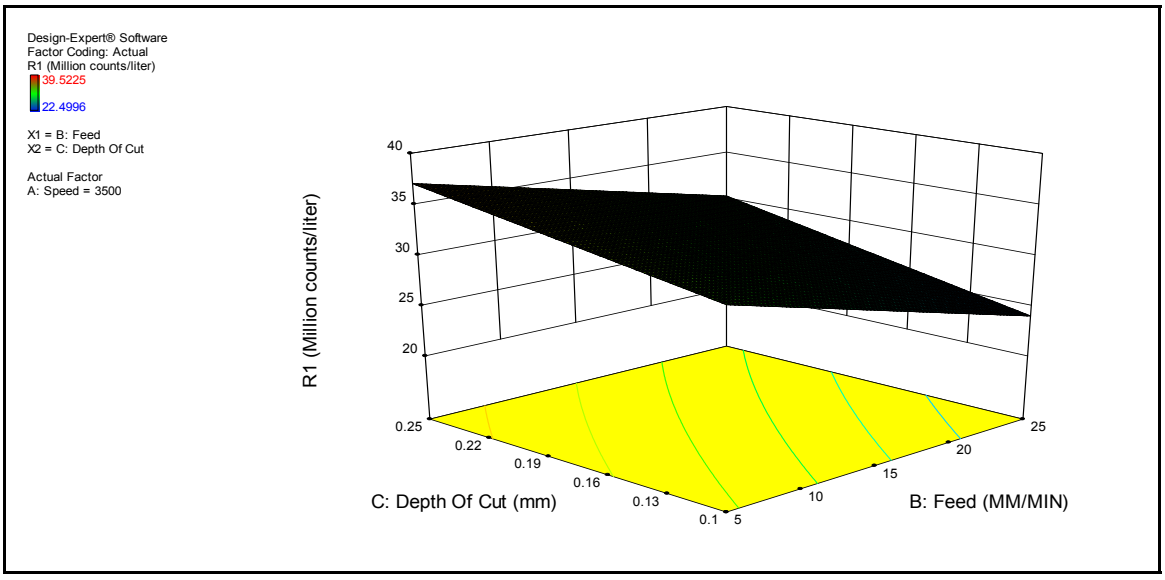

Figure 6-16: Effect of feed and depth of cut

From the Fig 6-16, it can be clearly seen that interaction effect plays a major role in the response. It can be seen that almost at all the areas of the plot the highest dust is generated at high depth and low feed, while the lowest counts are the points of high feed and low depth of cut.

6.5 Statistical Design Matrix for Concentration

The statistical analysis is conducted using Stat-Ease Design of Experiments. The factors considered were spindle speed, feed rate and cutting distance and the response was particle concentration. The statistical design selected for this study is Response surface design since it is the design used for factors subjected to 2 levels. In our study for Uni Directional composites, we had two spindle speeds, two feed rates and two axial depth of cuts. The spindle speeds are 1000 and 6000 rpm. The feed rates are 635 and 127 mm/min and the axial depth of cut are 2.54 and 6.35 mm. Following sections discuss in detail the statistical results. Table 6-9 shows the statistical design matrix.

Table 6-9: Design Matrix for Concentration

RUN NO	FACTOR 1 A:SPEED (RPM)	FACTOR 2 B:FEED(MM/MIN)	FACTOR 3 C:DOC (MM)	RESPONSE R1: GRIMM concentration (AVG) : mg/m^3
1	6000	635	6.35	31.53191
2	6000	635	2.54	25.68401
3	6000	127	6.35	39.52246
4	6000	127	2.54	34.59984
5	1000	635	6.35	29.26836
6	1000	635	2.54	22.4996
7	1000	127	6.35	34.75077
8	1000	127	2.54	30.0121

6.5.1 *Anova Output for Average Concentration*

Table 6-10: Anova output for mass concentration

Analysis of variance table [Partial sum of squares - Type III]						
Source	SS	dF	MS	F-Value	Prob > F	
Model	2875.581	6	479.2634743	294.3535	<0.05	*significant*
A-Speed	259.9955	1	259.9954537	159.6837	<0.05	*significant*
B-Feed	1509.482	1	1509.482171	927.0921	<0.05	*significant*
C-DOC	643.5208	1	643.520805	395.2369	<0.05	*significant*
Speed*Feed	7.384765	1	7.384765477	4.535567	0.086438372	*Not significant*
Speed*DOC	30.98367	1	30.98366734	19.02952	<0.05	*significant*
Feed*DOC	119.8985	1	119.8985422	73.63916	<0.05	*significant*
Residual	8.14095	5	1.628190055			
Lack of Fit	8.14095	1	8.140950277			
Pure Error	0	4	0			
Cor Total	2883.722	11				
Std. Dev.	1.276006		R-Squared	0.997177		
Mean	51.19681		Adj R-Squared	0.993789		
C.V. %	2.492354		Pred R-Squared	0.929039		
PRESS	204.6317		Adeq Precision	50.4846		

From the ANOVA table for average concentration (Table 6-10) we see that the model we have selected is significant since the prob>F value .05 is less than the significance start level value 0.1, which indicates the model terms are significant. Here the model terms refer to A, B, C that is spindle speed, feed rate and depth of cut. The ANOVA table shows that the response average counts mainly depends on individual effect of the factors and not on some interaction effect of the factors. ANOVA also gives an empirical relation between the responses and factors in the form of an equation from the experimental data. The equation is,

Concentration =
+24.80386
+2.97532E-003 * Speed
-0.020622 * Feed
+7.89809 * Depth Of Cut
+1.31033E-006 * Speed * Feed
-3.37397E-004 * Speed * Depth Of Cut
-6.92889E-003 * Feed * Depth Of Cut

6.5.2 ***Residual Analysis for Average Counts***

In order to check the validity of the Anova model, examination of residuals plots is conducted. To see that our model assumptions are not violated we need to see that the residuals for the normal probability plot are distributed along a straight line. For outlier plots we need to see that there is no unusual response in the experiment conducted, if our model is good all the residuals lie within the ± 3.5 limit. For residuals vs factor plots we need to see that the residuals are of constant variance. For residuals vs predicted we need to see that residuals do not follow any trend. Residual plots for average counts are shown in the Fig. 6-17. All the plots do not show any violation of model assumption and we can conclude that our model is good for prediction.

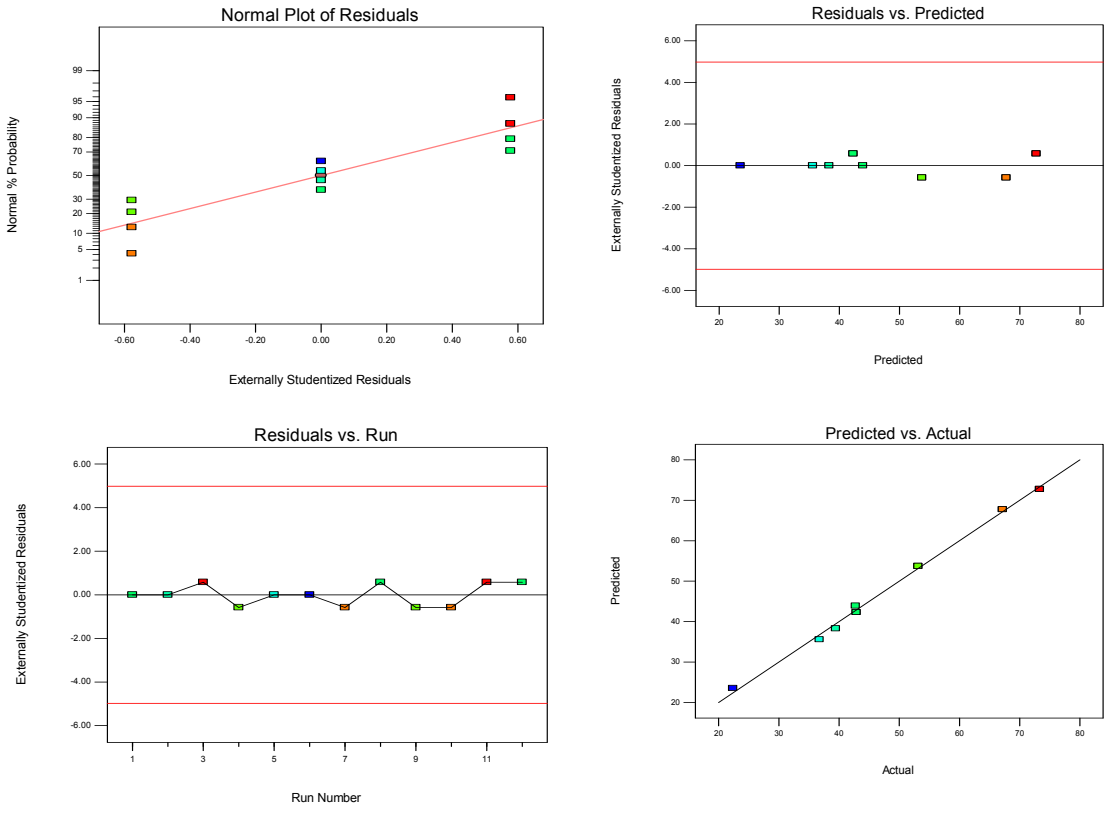

Figure 6-17: Residual Plots

6.5.3 *Contribution of the Different Factors on Concentration*

Table 6-11: Factors and Contribution

Source	Squares	% Contribution
A-Speed	259.9955	11
B-Feed	1509.482	55
C-DOC	643.5208	22
Speed*Feed	7.384765	1
Speed*DOC	30.98367	1
Feed*DOC	119.8985	8
Residual	8.14095	1
Lack of Fit	8.14095	1
Pure Error	0	0
Cor Total	2883.722	100

The percentage contribution of the main factors is found by dividing the sum of squares of the individual factors by the correlated total as seen in Table 6-11. The above table clearly shows that among the individual factors, feed is the most important factor, followed by depth of cut and then by the speed. It is important to note that the interaction factors also play an important role

6.5.4 *Effect of Feed Rate*

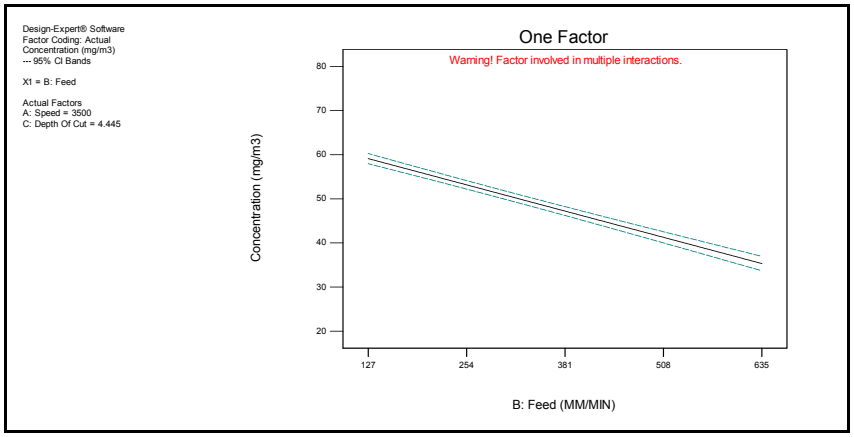

Figure 6-18: Effect of feed rate

From Fig. 6-15 it can be clearly seen that the concentration of particles decreases with an increase in feed rate. This can be explained from the fact that at a higher feed rate, the exposure time per area of the work piece is lower than in a low feed. Also when machining at a high feed rate, the cut is very coarse, meaning the particle sizes would be higher than in a slow feed. Cumulatively, the variation in the mass is very subtle as compared to the variation in counts. This means that at high feed even though the counts were lower by quite a few million particles, the excessive mass of the larger particles makes the difference in mass concentration seem subtle.

6.5.5 *Effect Of Spindle Speed*

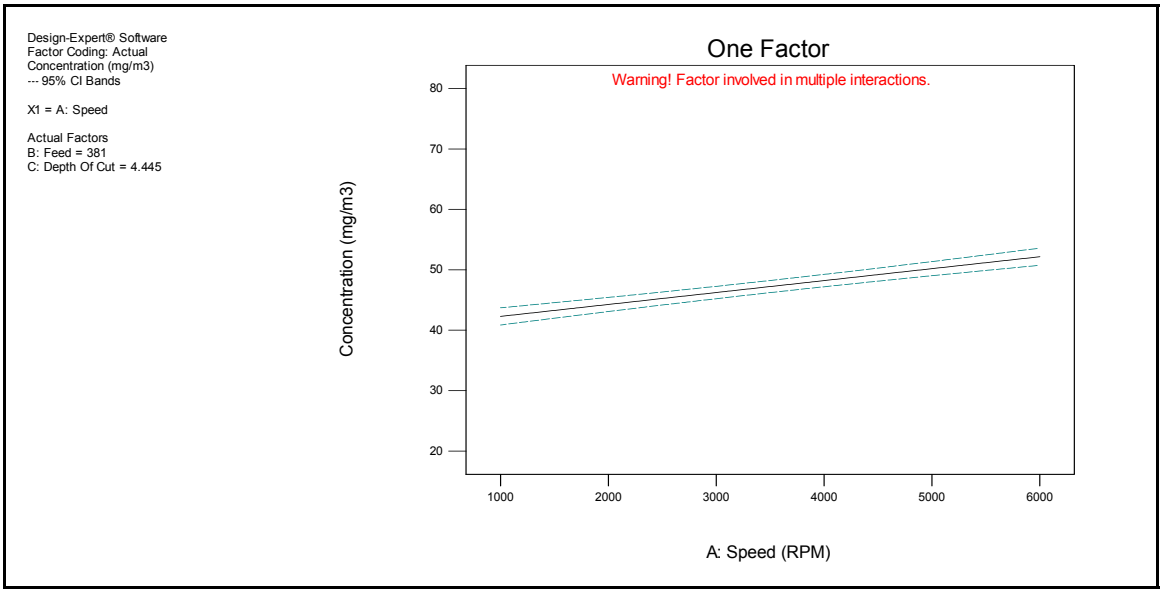

Figure 6-19: Effect of Spindle speed

As seen from the fig 6-19, even though spindle speed has a small effect on the concentration, we can see that as speed increases the mass concentration increases. This can be explained by the fact that as the speed rises more number of contacts occur between the tooth and work piece. Hence counts are higher and hence mass is higher. Similar argument holds true for lower speeds

6.5.6 *Effect of Depth of Cut*

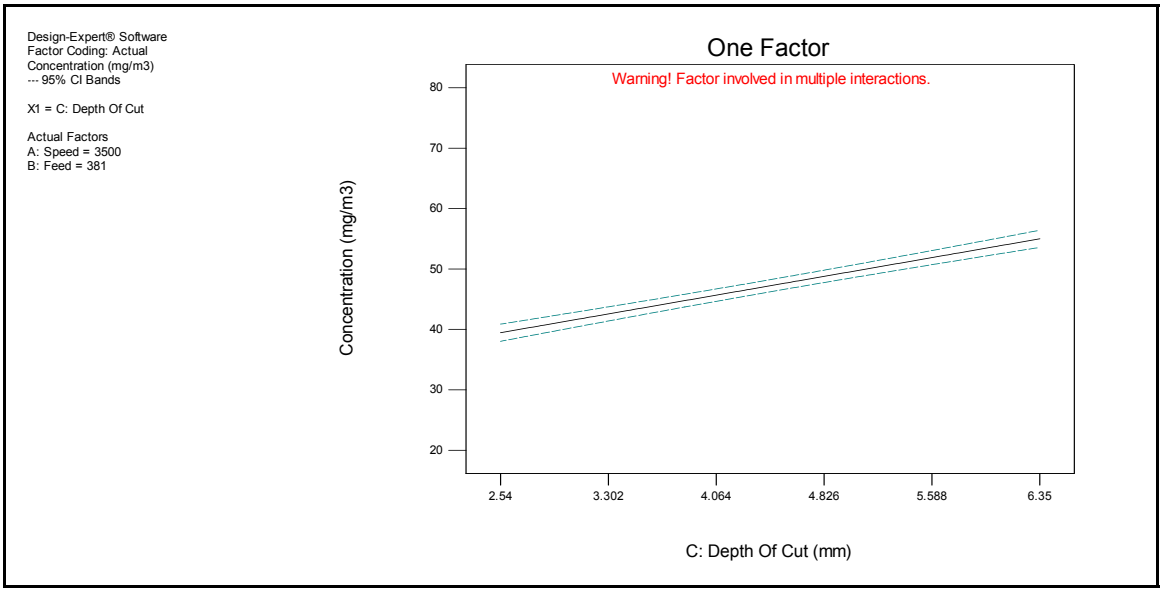

Figure 6-20: Effect of depth of cut

We can clearly see in Fig. 6-20, as the depth increases the concentration increases. This can be explained by the fact that higher volume of dust is cut per pass than at a lower depth of cut. So we should see a higher concentration at a higher depth of cut, which is what we observe.

6.5.7 *Interaction Effects of Feed and Doc*

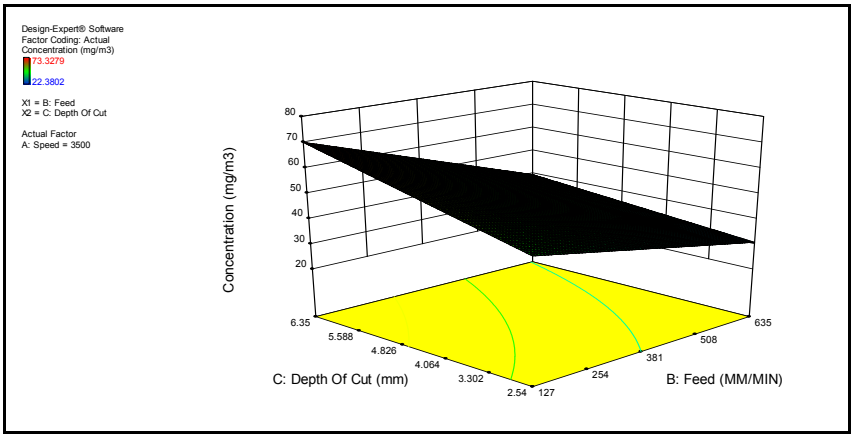

Figure 6-21: Effect of feed and DOC

From the fig. 6-21, it can be clearly seen that interaction effect plays a significant role in the response. It can be seen that at higher depth of cut and low feed, dust concentration is high, while its lowest at high feed and low depth of cut.

6.5.8 *Interaction Effects of Speed and Depth of Cut*

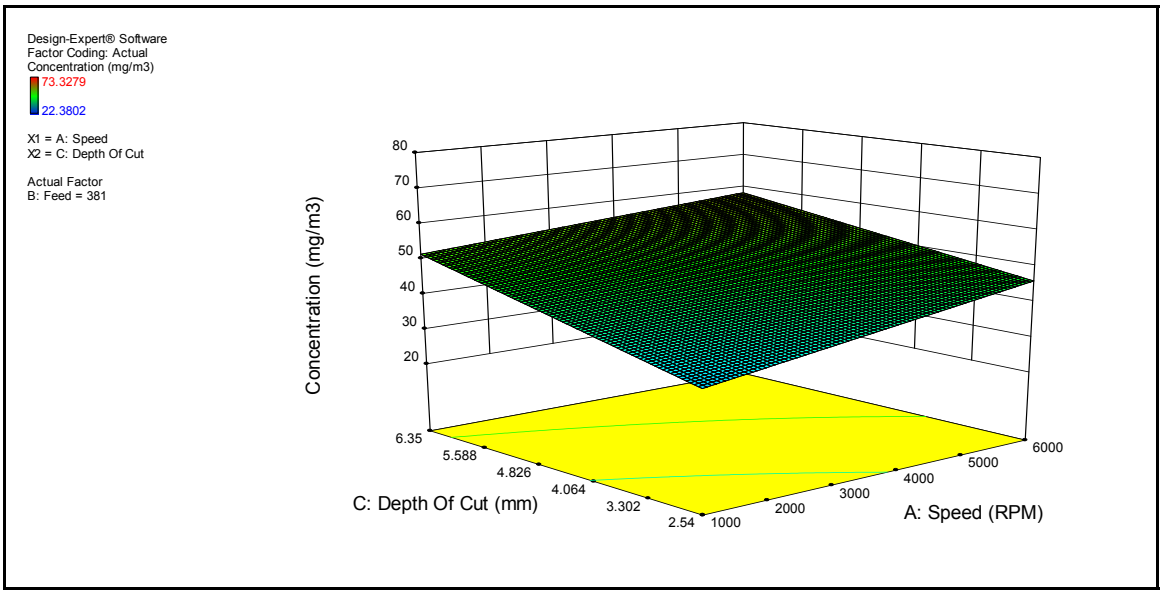

Figure 6-22: Effect of feed and depth of cut

From the Fig. 6-22, it can be clearly seen that interaction effect plays a major role in the response. It can be seen that at lower depth of cut and low speed, concentration is lower and is maximum at high speed and high depth of cut, which is expected.

6.6 *Conclusion*

From the above design of experiments it's clear that feed and depth of cut are the most important factors that affect the particle counts. The best cutting conditions for the least particle counts is low speed, high feed and low depth of cut. Cutting speed effects are negligible. It's a commonly researched fact that has been accepted which says that slow feed and high spindle speed are best cutting parameters for best surface finish and least

delamination. But this needs to be taken care of during machining composites, in order to generate least amount of dust, higher feeds and lower spindle speeds help. Hence in order to ensure a good finish and lower dust generation, a compromise is required. Hence the inferences drawn from machining of both CFRP Composites and HexMC® are similar.
In either case the best conditions for lowest dust counts or concentration is low speed, high feed and lower depth of cut.

7 Overall Conclusions

- The use of iso-kinetic sampling done during the process of these experiments proved that all the instruments show the exact same trend over a given test , both in terms of value and in terms of the nature of the plots.
- The Casella consistently records data between 0.1 mg/m^3 to 65 mg/m^3. The cyclone filters provided on the Casella can be analyzed to throw some more light on the type of fractures during trimming.
- The Grimm provides both counts and mass. The counts are somewhere in between 30 million counts/liter to 0.5 million counts/liter. The mass measured by the Grimm range from 0.5 mg/m^3 to 60 mg/m^3.
- The PTRAK Ultrafine counter measures the particle counts somewhere in between 25000 counts/ cc to as low as 300 counts/cc.
- Overall counts were found to be about 15% higher in the HexMC® material as compared to the Uni-Directional Composites. Same applies to the mass concentration as well.
- Aerodynamic diameters of the materials suggest that the Uni-Directional Composites produce finer particles than HexMC®. The UD-CFRP produces aerodynamic diameter of 0.19-0.23 µm while the HexMC® produces 0.28-0.35 µm.
- Mass concentration when edge trimming composites can exceed 50 mg/m^3 for total dust using real-time instrumentation, well above the OSHA limit for total dust of 15 mg/m^3 when measured at the source. However it was found that an excess of 30 mg/m^3 for respirable dust measured using real-time instrumentation, well above the OSHA limit for respirable dust of 5 mg/m^3 when measured at the source.

- During the machining of Composites, maximum damage, hence maximum dust was observed when the angle made by the cutting edge with the instantaneous fiber angle was ± 45°. Least was observed at 90°.
- Machining of composites using experimental methods yielded that for the least amount of dust generation during edge trimming, low speed, high feed and low depth of cut should be used. But it is commonly known that for the best surface finish, high speed and low feed is needed. Hence while trimming composites some kind of a compromise is required. Further research is needed to optimize the process conditions along with surface finish

7.1 Future Work

More tests can be performed on both materials to verify the effect of radial depth of cut on the optimum conditions for lower dust generation. Also different types of tools can be used to verify their effects on the generation of dust and process optimality. The same concept of iso-kinetic sampling can be applied to other machining processes like drilling, grinding etc.

8 References

1. Campbell, F.C., *Structural Composite Materials ,* ASM International, 2010.
2. SOFFAR, H., *The function of the respiratory system and the importance of respiration process.* American Journal of Public Health, 2015.
3. Mazumdar.SK, *Composites Manufacturing –Materials, Product and Process Engineering.* CRC PRESS, 2002.
4. Bhatia, S.C., *Interdisciplinary Labs Using Materials Science Module On Composites.* 2007.
5. Sheikh-Ahmad, J.Y., *Machining of Polymer Composites.* The Petroleum Institute, Department of Mechanical Engineering, United Arab Emirates, ISBN 978-0-387-35539-9, Ed. Springer Science, Abu Dhabi, 2009.
6. Keenoy, G.M.a.K., *F/A-18E/F ECP6038 forward fuselage: An affordability driven design. Presentation to the Society of Allied Weight Engineers, May 23, Arlington, Tex.* 2001.
7. Bralla, J.G., *Handbook of Product Design for Manufacturing.* McGraw-Hill (New York), 1986.
8. Teti, R., *Machining of composite materials,* CIRP Annals-Manufacturing Technology 2002. **51(2): 611-634**.
9. Colligan, K., Ramulu, M., *The effect of edge trimming on composite surface plies,* Manufacturing Review(USA) 5(4): 274-283, 1992.
10. T. G. Rogers , G.C.E., *A theory of machining of fiber-reinforced materials".* Journal of Composite Materials,, 1971. **Vol. 5, pp. 94-106.**
11. Santhanakrishnan, G., Krishnamurthy, R., Malhotra : *High Speed Steel Tool Wear Studies in Machining of Glass-Fiber-Reinforced Plastics..* S.K. Wear, 1989. **Vol. 132**: p. 327-336.
12. Ahmed, J., *Machining of Polymer Composites*. 2009: Springer Publications.
13. Koplev, A., Lystrup, A., Vorm, T, *The Cutting Process, Chips, and Cutting Forces in Machining CFRP.* Composites 1983. **Vol. 14(4)**: p. 371-376.
14. M.Ramulu,D.H.Wang,D.Arola,*Orthogonal cutting mechanisms of graphite/Epoxy composite part: 1 unidirectional laminates.* International Journal of Machine Tools and Manufacture, (1995) **Vol.35**: p. 1623-1638.
15. Colligan, K., Ramulu, M., *Delamination in surface plies of graphite/epoxy caused by the edge trimming process.* Processing and manufacturing of composite materials; Proceedings of the Symposium, 112th ASME Winter Annual Meeting, Atlanta, GA, Dec. 1-6, 1991 (A93-32021 12-37), p. 113-125, 1991.
16. H.Y. Puw and H. Hocheng, *Machinability test of carbon fiber reinforced plastics in milling.* 1993. **717-729**: p. 8(6).
17. A. I. Azmi, D. Bhattacharyy *Machinablity study of glass fiber reinforced polymer composites during end milling.* International Journal of Advance Manufacturing Technology, 2013. **Vol.64**: p. pp.247-261.
18. V. Schulze, K. Weidenmann, S. Dietrich., *Machining strategies for hole making in composites with minimal work piece damage by directing the process forces inwards.* Journal of Materials Processing Technology, 2011. **.211: 329–338**.

19. Davim, J., Mata, D., *Machinability of GFRP plastics using polycrystalline diamond and cemented carbide carbide (K15) tools.* Material and Design, 2007. **Vol. 28**: p. pp. 1050-1054.
20. Kalpakjian, S., *Manufacturing Processes for Engineering Materials.* Addison Wesley Longman, 1997.
21. ASME, *End Mill Cutters*, in *ANSI B94.19*. 1985.
22. Eyup, B., Birhan, Işık., *Investigation of surface roughness in turning unidirectional GFRP composites by using RS methodology and ANN.* The International Journal of Advanced Manufacturing Technology, 2006. **31**(1-2): p. 10-17.
23. http://www.aerosols.wustl.edu/education/AerosolBasics. 2010.
24. Basheera, A., *Modeling of surface roughness in precision machining of metal matrix composites using ANN.* Journal of Materials Processing Technology,, 2008. **197**(1-3): p. 439-444.
25. Gaines, M., *Composites Menace Crash Teams.* Flight International, 1991. **1**(17).
26. Hesterberg, T.W., W. C. Miller, E. E. McConnell, J. Chevalier, J. G. Hadley, D. M. and P.T. Bernstein, and R. Anderson, *Chronic Inhalation Toxicity of Size-Separated Glass Fibers in Fischer 344 Rats.* Fundamental and Applied Toxicology, 1993. **26**: p. 464-476.
27. Seibert, J.F., *Composite Fiber Hazard, Air Force Occupational and Environmental Health Laboratory.* Brooks AFB, TX, AFOEHL Report 90-EI00178MGA, 1990.
28. Thomson, S.A., *Toxicology of Carbon Fibers.* Proceedings Conference on Occupational Health Aspects of Advanced Composite Technology in the Aerospace Industry 1989.(Health Effects and Exposure Considerations): p. 164-170.
29. Kwan, J.K., *Health Hazard Evaluation of the Post-Curing Phase of Graphite Composite Operations* UCRL-LR-104684, 1990.
30. Ramulu, M., Kramlich, J, *Machining of Fiber Reinforced Composites: Review of Environmental and Health Effects.* International Journal of Environmentally Conscious Design & Manufacturing, 2004. **Vol. 11**: p. 1-19.
31. Haddad, M., Zitoune, R., Eyma, F., Castanie, B., Bougherara H, *Surface quality and dust analysis in high speed trimming of CFRP.* Applied Mechanics and Materials, Vol. 232, 2012. **232**(57-62).
32. Haddad, M., Zitoune, R., Eyma, F., Castanie, B. Bougherara H, *Study of the surface defects and dust generated during trimming of CFRP,Influence of tool geometry, machining parameters and cutting speed range.* Composites: Part A, 2014. **66**(142-154).
33. Miller, J.L., *Investigation of Machinability and Dust Emissions in Edge Trimming of Laminated Carbon Fiber Composites*, in *Department of Mechanical Engineering*. 2014, University of Washington: Seattle. p. 492.
34. http://www.airflowsciences.com/. 2010.
35. http://automationwiki.com/images/e/e2/Pitot_Tube.jpg. 2010.

9 Appendix

9.1 Appendix A

Combined Plots UDC CFRP Edge Trim

#	SPEED (RPM)	FEED(MM/MIN)	DOC (MM)	GRIMM (Counts/lit)	Grimm Concentration (mg/m3)	Casella Conc. (mg/m3)	PTRAK COUNTS (Counts/lit)
1	6000	635	3.81	23487560	29.289	28.89	27011000
2	3000	635	3.81	19825690	27.245	28.45	22800000
3	6000	635	2.54	18627540	34.270	36.27	21422000
4	6000	635	6.35	26752190	38.230	39.29	30765000
5	3000	635	2.54	17659070	32.560	34.76	20308000
6	1000	635	2.54	11453280	20.230	20.57	13171000
7	1000	635	6.35	16347590	30.130	33.78	18800000
8	1000	635	3.81	13258970	25.130	25.63	14585000
9	6000	381	6.35	26629430	53.230	51.23	29292000
10	6000	381	3.81	23145680	42.234	44.24	25460000
11	6000	381	2.54	19674540	43.950	41.65	21642000
12	3000	381	6.35	26897450	34.230	31.13	29587000
13	3000	381	3.81	24379570	38.230	39.15	26818000
14	3000	381	2.54	17682140	40.160	42.46	19450000
15	1000	381	2.54	19545340	29.950	27.36	21500000
16	1000	381	6.35	25408680	47.066	45.13	27950000
17	6000	127	3.81	31248970	53.36	54.36	34374000
18	3000	127	3.81	25432730	51.271	49.221	27976000
19	1000	127	3.81	23457860	48.230	50.13	25804000
20	1000	127	2.54	18675420	37.210	39.41	20543000
21	3000	127	2.54	24112960	48.220	49.45	26524000
22	6000	127	6.35	33531500	67.097	67.397	36885000
23	3000	127	6.35	29112960	51.220	49.45	32024000
24	1000	127	6.35	27786290	60.722	61.7342	30565000

Run #1

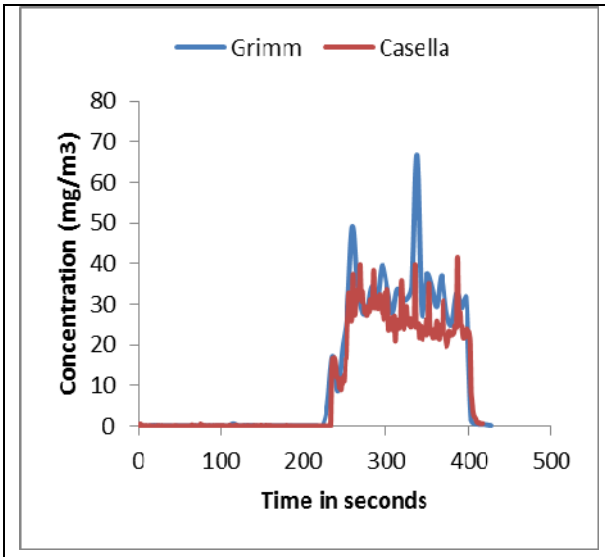

Speed: 6000 RPM
Feed: 635 mm/min
DOC: 3.81 mm

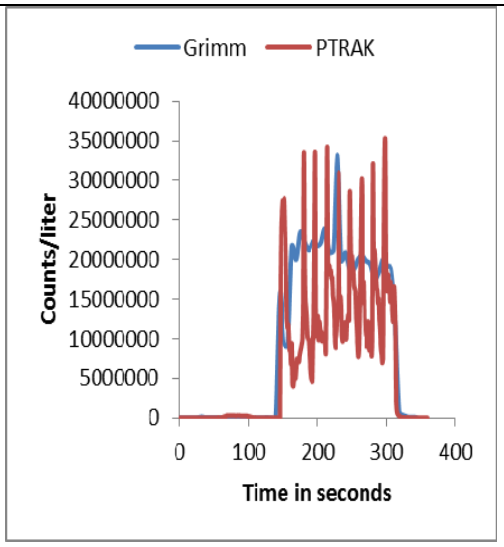

Speed: 6000 RPM
Feed: 635 mm/min
DOC: 3.81 mm

Run #2

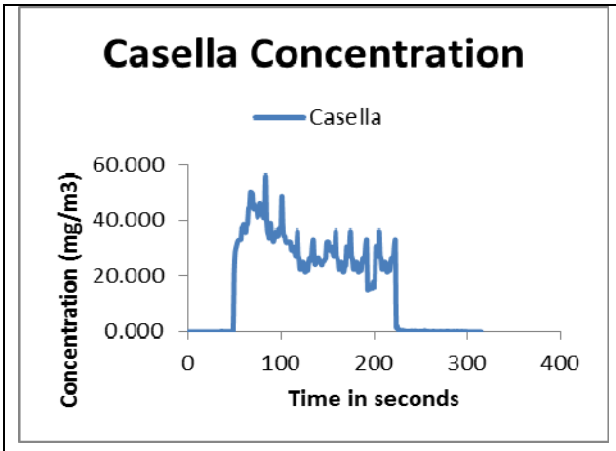

Speed: 3000 RPM
Feed: 635 mm/min
DOC: 3.81 mm

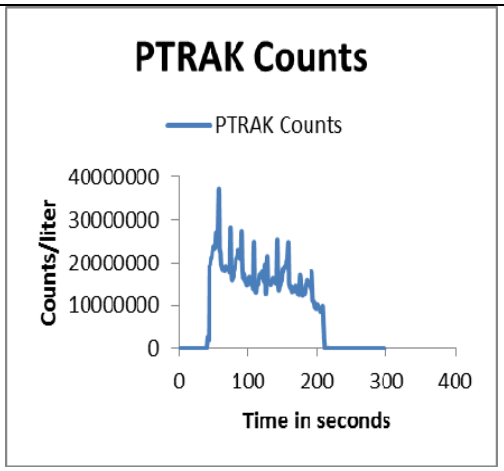

Speed: 3000 RPM
Feed: 635 mm/min
DOC: 3.81 mm

Run #3

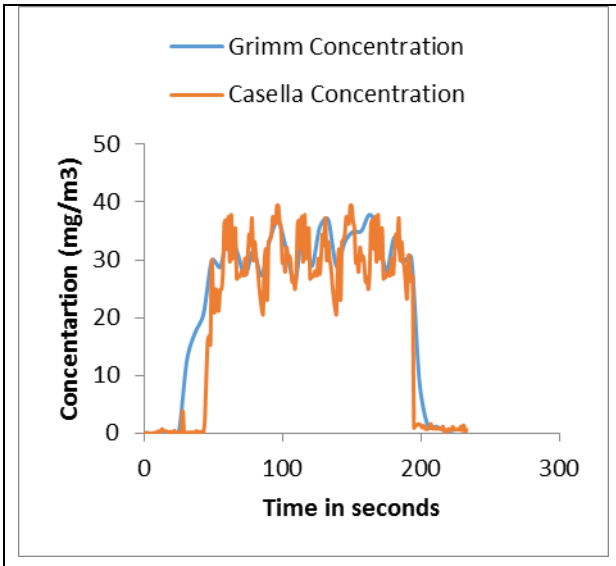

Speed: 6000 RPM
Feed: 635 mm/min
DOC: 2.54 mm

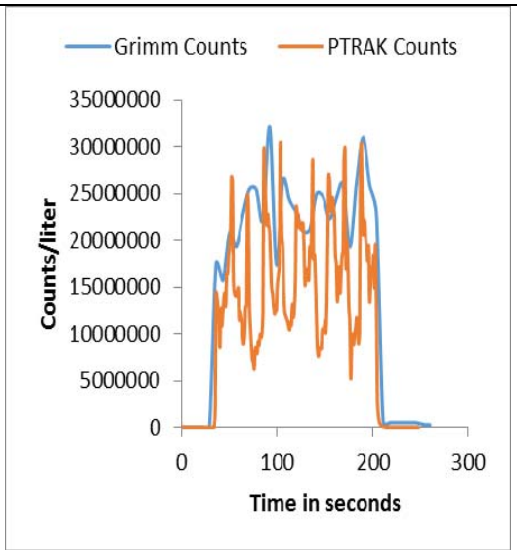

Speed: 6000 RPM
Feed: 635 mm/min
DOC: 2.54 mm

Run #4

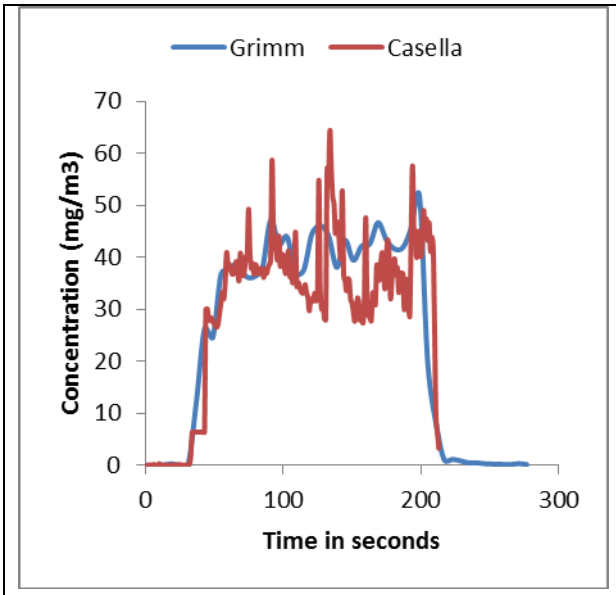

Speed: 6000 RPM
Feed: 635 mm/min
DOC: 6.35 mm

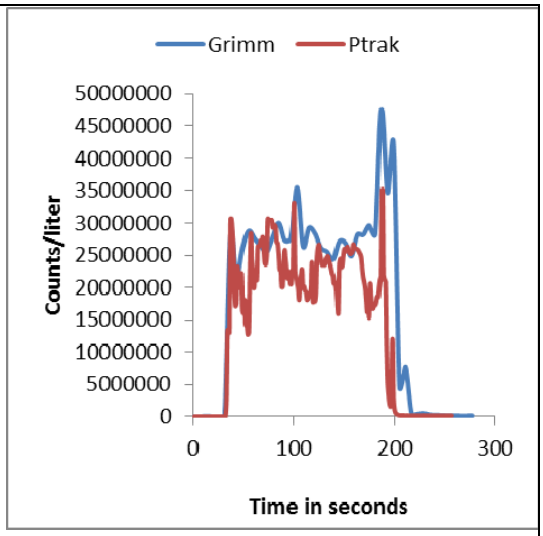

Speed: 6000 RPM
Feed: 635 mm/min
DOC: 6.35 mm

Run #5

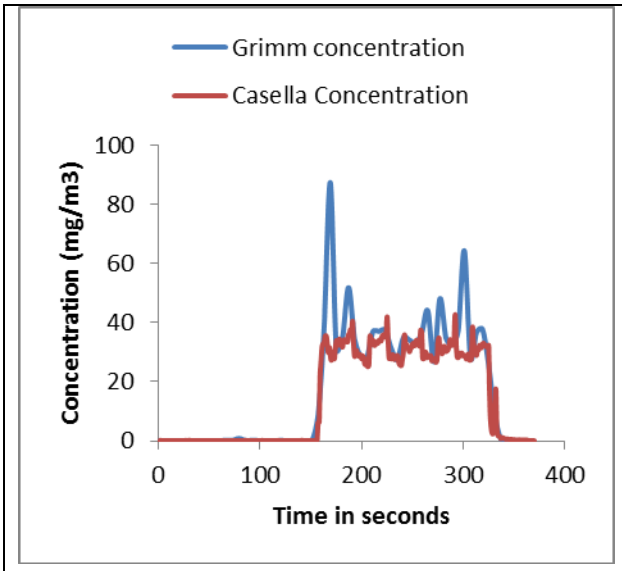

Speed: 3000 RPM
Feed: 635 mm/min
DOC: 2.54 mm

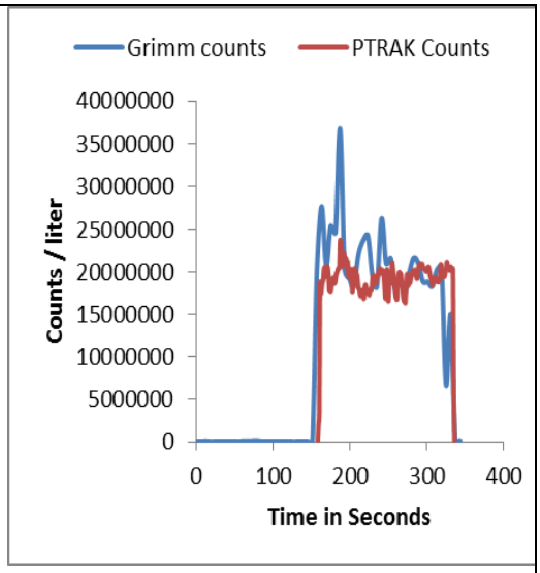

Speed: 3000 RPM
Feed: 635 mm/min
DOC: 2.54 mm

Run #6

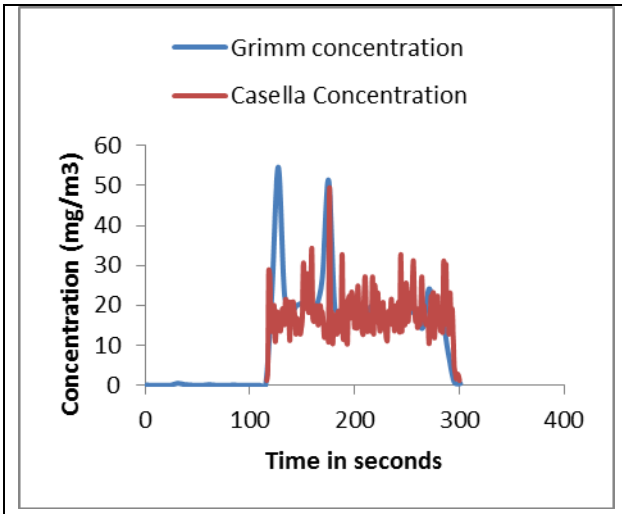

Speed: 1000 RPM
Feed: 635 mm/min
DOC: 2.54 mm

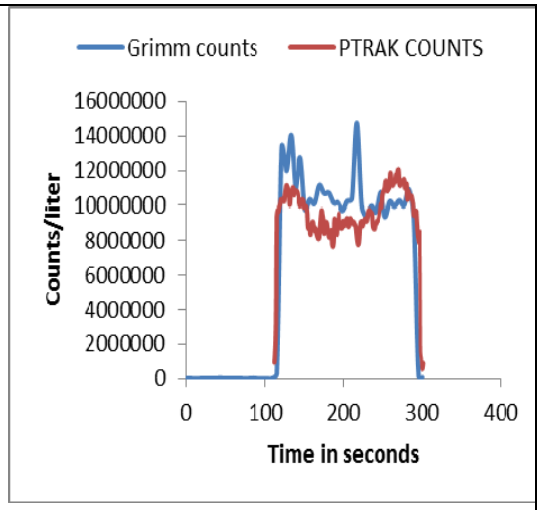

Speed: 1000 RPM
Feed: 635 mm/min
DOC: 2.54 mm

Run #7

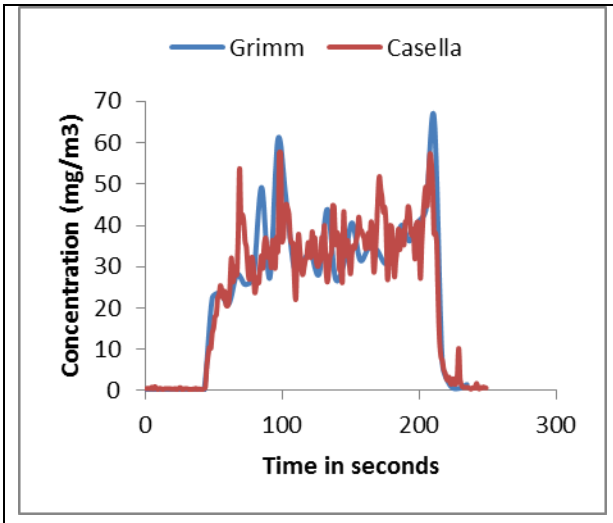

Speed: 1000 RPM
Feed: 635 mm/min
DOC: 6.35 mm

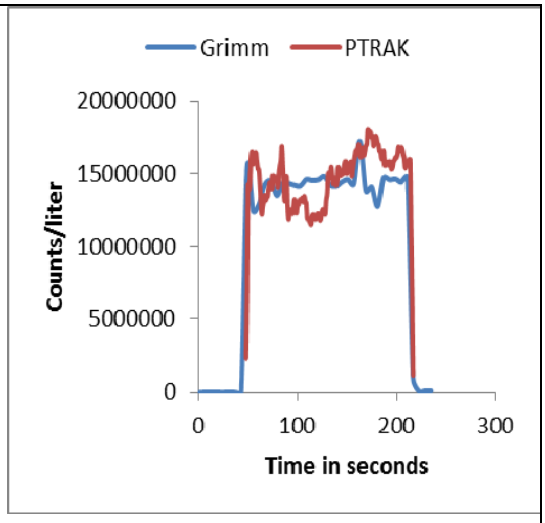

Speed: 1000 RPM
Feed: 635 mm/min
DOC: 6.35 mm

Run #8

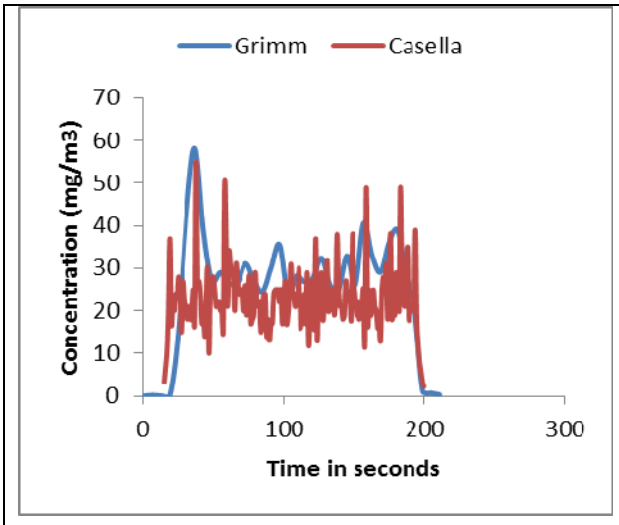

Speed: 1000 RPM
Feed: 635 mm/min
DOC: 3.81 mm

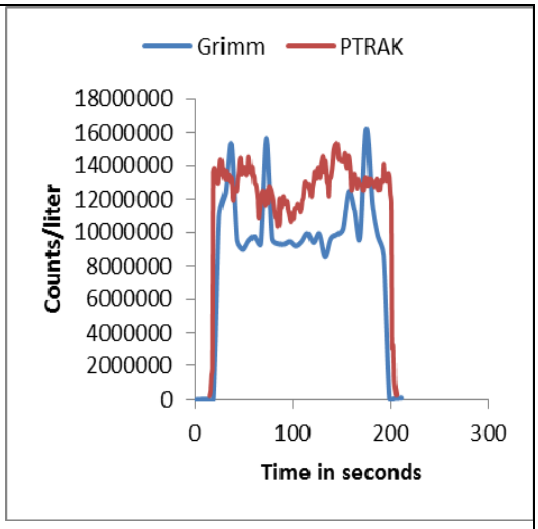

Speed: 1000 RPM
Feed: 635 mm/min
DOC: 3.81 mm

Run #9

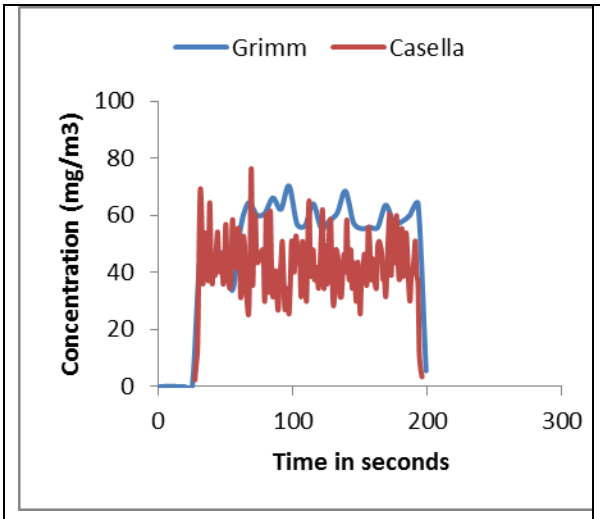

Speed: 6000 RPM
Feed: 381 mm/min
DOC: 6.35 mm

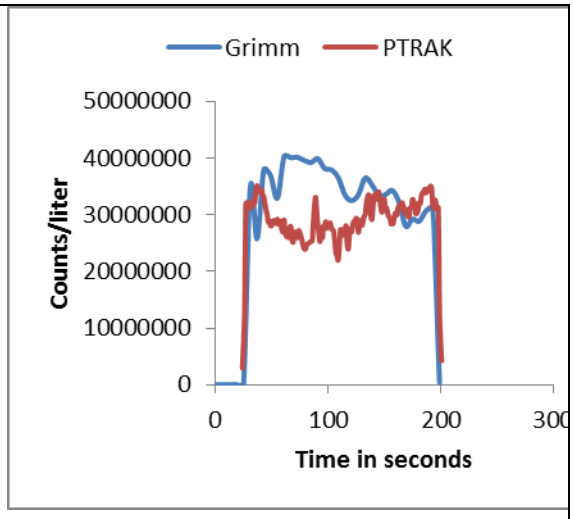

Speed: 6000 RPM
Feed: 381 mm/min
DOC: 6.35 mm

Run #10

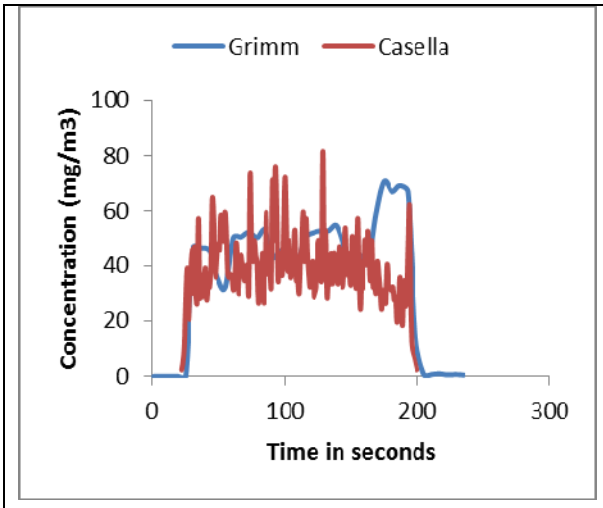

Speed: 6000 RPM
Feed: 381 mm/min
DOC: 3.81 mm

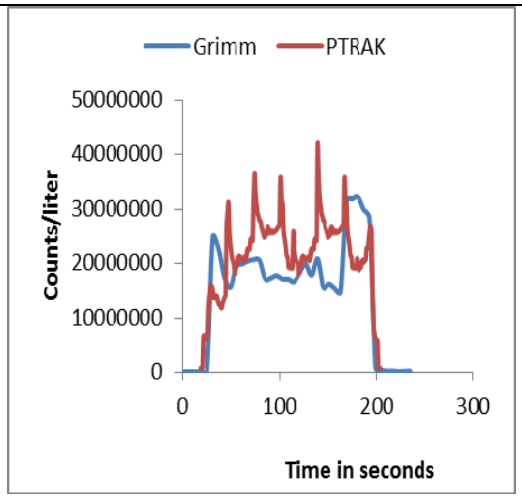

Speed: 6000 RPM
Feed: 381 mm/min
DOC: 3.81 mm

Run #11

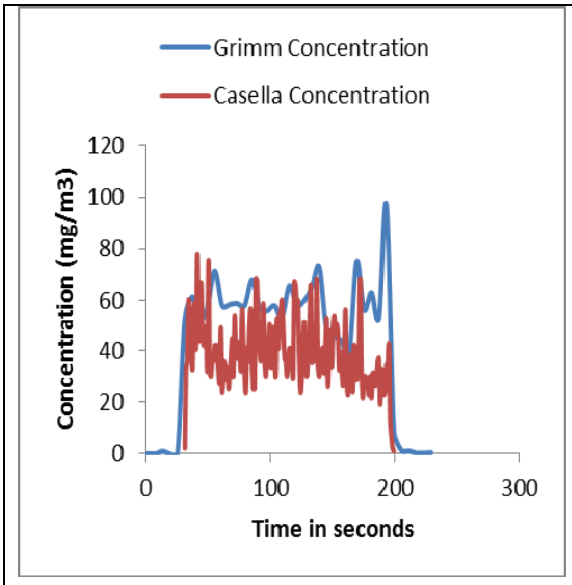

Speed: 6000 RPM
Feed: 381 mm/min
DOC: 2.54 mm

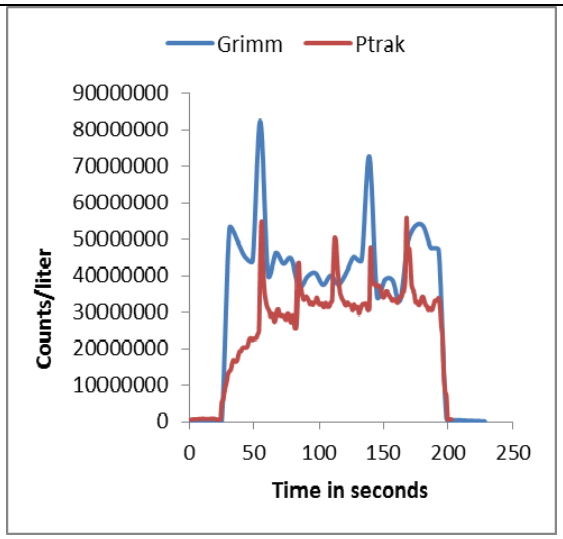

Speed: 6000 RPM
Feed: 381 mm/min
DOC: 2.54 mm

Run #12

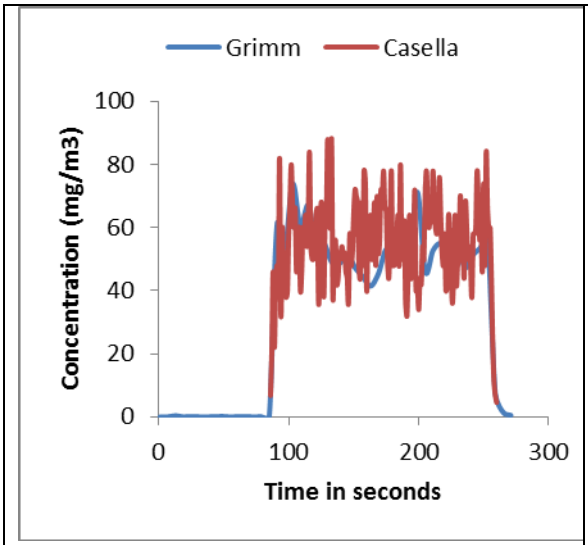

Speed: 3000 RPM
Feed: 381 mm/min
DOC: 6.35 mm

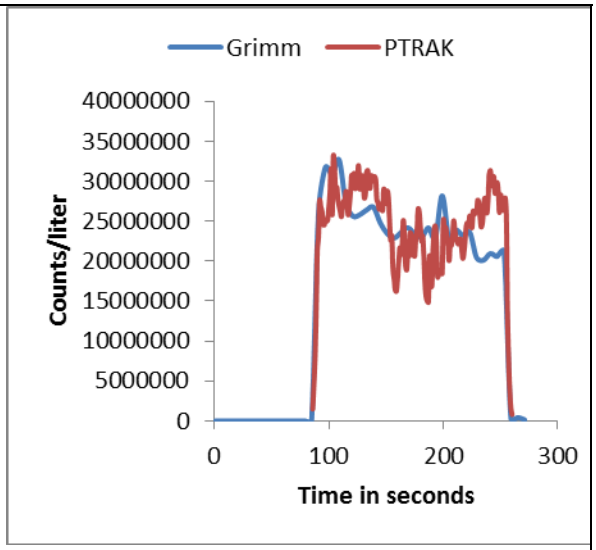

Speed: 3000 RPM
Feed: 381 mm/min
DOC: 6.35 mm

Run #13

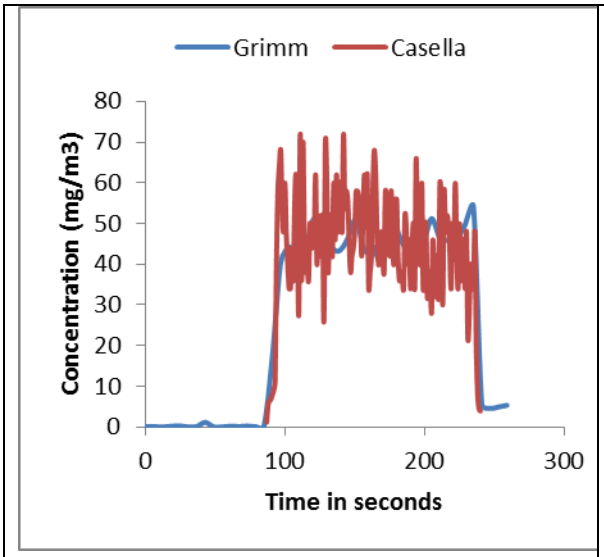

Speed: 3000 RPM
Feed: 381 mm/min
DOC: 3.81 mm

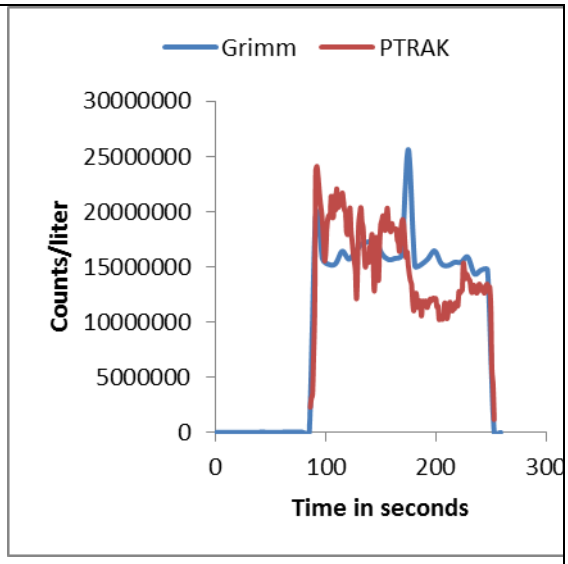

Speed: 3000 RPM
Feed: 381 mm/min
DOC: 3.81 mm

Run #14

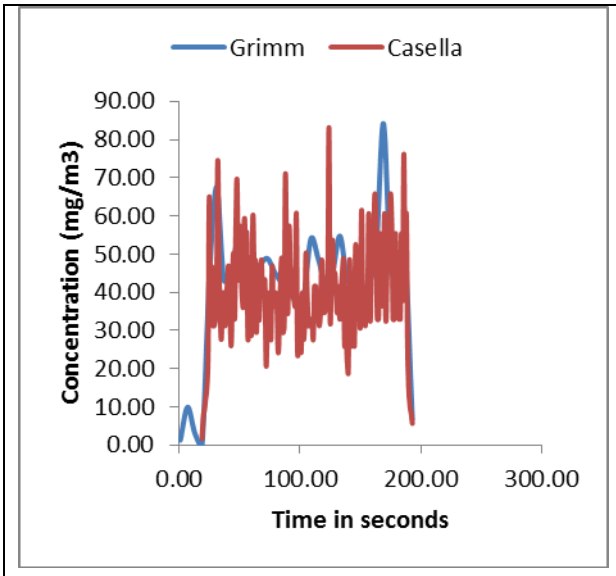

Speed: 3000 RPM
Feed: 381 mm/min
DOC: 2.54 mm

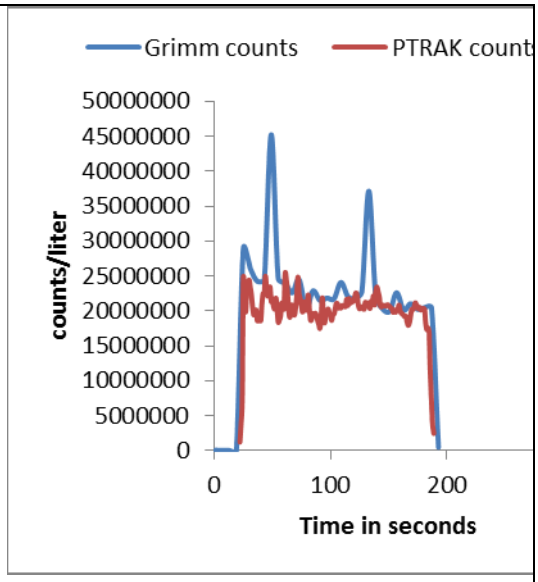

Speed: 3000 RPM
Feed: 381 mm/min
DOC: 2.54 mm

Run #15

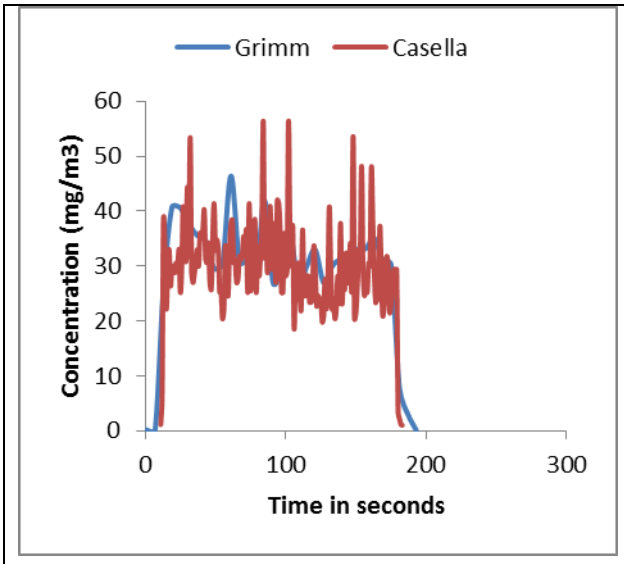

Speed: 1000 RPM
Feed: 381 mm/min
DOC: 2.54 mm

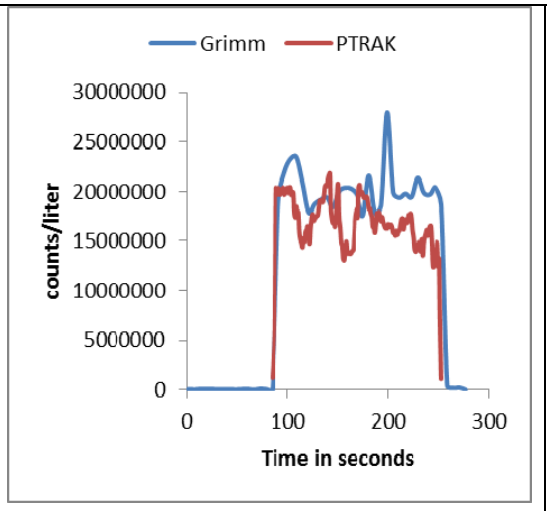

Speed: 1000 RPM
Feed: 381 mm/min
DOC: 2.54 mm

Run #16

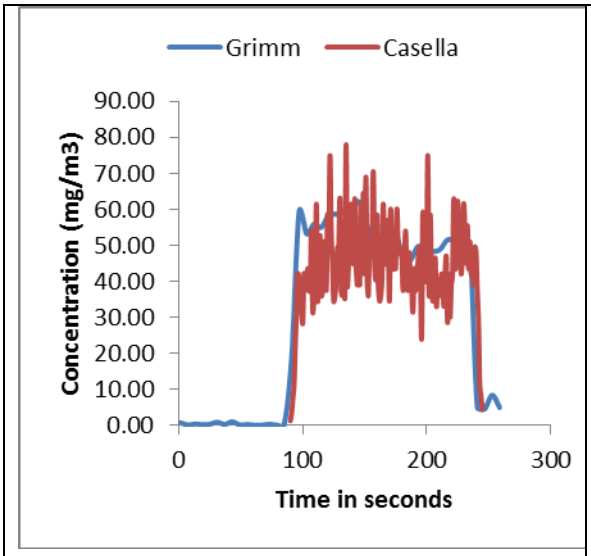

Speed: 1000 RPM
Feed: 381 mm/min
DOC: 6.35 mm

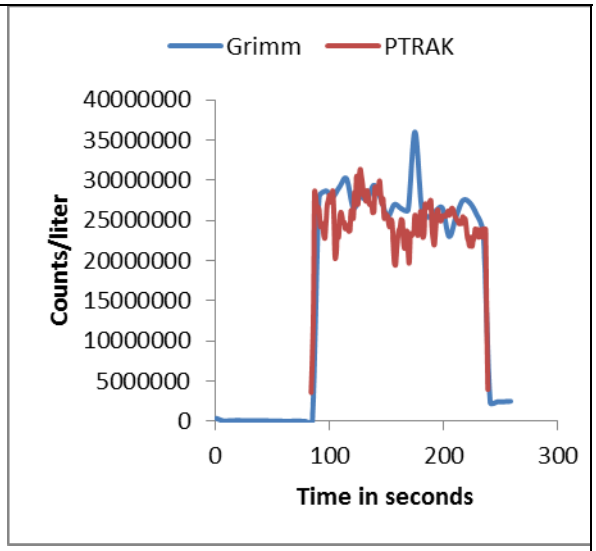

Speed: 1000 RPM
Feed: 381 mm/min
DOC: 6.35 mm

Run # 17

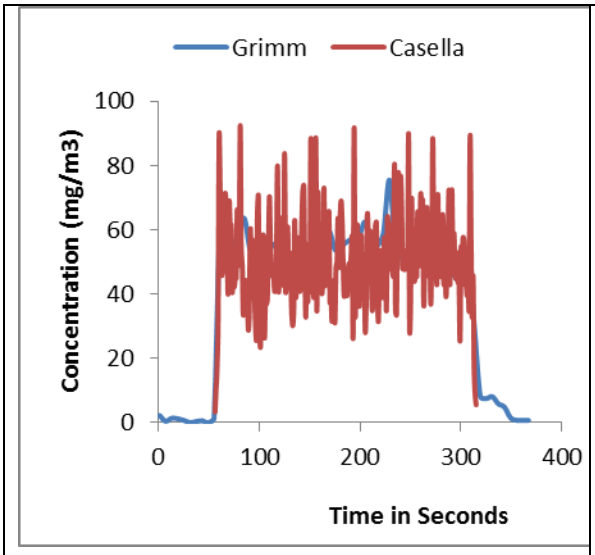

Speed: 6000 RPM
Feed: 127 mm/min
DOC: 3.81 mm

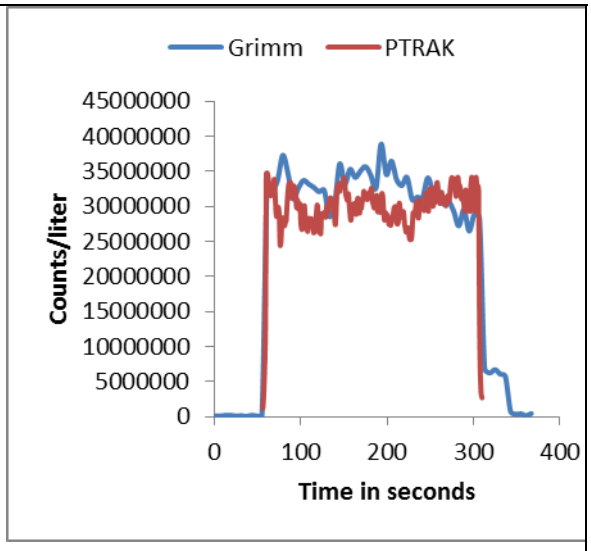

Speed: 6000 RPM
Feed: 127 mm/min
DOC: 3.81 mm

Run #18

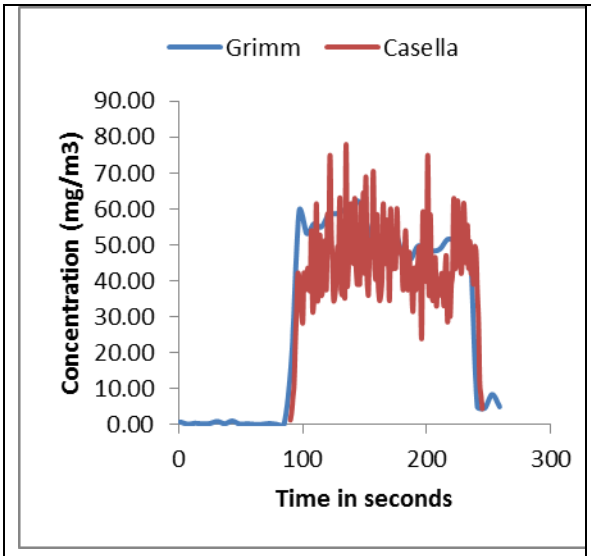

Speed: 3000 RPM
Feed: 127 mm/min
DOC: 3.81 mm

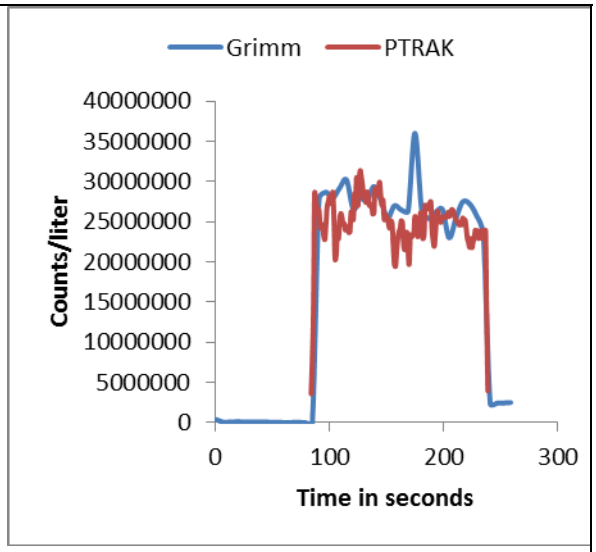

Speed: 3000 RPM
Feed: 127 mm/min
DOC: 3.81 mm

Run #19

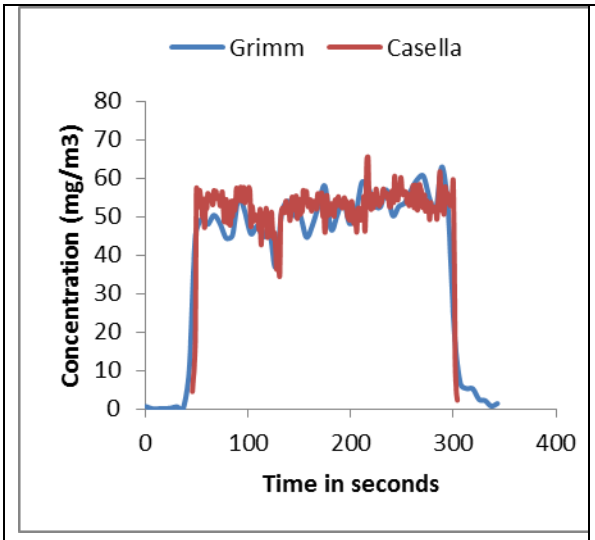

Speed: 1000 RPM
Feed: 127 mm/min
DOC: 3.81 mm

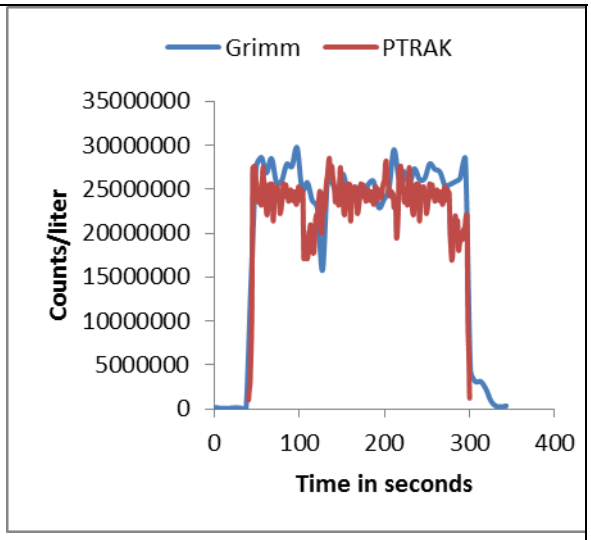

Speed: 1000 RPM
Feed: 127 mm/min
DOC: 3.81 mm

Run #20

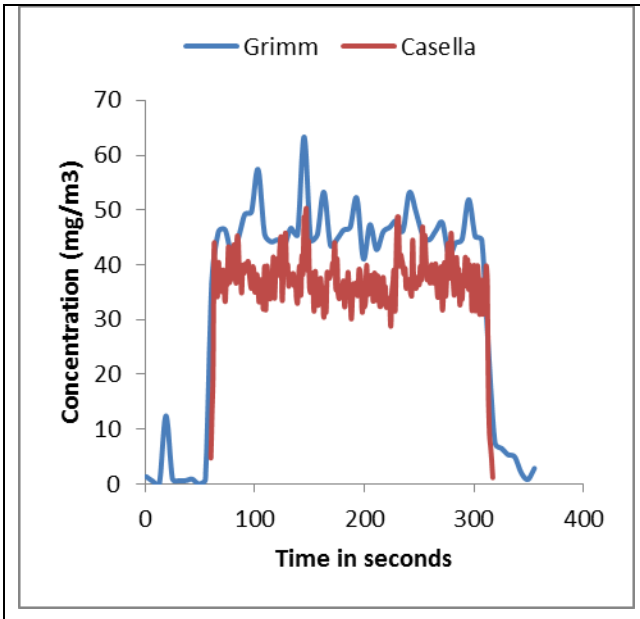

Speed: 1000 RPM
Feed: 127 mm/min
DOC: 2.54 mm

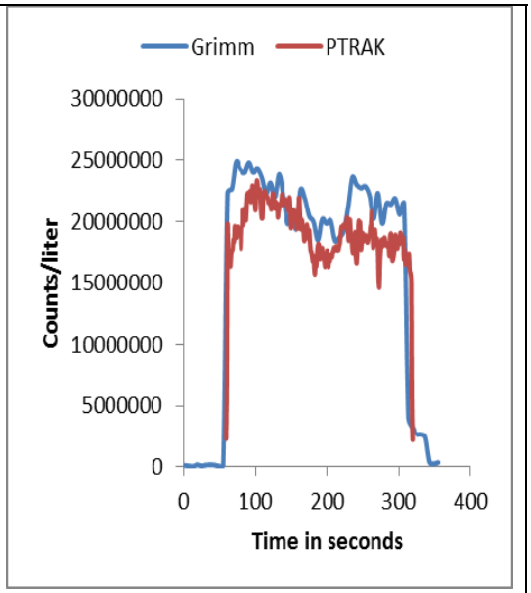

Speed: 1000 RPM
Feed: 127 mm/min
DOC: 2.54 mm

Run #21

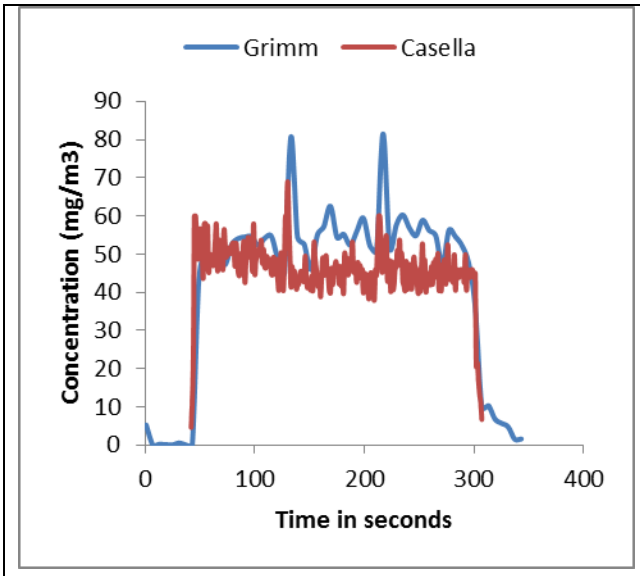

Speed: 3000 RPM
Feed: 127 mm/min
DOC: 2.54 mm

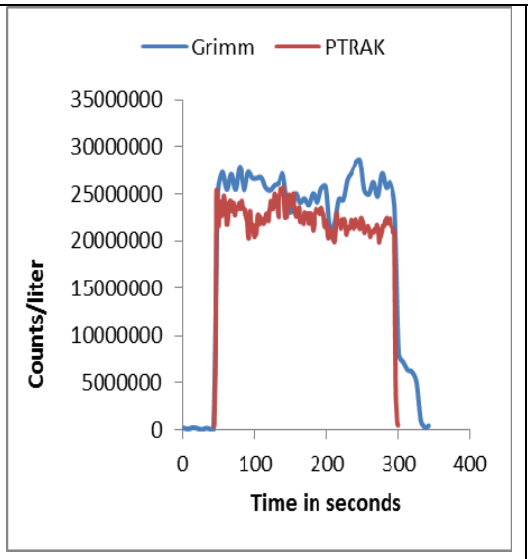

Speed: 3000 RPM
Feed: 127 mm/min
DOC: 2.54 mm

Run #22

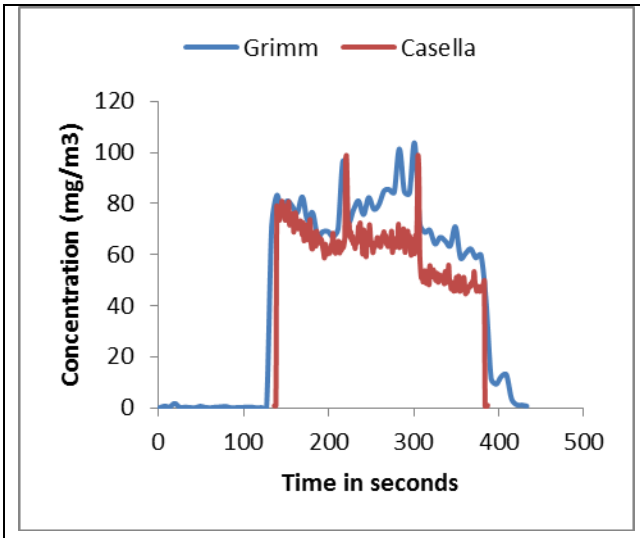

Speed: 6000 RPM
Feed: 127 mm/min
DOC: 6.35 mm

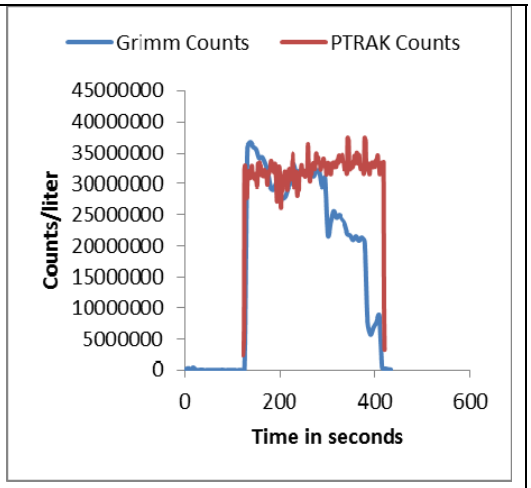

Speed: 6000 RPM
Feed: 127 mm/min
DOC: 6.35 mm

Run #23

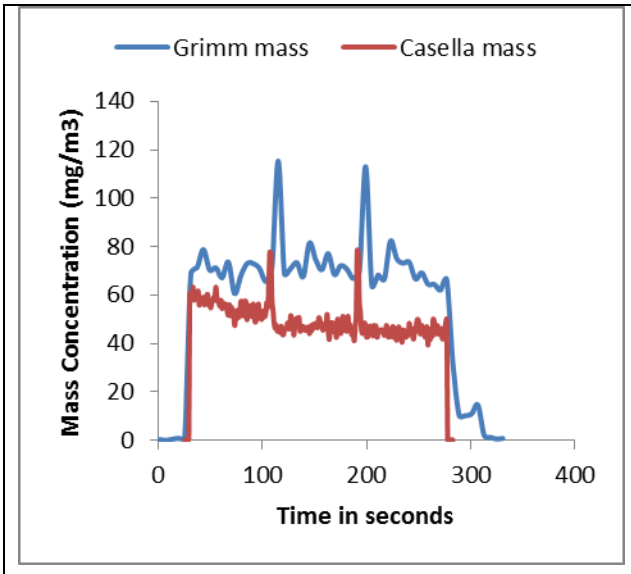

Speed: 3000 RPM
Feed: 127 mm/min
DOC: 6.35 mm

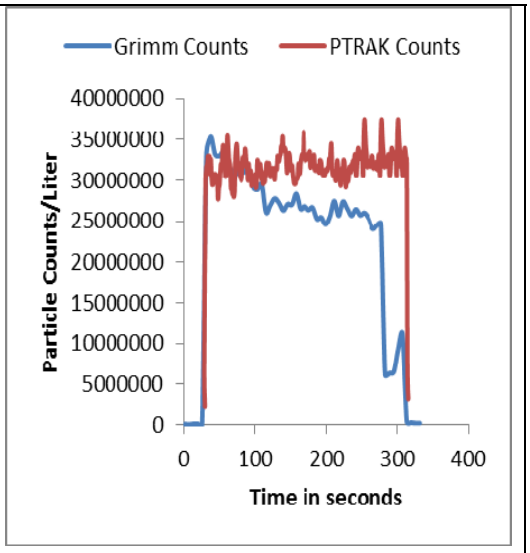

Speed: 3000 RPM
Feed: 127 mm/min
DOC: 6.35 mm

Run #24

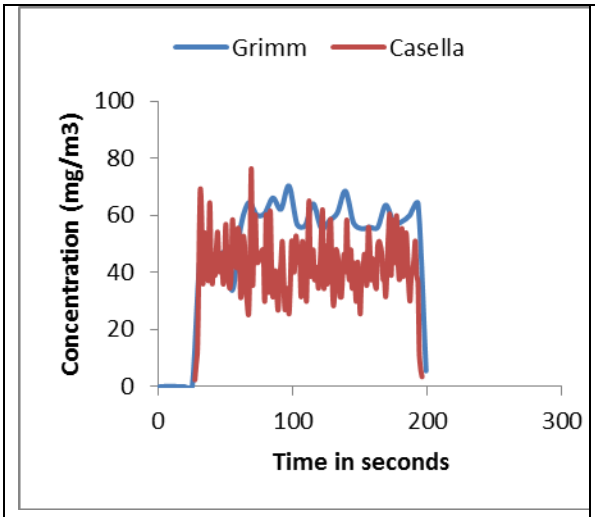

Speed: 1000 RPM
Feed: 127 mm/min
DOC: 6.35 mm

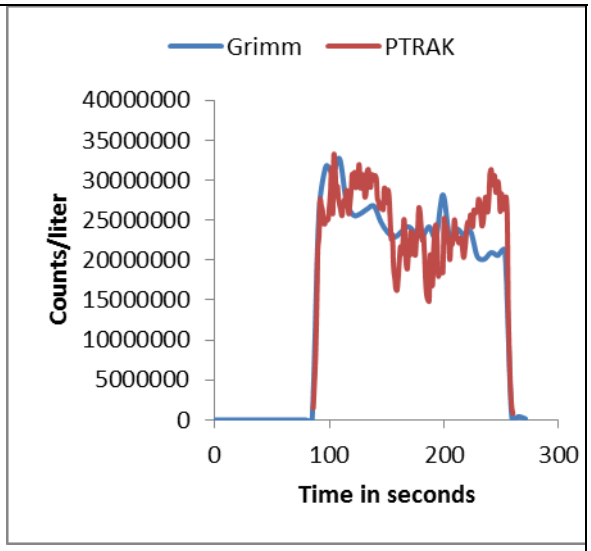

Speed: 1000 RPM
Feed: 127 mm/min
DOC: 6.35 mm

9.2 Appendix B

Combined Plots UDC HexMC® Edge Trim

#	SPEED (RPM)	FEED(MM/MIN)	DOC (MM)	GRIMM (Counts/lit)	Grimm Concentration (mg/m3)	Casella Conc. (mg/m3)	PTRAK COUNTS (Counts/lit)
1	6000	635	3.81	31531914	41.59424	42.74752	32236000
2	3000	635	3.81	27684009	37.28576	39.46176	26504000
3	6000	635	2.54	39522462	73.00154	73.32794	40272000
4	6000	635	6.35	33599836	49.87456	53.13696	30922000
5	3000	635	2.54	19268363	32.78144	36.75264	18091000
6	1000	635	2.54	13499598	22.01024	22.38016	12197000
7	1000	635	6.35	32750774	66.06554	67.16681	32560000
8	1000	635	3.81	22012100	40.48448	42.87808	24137000

Run #1

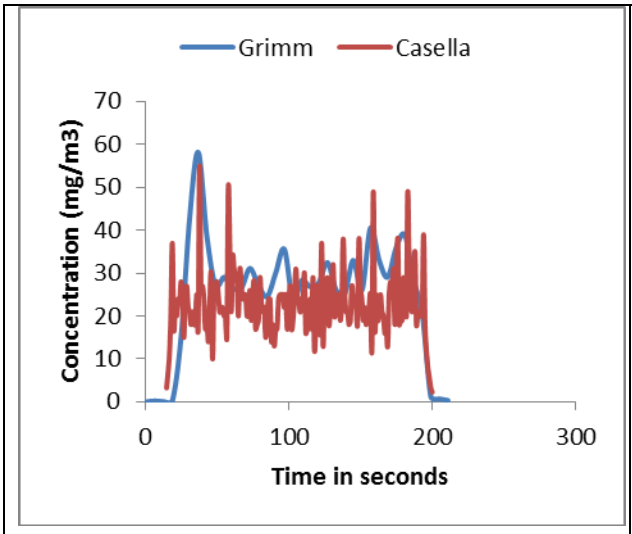

Speed: 6000 RPM
Feed: 635 mm/min
DOC: 6.35 mm

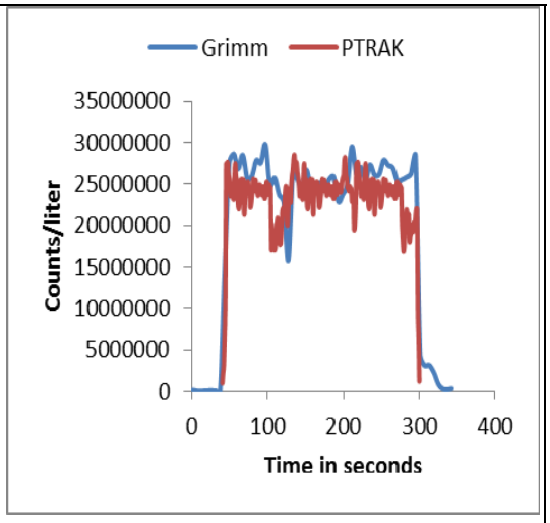

Speed: 6000 RPM
Feed: 635 mm/min
DOC: 6.35 mm

Run #2

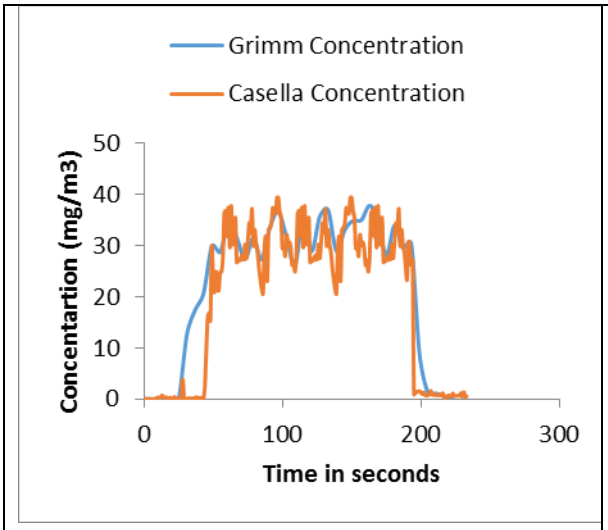

Speed: 6000 RPM
Feed: 635 mm/min
DOC: 2.54 mm

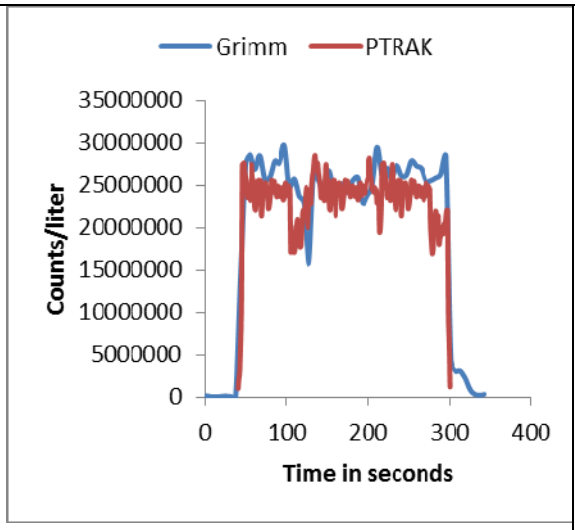

Speed: 6000 RPM
Feed: 635 mm/min
DOC: 2.54 mm

Run #3

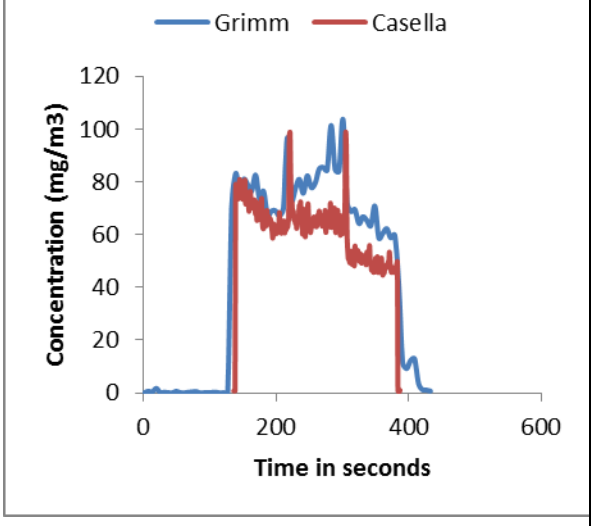

Speed: 6000 RPM
Feed: 127 mm/min
DOC: 6.35 mm

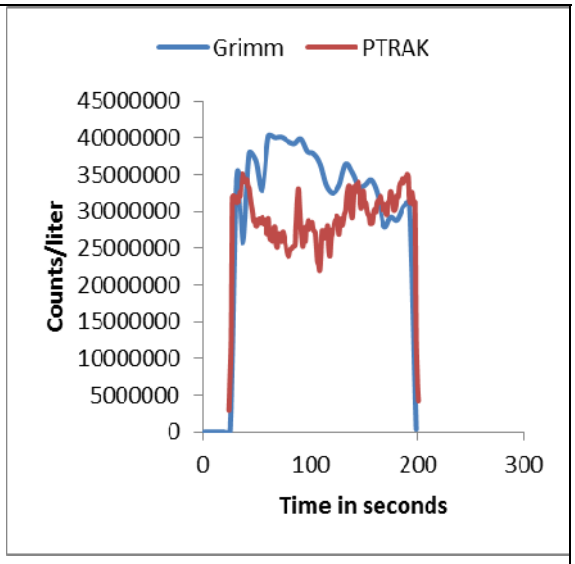

Speed: 6000 RPM
Feed: 127 mm/min
DOC: 6.35 mm

Run #4

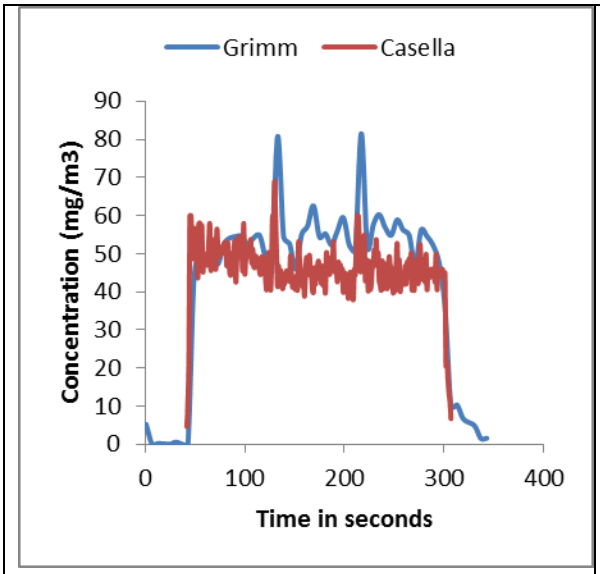

Speed: 6000 RPM
Feed: 127 mm/min
DOC: 6.35 mm

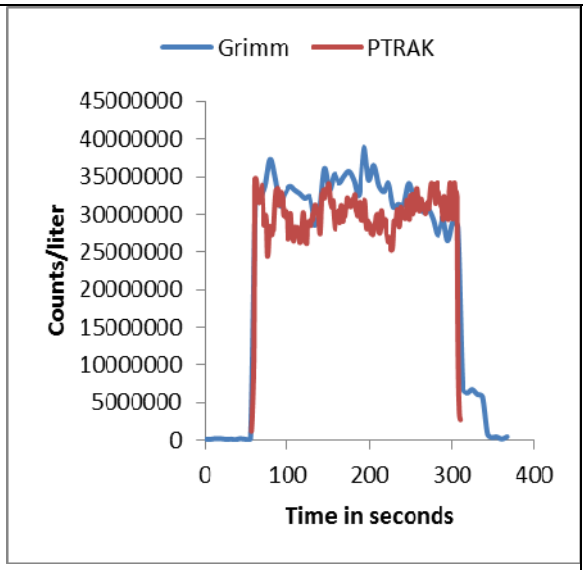

Speed: 6000 RPM
Feed: 127 mm/min
DOC: 6.35 mm

Run #5

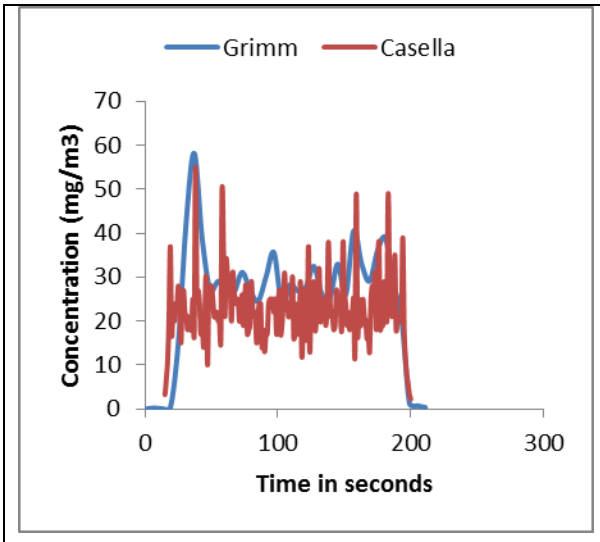

Speed: 1000 RPM
Feed: 635 mm/min
DOC: 6.35 mm

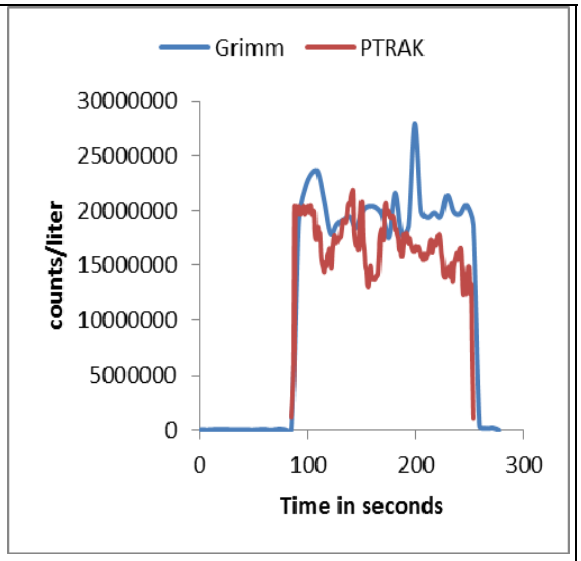

Speed: 1000 RPM
Feed: 635 mm/min
DOC: 6.35 mm

Run #6

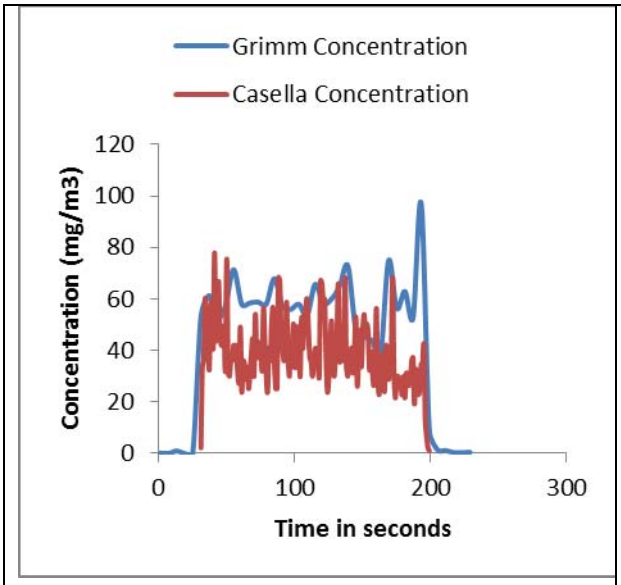

Speed: 1000 RPM
Feed: 635 mm/min
DOC: 2.54 mm

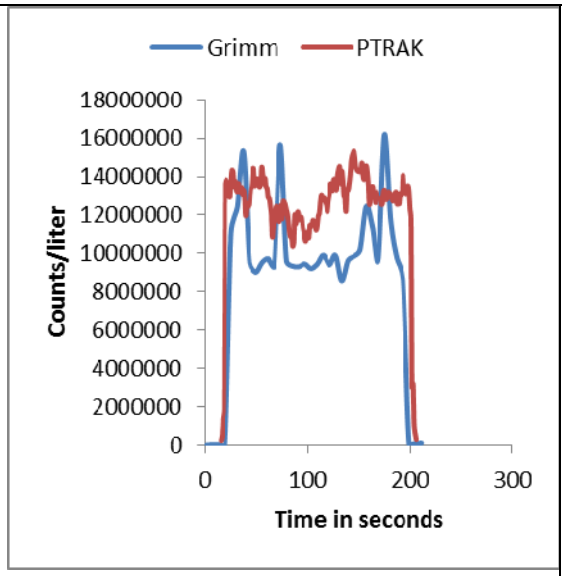

Speed: 1000 RPM
Feed: 635 mm/min
DOC: 2.54 mm

Run #7

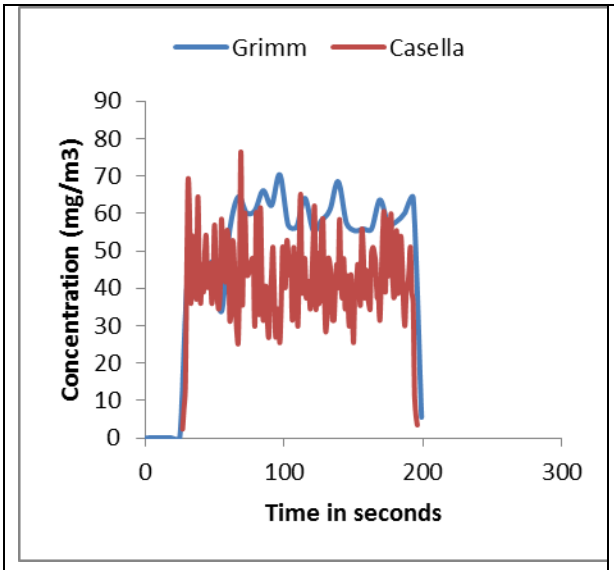

Speed: 1000 RPM
Feed: 127 mm/min
DOC: 6.35 mm

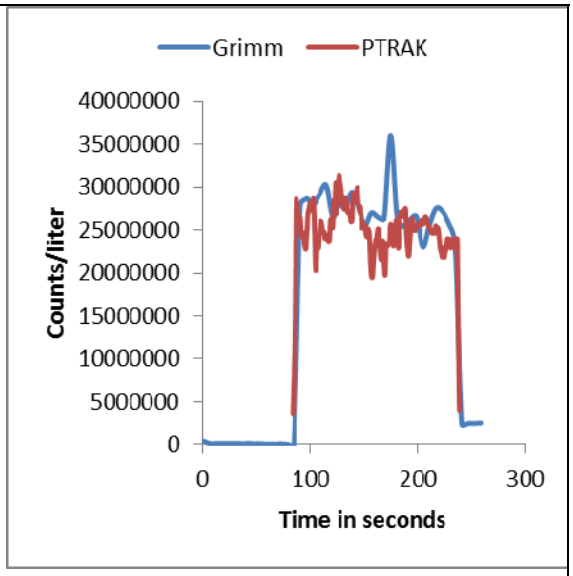

Speed: 1000 RPM
Feed: 127 mm/min
DOC: 6.35 mm

Run #8

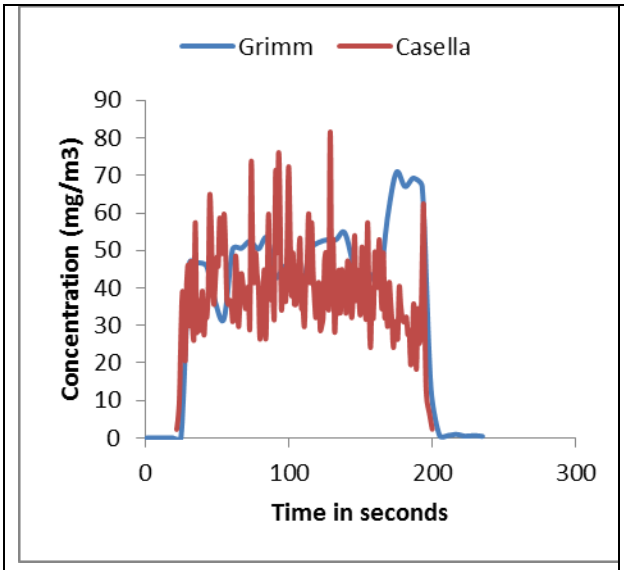

Speed: 1000 RPM
Feed: 127 mm/min
DOC: 6.35 mm

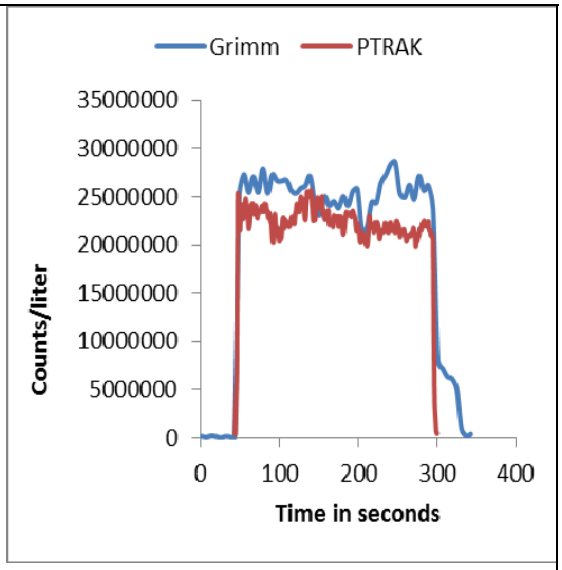

Speed: 1000 RPM
Feed: 127 mm/min
DOC: 6.35 mm

9.3 Appendix C

Aerodynamic Diameter Calculation Spreadsheet

In this spreadsheet and accompanying Matlab program, the user can convert from optical diameter to aerodynamic diameter. The purpose is to modify the GRIMM ranges for aerodynamic diameter in the previous tool. In this manner, the concentrations can be compared to gravimetric results from a cascade impactor. The user enters the constants including mean free diameter, standard density, ρa, particle density, ρe, dynamic shape factor, χ, and MP which is a multiplier for sizing between the bin low and high ranges where 0.5 is the midpoint. Individual densities can also be entered.

Constants			
λ	0.066	μm	Mean free path (fixed, used in Matlab)
ρ_a	1	g/cm3	Denisty equivalent aerodynamic particle (fixed, used in Matlab)
ρ_e	1.67	g/cm3	Density equivalent volume particle (can be modified for input into Matlab below for unique bin density)
χ	1.5		Shape factor (can be modified for input into Matlab for unique bin shape factor)
MP	0.5		Midpoint diameter (MP * (low bin + high bin)) (can be modified for calculations below, this is not used in Matlab)

ORIGINAL BIN STRUCTURE (EQUIVALENT VOLUME DIAMETER) - INPUT Paste cells C9:N12 into Matlab variable "equiv" cells C9:N12

ρ_e		1.67	1.67	1.67	1.67	1.67	1.67	1.67	1.67	1.67	1.67	1.67	1.67	1.67	1.67	1.67	1.67	1.67	1.67	1.67	1.67	1.67	1.67	1.67	1.67	1.67	1.67
χ		1.5	1.5	1.5	1.5	1.5	1.5	1.5	1.5	1.5	1.5	1.5	1.5	1.5	1.5	1.5	1.5	1.5	1.5	1.5	1.5	1.5	1.5	1.5	1.5	1.5	1.5
de (Low Bin)	blank	0.25	0.28	0.3	0.35	0.4	0.45	0.5	0.58	0.65	0.7	0.8	1	1.3	1.6	2	2.5	3	3.5	4	5	6.5	7.5	8.5	10	12.5	15
de (High Bin)	blank	0.28	0.3	0.35	0.4	0.45	0.5	0.58	0.65	0.7	0.8	1	1.3	1.6	2	2.5	3	3.5	4	5	6.5	7.5	8.5	10	12.5	15	17.5
MP		0.5	0.5	0.5	0.5	0.5	0.5	0.5	0.5	0.5	0.5	0.5	0.5	0.5	0.5	0.5	0.5	0.5	0.5	0.5	0.5	0.5	0.5	0.5	0.5	0.5	0.5

ORIGINAL BIN STRUCTURE (EQUIVALENT VOLUME DIAMETER) - reference

de (Low Bin)	User Defin	0.25	0.28	0.3	0.35	0.4	0.45	0.5	0.58	0.65	0.7	0.8	1	1.3	1.6	2	2.5	3	3.5	4	5	6.5	7.5	8.5	10	12.5	15
de (High Bin)	Backup	0.28	0.3	0.35	0.4	0.45	0.5	0.58	0.65	0.7	0.8	1	1.3	1.6	2	2.5	3	3.5	4	5	6.5	7.5	8.5	10	12.5	15	17.5
de (Bin Midpoint)	Filter	0.265	0.29	0.325	0.375	0.425	0.475	0.54	0.615	0.675	0.75	0.9	1.15	1.45	1.8	2.25	2.75	3.25	3.75	4.5	5.75	7	8	9.25	11.25	13.75	16.25
date & time (μg/m3)	Mass (μg/r	0.265 μm	0.290 μm	0.325 μm	0.375 μm	0.425 μm	0.475 μm	0.540 μm	0.615 μm	0.675 μm	0.750 μm	0.900 μm	1.150 μm	1.450 μm	1.800 μm	2.250 μm	2.750 μm	3.250 μm	3.750 μm	4.500 μm	5.750 μm	7.000 μm	8.000 μm	9.250 μm	11.250 μm	13.750 μm	16.250 μm

REVISED BIN STRUCTURE (AERODYNAMIC DIAMETER) pasted from Matlab. Paste cells from Matlab variable "aero" into cells C24:N29

ρ_e		1.67	1.67	1.67	1.67	1.67	1.67	1.67	1.67	1.67	1.67	1.67	1.67	1.67	1.67	1.67	1.67	1.67	1.67	1.67	1.67	1.67	1.67	1.67	1.67	1.67	1.67
χ		1.5	1.5	1.5	1.5	1.5	1.5	1.5	1.5	1.5	1.5	1.5	1.5	1.5	1.5	1.5	1.5	1.5	1.5	1.5	1.5	1.5	1.5	1.5	1.5	1.5	1.5
Ce (Low Bin)		1.6653	1.594	1.5544	1.4752	1.4158	1.3696	1.3326	1.2868	1.2559	1.2376	1.2079	1.1663	0	0	0	0	0	0	0	0	0	0	0	0	0	0
Ca (Low Bin)		1.6223	1.5562	1.5195	1.4459	1.3905	1.3474	1.3129	1.27	1.2411	1.2239	1.1961	1.157	0	0	0	0	0	0	0	0	0	0	0	0	0	0
Ce (High Bin)		1.594	1.5544	1.4752	1.4158	1.3696	1.3326	1.2868	1.2559	1.2376	1.2079	1.1663	0	0	0	0	0	0	0	0	0	0	0	0	0	0	0
Ca (High Bin)		1.5582	1.5195	1.4459	1.3905	1.3474	1.3129	1.27	1.2411	1.2239	1.1961	1.157	0	0	0	0	0	0	0	0	0	0	0	0	0	0	0
da (Low Bin)	User Defin	0.267	0.299	0.320	0.373	0.426	0.479	0.532	0.616	0.690	0.743	0.848	1.059	1.372	1.688	2.110	2.638	3.165	3.693	4.221	5.276	6.858	7.914	8.969	10.551	13.189	15.827
da (High Bin)	Backup	0.299	0.320	0.373	0.426	0.479	0.532	0.616	0.690	0.743	0.848	1.059	1.372	1.688	2.110	2.638	3.165	3.693	4.221	5.276	6.858	7.914	8.969	10.551	13.189	15.827	18.465
da (Bin Midpoint)	Filter	0.283	0.310	0.347	0.399	0.452	0.505	0.574	0.653	0.716	0.795	0.954	1.216	1.530	1.899	2.374	2.902	3.429	3.957	4.748	6.067	7.386	8.441	9.760	11.870	14.508	17.146
date & time (μg/m3	Mass (μg/r	0.283 μm	0.309 μm	0.346 μm	0.399 μm	0.452 μm	0.505 μm	0.573 μm	0.652 μm	0.716 μm	0.795 μm	0.953 μm	1.215 μm	1.529 μm	1.899 μm	2.374 μm	2.901 μm	3.429 μm	3.956 μm	4.748 μm	6.067 μm	7.386 μm	8.441 μm	9.760 μm	11.87 μm	14.50 μm	17.14 μm

9.4 Appendix D

SEM – Machining Dust on Casella Filter

Casella filter SEM – UD CFRP Composites

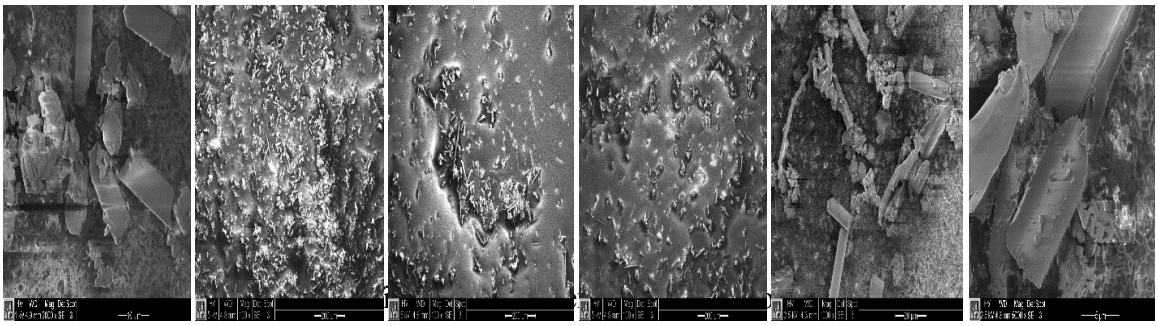

Casella filter SEM – HexMC Composites

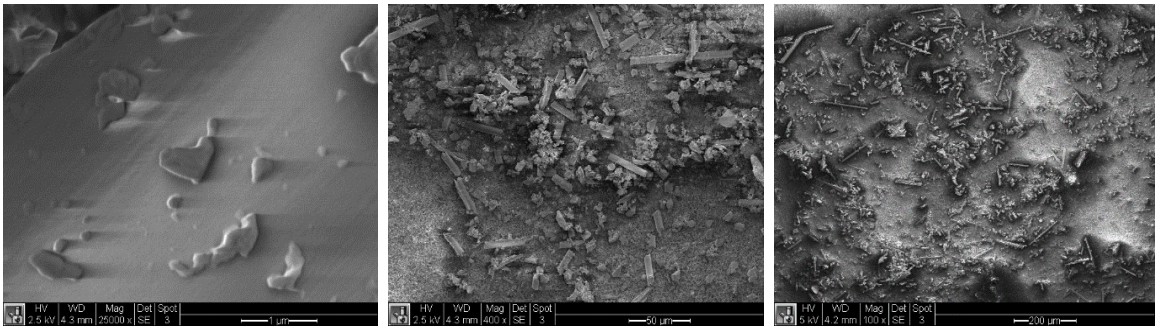

9.5 Appendix E

SEM – Machining Dust on Carbon Tape

UDC TAPE SEM (Feed 127 mm/min)

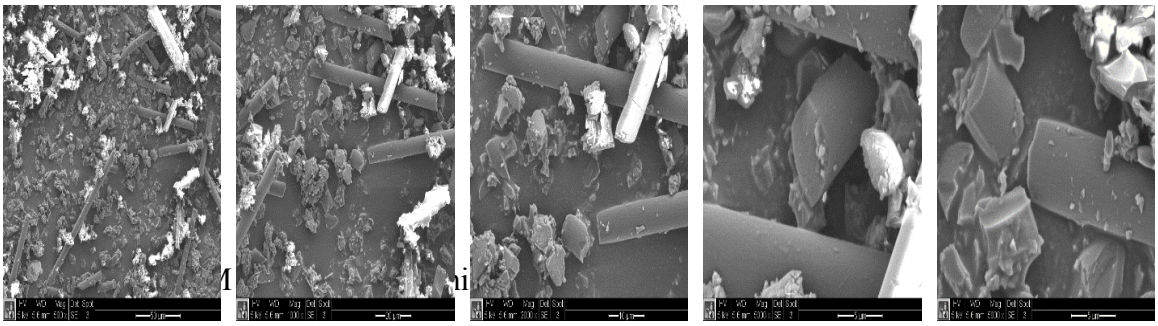

UDC TAPE SEM (Feed 381 mm/min)

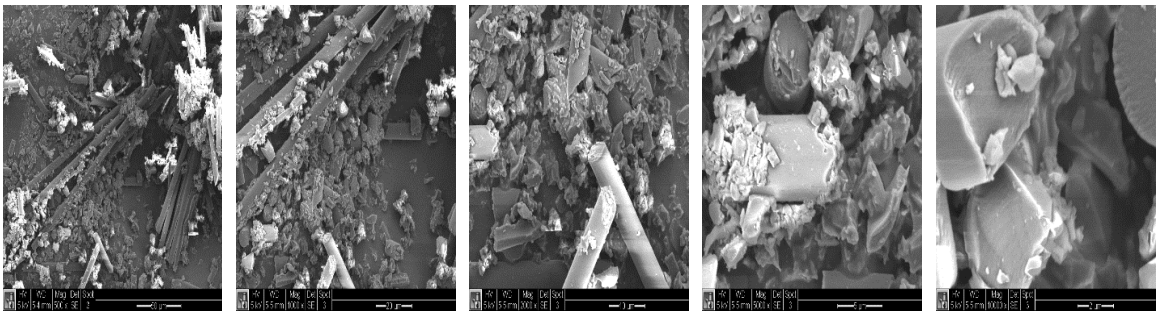

UDC TAPE SEM (Feed 635 mm/min)

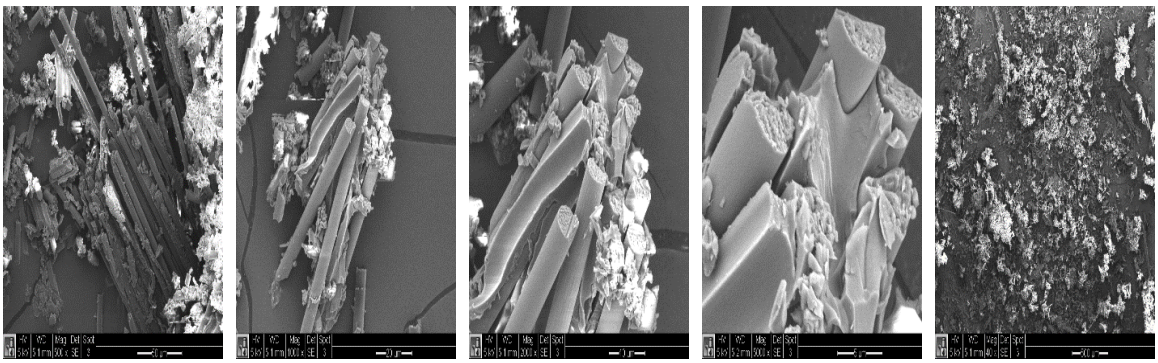

SEM – Machining Dust on Carbon Tape (cont.)

HexMC TAPE SEM (Feed 127 mm/min)

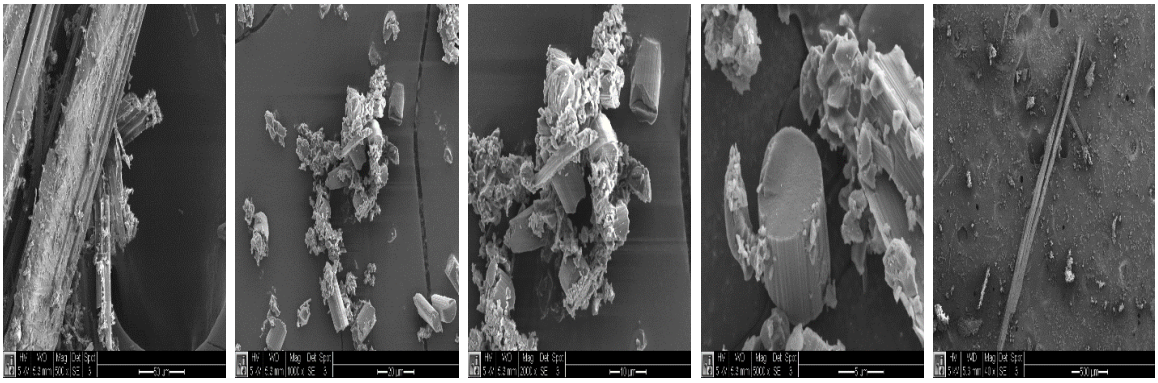

HexMC TAPE SEM (Feed 381 mm/min)

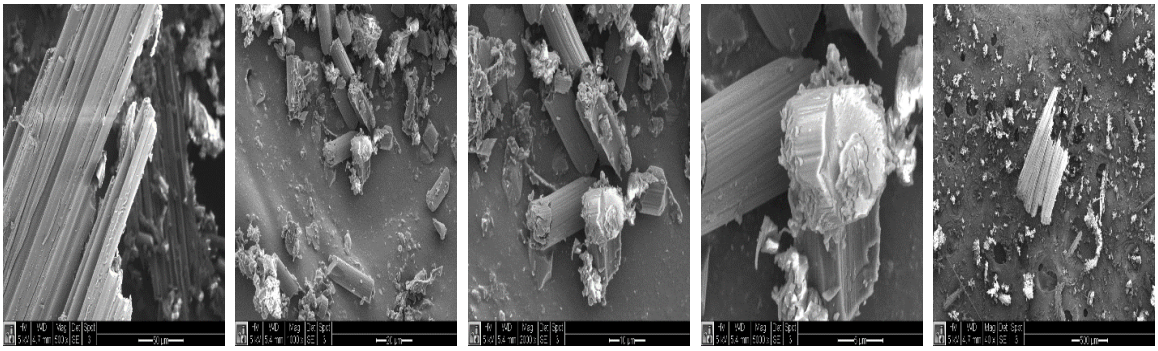

HexMC TAPE SEM (Feed 635 mm/min)

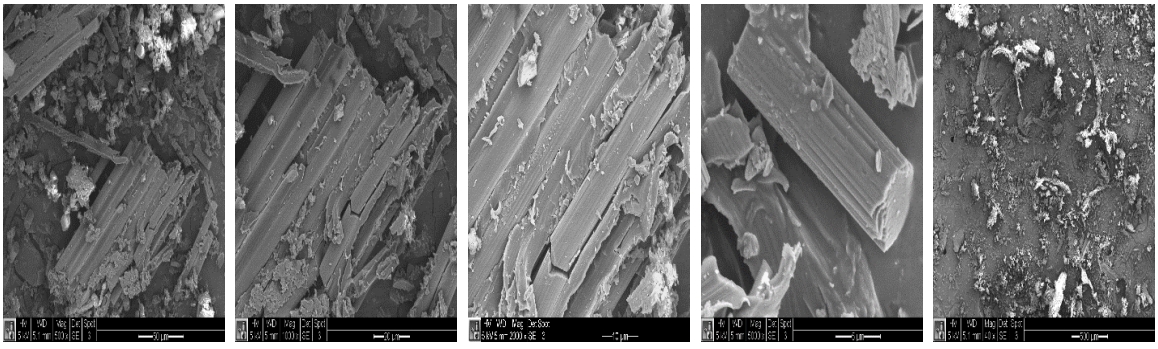

9.6 Appendix F

SEM – Machining Dust Sioutas Impactor stages for HexMC

SEM IMPACTOR STAGE A

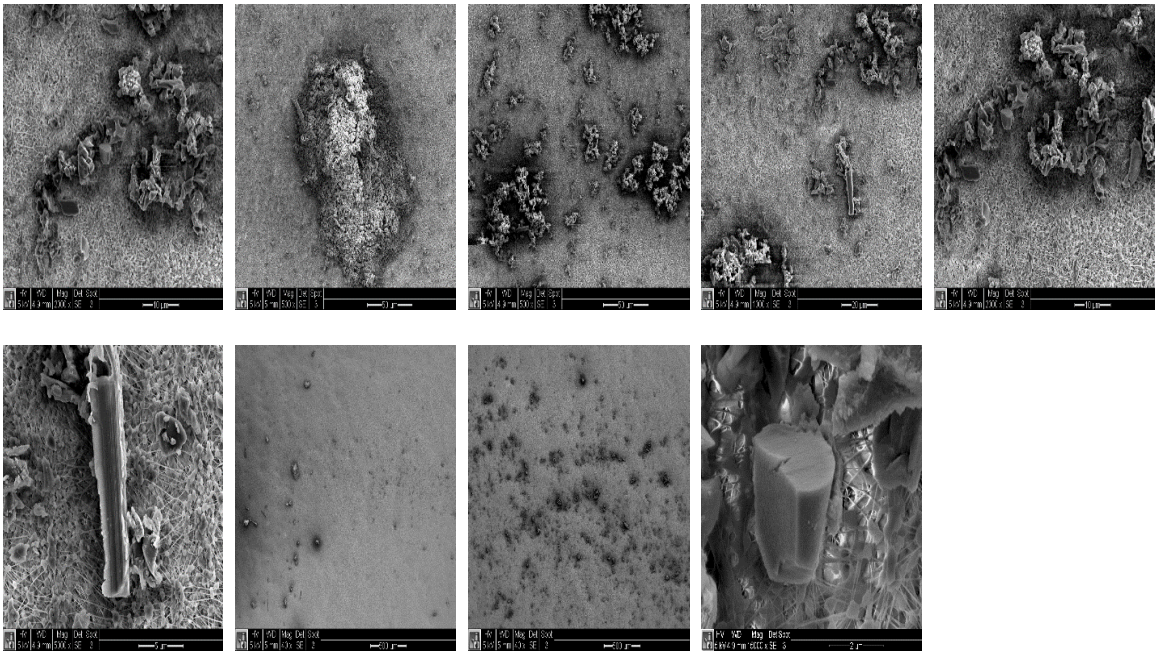

SEM IMPACTOR STAGE B

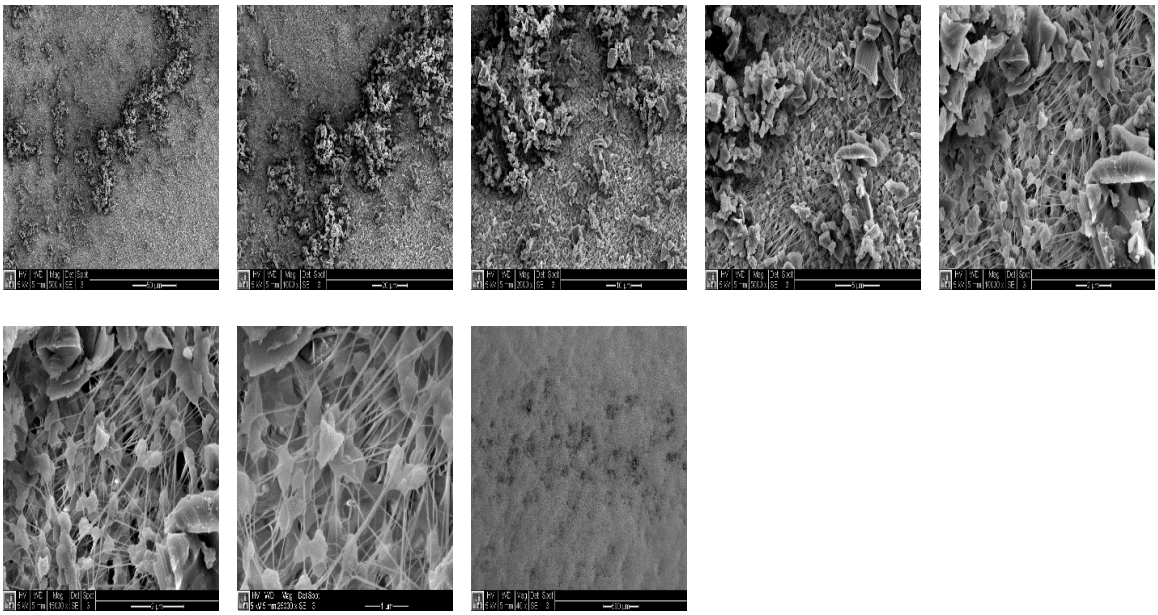

SEM – Machining Dust Sioutas Impactor stages for HexMC (cont.)

SEM IMPACTOR STAGE C

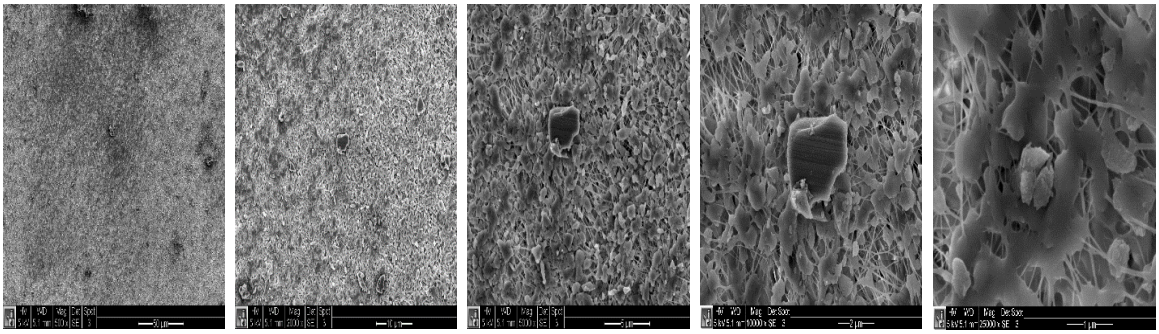

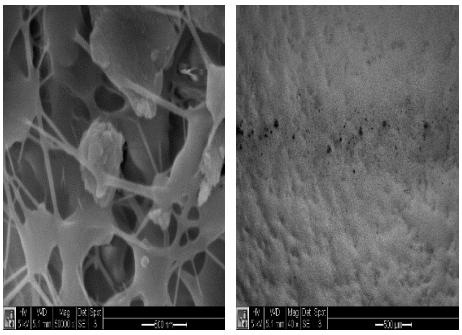

SEM IMPACTOR STAGE D

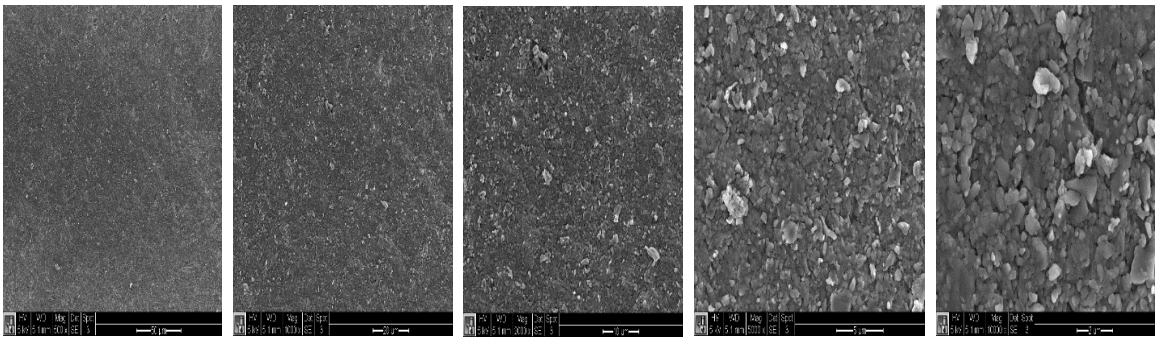

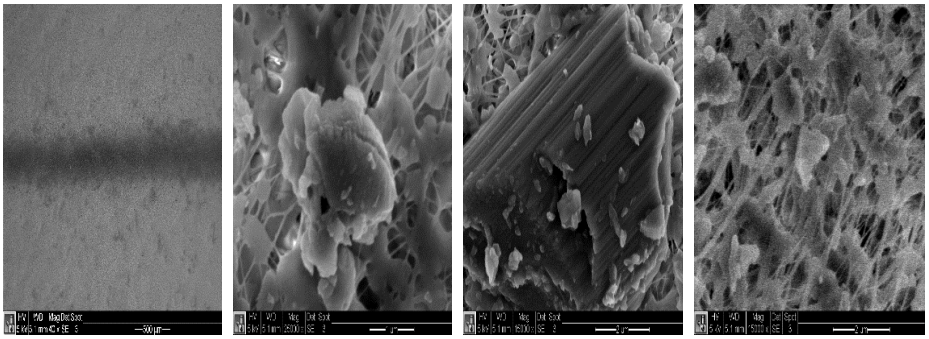

SEM – Machining Dust Sioutas Impactor stages for UD-CFRP

SEM IMPACTOR STAGE A

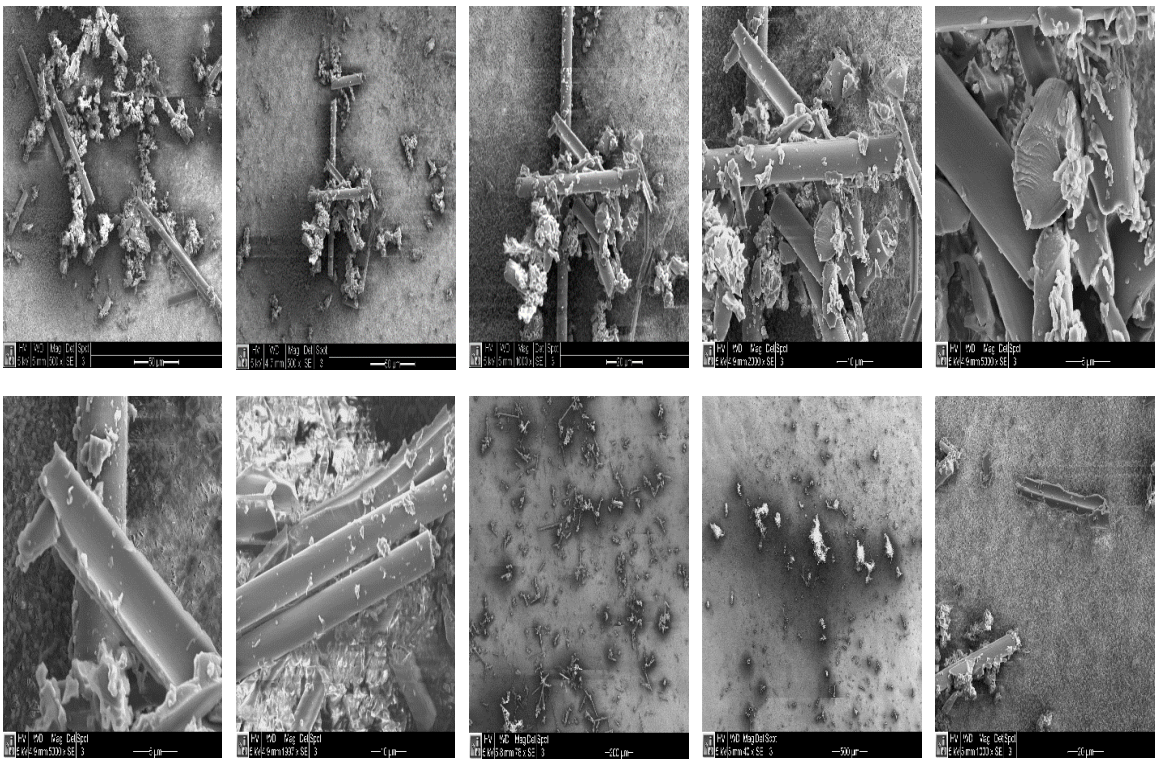

SEM IMPACTOR STAGE B

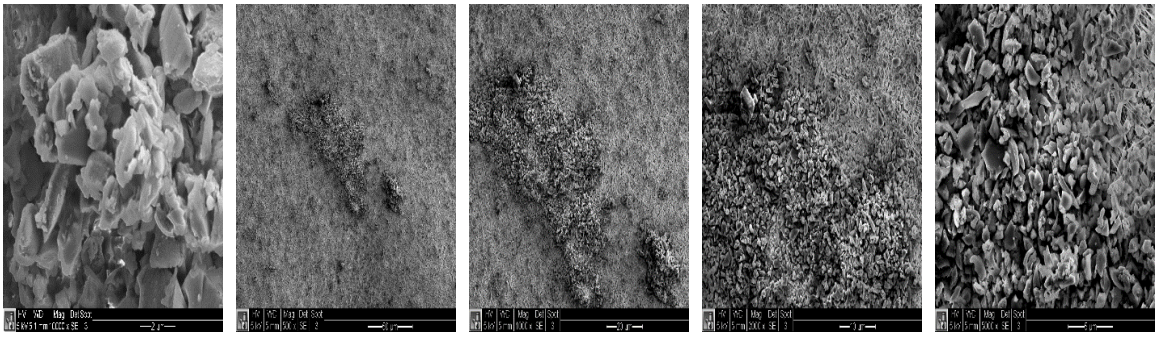

SEM – Machining Dust Sioutas Impactor stages for UD-CFRP (CONT.)

SEM IMPACTOR STAGE C

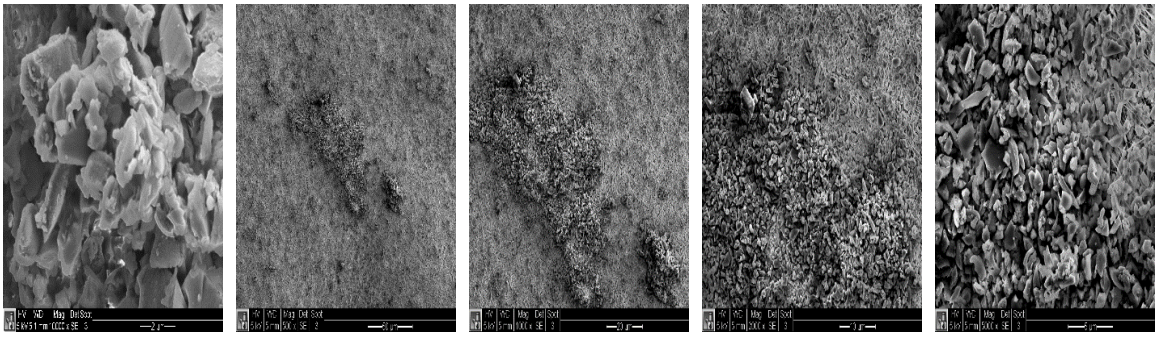

SEM IMPACTOR STAGE D

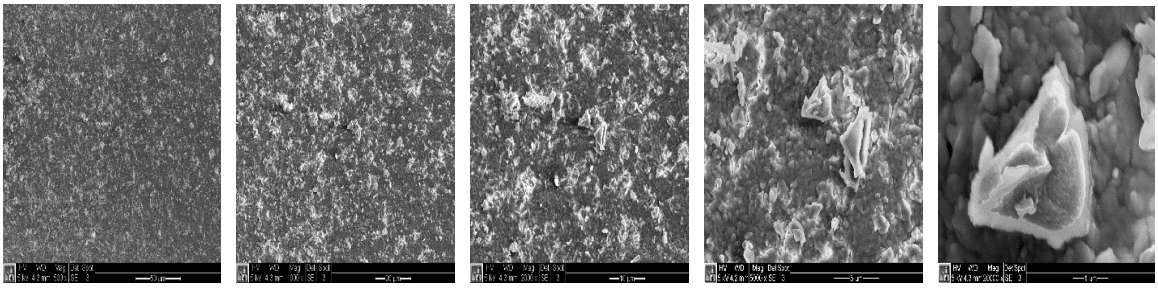

9.7 Appendix G

CNC Programs

Program 1:

```
O12363 (25 in/min edge trim for 3 minutes dust collection time)
T1 H01 G43
G91 (incremental)
M03 S6000 (spindle on CW)
G01 F25. Y0.03 (feed 25 .03 in Y)
G01 F25. X-7.0 (climb cut in X)
G01 F25. Y0.03 (feed into part .03)
G01 F25. X7.0 (Conventional cut in X)
G01 F25. Y0.03 (feed 25 .03 in Y)
G01 F25. X-7.0 (climb cut in X)
G01 F25. Y0.03 (feed into part .03)
G01 F25. X7.0 (Conventional cut in X)
G01 F25. Y0.03 (feed 25 .03 in Y)
G01 F25. X-7.0 (climb cut in X)
G01 F25. Y0.03 (feed 25 .03 in Y)
G01 F25. X7.0 (climb cut in X)
G01 F25. Y0.03 (feed into part .03)
G01 F25. X-7.0 (Conventional cut in X)
G01 F25. Y0.03 (feed 25 .03 in Y)
G01 F25. X7.0 (climb cut in X)
G01 F25. Y0.03 (feed into part .03)
G01 F25. X-7.0 (Conventional cut in X)
G01 F25. Y0.03 (feed 25 .03 in Y)
G01 F25. X7.0 (climb cut in X)
G01 F25. Y0.03 (feed into part .03)
G01 F25. X7.0 (Conventional cut in X)
M30 (end of program)
```

Program 2:

```
O12365 (15 in/min edge trim for 3 minutes dust collection time)
T1 H01 G43
G91 (incremental)
M03 S6000 (spindle on CW)
G01 F15. Y0.03 (feed 25 .03 in Y)
G01 F15. X-7.0 (climb cut in X)
G01 F15. Y0.03 (feed into part .03)
G01 F15. X7.0 (Conventional cut in X)
G01 F15. Y0.03 (feed 25 .03 in Y)
G01 F15. X-7.0 (climb cut in X)
G01 F15. Y0.03 (feed into part .03)
G01 F15. X7.0 (Conventional cut in X)
G01 F15. Y0.03 (feed 25 .03 in Y)
G01 F15. X-7.0 (climb cut in X)
G01 F15. Y0.03 (feed 25 .03 in Y)
G01 F15. X7.0 (climb cut in X)
M30 (end of program)
```

Program 3:

```
O12367 (5 in/min edge trim for 3 minutes dust collection time)
T1 H01 G43
G91 (incremental)
M03 S6000 (spindle on CW)
G01 F5. Y0.03 (feed 25 .03 in Y)
G01 F5. X-7.0 (climb cut in X)
G01 F5. Y0.03 (feed into part .03)
G01 F5. X7.0 (Conventional cut in X)
G01 F5. Y0.03 (feed 25 .03 in Y)
G01 F5. X-7.0 (climb cut in X)
G01 F5. X7.0 (No CUT RETURN PASS in X)
M30 (end of program)
```

Program 4:

```
O12369 (OCTAGON CUT)
T1 H01 G43
G91 (incremental)
M03 S1000 (spindle on CW)
G01 F1. Y0.4 (lead into the part)
G01 F1. X-1.414 Y1.414 (point a to b)
G01 F1. Y1.5 (point b to c)
G01 F1. X1.414 Y1.414 (POINT C TO D)
G01 F1. X2.0 (POINT D TO E)
G01 F1. X1.414 Y-1.414 (POINT E TO F)
G01 F1. Y-1.5 (POINT F TO G)
G01 F1. X-1.414 Y-1.414 (POINT G TO H)
G01 F1. X-2.0 (POINT H TO A)
M30 (end of program)
```

9.8 Appendix H

Comparing Worn and New Tools

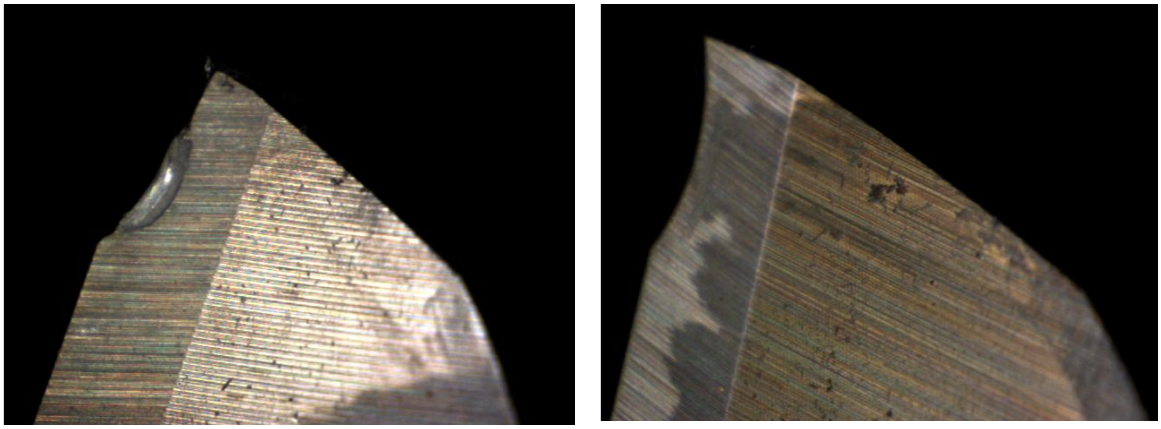

Figure 9-1: Worn Tool (left), New Tool (right)

The figure 9-1 shows the surface profiles of the new and used tool. The used tool shown in the figure was withdrawn from further testing after approximately 40 minutes of cutting.